Doctoral Dissertation
博士論文

Stochastic description and quantum aspects of curvature perturbations in the inflationary universe
（インフレーション宇宙における曲率ゆらぎの
確率的描像と量子的側面）

A Dissertation Submitted for the Degree of Doctor of Philosophy
December 2020
令和２年１２月博士（理学）申請

Department of Physics, Graduate School of Science,
The University of Tokyo
東京大学大学院理学系研究科物理学専攻

Kenta Ando
安藤　健太

Abstract

We study adiabatic curvature perturbations generated during inflation. The fundamental statistical quantities such as correlation functions of curvature perturbations can be calculated by means of a stochastic average while some quantum aspects may be probed via so-called improper operators. In this thesis, we shed light on both a stochastic description and quantum aspects. As for a stochastic description, we compute the power spectrum of curvature perturbations in stochastic inflation taking into account the deviation from the classical relationship between scales and field values at the time when a given scale exits the horizon. This allows the stochastic-δN formalism to make concrete contact with observations. As an application, we study how quantum diffusion near the end of inflation affects large-scale perturbations. We find that such a correction can be drastically large depending on the amount of diffusion, which means that the cosmic microwave background measurements can set explicit constraints on the entire inflationary potential. As for quantum aspects, we study bipartite temporal Bell inequalities for two-mode squeezed states, which are the quantum states of curvature perturbations. We find some regions in parameter space where they are indeed violated, which indicate a quantum signature. Since testing bipartite temporal Bell inequalities requires position measurements only, it evades a fundamental obstacle in Bell experiments in cosmology, where the decaying mode of curvature perturbations is too small to detect. Therefore, such Bell inequality violations could be probed in cosmology in principle, which would provide direct evidence that the structure of the present universe is of quantum origin.

Contents

Notation

- Greek indices μ, ν, $\cdots$ run over the spacetime coordinate labels $0, 1, 2, 3$. Latin indices i, j, $\cdots$ generally run over the spatial coordinate labels $1, 2, 3$.
- We take the sign of the metric as $(-, +, +, +)$ so that the Minkowski metric becomes

$$\eta_{\mu\nu} = \mathrm{diag}(-1, 1, 1, 1)\,.$$

- We adopt the natural units $c = \hbar = k_{\mathrm{B}} = 1$, where c, $\hbar$ and k_{B} are

speed of light	$c = 2.99792458 \times 10^{8}\,\mathrm{m/s}$
reduced Planck constant	$\hbar = 1.0545718 \times 10^{-34}\,\mathrm{J \cdot s}$
Boltzman constant	$k_{\mathrm{B}} = 1.38064852 \times 10^{-23}\,\mathrm{J/K}\,.$

- We use the reduced Planck mass

$$M_{\mathrm{Pl}} = \frac{1}{\sqrt{8\pi G}} = 4.341 \times 10^{-9}\,\mathrm{kg} = 2.435 \times 10^{18}\,\mathrm{GeV}$$

  instead of the gravitational constant.
- We take the normalization of the Fourier transform as

$$f(\boldsymbol{x}) = \int \frac{\mathrm{d}^3 k}{(2\pi)^{3/2}}\, \tilde{f}(\boldsymbol{k}) e^{i\boldsymbol{k}\cdot\boldsymbol{x}}$$
$$\tilde{f}(\boldsymbol{k}) = \int \frac{\mathrm{d}^3 x}{(2\pi)^{3/2}}\, f(\boldsymbol{x}) e^{-i\boldsymbol{k}\cdot\boldsymbol{x}}\,.$$

  unless stated otherwise.

Intorduction

Cosmological inflation stands for the accelerated expansion of the early universe [1–5]. It was originally advocated to solve initial condition problems of the Big Bang cosmology such as the horizon problem and the flatness problem. In typical models, inflation is caused by the vacuum energy of a scalar field called inflaton. Later, it was realized that quantum fluctuations of inflaton seed cosmological perturbations [6–11]. This theoretical prediction is consitent with observations of the cosmic microwave background (CMB) [12] and the large scale structure (LSS) [13–15]. Now inflation is a leading paradigm in cosmology.

One of the interesting features of cosmological inflation and perturbations is the interaction of the classical picture and the quantum picture. According to the inflation theory, the origin of cosmological perturbations is quantum fluctuations, but now we observe them as classical perturbations. This is denoted as a quantum-to-classical transition and such a transition is often thought to happen during inflation. Indeed, one can discuss it quantitatively from multiple perspectives. Cosmological perturbations take two-mode squeezed states, whose squeezing amplitude increases significantly during inflation [16]. Due to the high squeezing, the commutator of the field and its conjugate momentum disappears so that they commute like classical variables, which also corresponds to the fact that the decaying mode of perturbations becomes negligible outside of the horizon [17–20]. This is one demonstration of a quantum-to-classical transition during inflation. However, one should face this transition more carefully. For example, under two-mode squeezed states, any correlation functions of curvature perturbations can always be calculated by a stochastic average, that is to say, they can be described by means of classical probability [20–23]. This fact does not rely on the amount of squeezing. In contrast, a certain class of operators, so-called improper operators, can never have a stochastic description [21], which again holds regardless of the amount of squeezing. Hence, it is implied that, despite the common name "transition", many quantities regarding cosmological perturbations can always be described in a stochastic picture while there remain some features that can be described only by quantum theory. This thesis sheds light on both a stochastic description and quantum aspects.

Stochastic inflation

A stochastic description of perturbations gives rise to a theoretically interesting and also practically powerful picture of inflation that is called stochastic inflation [24,25]. Usually, the background evolution of inflaton is analyzed by the classical equation of motion and the perturbation is treated as a quantum field. However, the quantum fluctuations could affect the background evolution when they are large. Stochastic inflation incorporates the back reaction from the quantum fluctuations in the background equation as random noise. To say precisely, the inflaton field coarse-grained over the Hubble radius obeys

the Langevin equation, which is a stochastic differential equation (SDE). The probability density function of the field value at each time obeys the Fokker-Planck equation, which is a partial differential equation (PDE). The stochastic formalism has been shown to provide excellent agreement with usual quantum field theoretic (QFT) techniques in regimes where the two methods can be compared [25–35]. However the stochastic approach can go beyond perturbative QFT and describe the non-perturbative evolution of the coarse-grained fields through the full nonlinear equations of general relativity.

Stochastic inflation becomes rather predictive when it is combined with the δN formalism [8, 36–40]. According to the δN formalism, curvature perturbations on superhorizon scales are equivalent to fluctuations of e-folds, which is a nonperturbative relation. It relies on the separate universe approach [39, 41–46], where we assume that each part of the universe on superhorizon scales evolves in the same way as the unperturbed universe. When stochastic inflation is employed to describe the evolution of each patch, it gives rise to the stochastic-δN formalism [47–50]. In stochastic inflation, the number of e-folds passed from a certain field value to the end-of-inflation surface is a random variable, which we denote as $\mathcal{N}$, and its statistics describes the curvature perturbation nonperturbatively. Technically, it is achieved by the first-passage-time analysis of the stochastic process. One way to do this is to solve the Langevin equation many times numerically [50, 51]. Recently, analytical methods based on the Fokker-Planck equation have also been established [29, 52, 53], which can be used to derive the full probability distribution of the curvature perturbation [54, 55], finding large deviations from Gaussian statistics in the nonlinear tail of the distribution.

In fact, the problem that has been solved so far is the one when the initial conditions correspond to a fixed point $\mathbf{\Phi}$ in field space (here $\mathbf{\Phi}$ is a vector containing the values of all coarse-grained fields, and possibly of their conjugate momenta in the case where deviations from the slow-roll attractor are considered [56, 57]). However, the amplitude of the fluctuations at a given length scale is related to the statistics of the first-passage times from an initial condition that rather corresponds to when that scale crosses out the Hubble radius during inflation.

In regimes where quantum diffusion plays a negligible role, the fields driving inflation follow a classical, deterministic trajectory, so as a first approximation, there is a one-to-one correspondence between a scale k and the value of the fields $\mathbf{\Phi}$ at the time when k crosses out the Hubble radius. In other words, there exists a function $\mathbf{\Phi}_{\rm cl}(k)$ that relates k to a specific point in field space, which can be used as the initial condition for the first-passage-time problem.

However, there are regimes where this approximation may not be sufficient. In particular, in regions of the inflationary potential giving rise to large cosmological fluctuations, which may be relevant for primordial black holes, the effect of quantum diffusion is important [51, 54, 55, 58] and the classical trajectory cannot be used as a proxy for the typical realizations of the stochastic process. Furthermore, even if quantum diffusion plays an important role only at late time during inflation, and directly affects small scales only, it distorts the link between wavenumbers and field values at *all* scales, which implies that a substantial stochastic imprint may be left on the large scales observed in the CMB, even if they emerge at a time when quantum diffusion is negligible. In this thesis, we solve the first-passage-time problem associated with a given scale rather than with a given field value, in order to bridge the final gap between the stochastic-δN formalism and observable predictions.

Quantum aspects

Although a stochastic picture is powerful, there is a significant interest in quantum aspects themselves. As we already mentioned, the quantum states of the cosmological fluctuations is two-mode squeezed states, which are known as entangled states. Particularly, their infinite squeezing limit, which inflation virtually realizes, is nothing but the Einstein-Podolsky-Rosen (EPR) state [59], which is the entangled state advocated for the first time in history. Two-mode squeezed states are also commonly found in quantum optics [60–62] since they are realized by any quadratic Hamiltonian. In fact, inflation realizes the squeezing amplitude by far larger than that realized in laboratory experiments [23, 63]. Hence, one can expect some interactions between inflationary cosmology and quantum optics/information. In other words, one may be able to use the inflationary universe as a quantum laboratory, and at the same time, to study quantum aspects of inflation by means of the techniques developed in quantum information theory. In this thesis, we focus on the latter possibility.

So far, it is known that the prediction for cosmological perturbations sourced by quantum fluctuations of inflaton can be made to agree with the observations of the CMB and the LSS, that is to say,

$$\text{inflation \& quantum fluctuations} \quad \rightarrow \quad \text{CMB/LSS}\,. \tag{1}$$

This is a great success and may be already satisfactory, but one can be more ambitious. If a quantum signature is detected in cosmological observations themselves, namely,

$$\text{CMB/LSS} \quad \rightarrow \quad \text{quantum signature}\,, \tag{2}$$

it will be direct and strong evidence that the present structure of the universe comes from a quantum origin. This is a great goal worth aiming for although there will be a lot of theoretical and observational challenges on the way to go.

For the sake of that, one can make use of Bell inequalities [64]. In quantum theories, strong correlations that are impossible classically can be realized. Bell inequalities are used to characterize such a quantum nature. They are satisfied under classical assumptions such as realism and locality while their violations indicate a quantum signature. For example, the Clauser-Horne-Shimony-Holt (CHSH) scenario [65] provides an inequality about correlators of a spin operator between two subsystems, where the spatial direction of the measured spin is taken as a parameter. The violations of such inequalities have been found in laboratory experiments using photons, superconductors and so on (see *e.g.* Refs. [66–70]). This line of study has also been done in cosmology [23, 71–75]. The spin operator in Bell inequalities does not have to be an actual spin that expresses angular momentum. In fact, artificial spin operators called pseudo-spin operators can be constructed from continuous-variable operators. Hence, Bell experiments could be applied to cosmological scalar perturbations in principle.

However, there are some obstacles. It has been suggested that we cannot observe all the components of a pseudo-spin operator in cosmology because of the too tiny decaying mode of curvature perturbations to measure [75]. To overcome this, we are motivated to consider two-time correlators of a single dichotomic operator, namely, only one direction of a pseudo-spin operator. For instance, the Leggett-Garg inequalities [76, 77], which have already been applied to one-mode squeezed states, arise from three-time measurements of a single operator in a single system. However, it will be more natural to make use of two subsystems since cosmological perturbations are placed in two-mode squeezed states.

Indeed, there exists such a class of inequalities, which we call "bipartite temporal Bell inequalities" [23,78]. There, the same dichotomic variable is measured on each subsystem at different times. In this thesis, we test bipartite temporal Bell inequalities for two-mode squeezed states.

The value of this work is not restricted in cosmology since the states we consider are found in a broad range of systems. In particular, our study is helpful in general contexts where only one direction of a spin can be measured. Also, the use of bipartite systems can close the clumsiness loophole, which is a fundamental challenge in temporal Bell experiments [79].

Organization of this thesis

This thesis consists of two parts: a review part (Part I) and a part on our original works (Part II).

In Part I, we review the basics of inflationary cosmology and also explain technical things that our original works are based on. In Chap. 1, we review the standard cosmological perturbation theory. In Chap. 2, we discuss the generation of adiabatic perturbations during inflation focusing on their quantum states. Sec. 2.4 will be helpful to understand the relation between the two original works shown in Part II. In Chap. 3, we describe the stochastic formalism of inflation and how it can be used to predict observable quantities: curvature perturbations. This chapter is related to our work shown in Chap. 5. In Chap. 4, we review the preceding studies on Bell experiments in cosmology. This chapter is related to our work shown in Chap. 6.

In Part II, we present our two original works which focus on the stochastic picture and quantum aspects of the inflationary universe, respectively. In Chap. 5, we solve the first-passage-time problem associated with a given scale in the stochastic-δN formalism. In practice, we establish a computational program of the power spectrum of curvature perturbations. Also, as an application, we study the imprint of quantum diffusion near the end of inflation on large-scale perturbations. In Chap. 6, we test bipartite temporal Bell inequalities for two-mode squeezed states. After deriving a formula to compute two-time correlators and obtaining its asymptotic expressions, we show configurations where the Bell inequality violations are found. Chap. 5 and Chap. 6 are written based on our papers Ref. [80] and Ref. [81] respectively.

We show the conclusion of this thesis after these two parts.

Part I

Review Part

Chapter 1

Cosmological perturbation theory

In this chapter, we review the cosmological perturbation theory. After specifying the notation and describing the basic facts in the linear theory, we address the δN formalism, which is a nonlinear methodology.

1.1 Definition of perturbations

In this section, we specify our way of describing perturbations at first. The notation for cosmological perturbations differs among authors and sometimes induces confusion, hence one should take care of it.

Let us divide the spacetime metric into the background and the perturbation as

$$\mathrm{d}s^2 = \left[\bar{g}_{\mu\nu} + \delta g_{\mu\nu}\right] \mathrm{d}x^\mu \mathrm{d}x^\nu \,. \tag{1.1}$$

The background is the flat Friedmann-Lemaître-Robertson-Walker (FLRW) metric,

$$\bar{g}_{\mu\nu}\mathrm{d}x^\mu \mathrm{d}x^\nu = a^2 \left[-\mathrm{d}\eta^2 + \delta_{ij}\mathrm{d}x^i \mathrm{d}x^j\right] \tag{1.2}$$

where η is the conformal time. In the following, we raise and lower the spatial indices by means of δ_{ij}, δ^{ij}. The linearly perturbed FLRW metric can be written as

$$\begin{aligned} \mathrm{d}s^2 = a^2 \Big[& -(1-2\varphi)\,\mathrm{d}\eta^2 + 2\left(\partial_i B + S_i\right)\mathrm{d}\eta \mathrm{d}x^i \\ & \left((1+2\psi)\,\delta_{ij} + 2\partial_i\partial_j E + \partial_i F_j + \partial_j F_i + h_{ij}\right)\mathrm{d}x^i \mathrm{d}x^j \Big] \,, \end{aligned} \tag{1.3}$$

that is to say,

$$\delta g_{00} = 2a^2\varphi \tag{1.4}$$

$$\delta g_{0i} = a^2\left(\partial_i B + S_i\right) \tag{1.5}$$

$$\delta g_{ij} = a^2\left(2\psi\delta_{ij} + 2\partial_i\partial_j E + \partial_i F_j + \partial_j F_i + h_{ij}\right) \,. \tag{1.6}$$

Here, S_i and F_i are transverse ($\partial_i S^i = \partial_i F^i = 0$), and such perturbations are called vector perturbations in the cosmological perturbation theory. On the other hand, h_{ij} is transverse ($\partial_i h^i{}_j = 0$) and traceless ($h^i{}_i$=0), and such perturbations are called tensor perturbations. Finally, such perturbations as φ, ψ, B, E are called scalar perturbations. All the ten degrees of freedom in cosmological perturbations (4×1 in scalar, 2×2 in vector, 1×2 in tensor) are expressed with this notation. We focus on scalar perturbations in this

thesis, and our prime interest resides in ψ, which represents the curvature perturbation (in an arbitrary gauge).

Noting that the inverse matrix of the metric, $g^{\mu\nu}$, can be computed at linear order by

$$g^{\mu\nu} = \bar{g}^{\mu\nu} - \bar{g}^{\mu\rho}\,\delta g_{\rho\sigma}\,\bar{g}^{\sigma\nu}\,, \tag{1.7}$$

we can write each component as

$$g^{00} = -\frac{1}{a^2}\left(1+2\varphi\right) \tag{1.8}$$

$$g^{0i} = \frac{1}{a^2}\left(\partial^i B + S^i\right) \tag{1.9}$$

$$g^{ij} = \frac{1}{a^2}\left(\left(1-2\psi\right)\delta^{ij} - 2\partial^i\partial^j E - \partial^i F^j - \partial^j F^i + h^{ij}\right)\,. \tag{1.10}$$

Next, let us consider the 4-velocity of the fluid in the universe. Since we are using the conformal time, the background 4-velocity is expressed from $\bar{u}^\mu = \mathrm{d}x^\mu/(a\mathrm{d}\eta)$ as

$$\bar{u}^\mu = \left(\frac{1}{a}, \vec{0}\right) \tag{1.11}$$

$$\bar{u}_\mu = \left(-a, \vec{0}\right) \tag{1.12}$$

Noting that the perturbations of the 4-velocity are constrained by $g^{\mu\nu}u_\mu u_\nu = -1$, they are written in terms of a scalar perturbation ς and a vector perturbation ς_i $(\partial_i\varsigma^i = 0)$ as

$$u_\mu = \left(-a(1-\varphi), a\left(\partial_i\varsigma + \varsigma_i\right)\right) \tag{1.13}$$

$$u^\mu = \left(\frac{1}{a}(1+\varphi), \frac{1}{a}\left[\partial_i\left(\varsigma - B\right) + \varsigma_i - S_i\right]\right)\,. \tag{1.14}$$

Here, ς is called the velocity potential.

The stress-energy tensor of a perfect fluid is given by

$$T^\mu{}_\nu = \left(\rho + p\right)u^\mu u_\nu + p\delta^\mu_\nu \tag{1.15}$$

where $\rho = \bar{\rho} + \delta\rho$ is the energy density and $p = \bar{p} + \delta p$ is the pressure. Each component can be expressed as

$$T^0{}_0 = -\left({}^{(0)}\rho + \delta\rho\right) \tag{1.16}$$

$$T^0{}_i = \left({}^{(0)}\rho + {}^{(0)}p\right)\left(\partial_i\varsigma + \varsigma_i\right) \tag{1.17}$$

$$T^i{}_j = \left({}^{(0)}p + \delta p\right)\delta^i_j\,. \tag{1.18}$$

In general, the stress-energy tensor is written as

$$T^\mu{}_\nu = \left(\rho + p\right)u^\mu u_\nu + p\delta^\mu_\nu + \pi^\mu{}_\nu \tag{1.19}$$

where $\pi_{\mu\nu}$ is the anisotropic stress, which satisfies $\pi_{\mu\nu}u^\nu = 0$, $\pi^\mu{}_\mu = 0$ and hence has 5 degrees of freedom. One possible source for the anisotropic stress is freely streaming neutrino. In this thesis, we only consider the cases where the anisotropic stress is negligible.

1.2 Gauge-invariant quantities

In general relativity, a diffeomorphism is a gauge degree of freedom. In this section, we study how the perturbations defined in the previous section are transformed by the gauge transformation.

Let us consider the following infinitesimal transformation of the coordinate,

$$x^\mu \to \tilde{x}^\mu = x^\mu + \xi^\mu\left(x^\alpha\right) . \tag{1.20}$$

According to this, the spacetime metric is transformed as

$$\tilde{g}_{\mu\nu}\left(\tilde{x}^\alpha\right) = \frac{\partial x^\rho}{\partial \tilde{x}^\mu}\frac{\partial x^\sigma}{\partial \tilde{x}^\nu} g_{\rho\sigma}\left(x^\alpha\right) \simeq \bar{g}_{\mu\nu}\left(x^\alpha\right) + \delta g_{\mu\nu} - \bar{g}_{\mu\rho}\partial_\nu \xi^\rho - \bar{g}_{\nu\rho}\partial_\mu \xi^\rho \tag{1.21}$$

where $\tilde{x}^\alpha$ and x^α should be evaluated at the same world point. Let us also divide $\tilde{g}_{\mu\nu}$ into the background and the perturbation as

$$\tilde{g}_{\mu\nu}\left(\tilde{x}^\alpha\right) = \bar{g}_{\mu\nu}\left(\tilde{x}^\alpha\right) + \delta\tilde{g}_{\mu\nu} . \tag{1.22}$$

Noting

$$\bar{g}_{\mu\nu}\left(\tilde{x}^\alpha\right) \simeq \bar{g}_{\mu\nu}\left(x^\alpha\right) + \xi^\rho \partial_\rho \bar{g}_{\mu\nu} , \tag{1.23}$$

we finally obtain the transformation of the perturbation part as

$$\delta g_{\mu\nu} \to \delta\tilde{g}_{\mu\nu} = \delta g_{\mu\nu} - \xi^\rho \partial_\rho \bar{g}_{\mu\nu} - \bar{g}_{\mu\rho}\partial_\nu \xi^\rho - \bar{g}_{\nu\rho}\partial_\mu \xi^\rho . \tag{1.24}$$

In the same way, a 4-scalar and a 4-vector are transformed as (here we take the energy density ρ and the 4-velocity u_μ as examples)

$$\delta\rho \to \delta\tilde{\rho} = \delta\rho - \xi^\sigma \partial_\sigma \bar{\rho} \tag{1.25}$$

$$\delta u_\mu \to \delta\tilde{u}_\mu = \delta u_\mu - \xi^\sigma \partial_\sigma \bar{u}_\mu - \bar{u}_\sigma \partial_\mu \xi^\sigma . \tag{1.26}$$

Now, let us investigate how these transformations are represented in terms of the notation introduced in the previous section. For that sake, let us decompose the transformation parameter ξ^μ into scalar components ξ^0, ζ and a vector component χ_i ($\partial_i \chi^i = 0$) as

$$\xi^\mu = \left(\xi^0, \partial^i \zeta + \chi^i\right) . \tag{1.27}$$

Then, Eq. (1.24) becomes

$$\delta\tilde{g}_{00} = \delta g_{00} + 2a\left(a\xi^0\right)' \tag{1.28}$$

$$\delta\tilde{g}_{0i} = \delta g_{0i} + a^2\left[\partial_i\left(\xi^0 - \zeta'\right) - \chi_i'\right] \tag{1.29}$$

$$\delta\tilde{g}_{ij} = \delta g_{ij} - a^2\left[2\frac{a'}{a}\xi^0\delta_{ij} + 2\partial_i\partial_j\zeta + \partial_i\chi_j + \partial_j\chi_i\right] . \tag{1.30}$$

Here, a prime stands for the derivative with respect to the conformal time η. Let us take a closer look into these expressions. For example, the $(0\,i)$ component can be rewritten by using B, S_i as

$$\partial_i\tilde{B} + \tilde{S}_i = \partial_i B + S_i + \partial_i\left(\xi^0 - \zeta'\right) - \chi_i' . \tag{1.31}$$

Note that the rotation of $\partial_i \tilde{B}, \partial_i B + \partial_i \left(\xi^0 - \zeta'\right)$ is zero and also the divergence of $\tilde{S}_i, S_i - \chi_i'$ is zero. According to the Helmholtz theorem, a vector field can be decomposed into a rotation-free part and a divergence-free part. Therefore, we have

$$\partial_i \tilde{B} = \partial_i B + \partial_i \left(\xi^0 - \zeta'\right) \tag{1.32}$$

$$\tilde{S}_i = S_i - \chi_i' \,. \tag{1.33}$$

As shown in this example, in general, the scalar, vector and tensor sectors evolve independently at linear order in the perturbation theory. This fact is known as the decomposition theorem [82]. Note also that Eq. (1.32) indicates

$$\tilde{B} = B + \xi^0 - \zeta' \tag{1.34}$$

since it is an equation about perturbations.

The gauge transformation of the metric is summarized in the following.
Scalar:

$$\varphi \to \tilde{\varphi} = \varphi + \frac{1}{a}\left(a\xi^0\right)' \tag{1.35}$$

$$\psi \to \tilde{\psi} = \psi - \frac{a'}{a}\xi^0 \tag{1.36}$$

$$B \to \tilde{B} = B + \xi^0 - \zeta' \tag{1.37}$$

$$E \to \tilde{E} = E - \zeta \tag{1.38}$$

Vector:

$$S_i \to \tilde{S}_i = S_i - \chi_i' \tag{1.39}$$

$$F_i \to \tilde{F}_i = F_i - \chi_i \tag{1.40}$$

Tensor:

$$h_{ij} \to \tilde{h}_{ij} = h_{ij} \tag{1.41}$$

Also, perturbations of the 4-velocity are transformed as

$$\varsigma \to \tilde{\varsigma} = \varsigma + \xi^0 \tag{1.42}$$

$$\varsigma_i \to \tilde{\varsigma}_i = \varsigma_i \,. \tag{1.43}$$

Finally, a perturbation of a 4-scalar such as the energy density is transformed as

$$\delta\rho \to \delta\tilde{\rho} = \delta\rho - \xi^0 \bar{\rho}' \,. \tag{1.44}$$

The metric perturbations have ten degrees of freedom in general, but four of them are gauge redundancy and the number of physical degrees of freedom is six (2×1 in scalar, 1×2 in vector, 1×2 in tensor). Hereafter, we only consider scalar perturbations. From the counting shown above, we can impose two conditions at most on scalar degrees of freedom. We describe important gauge choices and gauge-invariant quantities in the following. Note that $\delta (\equiv \delta\rho/\bar{\rho})$ is the density contrast.

Conformal Newtonian gauge (Longitudinal gauge)

The conformal Newtonian gauge, also known as the longitudinal gauge, is defined as $B = E = 0$. Since $B - E'$ is transformed as $\tilde{B} - \tilde{E}' = B - E' + \xi^0$, we can define the following gauge-invariant quantities,

$$\Phi \equiv \varphi - \frac{1}{a}\left[a\left(B - E'\right)\right]' \tag{1.45}$$

$$\Psi \equiv \psi + \frac{a'}{a}\left(B - E'\right) \tag{1.46}$$

$$\delta_{\mathrm{L}} \equiv \delta + \frac{\bar{\rho}'}{\bar{\rho}}\left(B - E'\right) \tag{1.47}$$

$$\varsigma_{\mathrm{L}} \equiv \varsigma - \left(B - E'\right) . \tag{1.48}$$

Here, Ψ is gauge invariant and reduced to the curvature perturbation ψ when $B = E = 0$. Such a quantity is called the curvature perturbation in the conformal Newtonian gauge.

Uniform-density gauge

The uniform-density gauge is defined by $\delta\rho = 0$. The curvature perturbation in the uniform-density gauge

$$\zeta \equiv \psi - \mathcal{H}\frac{\delta\rho}{\bar{\rho}'} = \psi + \frac{\delta\rho}{3\left(\bar{\rho} + \bar{p}\right)} \tag{1.49}$$

is also called the adiabatic curvature perturbation. Here, $\mathcal{H} \equiv a'/a$ is the conformal Hubble. This quantity is very important in this thesis. If we simply say "curvature perturbation", we mean ζ.

Comoving gauge

The comoving gauge is defined by $\varsigma = 0$.[1] The curvature perturbation and the density contrast in the comoving gauge

$$\mathcal{R} \equiv \psi + \frac{a'}{a}\varsigma \tag{1.50}$$

$$\delta_{\mathrm{com}} \equiv \delta + \frac{\bar{\rho}'}{\bar{\rho}}\varsigma \tag{1.51}$$

are also used extensively.

Spatially flat gauge

The spatially flat gauge is defined by $\psi = 0$. As we will see later (see *e.g.* Eq. (2.28)), this gauge is suitable for seeing the perturbation of a scalar field ϕ, which is written in a gauge-invariant way as

$$\delta\phi_{\mathrm{flat}} \equiv \delta\phi - \frac{\bar{\phi}'}{\mathcal{H}}\psi . \tag{1.52}$$

[1] There are several definitions of the comoving gauge in the literature.

Uniform-N gauge

The uniform-N gauge is defined by $\delta N = 0$ where

$$\delta N = \psi + \frac{1}{3}\nabla^2 \int (E' - B)\mathrm{d}\eta \,, \tag{1.53}$$

see Eqs. (1.85) and (1.88). If we use the remaining degree of freedom to set $B = 0$, the definition can be recast as $\psi + \nabla^2 E/3 = 0$, $B = 0$. The stochastic inflation is usually established in this gauge. The uniform-N gauge is equivalent to the flat gauge on superhorizon scales as we will show nonlinearly in Sec. 1.4. This fact is crucial to justify the separate universe approach required by the stochastic inflation [57].

1.3 Linearized Einstein equation

In this section, we review the evolution of cosmological perturbations and the relation among the gauge-invariant quantities defined in the previous section. We restrict our analysis to scalar perturbations only.

The evolution of cosmological perturbations is determined by the linearized Einstein equation,

$$\delta G^\mu_\nu = \frac{1}{M_{\rm Pl}^2}\delta T^\mu_\nu \,. \tag{1.54}$$

The perturbations of the stress-energy tensor are shown in Eqs. (1.16)-(1.18). The computation of the Einstein tensor is complicated, so we only show the results here [83].

In the absence of the anisotropic stress, the (ij) component of the linearized Einstein equation with $i \neq j$ is written as

$$\partial_i \partial_j \left(\Phi - \Psi\right) = 0 \,, \tag{1.55}$$

which indicates

$$\Phi = \Psi \tag{1.56}$$

since they can not have a constant term. By using this, the (00), $(0i)$ and (ii) components are written as

$$\Delta\Psi - 3\mathcal{H}(\Psi' + \mathcal{H}\Psi) = -\frac{1}{2M_{\rm Pl}^2}a^2\delta\rho_{\rm L} \tag{1.57}$$

$$(\Psi' + \mathcal{H}\Psi) = \frac{1}{a}\left(a\Psi\right)' = \frac{1}{2M_{\rm Pl}^2}a^2(\bar{\rho} + \bar{p})\varsigma_{\rm L} \tag{1.58}$$

$$\Psi'' + 3\mathcal{H}\Psi' + \left(2\mathcal{H}' + \mathcal{H}^2\right)\Psi = -\frac{1}{2M_{\rm Pl}^2}a^2\delta p_{\rm L} \tag{1.59}$$

where the subscript "L" represents the Newtonian gauge. Let us see what is implied from these equations.

Removing $\Psi' + \mathcal{H}\Psi$ from Eqs. (1.57) and (1.58), one can show the Poisson equation

$$\Delta\Psi = -\frac{1}{2M_{\rm Pl}^2}a^2\bar{\rho}\,\delta_{\rm com} \tag{1.60}$$

or

$$\left(\frac{k}{aH}\right)^2 \Psi = \frac{3}{2}\delta_{\rm com} \tag{1.61}$$

where the comoving density perturbation $\delta_{\rm com}$ is defined in Eq. (1.51). This implies that $-\Phi$ corresponds to the gravitational potential in the Newtonian gravity.

From the definition of the adiabatic curvature perturbation ζ shown in Eq. (1.49), we have

$$\delta\rho_{\rm L} = 3(\bar{\rho} + \bar{p})(\zeta - \Psi)\,. \tag{1.62}$$

By substituting this into Eq. (1.57) and using

$$\mathcal{H}' - \mathcal{H}^2 = -\frac{1}{2M_P^2}(\bar{\rho} + \bar{p})a^2\,, \tag{1.63}$$

we obtain

$$\Delta\Psi - 3\mathcal{H}(\Psi' + \mathcal{H}\Psi) + 3(\mathcal{H}' - \mathcal{H}^2)\Psi = 3(\mathcal{H}' - \mathcal{H}^2)\zeta\,. \tag{1.64}$$

On the other hand, from the definition of the comoving curvature perturbation $\mathcal{R}$ shown in Eq. (1.50), we have

$$\varsigma_{\rm L} = \frac{\mathcal{R} - \Psi}{\mathcal{H}}\,. \tag{1.65}$$

By substituting this into Eq. (1.58), we obtain

$$-\mathcal{H}(\Psi' + \mathcal{H}\Psi) + (\mathcal{H}' - \mathcal{H}^2)\Psi = (\mathcal{H}' - \mathcal{H}^2)\mathcal{R}\,. \tag{1.66}$$

From Eqs. (1.64) and (1.66), we can show the relation between ζ and $\mathcal{R}$ as

$$\zeta - \mathcal{R} = -\frac{2M_{\rm Pl}^2\Delta\Psi}{3(\bar{\rho} + \bar{p})a^2} \sim \left(\frac{k}{aH}\right)^2 \Psi\,. \tag{1.67}$$

Hence, ζ coincides with $\mathcal{R}$ on superhorizon scales.

Let us show the conservation of the adiabatic perturbation ζ on superhorizon scales. The time derivative of Eq. (1.57) becomes

$$\delta\rho_{\rm L}' = -2\mathcal{H}\delta\rho_{\rm L} - \frac{2M_{\rm Pl}^2}{a^2}\left[\Delta\Psi' - 3\left(\mathcal{H}' + \mathcal{H}^2\right)\Psi' - 6\mathcal{H}\mathcal{H}'\Psi - 3\mathcal{H}\Psi''\right]\,. \tag{1.68}$$

Removing $\Delta\Psi'$ by means of Eq. (1.58) and removing Ψ'' by means of Eq. (1.59), we obtain

$$\delta\rho_{\rm L}' = -3\mathcal{H}(\delta\rho_{\rm L} + \delta p_{\rm L}) - 3(\bar{\rho} + \bar{p})\Psi' - (\bar{\rho} + \bar{p})\Delta_{\varsigma_{\rm L}}\,. \tag{1.69}$$

By using this, the time derivative of ζ can be calculated from

$$\zeta' = \Psi' + \frac{\delta\rho_{\rm L}'}{3(\bar{\rho} + \bar{p})} - \frac{\bar{\rho}' + \bar{p}'}{3(\bar{\rho} + \bar{p})^2}\delta\rho_{\rm L} \tag{1.70}$$

as

$$\zeta' = -\mathcal{H}\frac{\delta p_{\rm nad}}{\bar{\rho} + \bar{p}} - \frac{1}{3}\Delta_{\varsigma_{\rm L}}\,. \tag{1.71}$$

Here, $\delta p_{\rm nad}$ is the non-adiabatic pressure perturbation [84],

$$\delta p_{\rm nad} = \delta p - \frac{\bar{p}'}{\bar{\rho}'}\delta\rho\,. \tag{1.72}$$

Eq. (1.71) indicates that ζ (or equivalently $\mathcal{R}$) is conserved on superhorizon scales if $\delta p_{\rm nad} = 0$. If the universe is described by only one degree of freedom, we can write $p = p(\rho)$ and the non-adiabatic pressure perturbation indeed vanishes. One can also show that the tensor perturbation h_{ij} is conserved on superhorizon scales as well.

1.4 δN formalism

So far, we have discussed the linear perturbation theory. The δN formalism is a powerful method that can evaluate long-wavelength curvature perturbations nonlinearly as fluctuations of e-folds N. In this section, we review the δN formalism referring to Ref. [85].

Let us expand the spacetime metric with the Arnowitt-Deser-Misner (ADM) formalism as

$$\begin{aligned} {\rm d}s^2 &= -\mathcal{N}^2{\rm d}t^2 + \gamma_{ij}({\rm d}x^i + \beta^i{\rm d}t)({\rm d}x^j + \beta^j{\rm d}t) &(1.73)\\ &= -(\mathcal{N}^2 - \beta^k\beta_k){\rm d}t^2 + 2\beta_i{\rm d}t{\rm d}x^i + \gamma_{ij}{\rm d}x^i{\rm d}x^j\,. &(1.74)\end{aligned}$$

$\mathcal{N}$ is the lapse function and β_i is the shift vector. We raise and lower the spatial indices by means of the spatial metric γ_{ij}. The metric and its inverse are written in the matrix form as

$$g_{\mu\nu} = \begin{pmatrix} -(\mathcal{N}^2 - \beta^k\beta_k) & \beta_j \\ \beta_i & \gamma_{ij} \end{pmatrix}, \quad g^{\mu\nu} = \begin{pmatrix} -\mathcal{N}^{-2} & \mathcal{N}^{-2}\beta^j \\ \mathcal{N}^{-2}\beta^i & \gamma^{ij} - \mathcal{N}^{-2}\beta^i\beta^j \end{pmatrix} \tag{1.75}$$

where γ^{ij} is the inverse matrix of γ_{ij}. The spatial metric γ_{ij} is written as

$$\gamma_{ij} = a^2 e^{2\psi}\left(e^{\chi}\right)_{ij} \tag{1.76}$$

where χ_{ij} is traceless ($\chi^i{}_i = 0$) and written in turn as

$$\chi_{ij} = \partial_i C_j + \partial_j C_i - \frac{2}{3}\delta_{ij}\partial_k C^k + h_{ij}\,. \tag{1.77}$$

Here, C_i includes both scalar perturbations and vector perturbations.

The determinant of the metric is calculated as

$$\begin{aligned} g &= = -\mathcal{N}^2\gamma \quad (\gamma \equiv \det\gamma_{ij}) &(1.78)\\ &= -\mathcal{N}^2(a^2e^{2\psi})^3\,. &(1.79)\end{aligned}$$

When ψ and χ_{ij} are small, γ_{ij} becomes[2]

$$\gamma_{ij} = a^2(t)\left[(1+2\psi)\delta_{ij} + \chi_{ij}\right]\,. \tag{1.80}$$

We are interested in nonlinear perturbations on superhorizon scales ($k \ll aH$). On sufficiently large scales, the metric should be well approximated by the FLRW metric. Hence, we postulate

$$\beta_i = \mathcal{O}\left(\epsilon\right) \tag{1.81}$$

[2]Hence, ψ used here corresponds to $\psi + \nabla^2 E/3$ in terms of linear perturbations introduced in Eq. (1.6). Obviously, their difference vanishes on superhorizon scales.

with $\epsilon \equiv k/(aH)$.

Let us take a gauge where the spatial components of the 4-velocity, u^i, are zero. Then, $g_{\mu\nu}u^\mu u^\nu = -1$ leads to

$$u^\mu = \left(\frac{1}{\sqrt{\mathcal{N}^2 - \beta^k \beta_k}}, 0 \right) = \left(\frac{1}{\mathcal{N}}, 0 \right) + \mathcal{O}\left(\epsilon^2\right) . \tag{1.82}$$

The expansion

$$\theta \equiv \nabla_\mu u^\mu \tag{1.83}$$

can be calculated as

$$\theta = \frac{1}{\sqrt{-g}} \partial_\mu \left(\sqrt{-g} u^\mu \right) \tag{1.84}$$

$$= \frac{1}{\mathcal{N} a^3 e^{3\psi}} \partial_0 \left(\frac{\mathcal{N} a^3 e^{3\psi}}{\sqrt{\mathcal{N}^2 - \beta^k \beta_k}} \right) \tag{1.85}$$

$$= \frac{1}{\mathcal{N}} \left(3\frac{\dot{a}}{a} + 3\dot{\psi} \right) + \mathcal{O}(\epsilon^2) \tag{1.86}$$

where the dot represents the derivative with respect to t. The local Hubble is expressed as

$$\tilde{H} \equiv \frac{\theta}{3} = \frac{1}{\mathcal{N}} \left(\frac{\dot{a}}{a} + \dot{\psi} \right) + \mathcal{O}(\epsilon^2) . \tag{1.87}$$

The local e-fold is expressed as

$$N(t_f, t_i, \boldsymbol{x}) = \int_{t_i}^{t_f} \tilde{H} \mathcal{N} \mathrm{d}t . \tag{1.88}$$

From Eq. (1.87), it is calculated as

$$N(t_f, t_i, \boldsymbol{x}) = \int_{t_i}^{t_f} \left(\frac{\dot{a}}{a} + \dot{\psi} \right) \mathrm{d}t \tag{1.89}$$

$$= \log \left[\frac{a(t_f)}{a(t_i)} \right] + \psi(t_f, \boldsymbol{x}) - \psi(t_i, \boldsymbol{x}) \tag{1.90}$$

$$= N_0(t_f, t_i) + \psi(t_f, \boldsymbol{x}) - \psi(t_i, \boldsymbol{x}) \tag{1.91}$$

where $N_0 = \log\left[a(t_f)/a(t_i)\right]$ is the background e-folds.

As in the linear theory, we define ζ as the curvature perturbation in the uniform-density gauge,

$$\zeta \equiv \psi|_{\delta\rho=0} . \tag{1.92}$$

If we take the flat surface ($\psi = 0$) at $t = t_i$ and the uniform-density surface ($\delta\rho = 0$) at $t = t_f$, Eq. (1.91) becomes

$$\zeta(t_f, \boldsymbol{x}) = \delta N(t_f, t_i, \boldsymbol{x}) \tag{1.93}$$

where $\delta N(t_f, t_i, \boldsymbol{x})$ is the fluctuation of the e-folds from the initial flat surface to the final uniform-density surface. Eq. (1.93) is the central equation in the δN formalism and includes nonlinear perturbations.

In Eq. (1.71), we showed at linear order that ζ is conserved on superhorizon scales if the universe is adiabatic ($p = p(\rho)$). In fact, this is closely related to energy conservation. By applying the stress-energy tensor of a perfect fluid shown in Eq. (1.15) to the equation of the energy conservation, $\nabla_\nu T^{\mu\nu} = 0$, we obtain

$$\begin{aligned} u_\mu \nabla_\nu T^{\mu\nu} &= u_\mu \nabla_\nu \left[(\rho + p)\, u^\mu u^\nu + p g^{\mu\nu} \right] \\ &= -u^\nu \partial_\nu (\rho + p) - (\rho + p) \nabla_\nu u^\nu + (\rho + p) u^\nu u_\mu \nabla_\nu u^\mu + u^\mu \partial_\mu p \\ &= 0\,. \end{aligned} \tag{1.94}$$

Because of $u^\nu \partial_\nu = (\mathrm{d}x^\nu/\mathrm{d}\tau)\, \partial/\partial x^\nu = \mathrm{d}/\mathrm{d}\tau$ and $u_\mu \nabla_\nu u^\mu = \nabla_\nu (u^\mu u_\mu)/2 = 0$, this is rewritten as

$$\frac{\mathrm{d}}{\mathrm{d}\tau} \rho + (\rho + p)\, \theta = 0\,. \tag{1.95}$$

Since the proper time τ is given by $\mathrm{d}\tau = \sqrt{\mathcal{N}^2 - \beta^k \beta_k}\mathrm{d}t \simeq \mathcal{N}\mathrm{d}t$, Eq. (1.87) becomes

$$\tilde{H} = -\frac{1}{\mathcal{N}} \frac{\dot{\rho}}{3(\rho + p)} + \mathcal{O}(\epsilon^2) = \frac{1}{\mathcal{N}} \left(\frac{\dot{a}}{a} + \dot{\psi} \right) + \mathcal{O}(\epsilon^2)\,. \tag{1.96}$$

Noting that $\delta\rho = 0$ means $\delta p = 0$ if the perturbation is adiabatic ($p = p(\rho)$), the time derivative of ζ is calculated as

$$\dot{\zeta} = \dot{\psi}\Big|_{\delta\rho = 0} \tag{1.97}$$

$$= -H - \frac{\dot{\rho}}{3(\rho + p)}\bigg|_{\delta\rho = 0} \tag{1.98}$$

$$= -H - \frac{\dot{\bar{\rho}}}{3(\bar{\rho} + \bar{p})} \tag{1.99}$$

$$= 0 \qquad \text{(adiabatic, superhorizon)} \tag{1.100}$$

where we used $\dot{\bar{\rho}} = -3H(\bar{\rho} + \bar{p})$, which holds at the background level. Therefore, energy conservation ensures the conservation of ζ nonlinearly.

Chapter 2

Inflation and generation of cosmological perturbations

The Big Bang cosmology has been observationally confirmed by the Big Bang nucleosynthesis, the Hubble law, the CMB and so on. However, it involved theoretical problems about its initial conditions such as the horizon problem and the flatness problem. Then, the inflation theory was advocated and it was realized that an accelerated expansion in the early stage of the universe can solve the initial condition problems. Furthermore, inflation can also explain the generation of primordial cosmological perturbations and it has been supported by the observation of the CMB and the LSS. In this chapter, we review the generation of perturbations in single-field slow-roll inflation and also address the so-called quantum-to-classical transition.

2.1 Single-field slow-roll inflation

From

$$\frac{\ddot{a}}{a} = \dot{H} + H^2 = -\frac{1}{6M_{\rm Pl}^2}\left(\rho + 3p\right) , \tag{2.1}$$

the necessary condition for an accelerated expansion is $p < -\rho/3$. Also, from

$$\dot{H} = -\frac{1}{2M_{\rm Pl}^2}\left(\rho + p\right) , \tag{2.2}$$

$p \simeq -\rho$ is required in order for an exponential expansion $a \sim e^{Ht}$ to last long enough.

In the simplest class of models, inflation is realized by the vacuum energy of a single scalar field. Let us consider the Einstein-Hilbert action with a canonical scalar field in the matter sector,

$$S = \int \mathrm{d}^4x\sqrt{-g}\left[\frac{M_{\rm Pl}^2}{2}R - \frac{1}{2}g^{\mu\nu}\partial_\mu\phi\partial_\nu\phi - V(\phi)\right] . \tag{2.3}$$

In general, the stress-energy tensor is given by

$$T_{\mu\nu} \equiv -\frac{2}{\sqrt{-g}}\frac{\delta\left(\sqrt{-g}\mathcal{L}_m\right)}{\delta g^{\mu\nu}} = -2\frac{\delta\mathcal{L}_m}{\delta g^{\mu\nu}} + g_{\mu\nu}\mathcal{L}_m \tag{2.4}$$

$$= -\frac{2}{\sqrt{-g}}\left[\frac{\partial(\mathcal{L}_m\sqrt{-g})}{\partial g^{\mu\nu}} - \frac{\partial}{\partial x^\alpha}\frac{\partial(\mathcal{L}_m\sqrt{-g})}{\partial(\partial_\alpha g^{\mu\nu})}\right] \tag{2.5}$$

where $\mathcal{L}_m$ is the Lagrangian for the matter sector. Hence, the stress-energy tensor for a scalar field becomes

$$T_{\mu\nu} = \partial_\mu\phi\partial_\nu\phi + g_{\mu\nu}\left[-\frac{1}{2}g^{\rho\sigma}\partial_\rho\phi\partial_\sigma\phi - V(\phi)\right] \tag{2.6}$$

where we used $\partial\sqrt{-g}/\partial g^{\mu\nu} = -\sqrt{-g}g_{\mu\nu}/2$.

Regarding the homogeneous modes, the energy density and the pressure are given by

$$\bar{\rho} = \frac{1}{2}\dot{\bar{\phi}}^2 + V(\bar{\phi}) \tag{2.7}$$

$$\bar{p} = \frac{1}{2}\dot{\bar{\phi}}^2 - V(\bar{\phi})\,. \tag{2.8}$$

Hence, $p \simeq -\rho$ is realized when the field rolls down the potential slowly, namely, $\dot{\phi}^2 \ll V$. A scalar field that causes inflation like ϕ here is called inflaton.

For future reference, the perturbations introduced in Eqs. (1.16)-(1.18) are expressed as

$$\delta\rho = \dot{\bar{\phi}}\delta\dot{\phi} + \partial_\phi V\delta\phi + \dot{\bar{\phi}}^2\varphi \tag{2.9}$$

$$\delta p = \dot{\bar{\phi}}\delta\dot{\phi} - \partial_\phi V\delta\phi + \dot{\bar{\phi}}^2\varphi \tag{2.10}$$

$$\varsigma = -\frac{\delta\phi}{a\dot{\bar{\phi}}} \tag{2.11}$$

where φ is a metric perturbation introduced in Eq. (1.3).

Hereafter, we omit overlines put on homogeneous quantities. In the rest of this section, we write down equations for the homogeneous modes. The equation of motion of inflaton can be obtained by varying the action with respect to ϕ as

$$\ddot{\phi} + 3H\dot{\phi} + \partial_\phi V = 0\,. \tag{2.12}$$

The Friedmann equation is written as

$$H^2 = \frac{1}{3M_{\rm Pl}^2}\left[\frac{1}{2}\dot{\phi}^2 + V\right]\,. \tag{2.13}$$

When discussing inflation, the number of e-folds

$$N = \int H\mathrm{d}t \tag{2.14}$$

is a convenient time variable. The slow-roll parameters are defined by

$$\epsilon_1 \equiv \frac{\mathrm{d}\ln H^{-1}}{\mathrm{d}N} = -\frac{\dot{H}}{H^2} \tag{2.15}$$

$$\epsilon_n \equiv \frac{\mathrm{d}\ln|\epsilon_{n-1}|}{\mathrm{d}N} \quad \text{for} \quad n \geq 2\,. \tag{2.16}$$

For single-field inflation, the first and second slow-roll parameters can be written as

$$\epsilon_1 = \frac{1}{2M_{\rm Pl}^2}\left(\frac{\mathrm{d}\phi}{\mathrm{d}N}\right)^2 \tag{2.17}$$

$$\epsilon_2 = 2\frac{\mathrm{d}^2\phi}{\mathrm{d}N^2}\left(\frac{\mathrm{d}\phi}{\mathrm{d}N}\right)^{-1} \tag{2.18}$$

where we used $\rho + p = \dot{\phi}^2$ and Eq. (2.2). The equation of motion of inflaton, Eq. (2.12), and the Friedmann equation, Eq. (2.13) , can be rewritten in terms of e-folds and the slow-roll parameters as

$$\frac{\mathrm{d}^2\phi}{\mathrm{d}N^2} + (3 - \epsilon_1)\frac{\mathrm{d}\phi}{\mathrm{d}N} + \frac{\partial_\phi V}{H^2} = 0 \tag{2.19}$$

$$(3 - \epsilon_1)H^2 M_{\rm Pl}^2 = V\,. \tag{2.20}$$

If we assume the slow-roll conditions, that is,

$$\epsilon_n \ll 1 \quad \text{for} \quad \forall n\,, \tag{2.21}$$

the equation of motion of inflaton and the Friedmann equation can be further rewritten approximately as

$$\frac{\mathrm{d}\phi}{\mathrm{d}N} \simeq -\frac{\partial_\phi V}{3H^2} \simeq -M_{\rm Pl}^2\frac{\partial_\phi V}{V} \tag{2.22}$$

$$3H^2 M_{\rm Pl}^2 \simeq V\,. \tag{2.23}$$

This, in turn, leads to approximate expressions for the slow roll parameters,

$$\epsilon_1 \simeq \frac{M_{\rm Pl}^2}{2}\left(\frac{\partial_\phi V}{V}\right)^2 \tag{2.24}$$

$$\epsilon_2 \simeq -2M_{\rm Pl}^2\frac{\partial_\phi^2 V}{V} + 2M_{\rm Pl}^2\left(\frac{\partial_\phi V}{V}\right)^2\,. \tag{2.25}$$

From Eqs. (2.1) and (2.15), inflation ends when $\epsilon_1 \simeq 1$. The number of e-folds elapsed from a certain field value, ϕ_*, until the end of inflation is evaluated by means of Eq. (2.17) as

$$N = \frac{1}{M_{\rm Pl}}\int_{\phi_{\rm end}}^{\phi_*}\frac{\mathrm{d}\phi}{\sqrt{2\epsilon_1}} \tag{2.26}$$

where $\phi_{\rm end}$ is a field value where $\epsilon_1 \simeq 1$ and we assumed $\phi_{\rm end} < \phi_*$.

2.2 Generation of scalar perturbations

From Eqs. (1.57)-(1.59) and Eqs. (2.9)-(2.11), one can show that the perturbations of the inflaton field obey

$$\delta\phi'' + 2\frac{a'}{a}\delta\phi' - \Delta\delta\phi + a^2\partial_\phi^2 V\delta\phi = 2a^2\partial_\phi V\varphi - \phi'\left[\varphi' + 3\psi' - \Delta\left(B - E'\right)\right]\,. \tag{2.27}$$

This equation of motion includes metric perturbations. However, by using Eqs. (1.57)-(1.59) again, it is simplified on the spatially-flat slicing as [37, 84, 86]

$$\delta\phi_{\rm flat}'' + 2\frac{a'}{a}\delta\phi_{\rm flat}' - \Delta\delta\phi_{\rm flat} + a^2\left[\partial_\phi^2 V - \frac{1}{a^4 M_{\rm Pl}^2}\left(\frac{a^2\phi'^2}{\mathcal{H}}\right)'\right]\delta\phi_{\rm flat} = 0 \tag{2.28}$$

where $\delta\phi_{\rm flat}$ is defined in Eq. (1.52). Note that Eq. (2.28) is valid at linear order while its derivation of Eq. (2.28) does not rely on the slow-roll approximation.

On the other hand, it is known that the adiabatic scalar perturbations of the universe can be described by the so-called Mukhanov-Sasaki variable [87, 88] defined as

$$v(\eta, \boldsymbol{x}) \equiv z(\eta)\mathcal{R}(\eta, \boldsymbol{x}) \tag{2.29}$$

with

$$z(\eta) \equiv aM_{\rm Pl}\sqrt{2\epsilon_1}\,. \tag{2.30}$$

This is also often written as $v = z\zeta$ in the literature. Note also that $\mathcal{R}$ coincides with ζ once one takes either the slow-roll limit or the long-wavelength limit. Up to second order in the perturbations, the gauge-invariant scalar perturbations obey the following action, [89–92]

$$S = \int \mathrm{d}t\mathrm{d}^3x\, a^3 M_{\rm Pl}^2 \left(-\frac{\dot{H}}{H^2}\right)\left[\dot{\mathcal{R}}^2 - \frac{1}{a^2}\left(\nabla\mathcal{R}\right)^2\right] \tag{2.31}$$

$$= \int \mathrm{d}\eta\mathrm{d}^3x\, \frac{1}{2}\left[v'^2 - \left(\nabla v\right)^2 - 2\frac{z'}{z}vv' + \frac{z'^2}{z^2}v^2\right] \tag{2.32}$$

$$= \int \mathrm{d}\eta\mathrm{d}^3x\, \frac{1}{2}\left[v'^2 - \left(\nabla v\right)^2 + \frac{z''}{z}v^2\right] \tag{2.33}$$

where we performed integration by parts in the last equality. Hence, v can be viewed as a canonical field and it obeys the Mukhanov-Sasaki equation,

$$v'' + \left(-\Delta - \frac{z''}{z}\right)v = 0\,. \tag{2.34}$$

For single-field inflation, since $\mathcal{R}$ is expressed as

$$\mathcal{R} = -\mathcal{H}\frac{\delta\phi_{\rm flat}}{\phi'} = -\frac{\delta\phi_{\rm flat}}{\frac{\mathrm{d}\phi}{\mathrm{d}N}}\,, \tag{2.35}$$

v and z can be rewritten as

$$|v| = a\left|\delta\phi_{\rm flat}\right|\,, \qquad z = a\left|\frac{\phi'}{\mathcal{H}}\right| = a\left|\frac{\mathrm{d}\phi}{\mathrm{d}N}\right|\,. \tag{2.36}$$

One can check that Eq. (2.28) and Eq. (2.34) are indeed equivalent.

Let us promote $v(\eta, \boldsymbol{x})$ to a quantum field $\hat{v}(\eta, \boldsymbol{x})$ and expand it by Fourier modes,

$$\hat{v}(\eta, \boldsymbol{x}) = \int \frac{\mathrm{d}^3k}{(2\pi)^{3/2}}\hat{v}_{\boldsymbol{k}}(\eta)e^{i\boldsymbol{k}\cdot\boldsymbol{x}} \tag{2.37}$$

$$= \int \frac{\mathrm{d}^3k}{(2\pi)^{3/2}}\frac{\hat{c}_{\boldsymbol{k}}v_k(\eta) + \hat{c}^\dagger_{-\boldsymbol{k}}v^*_k(\eta)}{\sqrt{2k}}e^{i\boldsymbol{k}\cdot\boldsymbol{x}} \tag{2.38}$$

$$= \int \frac{\mathrm{d}^3k}{(2\pi)^{3/2}}\frac{1}{\sqrt{2k}}\left[\hat{c}_{\boldsymbol{k}}v_k(\eta)e^{i\boldsymbol{k}\cdot\boldsymbol{x}} + \hat{c}^\dagger_{\boldsymbol{k}}v^*_k(\eta)e^{-i\boldsymbol{k}\cdot\boldsymbol{x}}\right] \tag{2.39}$$

where $\hat{c}_{\boldsymbol{k}}$ and $\hat{c}^\dagger_{\boldsymbol{k}}$ are annihilation and creation operators in the Schrödinger representation satisfying the commutation relation

$$\left[\hat{c}_{\boldsymbol{k}}, \hat{c}^\dagger_{\boldsymbol{p}}\right] = \delta\left(\boldsymbol{k} - \boldsymbol{p}\right) \tag{2.40}$$

$$\left[\hat{c}_{\boldsymbol{k}}, \hat{c}_{\boldsymbol{p}}\right] = 0, \quad \left[\hat{c}^\dagger_{\boldsymbol{k}}, \hat{c}^\dagger_{\boldsymbol{p}}\right] = 0 \tag{2.41}$$

and $v_k(\eta)$ (or $v_k(\eta)/\sqrt{2k}$) is called the mode function. Note that the property $\hat{v}_{-\boldsymbol{k}} = \hat{v}^\dagger_{\boldsymbol{k}}$ ensures $\hat{v}$ is real. Imposing the canonical commutation relation

$$[\hat{v}(\eta, \boldsymbol{x}), \hat{v}'(\eta, \boldsymbol{y})] = i\delta(\boldsymbol{x} - \boldsymbol{y})\,, \tag{2.42}$$

one can realize that the mode function should be normalized as

$$\frac{v_k v_k'^* - v_k' v_k^*}{2k} = i\,. \tag{2.43}$$

The vacuum is determined by $\hat{c}_{\boldsymbol{k}}\,|0\rangle = 0$ but it depends on the mode function. A common assumption in inflationary cosmology is that the mode function takes that in the Minkowski space in the infinite past,

$$\frac{v_k(\eta)}{\sqrt{2k}} \to \frac{e^{-ik\eta}}{\sqrt{2k}} \qquad \text{for} \qquad -k\eta \to \infty \tag{2.44}$$

since a quantum field is not affected by the cosmic expansion deep inside the horizon. The vacuum state determined by this mode function is called the Bunch-Davies vacuum. As we will see later, Eq. (2.34) also holds for the quantum field (see the discussion below Eq. (2.93)) and hence

$$v_k'' + \left(k^2 - \frac{z''}{z}\right) v_k = 0\,. \tag{2.45}$$

Before solving the differential equation, let us investigate more about the term z''/z. It is expressed in general as

$$\frac{z''}{z} = a^2H^2\left(2 - \epsilon_1 + \frac{3}{2}\epsilon_2 - \frac{1}{2}\epsilon_1\epsilon_2 + \frac{1}{4}\epsilon_2^2 + \frac{1}{2}\epsilon_2\epsilon_3\right)\,. \tag{2.46}$$

Since the conformal time η is computed at linear order in slow roll as

$$\eta = \int \frac{dt}{a} \simeq -\frac{1}{aH}\left(1 + \epsilon_1\right)\,, \tag{2.47}$$

it becomes

$$\frac{z''}{z} \simeq \frac{1}{\eta^2}\left(2 + \epsilon_1 + \frac{3}{2}\epsilon_2\right)\,. \tag{2.48}$$

If one takes into account only the mass term in the potential, $m^2 = \partial_\phi^2 V$, because of Eqs. (2.24) and (2.25), the above expression is reduced to

$$\frac{z''}{z} \simeq \frac{1}{\eta^2}\left(2 - \frac{m^2}{H^2}\right) \tag{2.49}$$

but we will keep using the general form shown in Eq. (2.48). Let us define ν by

$$\frac{z''}{z} \equiv \frac{1}{\eta^2}\left(\nu^2 - 1\right)\,. \tag{2.50}$$

Then, ν is expressed at linear order in slow roll as

$$\nu \simeq \sqrt{\frac{9}{4} + \epsilon_1 + \frac{3}{2}\epsilon_2} \simeq \frac{3}{2} + \epsilon_1 + \frac{1}{2}\epsilon_2\,. \tag{2.51}$$

Assuming that ν defined above is approximately time independent, the general solution of Eq. (2.45) is given by a linear combination of the Hankel functions as

$$\frac{v_k(\eta)}{\sqrt{2k}} = C_1(k)\sqrt{-\eta}H_\nu^{(1)}(-k\eta) + C_2(k)\sqrt{-\eta}H_\nu^{(2)}(-k\eta)\,. \tag{2.52}$$

Noting the asymptotic expression of the Hankel function

$$H_\nu^{(1)}(z) = \left(H_\nu^{(2)}(z)\right)^* \simeq \sqrt{\frac{2}{\pi z}}e^{i\left(z-\frac{2\nu+1}{4}\pi\right)} \quad \text{for} \quad |z| \to \infty\,, \tag{2.53}$$

the coefficient is determined from the condition shown in Eq. (2.44) as

$$C_1(k) = \frac{\sqrt{\pi}}{2}e^{i\frac{2\nu+1}{4}\pi}, \qquad C_2(k) = 0\,. \tag{2.54}$$

Hence, the mode function is determined as[1]

$$\frac{v_k(\eta)}{\sqrt{2k}} = \frac{\sqrt{\pi}}{2}e^{i\frac{2\nu+1}{4}\pi}\sqrt{-\eta}H_\nu^{(1)}(-k\eta)\,. \tag{2.55}$$

The Hankel function for $\nu = 3/2$ can be written in terms of elementary functions as

$$H_{3/2}^{(1)}(x) = -\sqrt{\frac{2}{\pi x}}\left(1+\frac{i}{x}\right)e^{ix} \quad \text{for} \quad x > 0\,. \tag{2.56}$$

Hence, at leading order $\nu = 3/2$, the mode function can be written as

$$\frac{v_k(\eta)}{\sqrt{2k}} = \frac{1}{\sqrt{2k}}\left(1-\frac{i}{k\eta}\right)e^{-ik\eta} \quad \text{for} \quad \nu = \frac{3}{2}\,. \tag{2.57}$$

Now, let us investigate the behavior of the mode function on superhorizon scales ($-k\eta \ll 1$). Since the Hankel function has an asymptotic expression for $\nu \in \mathbb{R}$

$$H_\nu^{(1)}(z) \simeq \sqrt{\frac{2}{\pi}}e^{-i\frac{\pi}{2}}2^{\nu-\frac{3}{2}}\frac{\Gamma(\nu)}{\Gamma(3/2)}z^{-\nu} \quad \text{for} \quad |z| \to 0\,, \tag{2.58}$$

the mode function becomes

$$\frac{v_k(\eta)}{\sqrt{2k}} = 2^{\nu-\frac{3}{2}}\frac{\Gamma(\nu)}{\Gamma(3/2)}e^{i\frac{2\nu-1}{4}\pi}\frac{aH}{\sqrt{2k^3}}\left(\frac{k}{aH}\right)^{\frac{3}{2}-\nu} \quad \text{for} \quad -k\eta \to 0\,. \tag{2.59}$$

Substituting the expression for ν in the slow-roll regime shown in Eq. (2.51), one obtains

$$\frac{v_k(\eta)}{\sqrt{2k}} \simeq i\frac{aH}{\sqrt{2k^3}}\left(\frac{k}{aH}\right)^{-\epsilon_1-\epsilon_2/2} \quad \text{for} \quad -k\eta \to 0\,. \tag{2.60}$$

The power spectrum of the field perturbations is defined by

$$\langle \delta\phi_{\boldsymbol{k}}\delta\phi_{\boldsymbol{p}}\rangle \equiv \frac{2\pi^2}{k^3}\mathcal{P}_{\delta\phi}(k)\delta(\boldsymbol{k}+\boldsymbol{p})\,. \tag{2.61}$$

[1]Note that the overall phase of the mode function is irrelevant since it is absorbed by shift of time coordinate. It also corresponds to the constant term in Eq. (2.110).

Noting $\delta\phi_{\boldsymbol{k}} = v_{\boldsymbol{k}}/a$, where $\delta\phi_{\boldsymbol{k}}$ is evaluated on the spatially-flat gauge, and Eq. (2.38), the left-hand side is calculated as

$$\langle \delta\phi_{\boldsymbol{k}} \delta\phi_{\boldsymbol{p}} \rangle = \frac{1}{a^2}\frac{|v_k|^2}{2k}\delta(\boldsymbol{k}+\boldsymbol{p}) = \frac{H^2}{2k^3}\left(\frac{k}{aH}\right)^{-2\epsilon_1-\epsilon_2}\delta(\boldsymbol{k}+\boldsymbol{p})\,. \tag{2.62}$$

Hence, the power spectrum of the field perturbations on superhorizon scales is evaluated as

$$\mathcal{P}_{\delta\phi}(k) = \left(\frac{H}{2\pi}\right)^2\left(\frac{k}{aH}\right)^{-2\epsilon_1-\epsilon_2}\,. \tag{2.63}$$

Note that the spectrum is almost scale invariant. In particular, it is evaluated at the horizon exit of the scale ($k \simeq aH$) as

$$\mathcal{P}_{\delta\phi}(k) = \left(\frac{H}{2\pi}\right)^2\,. \tag{2.64}$$

Similarly, the power spectrum of the curvature perturbations is defined by

$$\langle \zeta_{\boldsymbol{k}} \zeta_{\boldsymbol{p}} \rangle \equiv \frac{2\pi^2}{k^3}\mathcal{P}_\zeta(k)\delta(\boldsymbol{k}+\boldsymbol{p})\,. \tag{2.65}$$

Noting $\zeta_{\boldsymbol{k}} = v_{\boldsymbol{k}}/z = \delta\phi_{\boldsymbol{k}}/(M_{\rm Pl}\sqrt{2\epsilon_1})$, the power spectrum of the curvature perturbations can also be calculated by means of the mode function shown in Eq. (2.60). As we showed in Eq. (1.100), the curvature perturbations are conserved on superhorizon scales, $\dot{\zeta} = 0$. However, Eq. (2.60) implies fictitious time dependence at the order of the slow-roll parameters, $\dot{\zeta} \sim H\zeta\mathcal{O}(\epsilon_n)$. This is because the calculation leading to Eq. (2.60) relies on the slow-roll approximation although the Mukhanov-Sasaki equation (2.45) does not rely on that approximation. Therefore, one should evaluate the curvature perturbations around the time of the horizon exit of a scale of interest. For scales around a certain scale $k_{\rm p}$, one obtains the power spectrum as

$$\mathcal{P}_\zeta(k) = \frac{1}{2\epsilon_1}\left(\frac{H}{2\pi M_{\rm Pl}}\right)^2\left(\frac{k}{k_{\rm p}}\right)^{-2\epsilon_1-\epsilon_2} \simeq \frac{1}{12\pi^2 M_{\rm Pl}^6}\frac{V^3}{(\partial_\varphi V)^2}\left(\frac{k}{k_{\rm p}}\right)^{-2\epsilon_1-\epsilon_2} \tag{2.66}$$

where the right-hand side is evaluated at the time when $k_{\rm p} \simeq aH$. This result agrees with the δN formalism, which says $\zeta = \delta N$, on top of Eq. (2.26). The scale dependence of the power spectrum is represented by the scalar tilt defined as

$$n_{\rm s} - 1 \equiv \frac{{\rm d}\ln\mathcal{P}_\zeta(k)}{{\rm d}\ln k}\,. \tag{2.67}$$

Eq. (2.66) indicates

$$n_{\rm s} - 1 = -2\epsilon_1 - \epsilon_2 \simeq -3M_{\rm Pl}^2\left(\frac{\partial_\phi V}{V}\right)^2 + 2M_{\rm Pl}^2\frac{\partial_\phi^2 V}{V} \tag{2.68}$$

where we used Eqs. (2.24)-(2.25).

The amplitude of $\mathcal{P}_\zeta$ and $n_{\rm s}$ are important quantities to connect inflation theory with observations. Denoting

$$\mathcal{P}_\zeta(k) = A_{\rm s}\left(\frac{k}{k_{\rm p}}\right)^{n_{\rm s}-1} \tag{2.69}$$

for the pivot scale $k_{\rm p} = 0.05\,{\rm Mpc}^{-1}$, the observation of the CMB anisotropy by Planck 2018 provides [12]

$$\ln\left(10^{10}A_{\rm s}\right) = 3.044 \pm 0.014\,, \quad n_{\rm s} = 0.9649 \pm 0.0042 \tag{2.70}$$

where the errors are given at the 68% confidence level. The duration of inflation from the horizon exit of the pivot scale can be estimated as $N \simeq$ 50-60.

At last in this section, let us briefly mention tensor perturbations generated during inflation, namely primordial gravitational waves. Tensor perturbations are described by the following action,

$$S = \frac{M_{\rm Pl}^2}{8}\int {\rm d}\eta \int {\rm d}^3x a^2 \left[\left(h_{ij}'\right)^2 - \left(\nabla h_{ij}\right)^2\right]\,. \tag{2.71}$$

Using the polarization tensors that are transverse, tranceless and normalized as $e^{r,ij}\left(\boldsymbol{k}\right)e^{s}_{ij}\left(\boldsymbol{k}\right) = \delta^{rs}$, tensor perturbations can be expanded as

$$h_{ij}(\eta,\boldsymbol{x}) = \int \frac{{\rm d}^3k}{(2\pi)^{3/2}}\left[h^{(+)}_{\boldsymbol{k}}(\eta)e^{(+)}_{ij}(\boldsymbol{k}) + h^{(\times)}_{\boldsymbol{k}}(\eta)e^{(\times)}_{ij}(\boldsymbol{k})\right]e^{i\boldsymbol{k}\cdot\boldsymbol{x}}\,. \tag{2.72}$$

Then, the evolution of $h^r_{\boldsymbol{k}}(\eta)$ can be investigated parallelly with the method for scalar perturbations described above. The power spectrum for each polarization is defined by

$$\left\langle h^r_{\boldsymbol{k}}h^s_{\boldsymbol{p}}\right\rangle \equiv \frac{2\pi^2}{k^3}\mathcal{P}_h(k)\delta(\boldsymbol{k}+\boldsymbol{p})\delta^{rs} \tag{2.73}$$

and calculated as

$$\mathcal{P}_h(k) = \frac{H^2}{\pi^2 M_{\rm Pl}^2}\,. \tag{2.74}$$

The tensor tilt is evaluated with the slow-roll approximation as

$$n_t \equiv \frac{{\rm d}\ln\mathcal{P}_\zeta(k)}{{\rm d}\ln k} \simeq -2\epsilon_1\,. \tag{2.75}$$

The tensor-to-scalar ratio

$$r \equiv \frac{2\mathcal{P}_h}{\mathcal{P}_\zeta} \simeq 16\epsilon_1 \tag{2.76}$$

is another observationally important quantity. The current observations impose an upper bound on it, [12]

$$r(k = 0.002\,{\rm Mpc}^{-1}) < 0.056 \quad \text{(95\%CL, Planck TT,TE,EE+lowE+lensing+BK15)}\,. \tag{2.77}$$

2.3 Quantum states of cosmological perturbations

In the previous section, we evaluated the amplitude of scalar perturbations working in the Heisenberg picture as is usual in cosmology. In this section, we consider how the quantum states evolves in the Schrödinger picture. For that sake, our first step will be to write down the Hamiltonian in terms of creation and annihilation operators. Then, we will identify the time evolution operator $\hat{U}(t)$. Finally, we will operate it to the Bunch-Davies vacuum to see the quantum states of cosmological perturbations as $|\Psi(t)\rangle = \hat{U}(t)\,|0\rangle$. We will figure out that cosmological perturbations are placed in two-mode squeezed states. This section is written mainly based on Ref. [16, 17, 20, 23].

Let us start with the quadratic action expressed in the way of Eq. (2.32). According to this action, the conjugate momentum of $v(\eta, \boldsymbol{x})$ is given by

$$p(\eta, \boldsymbol{x}) = \frac{\partial \mathcal{L}}{\partial v'} = v' - \frac{z'}{z} v \,. \tag{2.78}$$

Note that, while v is associated with the curvature perturbations as $\zeta = v/z$, p is associated with its time derivative as $\zeta' = p/z$. The Hamiltonian is derived as

$$H = \int \mathrm{d}^3x \left(pv' - \mathcal{L}\right) \tag{2.79}$$

$$= \int \mathrm{d}^3x \frac{1}{2}\left[p^2 + 2\frac{z'}{z}pv + (\nabla v)^2\right] . \tag{2.80}$$

It is expressed in the Fourier space as

$$H = \int_{\mathbb{R}^{3+}} \mathrm{d}^3k \left[p_{\boldsymbol{k}} p^*_{\boldsymbol{k}} + \frac{z'}{z}\left(p^*_{\boldsymbol{k}} v_{\boldsymbol{k}} + p_{\boldsymbol{k}} v^*_{\boldsymbol{k}}\right) + k^2 v_{\boldsymbol{k}} v^*_{\boldsymbol{k}}\right] \tag{2.81}$$

where we restricted the integral into half of the full momentum space, $\mathbb{R}^{3+}$, in order to deal with only independent variables. Let us quantize this system. Here, instead of expanding

$$\hat{v}_{\boldsymbol{k}} = \frac{\hat{c}_{\boldsymbol{k}} v_k(\eta) + \hat{c}^\dagger_{-\boldsymbol{k}} v^*_k(\eta)}{\sqrt{2k}} \tag{2.82}$$

as is done in Eq. (2.38), let us introduce creation and annihilation operators in the Heisenberg representation,

$$\hat{c}^{\mathrm{H}}_{\boldsymbol{k}}(\eta) \equiv \frac{1}{\sqrt{2}}\left(\sqrt{k}\hat{v}_{\boldsymbol{k}} + \frac{i}{\sqrt{k}}\hat{p}_{\boldsymbol{k}}\right) \tag{2.83}$$

$$\hat{c}^{\mathrm{H}\dagger}_{\boldsymbol{k}}(\eta) \equiv \frac{1}{\sqrt{2}}\left(\sqrt{k}\hat{v}^\dagger_{\boldsymbol{k}} - \frac{i}{\sqrt{k}}\hat{p}^\dagger_{\boldsymbol{k}}\right) . \tag{2.84}$$

The canonical commutation relation of the phase-space variables, $[\hat{v}_{\boldsymbol{k}}, \hat{p}_{\boldsymbol{q}}] = i\delta(\boldsymbol{k} + \boldsymbol{q})$, leads to that of the creation and annihilation operators, $\left[\hat{c}^{\mathrm{H}}_{\boldsymbol{k}}, \hat{c}^{\mathrm{H}\dagger}_{\boldsymbol{q}}\right] = \delta(\boldsymbol{k} - \boldsymbol{q})$. The phase-space variables are expressed as

$$\hat{v}_{\boldsymbol{k}} = \frac{1}{\sqrt{2k}}\left(\hat{c}^{\mathrm{H}}_{\boldsymbol{k}} + \hat{c}^{\mathrm{H}\dagger}_{-\boldsymbol{k}}\right) \tag{2.85}$$

$$\hat{p}_{\boldsymbol{k}} = -i\sqrt{\frac{k}{2}}\left(\hat{c}^{\mathrm{H}}_{\boldsymbol{k}} - \hat{c}^{\mathrm{H}\dagger}_{-\boldsymbol{k}}\right) . \tag{2.86}$$

Therefore, the Hamiltonian given in Eq. (2.81) is quantized as

$$\hat{H} = \frac{1}{2}\int_{\mathbb{R}^3} \mathrm{d}^3k \left[k\left(\hat{c}^{\mathrm{H}}_{\boldsymbol{k}} \hat{c}^{\mathrm{H}\dagger}_{\boldsymbol{k}} + \hat{c}^{\mathrm{H}\dagger}_{-\boldsymbol{k}} \hat{c}^{\mathrm{H}}_{-\boldsymbol{k}} \right) - i\frac{z'}{z}\left(\hat{c}^{\mathrm{H}}_{\boldsymbol{k}} \hat{c}^{\mathrm{H}}_{-\boldsymbol{k}} - \hat{c}^{\mathrm{H}\dagger}_{-\boldsymbol{k}} \hat{c}^{\mathrm{H}\dagger}_{\boldsymbol{k}} \right) \right] \tag{2.87}$$

up to terms including $\delta(\boldsymbol{0})$, which express the vacuum energy. This is the Hamiltonian that describes cosmological perturbations. The former part of this Hamiltonian represents the familiar one for the free field. On the other hand, the latter part comes from the cosmic expansion and implies that the classical source, which is gravity here, induces creation of pair of particles (energy excitations) with opposite momenta.

The time evolution of $\hat{c}^{\mathrm{H}}_{\boldsymbol{k}}$ is described by the Heisenberg equation,

$$\frac{\mathrm{d}\hat{c}^{\mathrm{H}}_{\boldsymbol{k}}}{\mathrm{d}\eta} = i\left[\hat{H}, \hat{c}^{\mathrm{H}}_{\boldsymbol{k}} \right] \tag{2.88}$$

$$= -ik\hat{c}^{\mathrm{H}}_{\boldsymbol{k}} + \frac{z'}{z}\hat{c}^{\mathrm{H}\dagger}_{-\boldsymbol{k}} \,. \tag{2.89}$$

It can be solved by means of the Bogoliubov transformation

$$\hat{c}^{\mathrm{H}}_{\boldsymbol{k}}(\eta) = \alpha_k(\eta)\hat{c}_{\boldsymbol{k}} + \beta_k(\eta)\hat{c}^{\dagger}_{-\boldsymbol{k}} \tag{2.90}$$

where the operator $\hat{c}_{\boldsymbol{k}}$ without a superscript "H" stands for that in the Schrödinger representation and one can interpret it as $\hat{c}_{\boldsymbol{k}} = \hat{c}^{\mathrm{H}}_{\boldsymbol{k}}(\eta_{\mathrm{ini}})$. The coefficients must satisfy the following differential equations,

$$\frac{\mathrm{d}\alpha_k}{\mathrm{d}\eta} = -ik\alpha_k + \frac{z'}{z}\beta_k^* \tag{2.91}$$

$$\frac{\mathrm{d}\beta_k}{\mathrm{d}\eta} = -ik\beta_k + \frac{z'}{z}\alpha_k^* \tag{2.92}$$

and be normalized as

$$\left|\alpha_k^2\right| - \left|\beta_k\right|^2 = 1 \tag{2.93}$$

because of the commutation relation of the creation and annihilation operators. Eqs. (2.82), (2.85) and (2.90) indicate that $\alpha_k + \beta_k^*$ corresponds to the Mukhanov-Sasaki mode function v_k, and Eqs. (2.91) and (2.92) indicate that it indeed satisfies the Mukhanov-Sasaki equation shown in Eq. (2.45).

On the other hand, the time evolution of $\hat{c}^{\mathrm{H}}_{\boldsymbol{k}}$ should also be described by means of the time evolution operator as

$$\hat{c}^{\mathrm{H}}_{\boldsymbol{k}}(\eta) = \hat{U}^{\dagger}(\eta)\hat{c}_{\boldsymbol{k}}\hat{U}(\eta) \,. \tag{2.94}$$

It is known that the time evolution operator $\hat{U}$ which realizes Eq. (2.90) is expressed as a product of the (two-mode) squeezing operator $\hat{U}_S$ and the rotation operator $\hat{R}$ defined as

$$\hat{U} = \hat{U}_S\hat{R} \tag{2.95}$$

$$\hat{U}_S = \exp\left[re^{-2i\varphi}\hat{c}^{\dagger}_{\boldsymbol{k}}\hat{c}^{\dagger}_{-\boldsymbol{k}} - re^{2i\varphi}\hat{c}_{\boldsymbol{k}}\hat{c}_{-\boldsymbol{k}} \right] \tag{2.96}$$

$$\hat{R} = \exp\left[i\theta\hat{c}^{\dagger}_{\boldsymbol{k}}\hat{c}_{\boldsymbol{k}} + i\theta\hat{c}^{\dagger}_{-\boldsymbol{k}}\hat{c}_{-\boldsymbol{k}} \right] = e^{i\theta\hat{n}_{\boldsymbol{k}}}e^{i\theta\hat{n}_{-\boldsymbol{k}}} \tag{2.97}$$

where r, φ and θ are real-valued functions of time assigned for each bipartite system. Note that $\hat{U}$ given above is symmetric with respect to $\boldsymbol{k}$ and $-\boldsymbol{k}$ as it should be.

Before checking that this is a correct time evolution operator, let us discuss the space we deal with and the normalization of operators. From the Hamiltonian given in Eq. (2.87), the full Hilbert space $\mathcal{E}$ can be factorized into a product of bipartite systems each composed of the $\boldsymbol{k}$ and $-\boldsymbol{k}$ modes,

$$\mathcal{E} = \prod_{\boldsymbol{k}\in\mathbb{R}^{3+}} \mathcal{E}_{\boldsymbol{k}} \otimes \mathcal{E}_{-\boldsymbol{k}} \,. \tag{2.98}$$

We focus on one bipartite system $\mathcal{E}_{\boldsymbol{k}} \otimes \mathcal{E}_{-\boldsymbol{k}}$ from now on. Then, we encounter such commutation relations as

$$\left[\hat{c}_{\boldsymbol{k}}, \hat{c}^{\dagger}_{\boldsymbol{k}}\right] = \delta\left(\boldsymbol{0}\right). \tag{2.99}$$

The diverging delta function in the right-hand side can be interpreted as the volume V. Hereafter, we denote the subsystems of the mode $\boldsymbol{k}$ and $-\boldsymbol{k}$ also as '1' and '2' subsystems respectively. Then we can write the commutation relation as

$$\left[\hat{c}_i, \hat{c}^{\dagger}_j\right] = V\delta_{ij} \qquad (i,j=1,2)\,. \tag{2.100}$$

Now, let us redefine the operator $\hat{c}_{\boldsymbol{k}}$ as the old one divided by $\sqrt{V}$ i.e. $\hat{c}_{\boldsymbol{k}}/\sqrt{V} \to \hat{c}_{\boldsymbol{k}}$. Accordingly, the mass dimension of $\hat{c}_{\boldsymbol{k}}$ is changed as $-3/2 \to 0$. The redefined operators have the following commutation relation

$$\left[\hat{c}_i, \hat{c}^{\dagger}_j\right] = \delta_{ij}\,, \qquad (i,j=1,2)\,. \tag{2.101}$$

The situation depicted in Eq. (2.99) is particular in field theory, but with the normalization that gives Eq. (2.101), we can make use of the techniques of quantum information theory.

By using the Baker-Campbell-Hausdorff formula, Eq. (2.94) can be calculated with $\hat{U}$ given in Eq. (2.95) as

$$\hat{U}^{\dagger}(\eta)\hat{c}_{\boldsymbol{k}}\hat{U}(\eta) = e^{i\theta}\cosh r\hat{c}_{\boldsymbol{k}} + e^{-i\theta-2i\varphi}\sinh r\hat{c}^{\dagger}_{-\boldsymbol{k}}\,. \tag{2.102}$$

Identifying Eq. (2.90) and Eq. (2.102), one can translate the differential equations for α and β shown in Eqs. (2.91)-(2.91) into those of r, φ and θ as

$$\frac{\mathrm{d}r}{\mathrm{d}\eta} = \frac{z'}{z}\cos(2\varphi) \tag{2.103}$$

$$\frac{\mathrm{d}\varphi}{\mathrm{d}\eta} = k - \frac{z'}{z}\coth(2r)\sin(2\varphi) \tag{2.104}$$

$$\frac{\mathrm{d}\theta}{\mathrm{d}\eta} = -k + \frac{z'}{z}\tanh(r)\sin(2\varphi)\,. \tag{2.105}$$

Eq. (2.102) also satisfies the normalization imposed by Eq. (2.93). Therefore, if r, φ and θ obey the above differential equations, Eq. (2.95) provides the correct time evolution operator.

Now that we have identified the time evolution operator $\hat{U}$, let us work fully in the Schrödinger picture from now on. Thanks to the operator ordering theorem, the squeezing operator $\hat{U}_S$ given in Eq. (2.96) can be written as (see Appendix C.1 for the derivation)

$$\begin{aligned}\hat{U}_S(\eta) = \exp\left[e^{-2i\varphi}\tanh r\,\hat{c}^\dagger_{\boldsymbol{k}}\hat{c}^\dagger_{-\boldsymbol{k}}\right]\exp\left[-\ln(\cosh r)\left[\hat{c}^\dagger_{\boldsymbol{k}}\hat{c}_{\boldsymbol{k}}+\hat{c}_{-\boldsymbol{k}}\hat{c}^\dagger_{-\boldsymbol{k}}\right]\right]\\ \times\exp\left[-e^{2i\varphi}\tanh r\,\hat{c}_{\boldsymbol{k}}\hat{c}_{-\boldsymbol{k}}\right]\,.\end{aligned} \tag{2.106}$$

This formula makes it easy to calculate the evolution of the state. Starting from the vacuum state $|0,0\rangle$, the bipartite system evolves as

$$\hat{U}(\eta)\,|0,0\rangle = \frac{1}{\cosh(r)}\sum_{n=0}^{\infty}e^{-2in\varphi}\tanh^n(r)\,|n,n\rangle \equiv |\Psi_{\rm 2sq}(\eta)\rangle \tag{2.107}$$

where $|n,m\rangle$ denotes the state with n particles in the $\boldsymbol{k}$ mode and m particles in the $-\boldsymbol{k}$ mode. The resultant state is called the two-mode squeezed state. It is characterized by three time-dependent parameters: the squeezing amplitude r, the squeezing angle φ and the rotation angle θ. Note that the expression for a two-mode squeezed state, Eq. (2.107), does not include the rotation angle θ since the vacuum state is invariant under rotations, $\hat{R}(t)\,|0,0\rangle = |0,0\rangle$. This implies that measurements performed at the same time are insensitive to θ, since θ simply adds an overall phase to the wavefunction. However, as will be made explicit in Chap. 6, when multiple-time measurements are performed, this is not the case any more and the result becomes sensitive to the change in the overall phase between the measurement times. This can be interpreted as a consequence of the fact that, after performing the first measurement, a two-mode squeezed state is projected onto the eigenstate of a spin operator, which is not a two-mode squeezed state anymore, and which is therefore not invariant under rotations. This is why, contrary to what is usually done, θ is carefully kept in this thesis.

For a pure de Sitter spacetime, where $z'/z = -1/\eta$, there are analytical solutions for the differential equations given in Eqs. (2.103)-(2.105) as

$$r = -\mathrm{arc\,sinh}\left(\frac{1}{2k\eta}\right) \tag{2.108}$$

$$\varphi = \frac{\pi}{4}+\frac{1}{2}\mathrm{arc\,tan}\left(\frac{1}{2k\eta}\right) \tag{2.109}$$

$$\theta = -k\eta+\mathrm{arc\,tan}\,(2k\eta)\ \ (+\,\mathrm{const.}). \tag{2.110}$$

The quantities appearing here evolve from the beginning to the end of inflation as

$$\begin{aligned}&\eta : -\infty && \to\ 0\\ &r : 0\left(\sim -\frac{1}{2k\eta}\right) && \to\ +\infty\left(\sim \log\left(-\frac{1}{k\eta}\right)\sim N\right)\\ &\varphi : \frac{\pi}{4}\left(\sim\frac{\pi}{4}+\frac{1}{4k\eta}\right) && \to\ 0\,(\sim -k\eta)\\ &\theta : +\infty\,(\sim -k\eta) && \to\ 0\,(\sim k\eta)\end{aligned}\,. \tag{2.111}$$

It is remarkable that the squeezing parameter r, which is a measure of the magnitude of squeezing, grows in proportion to the e-folds after the horizon exit. Hence, $r\sim 50$ is achieved. Noting that r appears in the form of e^r in many quantities, it is a very high

squeezing $e^r \gg 1$. In the laboratory experiment, $r \sim 1.7$ is the world record [63]. One could come up with the following analogy. Regarding the homogeneous mode, the CMB is the almost ideal black body radiation. Similarly, the anisotropy originates from the best squeezed states realized in nature. Two-mode squeezed states are entangled states that arise in a large variety of physical situations, since any quadratic Hamiltonian produces squeezed states. They are therefore commonly found in quantum optics [60–62]. In the large-squeezing limit, they also provide a realization of the Einstein-Podolsky-Rosen (EPR) state [59]. This discussion implies the possibility that the universe works as a quantum laboratory or that the techniques developed in quantum information theory is helpful to understand cosmological perturbations. In Chap. 6, we study general squeezed states keeping r, φ and θ unknown parameters for two reasons: 1) the evolution of r, φ and θ is not known and left for future work 2) squeezed states are realized in a broad range of systems as mentioned above.

2.4 Quantum-to-classical transition

In this section, we discuss what is called the quantum-to-classical transition of cosmological perturbations. The words "quantum" and "classical" are somewhat vague. There are several quantities and properties which represent "quantumness" and "classicality". We intend to make only robust statements about them. Here, we focus particularly on the relation between the quantum average and the stochastic average [23, 75]. Other ways of describing this issue are also mentioned at the end of this section.

As can be seen in Eqs. (2.85) and (2.86), in quantum field theory, a quantum field generically mixes the $\boldsymbol{k}$ and $-\boldsymbol{k}$ modes of the creation and annihilation operators. However, this is not familiar to quantum information theory. In order to make use of techniques developed there, we define the "position" and "momentum" operators for each mode as

$$\hat{q}_{\boldsymbol{k}} = \frac{1}{\sqrt{2k}}\left(\hat{c}_{\boldsymbol{k}} + \hat{c}^{\dagger}_{\boldsymbol{k}}\right) \tag{2.112}$$

$$\hat{\pi}_{\boldsymbol{k}} = -i\sqrt{\frac{k}{2}}\left(\hat{c}_{\boldsymbol{k}} - \hat{c}^{\dagger}_{\boldsymbol{k}}\right). \tag{2.113}$$

These are Hermitian in contrast with $v_{\boldsymbol{k}}$ and $p_{\boldsymbol{k}}$. They obey the commutation relation $[\hat{q}_{\boldsymbol{k}}, \hat{\pi}_{\boldsymbol{q}}] = i\delta(\boldsymbol{k} - \boldsymbol{q})$. We can also introduce $\hat{Q}_{\boldsymbol{k}}$, $\hat{P}_{\boldsymbol{k}}$ for convenience as

$$\hat{Q}_{\boldsymbol{k}} = \sqrt{k}\hat{q}_{\boldsymbol{k}} \tag{2.114}$$

$$\hat{P}_{\boldsymbol{k}} = \frac{1}{\sqrt{k}}\hat{\pi}_{\boldsymbol{k}}. \tag{2.115}$$

Again, they obey the commutation relation $\left[\hat{Q}_{\boldsymbol{k}}, \hat{P}_{\boldsymbol{q}}\right] = i\delta(\boldsymbol{k} - \boldsymbol{q})$. The eigenstate of $\hat{q}_{\boldsymbol{k}}$ with the eignevalue q, $|q\rangle_{\boldsymbol{k}}$, and that of $\hat{Q}_{\boldsymbol{k}}$ with the eignevalue $Q \equiv \sqrt{k}q$, $|Q\rangle_{\boldsymbol{k}}$, are related as $|q\rangle_{\boldsymbol{k}} = k^{1/4}|Q\rangle_{\boldsymbol{k}}$. The creation and annihilation operators are expressed as

$$\hat{c}_{\boldsymbol{k}} = \frac{1}{\sqrt{2}}\left(\sqrt{k}\hat{q}_{\boldsymbol{k}} + \frac{i}{\sqrt{k}}\hat{\pi}_{\boldsymbol{k}}\right) = \frac{1}{\sqrt{2}}\left(\hat{Q}_{\boldsymbol{k}} + i\hat{P}_{\boldsymbol{k}}\right) \tag{2.116}$$

$$\hat{c}^{\dagger}_{\boldsymbol{k}} = \frac{1}{\sqrt{2}}\left(\sqrt{k}\hat{q}_{\boldsymbol{k}} - \frac{i}{\sqrt{k}}\hat{\pi}_{\boldsymbol{k}}\right) = \frac{1}{\sqrt{2}}\left(\hat{Q}_{\boldsymbol{k}} - i\hat{P}_{\boldsymbol{k}}\right). \tag{2.117}$$

These expressions can be compared with Eqs. (2.83) and (2.84). The mass dimensions of some quantities are summarized below.

$$\hat{c}_{\boldsymbol{k}} : -\frac{3}{2}, \quad \hat{q}_{\boldsymbol{k}} : -2, \quad \hat{\pi}_{\boldsymbol{k}} : -1, \quad \hat{Q}_{\boldsymbol{k}} : -\frac{3}{2}, \quad \hat{P}_{\boldsymbol{k}} : -\frac{3}{2} \tag{2.118}$$

Applying the renormalization $\hat{c}_{\boldsymbol{k}}/\sqrt{V} \to \hat{c}_{\boldsymbol{k}}$ as is described around Eq. (2.101) and redefining the other operators $\hat{q}_{\boldsymbol{k}}, \hat{\pi}_{\boldsymbol{k}}, \hat{Q}_{\boldsymbol{k}}, \hat{P}_{\boldsymbol{k}}$ according to the new $\hat{c}_{\boldsymbol{k}}$, these redefined operators have the commutation relations as

$$\left[\hat{c}_i, \hat{c}_j^\dagger\right] = \delta_{ij}, \quad [\hat{q}_i, \hat{\pi}_j] = \left[\hat{Q}_i, \hat{P}_j\right] = i\delta_{ij} \qquad (i, j = 1, 2 = \boldsymbol{k}, -\boldsymbol{k})\,. \tag{2.119}$$

The mass dimensions shown in Eq. (2.118) are changed into

$$\hat{c}_{\boldsymbol{k}} : 0, \quad \hat{q}_{\boldsymbol{k}} : -\frac{1}{2}, \quad \hat{\pi}_{\boldsymbol{k}} : \frac{1}{2}, \quad \hat{Q}_{\boldsymbol{k}} : 0, \quad \hat{P}_{\boldsymbol{k}} : 0\,. \tag{2.120}$$

Since we are considering a bipartite system of the $\boldsymbol{k}$ and $-\boldsymbol{k}$ modes, the phase-space variables consist of $X \equiv (Q_{\boldsymbol{k}}, P_{\boldsymbol{k}}, Q_{-\boldsymbol{k}}, P_{-\boldsymbol{k}})$. Let us consider a general quantity $O(X)$ defined as a function of phase-space variables. This can be read as a quantum operator $\hat{O}(\hat{X})$ as well. The stochastic average is expressed as

$$\langle O \rangle_{\text{stoch}} = \int \mathrm{d}^4 X\, O(X) P(X) \tag{2.121}$$

where $P(X)$ is the classical probability density function. Let us consider when a quantum average has a stochastic description.

The Weyl transform of the operator $\hat{O}(\hat{X})$ is defined by

$$\tilde{O}(X) = \int \mathrm{d}x\, \mathrm{d}y\, e^{-iP_{\boldsymbol{k}}x - iP_{-\boldsymbol{k}}y} \left\langle Q_{\boldsymbol{k}} + \frac{x}{2}, Q_{-\boldsymbol{k}} + \frac{y}{2} \middle| \hat{O} \middle| Q_{\boldsymbol{k}} - \frac{x}{2}, Q_{-\boldsymbol{k}} - \frac{y}{2} \right\rangle . \tag{2.122}$$

This is a map from an operator to a function of phase-space variables. A fundamental property of the Weyl transform is

$$\mathrm{Tr}\left(\hat{A}\hat{B}\right) = \frac{1}{(2\pi)^2} \int \tilde{A}(X) \tilde{B}(X) \mathrm{d}^4 X\,. \tag{2.123}$$

Therefore, the quantum average can be computed as

$$\left\langle \hat{O} \right\rangle_{\text{quant}} = \mathrm{Tr}\left(\hat{\rho}\hat{O}\right) = \frac{1}{(2\pi)^2} \int \tilde{\rho}(X) \tilde{O}(X) \mathrm{d}^4 X = \int \tilde{O}(X) W(X) \mathrm{d}^4 X \tag{2.124}$$

where $\hat{\rho}$ is the density matrix and $W(X)$ is the Wigner function defined by

$$W(X) = \frac{1}{(2\pi)^2} \tilde{\rho}(X) \tag{2.125}$$

$$= \frac{1}{(2\pi)^2} \int \mathrm{d}x\, \mathrm{d}y\, e^{-iP_{\boldsymbol{k}}x - iP_{-\boldsymbol{k}}y} \left\langle Q_{\boldsymbol{k}} + \frac{x}{2}, Q_{-\boldsymbol{k}} + \frac{y}{2} \middle| \hat{\rho} \middle| Q_{\boldsymbol{k}} - \frac{x}{2}, Q_{-\boldsymbol{k}} - \frac{y}{2} \right\rangle . \tag{2.126}$$

The quantum version of the characteristic function is defined by

$$\chi(\kappa) = \mathrm{Tr}\left[\hat{\rho}\, e^{i\kappa^{\mathrm{T}} \cdot \hat{X}}\right], \tag{2.127}$$

where κ is a vector with four components. The Wigner function can be calculated as the Fourier transform of this characteristic function

$$W(X) = \frac{1}{(2\pi)^4} \int \mathrm{d}^4\kappa \, e^{-i\kappa^{\mathrm{T}}\cdot X} \chi(\kappa) \,. \tag{2.128}$$

Hence, the Wigner function is the quantum generalization of the classical distribution in phase space. Note however that the Wigner function is not ensured to be positive.

There are two conditions for the quantum average expressed in Eq. (2.124) to have a stochastic description: 1) the Wigner function is positive definite, 2) $\tilde{O}(X) = O(X)$. These two conditions allow one to interpret the last expression of Eq. (2.124) as an average of a random variable with a classical probability density function just as Eq. (2.121). The second condition can be restated as "the operator $\hat{O}$ is proper", where a proper operator is defined as an operator $\hat{O}$ whose Weyl transform $\tilde{O}(X)$ takes all and only the eigenvalues of $\hat{O}$. An operator that is not proper is called an improper operator. It can be shown that the Wigner function of a squeezed state is Gaussian and hence positive definite. Therefore, only whether the second condition is satisfied or not is to be checked.

People are primarily interested in operators that represent correlation functions of curvature perturbations, namely $\hat{\zeta}^n_{\boldsymbol{k}}$. From Eqs. (2.78), (2.85), (2.86), (2.116) and (2.117), $\zeta_{\boldsymbol{k}}$ and its time derivative can be expressed in terms of $\hat{Q}_{\boldsymbol{k}}$ and $\hat{P}_{\boldsymbol{k}}$ as

$$z\hat{\zeta}_{\boldsymbol{k}} = \hat{v}_{\boldsymbol{k}} = \frac{1}{2\sqrt{k}} \left[\hat{Q}_{\boldsymbol{k}} + \hat{Q}_{-\boldsymbol{k}} + i\left(\hat{P}_{\boldsymbol{k}} - \hat{P}_{-\boldsymbol{k}}\right)\right] \tag{2.129}$$

$$z\hat{\zeta}'_{\boldsymbol{k}} = \hat{p}_{\boldsymbol{k}} = \frac{\sqrt{k}}{2i} \left[\hat{Q}_{\boldsymbol{k}} - \hat{Q}_{-\boldsymbol{k}} + i\left(\hat{P}_{\boldsymbol{k}} + \hat{P}_{-\boldsymbol{k}}\right)\right] \tag{2.130}$$

where every operator is represented in the Schrödinger picture. The condition $\tilde{O}(X) = O(X)$ is valid for $\hat{Q}^n_{\boldsymbol{k}}$ and $\hat{P}^n_{\boldsymbol{k}}$, namely, $\widetilde{Q^n_{\boldsymbol{k}}} = Q^n_{\boldsymbol{k}}$ and $\widetilde{P^n_{\boldsymbol{k}}} = P^n_{\boldsymbol{k}}$. However, the Weyl transform of their products can produce nontrivial terms e.g. $\widetilde{Q_{\boldsymbol{k}}P_{\boldsymbol{k}}} = Q_{\boldsymbol{k}}P_{\boldsymbol{k}} + i/2$. Nevertheless, one can show that such nontrivial terms cancel and eventually $\widetilde{\zeta^n_{\boldsymbol{k}}} = \zeta^n_{\boldsymbol{k}}$ is true [22]. This means that correlation functions of ζ such as $\left\langle \hat{\zeta}(\eta, \boldsymbol{x})\hat{\zeta}(\eta, \boldsymbol{y}) \right\rangle$ can be reproduced by a stochastic approach. The discussion so far does not rely on the large squeezing limit. Therefore, correlation functions of ζ always have a stochastic description despite the common name, the quantum-to-classical "transition". On the other hand, one can define improper operators, which implies the possibility that a quantum signature can be captured in cosmological perturbations. Among the following contents, Chap. 3 and Chap. 5 focus on a stochastic description while Chap. 4 and Chap. 6 focus on quantum aspects.

At last, let us briefly mention other arguments regarding the quantum-to-classical transition. The canonical commutation relation of the Mukhanov-Sasaki variable $[\hat{v}_{\boldsymbol{k}}, \hat{p}_{\boldsymbol{q}}] = i\delta\left(\boldsymbol{k} + \boldsymbol{q}\right)$ can be recast in terms of the field perturbation as

$$\left[\delta\hat{\phi}_{\boldsymbol{k}}, \delta\hat{\dot{\phi}}_{\boldsymbol{q}}\right] = \frac{i}{a^3}\delta(\boldsymbol{k} + \boldsymbol{q}) \,. \tag{2.131}$$

where we used $\hat{v}_{\boldsymbol{k}} = a\delta\hat{\phi}_{\boldsymbol{k}}$ and $\hat{p}_{\boldsymbol{k}} = a\delta\hat{\phi}'_{\boldsymbol{k}}$ at leading order in slow roll. When a scalar field is quantized on the Minkowski spacetime, the right-hand side should be simply

$i\delta(\boldsymbol{k}+\boldsymbol{q})$. However, the above expression suggests that $\delta\hat{\phi}_{\boldsymbol{k}}$ and $\delta\hat{\dot{\phi}}_{\boldsymbol{q}}$ become commutable like a classical field. Actually, this is ensured from the fact that the decaying mode of the curvature perturbation becomes negligible compared with the constant mode on superhorizon scales due to the large squeezing [17]. Indeed, from Eqs. (2.85), (2.86), (2.90), (2.102) and (2.111), we can see

$$v_k(\eta) = \alpha_k + \beta_k^* \simeq \cosh r + \sinh r \simeq e^r \tag{2.132}$$

$$p_k(\eta) = \alpha_k - \beta_k^* \simeq \cosh r - \sinh r \simeq e^{-r} \tag{2.133}$$

on superhorizon scales.

On the other hand, there is a fact that seems to suggest the opposite, that is to say, the enhancement of the entanglement. Quantum discord is defined as a difference that arises by evaluating two classically equivalent expressions for the mutual information in a quantum mechanical way. It was found that quantum discord increases due to the large squeezing [20]. This reminds us that the highly squeezed state is a physical realization of the EPR state.

The effects of decoherence have also been studied phenomenologically [93–95]. It is suggested that interaction with the environment reduces a quantum signature but the precise property of the decoherence in cosmology remains an open question.

Chapter 3

Stochastic inflation

In this chapter, we review the stochastic formalism of inflation, also called the stochastic inflation, and how it predicts observable quantities. This chapter is supposed to be preparation for Chap. 5 but is not minimal for that purpose. A reader who intends to go ahead to Chap. 5 quickly can jump to Sec. 3.3 after just noting that coarse-grained inflaton fields obey the Langevin equation (3.21) and their probability density function evolves according to the Fokker-Planck equation (3.23).

3.1 Stochastic equation of motion

In this section, we show the derivation of the Langevin equation by decomposing inflaton fields into IR fields and UV fields in their equation of motion. This method was developed in original works of the stochastic inflation and has been studied further including the extension to multi-field setups and the phase-space formulation, which is applicable beyond slow-roll [24,25,49,56,57,96]. On the other hand, this original method nowadays tends to be called the "heuristic" method because the first-principle derivation which makes use of the Schwinger-Keldysh formalism has been established recently [33,96]. Nevertheless, the heuristic approach has the advantage of being intuitive.

Let us consider the following action for multiple scalar fields with a canonical kinetic term,

$$S = \int \mathrm{d}^4x\,\sqrt{-g}\left[\frac{M_{\rm Pl}^2}{2}R - \frac{1}{2}g^{\mu\nu}\delta_{IJ}\partial_\mu\phi^I\partial_\nu\phi^J - V(\phi)\right]. \tag{3.1}$$

In more general contexts, the Kronecker delta δ_{IJ} can be replaced with a field space metric $G_{IJ}(\phi)$. The stochastic inflation with a non-canonical kinetic term has also been studied [34,96,97]. In what follows, we assume a canonical kinetic term for simplicity but do not assume slow roll.

The Hamilton equations for the background fields read

$$\frac{\mathrm{d}\hat{\phi}^I}{\mathrm{d}N} = \hat{\varpi}^I \tag{3.2}$$

$$\frac{\mathrm{d}\hat{\varpi}^I}{\mathrm{d}N} = -(3-\epsilon_1)\hat{\varpi}^I - \frac{\partial_{\phi^I}V(\hat{\phi})}{H^2} \tag{3.3}$$

where $\hat{\varpi}^I$ represents the (rescaled) conjugate momenta. At this stage, $\hat{\phi}^I$ and $\hat{\varpi}^I$ are quantum fields. In the standard perturbation theory, which is discussed until the previous

chapter, a full scalar field is decomposed into the background and the perturbation as $\phi^I(N,\boldsymbol{x}) = \bar{\phi}^I(N) + \delta\phi^I(N,\boldsymbol{x})$, where the background is treated as a classical field and the perturbation is treated as a quantum field. On the other hand, in stochastic inflation, a full scalar field is decomposed into the IR field (also known as the coarse-grained field) and the UV field as

$$\hat{\phi}^I = \hat{\phi}^I_{\rm IR} + \hat{\phi}^I_{\rm UV} \tag{3.4}$$

$$\hat{\phi}^I_{\rm IR} = \int \frac{{\rm d}^3k}{(2\pi)^{3/2}} \mathcal{W}\left(\frac{k}{k_\sigma(N)}\right) \hat{\phi}^I_{\boldsymbol{k}}\, e^{i\boldsymbol{k}\cdot\boldsymbol{x}} \tag{3.5}$$

$$\hat{\phi}^I_{\rm UV} = \int \frac{{\rm d}^3k}{(2\pi)^{3/2}} \left[1 - \mathcal{W}\left(\frac{k}{k_\sigma(N)}\right)\right] \hat{\phi}^I_{\boldsymbol{k}}\, e^{i\boldsymbol{k}\cdot\boldsymbol{x}} \tag{3.6}$$

where $k_\sigma(N) \equiv \sigma a H$ with $\sigma \ll 1$ is a coarse-graining scale and $\mathcal{W}\left(k/k_\sigma(N)\right)$ is a window function which collects larger scales than $k_\sigma(N)$, namely, k such that $k < k_\sigma(N)$ The same decomposition goes also for the conjugate momentum,

$$\hat{\varpi}^I = \hat{\varpi}^I_{\rm IR} + \hat{\varpi}^I_{\rm UV} \tag{3.7}$$

$$\hat{\varpi}^I_{\rm IR} = \int \frac{{\rm d}^3k}{(2\pi)^{3/2}} \mathcal{W}\left(\frac{k}{k_\sigma(N)}\right) \hat{\varpi}^I_{\boldsymbol{k}}\, e^{i\boldsymbol{k}\cdot\boldsymbol{x}} \tag{3.8}$$

$$\hat{\varpi}^I_{\rm UV} = \int \frac{{\rm d}^3k}{(2\pi)^{3/2}} \left[1 - \mathcal{W}\left(\frac{k}{k_\sigma(N)}\right)\right] \hat{\varpi}^I_{\boldsymbol{k}}\, e^{i\boldsymbol{k}\cdot\boldsymbol{x}} \tag{3.9}$$

with $\hat{\varpi}^I_{\boldsymbol{k}} = {\rm d}\hat{\phi}^I_{\boldsymbol{k}}/{\rm d}N$.

Then, stochastic inflation makes use of the separate universe approach [39, 41–46], where the homogeneous equations of motion are able to describe the inhomogeneous fields at leading order in the gradient expansion. By substituting the decompositions (3.4) and (3.7) into the unperturbed equations motion (3.2) and (3.3), up to linear order in the UV sector, one obtains the nonlinear equations of motion for the IR sector as

$$\frac{{\rm d}\hat{\phi}^I_{\rm IR}}{{\rm d}N} = \hat{\varpi}^I_{\rm IR} + \hat{\xi}^I_\phi(N) \tag{3.10}$$

$$\frac{{\rm d}\hat{\varpi}^I_{\rm IR}}{{\rm d}N} = -(3-\epsilon_1)\hat{\varpi}^I_{\rm IR} - \frac{\partial_{\phi^I} V(\hat{\phi}_{\rm IR})}{H^2} + \hat{\xi}^I_\varpi(N) \tag{3.11}$$

where the noise terms $\hat{\xi}^I_\phi$ and $\hat{\xi}^I_\varpi$ are given by

$$\hat{\xi}^I_\phi = \int \frac{{\rm d}^3k}{(2\pi)^{3/2}} \frac{{\rm d}\mathcal{W}}{{\rm d}N}\left(\frac{k}{k_\sigma(N)}\right) \hat{\phi}^I_{\boldsymbol{k}}\, e^{i\boldsymbol{k}\cdot\boldsymbol{x}} \tag{3.12}$$

$$\hat{\xi}^I_\varpi = \int \frac{{\rm d}^3k}{(2\pi)^{3/2}} \frac{{\rm d}\mathcal{W}}{{\rm d}N}\left(\frac{k}{k_\sigma(N)}\right) \hat{\varpi}^I_{\boldsymbol{k}}\, e^{i\boldsymbol{k}\cdot\boldsymbol{x}}\,. \tag{3.13}$$

Usually, the window function is taken as a Heaviside function $\mathcal{W}(k/k_\sigma(N)) = \theta(k_\sigma(N) - k)$. Then, its derivative gives a Dirac delta function and the correlations of the noise terms can be calculated as

$$\left\langle \hat{\xi}^I_\phi(N)\hat{\xi}^J_\phi(N')\right\rangle = \frac{{\rm d}\ln k_\sigma}{{\rm d}N}\mathcal{P}^{IJ}_{\phi\phi}\left(N, k_\sigma(N)\right)\delta(N-N') \tag{3.14}$$

$$\left\langle \hat{\xi}^I_\varpi(N)\hat{\xi}^J_\varpi(N')\right\rangle = \frac{{\rm d}\ln k_\sigma}{{\rm d}N}\mathcal{P}^{IJ}_{\varpi\varpi}\left(N, k_\sigma(N)\right)\delta(N-N') \tag{3.15}$$

$$\left\langle \hat{\xi}^I_\phi(N)\hat{\xi}^J_\varpi(N')\right\rangle = \left\langle \hat{\xi}^J_\varpi(N)\hat{\xi}^I_\phi(N')\right\rangle^* = \frac{{\rm d}\ln k_\sigma}{{\rm d}N}\mathcal{P}^{IJ}_{\phi\varpi}\left(N, k_\sigma(N)\right)\delta(N-N')\,. \tag{3.16}$$

Here, the amplitude of the noises is given by power spectra defined as

$$\left\langle \hat{A}^I_{\boldsymbol{k}}(N)\hat{B}^J_{\boldsymbol{p}}(N)\right\rangle = \frac{2\pi^2}{k^3}\mathcal{P}^{IJ}_{AB}(N,k)\delta(\boldsymbol{k}+\boldsymbol{p}) \tag{3.17}$$

where A, B represent ϕ or ϖ. Since $\mathrm{d}\ln k_\sigma/\mathrm{d}N = 1-\epsilon_1$, this quantity can be replaced by unity in the slow-roll regime and this approximation is even better for the ultra-slow-roll regime. Eqs. (3.14)-(3.16) are computed for a single spatial point. When computed for two different points, the right-hand sides should be multiplied by a cardinal sine function $\sin(k_\sigma r)/(k_\sigma r)$ where r represents the distance between the two points. However, the precise form of the spatial correlation depends on the window function. A common prescription is to replace the cardinal sine function with a Heaviside function, that is to say, to assume correlation 1 inside the coarse-graining scale and 0 outside.

The last step is to view the quantum operators $\hat{\xi}^I_\phi$ and $\hat{\xi}^I_\varpi$ as stochastic Gaussian noises with zero mean and (co-)variances given by Eqs. (3.14)-(3.16). This requires the real part of Eq. (3.16) to be much larger than its imaginary part, which is indeed true on superhorizon scales as is implied from Eqs. (2.132) and (2.133). Then, Eqs. (3.10) and (3.11) can be interpreted as the stochastic Langevin equations for the IR fields ϕ_{IR} and ϖ_{IR},

$$\frac{\mathrm{d}\phi^I_{\mathrm{IR}}}{\mathrm{d}N} = \varpi^I_{\mathrm{IR}} + \xi^I_\phi(N) \tag{3.18}$$

$$\frac{\mathrm{d}\varpi^I_{\mathrm{IR}}}{\mathrm{d}N} = -(3-\epsilon_1)\varpi^I_{\mathrm{IR}} - \frac{\partial_{\phi^I}V(\phi_{\mathrm{IR}})}{H^2(\phi_{\mathrm{IR}},\varpi_{\mathrm{IR}})} + \xi^I_\varpi(N) \tag{3.19}$$

where we have removed the hats to stress that we now work with stochastic quantities rather than quantum operators. Since the coarse-graining scale depends on time, new modes come from the UV modes to the IR modes as time passes, which is a physical interpretation of the origin of the noise terms. Hereafter, we will remove the subscript 'IR' for the conciseness of the display.

Let us comment on the validity of the separate universe approach. In the first place, Eqs. (3.2) and (3.3) hold for the background fields which do not have spatial dependence. In the computation leading to Eqs. (3.10) and (3.11), we assumed that the fields including perturbations also obey Eqs. (3.2) and (3.3) on superhorizon scales. In contrast, it has been pointed out that, when slow roll is violated, the perturbed background equation of motion with $\phi \to \phi + \delta\phi$ does not reproduce the correct perturbation equation obtained from the standard perturbations theory [98]. However, this happens just because one neglects metric perturbations. In fact, if one perturbs the time variable as well as the field, the resultant perturbed background equation coincides with the perturbation equation. This means that the separate universe approach is valid beyond slow roll [57]. Note also that when deriving the Langevin equations, the time coordinate (here the number of e-folds N) has not been perturbed, so the power spectra must be evaluated in the uniform-N gauge. On the other hand, the power spectra of the field perturbations are usually computed in the spatially-flat gauge. Since these two gauge choices are equivalent on superhorizon scales as discussed in Sec. 1.2, we can conclude that the e-folds N is the appropriate time variable in stochastic inflation [29, 57]. Otherwise, one would have to evaluate gauge corrections that arise in the noise terms.

Let us also mention the Markovian property of the stochastic process, where a Markovian process is such a process whose future behavior does not depend on its past history. The Langevin equations we obtained here do not strictly represent Markovian processes

since their diffusion terms are evaluated by the UV modes which evolve on the IR stochastic background. Nevertheless, the Markovian approximation is often adopted by assuming that the noise amplitude depends only on the IR fields themselves, which makes it possible to make use of the Fokker-Planck equation. This is safely justified for slowly-rolling light scalar fields [96]. We also obey this prescription in this thesis.

In slow-roll setups, the conjugate momenta are inferred from the fields as $\varpi \simeq -\partial_\phi V/(3H^2)$. It has also been shown that the quantum kick occurs in the direction of the slow-roll attractor [56]. Hence, we can discard the momenta from the dynamical variables in this case, and the Langevin equations for the coarse-grained fields become [52, 53]

$$\frac{\mathrm{d}\phi^I}{\mathrm{d}N} = -\frac{\partial_{\phi^I} V}{3H^2} + \frac{H}{2\pi}\xi^I(N) \tag{3.20}$$

with $\left\langle \xi^I(N)\xi^J(N')\right\rangle = \delta^{IJ}\delta(N-N')$, where the power spectra of the fields were deduced for light fields from Eq. (2.64).

The main point in this section is summarised in a general form as follows. At leading order in the gradient expansion, the quantum fields $\hat{\boldsymbol{\Phi}}$ can be described by classical random variables $\boldsymbol{\Phi}$. Here, $\boldsymbol{\Phi}$ is a vector containing the values of all coarse-grained fields, and possibly of their conjugate momenta in the case where deviations from the slow-roll attractor are considered. They obey stochastic Langevin equations of the form

$$\frac{\mathrm{d}\boldsymbol{\Phi}}{\mathrm{d}N} = \boldsymbol{F}_{\mathrm{cl}}\left(\boldsymbol{\Phi}\right) + \boldsymbol{\Xi}, \tag{3.21}$$

where $\boldsymbol{F}_{\mathrm{cl}}\left(\boldsymbol{\Phi}\right)$ encodes the classical equations of motion, and $\boldsymbol{\Xi}$ is a white Gaussian noise with vanishing mean, and variance given by

$$\left\langle \Xi_i\left(\boldsymbol{x},N\right)\Xi_j\left(\boldsymbol{x},N'\right)\right\rangle = \frac{\mathrm{d}\ln k_\sigma}{\mathrm{d}N}\mathcal{P}_{\Phi_i,\Phi_j}\left(N,k_\sigma(N)\right)\delta(N-N'), \tag{3.22}$$

which describes the continuous inflow of modes into the coarse-grained sector.

3.2 Fokker-Planck equation and Ito-Stratonovich dilemma

The Langevin equation (3.21) gives rise to a Fokker-Planck equation that drives the probability to find the field at position $\boldsymbol{\Phi}$ in field space at time N, given that it was at position $\boldsymbol{\Phi}_{\mathrm{in}}$ at a previous time N_{in},

$$\frac{\partial}{\partial N}P\left(\boldsymbol{\Phi},N|\boldsymbol{\Phi}_{\mathrm{in}},N_{\mathrm{in}}\right) = \mathcal{L}_{\mathrm{FP}}\left(\boldsymbol{\Phi}\right)\cdot P\left(\boldsymbol{\Phi},N|\boldsymbol{\Phi}_{\mathrm{in}},N_{\mathrm{in}}\right). \tag{3.23}$$

In this expression, $\mathcal{L}_{\mathrm{FP}}\left(\boldsymbol{\Phi}\right)$ is a differential operator of second order in phase space (*i.e.* it contains first and second derivatives with respect to the field coordinates Φ_i), called the Fokker-Planck operator. In order to write down the precise form of the Fokker-Planck operator, we need to address the so-called Ito-Stratonovich dilemma. As will be mentioned at the end of this section, this problem has less importance in our work presented in Chap. 5, so the following is dedicated to a comprehensive review. See *e.g.* Refs. [99, 100] for the details of the mathematics explained below.

In fact, the Langevin equation (3.21) does not *a priori* determine the physics uniquely because of the non-uniqueness of the definition of the stochastic integral. To illustrate

this simply, let us consider a one-dimensional autonomous SDE for a stochastic process $X(t)$,

$$\frac{\mathrm{d}X(t)}{\mathrm{d}t} = h\left(X(t)\right) + g\left(X(t)\right)\xi(t) \tag{3.24}$$

with $\langle \xi(t)\xi(t')\rangle = \delta(t-t')$.[1] It can be written in integral form as

$$X(T) - X(0) = \int_0^T h\left(X(t)\right)\mathrm{d}t + \int_0^T g\left(X(t)\right)\mathrm{d}W(t) \tag{3.25}$$

where $W(t)$ is the Wiener process, which is a continuous stochastic process with $W(0) = 0$ that satisfies the following property: for a partition of time, $0 = t_0 \leq t_1 \leq \cdots \leq t_n = T$, the increments $\{W(t_{j+1}) - W(t_j)\}_j$ are independent and each of them obeys a Gaussian distribution with mean 0 and variance $t_{j+1} - t_j$. Mathematically, this process is indifferentiable while physicists often write $\xi(t) = \mathrm{d}W(t)/\mathrm{d}t$. The first term of Eq. (3.25) is the Riemann integral, whose definition

$$\int_0^T h\left(X(t)\right)\mathrm{d}t = \lim_{n\to\infty}\sum_{j=0}^{n-1} h\left(X(t_{*j})\right)\left(t_{j+1} - t_j\right) \tag{3.26}$$

does not depend on the precise position of the representative points $t_{*j} \in [t_j, t_{j+1}]$. On the other hand, the second term is a stochastic integral, whose definition

$$\int_0^T g\left(X(t)\right)\mathrm{d}W(t) = \lim_{n\to\infty}\sum_{j=0}^{n-1} g\left(X(t_{*j})\right)\left(W(t_{j+1}) - W(t_j)\right)\,. \tag{3.27}$$

does depend on how to take t_{*j}. It is often parametrized by α with $t_{*j} = (1-\alpha)t_j + \alpha t_{j+1}$. There are two common choices; $\alpha = 0$ defines the Ito integral [101] while $\alpha = 1/2$ defines the Stratonovich integral [102]. Let us explain some properties of them. For a function $f(x)$, the standard chain rule for derivatives holds only for the Stratonovich integral,

$$\begin{aligned}
\mathrm{d}f\left(X(t)\right) &= f'\left(X(t)\right)\mathrm{d}X(t) && (3.28)\\
&= f'\left(X(t)\right)h\left(X(t)\right)\mathrm{d}t + f'\left(X(t)\right)g\left(X(t)\right)\circ\mathrm{d}W(t) \qquad \text{(Stratonovich)} && (3.29)
\end{aligned}$$

where we followed the convention to write $\circ\,\mathrm{d}W(t)$ for the Stratonovich integral. For the Ito integral, it becomes

$$\begin{aligned}
\mathrm{d}f\left(X(t)\right) = &\left[f'\left(X(t)\right)h\left(X(t)\right) + \frac{1}{2}f''\left(X(t)\right)g^2\left(X(t)\right)\right]\mathrm{d}t\\
&+ f'\left(X(t)\right)g\left(X(t)\right)\mathrm{d}W(t) \qquad \text{(Ito)}\,. \qquad (3.30)
\end{aligned}$$

This relation is called the Ito lemma, which is summarized symbolically as

$$\mathrm{d}W(t)\mathrm{d}W(t) = \mathrm{d}t, \quad \mathrm{d}W(t)\mathrm{d}t = 0, \quad \mathrm{d}t\mathrm{d}t = 0 \qquad \text{(Ito)}\,. \tag{3.31}$$

In addition, it can be shown that the expectation value of the Ito integral is always zero. For example, by taking $h = 0$, $g = 1$ and $f(x) = x^2/2$, one can show that

[1] If the diffusion term depends only on time, which is the case for spectator fields, there is not subtlety described below. However, the diffusion terms in the Langevin equations for inflaton fields do depend on the fields.

$\int_0^T W(t)\mathrm{d}W(t) = W^2(T)/2 - T/2$ for the Ito integral and $\int_0^T W(t) \circ \mathrm{d}W(t) = W^2(T)/2$ for the Stratonovich integral. Provided that a stochastic process $X(t)$ obeys an Ito SDE written as Eq. (3.24), the same process can also be described by a Stratonovich SDE

$$\frac{\mathrm{d}X(t)}{\mathrm{d}t} = h\left(X(t)\right) - \frac{1}{2}g\left(X(t)\right)g'\left(X(t)\right) + g\left(X(t)\right) \circ \xi(t)\,. \tag{3.32}$$

Now let us discuss what the non-uniqueness of the stochastic integral explained above implies to the stochastic inflation. In the stochastic inflation, the Langevin equation (3.21) does not come with any scheme of the stochastic integral. Depending on which type of SDE we interpret it as, it gives different physical predictions, that is to say,

$$\text{SDE} \to \begin{cases} \text{Theory 1} \\ \text{Theory 2} \end{cases}. \tag{3.33}$$

On the other hand, the actual physical theory should be determined uniquely and it can be described by either Ito or Stratonovich SDE as illustrated in Eq. (3.32), namely,

$$\text{Theory} \to \begin{cases} \text{Ito SDE} \\ \text{Stratonovich SDE}\,. \end{cases} \tag{3.34}$$

Then, the question is which type of SDE the Langevin equation of the form of Eq. (3.21) should represent, which has been under dispute [29, 33, 50, 96, 97, 103]. The recent works [96,97] showed, by considering a general curved field space, that only the Stratonovich scheme respects the field-space covariance because it validates the standard chain rule. They also stressed that the original Langevin equations with the Stratonovich interpretation is equivalent to an Ito-type Langevin equation with the same form where the derivatives are replaced with what they call the Ito-covariant derivatives.

In the case of a flat field space, the Langevin equation Eq. (3.21) can be recast as the Fokker-Planck equation, which is expressed for each scheme as

$$\frac{\partial}{\partial N}P = -\frac{\partial}{\partial \Phi_i}\left[F_{\mathrm{cl},i}P\right] + \frac{1}{2}\frac{\partial^2}{\partial\Phi_i\partial\Phi_j}\left[G_{ia}G_{ja}P\right] \qquad \text{(Ito)} \tag{3.35}$$

$$\frac{\partial}{\partial N}P = -\frac{\partial}{\partial \Phi_i}\left[\left(F_{\mathrm{cl},i} + \frac{1}{2}G_{ja}\frac{\partial}{\partial\Phi_j}G_{ia}\right)P\right] + \frac{1}{2}\frac{\partial^2}{\partial\Phi_i\partial\Phi_j}\left[G_{ia}G_{ja}P\right] \tag{3.36}$$

$$= -\frac{\partial}{\partial \Phi_i}\left[F_{\mathrm{cl},i}P\right] + \frac{1}{2}\frac{\partial}{\partial\Phi_i}\left[G_{ia}\frac{\partial}{\partial\Phi_j}\left(G_{ja}P\right)\right] \qquad \text{(Stratonovich)} \tag{3.37}$$

with $P \equiv P\left(\boldsymbol{\Phi}, N|\boldsymbol{\Phi}_{\mathrm{in}}, N_{\mathrm{in}}\right)$. When writing down these expressions, we assumed that the diffusion term is written as $\Xi_i = G_{ia}\xi_a$ with $\langle\xi_a(N)\xi_b(N')\rangle = \delta_{ab}\delta(N-N')$. Note that the covariance matrix of $\boldsymbol{\Xi}$ does not uniquely determine the "square root" G_{ia}. Hence, although the Ito Fokker-Planck equation depends only on the covariance matrix $G_{ia}G_{ja}$, for other schemes, the choice of G_{ia} (*i.e.* the choice of vielbeins) would induce the field-space frame dependence in general. However, in stochastic inflation, there is a natural frame preferred by independent creation and annihilation operators [96].

The generic formalism we construct in Sec. 5.1 does not specify the details of the Fokker-Planck operator and is therefore independent of the choice of discretization scheme. Since the differences amongst the discretization schemes arise from the derivative of the diffusion term with respect to the fields, those differences are invisible in the single-field slow-roll case, where the diffusion term is given by the almost constant Hubble parameter. Therefore, for the specific model we later consider in Sec. 5.2, all discretization schemes give the same result.

3.3 Stochastic-δN formalism and first-passage-time analysis

We have seen that the inflaton fields coarse-grained over superhorizon scales obey the Langevin equation (3.21) and its probability density function evolves according to the Fokker-Planck equation (3.23). In this section, we show how this picture can predict observable quantities. A similar review is also shown in our previous paper [80].

3.3.1 Stochastic-δN formalism

Recall that, as we showed in Sec. 1.4, curvature perturbations on superhorizon scales are related to the amount of expansion $N = \ln a$ from an initial flat space-time slice to a final space-time slice of uniform energy density ρ,

$$\zeta(t, \boldsymbol{x}) = N(t, \boldsymbol{x}) - \overline{N}(t) \equiv \delta N \,, \tag{3.38}$$

where $\overline{N}(t)$ is the unperturbed number of e-folds. In the separate universe approach (the validity of which has recently been shown to extend beyond slow roll in Ref. [57]), on superhorizon scales, gradients can be neglected, so $N(t, \boldsymbol{x})$ is the amount of expansion in unperturbed, homogeneous universes. The curvature perturbations ζ can thus be extracted from the knowledge of the durations of inflation in such universes. These durations vary under quantum fluctuations in the fields that drive inflation, which can be described in the stochastic inflation formalism.

The duration of inflation under the process (3.21), starting from the location $\boldsymbol{\Phi}_{\rm in}$ in field space, is a random variable that we denote $\mathcal{N}$. The probability density function $\mathcal{N}$, $P_{\rm FPT}(\mathcal{N}, \boldsymbol{\Phi}_{\rm in})$, can be shown to obey the adjoint Fokker-Planck equation [29, 54]

$$\frac{\mathrm{d}P_{\rm FPT}(\mathcal{N}, \boldsymbol{\Phi})}{\mathrm{d}\mathcal{N}} = \mathcal{L}^{\dagger}_{\rm FP}\left(\boldsymbol{\Phi}\right) \cdot P_{\rm FPT}(\mathcal{N}, \boldsymbol{\Phi}), \tag{3.39}$$

where $\mathcal{L}^{\dagger}_{\rm FP}(\boldsymbol{\Phi})$ is the adjoint Fokker-Planck operator, related to the Fokker-Planck operator via $\int \mathrm{d}\boldsymbol{\Phi}\, f_1(\boldsymbol{\Phi}) \mathcal{L}_{\rm FP}(\boldsymbol{\Phi}) \cdot f_2(\boldsymbol{\Phi}) = \int \mathrm{d}\boldsymbol{\Phi}\, f_2(\boldsymbol{\Phi}) \mathcal{L}^{\dagger}_{\rm FP}(\boldsymbol{\Phi}) \cdot f_1(\boldsymbol{\Phi})$. Since Eq. (3.39) is a partial differential equation, it needs to be solved with some boundary conditions. The first condition is given by the end-of-inflation surface $\mathcal{C}_{\rm end} = \{\boldsymbol{\Phi}, \rho(\boldsymbol{\Phi}) = \rho_{\rm end}\}$,[2] where the number of inflationary e-folds necessarily vanishes, hence $P_{\rm FPT}(\mathcal{N}, \boldsymbol{\Phi}) = \delta(\mathcal{N})$ for $\boldsymbol{\Phi} \in \mathcal{C}_{\rm end}$. In hilltop models, $\mathcal{C}_{\rm end}$ makes the inflating domain of field space compact and is enough to fully specify the problem. Otherwise, another boundary condition has to be added, which in practice we take to be a reflective boundary condition high enough in the potential [52, 53], along some surface $\mathcal{C}_{\rm uv}$, such that $[\boldsymbol{u}(\boldsymbol{\Phi}) \cdot \boldsymbol{\nabla}] P_{\boldsymbol{\Phi}}\left(\mathcal{N}\right) = 0$ when $\boldsymbol{\Phi} \in \mathcal{C}_{\rm uv}$, where $\boldsymbol{u}$ is a field-space vector orthogonal to $\mathcal{C}_{\rm uv}$. The details of this second boundary condition are anyway irrelevant as long as inflation proceeds at sub-Planckian energies [52, 53].

From Eq. (3.39), the statistics of $\mathcal{N}$, hence of $\delta\mathcal{N} = \mathcal{N} - \langle\mathcal{N}\rangle$ (where $\langle\cdot\rangle$ denotes statistical average), and in turn, the one of ζ through Eq. (3.38), can be inferred. This is

[2] In single-field inflation, assuming that the slow-roll attractor has been reached before the end of inflation, the field and its conjugated momentum are directly related, so inflation ends through a single point in field phase space, and $\rho_{\rm end}$ can be taken as the energy density at that point. The situation is more involved in multiple-field systems, but assuming that quantum diffusion becomes negligible when inflation terminates, the choice of the precise value for $\rho_{\rm end}$ becomes irrelevant.

the stochastic-δN program. Since the power spectrum corresponds to the two-point function of curvature perturbations, in practice, one needs to compute the two first moments of $\mathcal{N}$, given that $\langle\delta\mathcal{N}^2\rangle = \langle\mathcal{N}^2\rangle - \langle\mathcal{N}\rangle^2$. By applying the adjoint Fokker-Planck operator to the definition of the $n^{\rm th}$ moment of $\mathcal{N}$, $\langle\mathcal{N}^n\rangle(\mathbf{\Phi}) = \int P_{\rm FPT}(\mathcal{N},\mathbf{\Phi})\mathcal{N}^n \mathrm{d}\mathcal{N}$, after integration by part, one obtains the iterative set of differential equations [29]

$$\mathcal{L}^\dagger_{\rm FP}\left(\mathbf{\Phi}\right)\cdot\langle\mathcal{N}^n\rangle(\mathbf{\Phi}) = -n\langle\mathcal{N}^{n-1}\rangle(\mathbf{\Phi}). \tag{3.40}$$

Starting from $\langle\mathcal{N}^0\rangle = 1$, one can then solve iteratively for $\langle\mathcal{N}\rangle$ and $\langle\mathcal{N}^2\rangle$.

Let us stress that $P_{\rm FPT}(\mathcal{N},\mathbf{\Phi})$ corresponds to the distribution of $\mathcal{N}$ associated with a given initial point $\mathbf{\Phi}$ in field space. However, as explained in Introduction, in order to make contact with observations, one should determine the distribution of $\mathcal{N}$ associated with a given scale k. The link between $\mathbf{\Phi}$ and k thus remains to be specified, and this is the goal of our work presented in Chap. 5.

3.3.2 Power spectrum in the low-diffusion limit

In the regime where the stochastic noise plays a negligible role in the Langevin equation (3.21), at first order in the noise, all realisations follow the classical, deterministic equation of motion. The value of the fields $\mathbf{\Phi}$ at the time when the scale k crosses out the Hubble radius, *i.e.* when $k = aH$, is therefore the same for all realizations, which defines the function $\mathbf{\Phi}_{\rm cl}(k)$, which can be inverted into the function $k_{\rm cl}(\mathbf{\Phi})$.

At this order, the fluctuations in the duration of inflation starting from $\mathbf{\Phi}_{\rm in}$ will receive a contribution from all modes that cross out the Hubble radius between the time when $\mathbf{\Phi} = \mathbf{\Phi}_{\rm in}$ and the end of inflation, *i.e.* from all modes k such that $k_{\rm cl}(\mathbf{\Phi}_{\rm in}) < k < k_{\rm end}$, where $k_{\rm end}$ corresponds to the Hubble scale at the end of inflation. One thus has [49]

$$\left\langle\delta\mathcal{N}^2(\mathbf{\Phi})\right\rangle = \int_{k_{\rm cl}(\mathbf{\Phi})<k<k_{\rm end}} \mathcal{P}_\zeta(k)\mathrm{d}\ln k. \tag{3.41}$$

A detailed derivation of this (otherwise intuitive) formula will be provided in Sec. 5.1, but for now, let us note that by differentiating both hands with respect to the field-space coordinate along the background, classical trajectory, one obtains

$$\mathcal{P}_\zeta(k) = -\frac{\mathrm{d}\left\langle\delta\mathcal{N}^2\right\rangle\left[\mathbf{\Phi}_{\rm cl}(k)\right]}{\mathrm{d}\ln(k)}\,. \tag{3.42}$$

3.3.3 Case of a slowly-rolling single field

For illustrative purpose, let us apply the above calculational program to the case of a single field in the slow-roll regime, and see how the standard formula for the power spectrum can be recovered. For a single scalar field ϕ with a canonical kinetic term and potential function $V(\phi)$, in the slow-roll regime, the Fokker-Planck and adjoint Fokker-Planck operators are respectively given by [24, 25] (see Eqs. (3.20) and (3.35))[3]

$$\frac{1}{M_{\rm Pl}^2}\mathcal{L}_{\rm FP}(\phi)\cdot f = \frac{\partial}{\partial\phi}\left[\frac{v'(\phi)}{v(\phi)}f(\phi)\right] + \frac{\partial^2}{\partial\phi^2}\left[v(\phi)f(\phi)\right] \tag{3.43}$$

$$\frac{1}{M_{\rm Pl}^2}\mathcal{L}^\dagger_{\rm FP}(\phi)\cdot f = -\frac{v'(\phi)}{v(\phi)}\frac{\partial}{\partial\phi}f(\phi) + v\frac{\partial^2}{\partial\phi^2}f(\phi)\,, \tag{3.44}$$

[3] Although these are expressed for the Ito scheme, the difference from other schemes is suppressed as $\sim V/M_{\rm Pl}^4$ in this case.

where f is a dummy function on which the differential operators act, a prime denotes the derivative with respect to the field value ϕ, and we have introduced the reduced potential

$$v(\phi) = \frac{V(\phi)}{24\pi^2 M_{\rm Pl}^4} \tag{3.45}$$

for convenience. This allows one to integrate Eq. (3.40) exactly, and one obtains [29, 52]

$$\langle \mathcal{N}^n \rangle (\phi) = n \int_{\phi_{\rm end}}^{\phi} \frac{{\rm d}\phi_1}{M_{\rm Pl}} \int_{\phi_1}^{\phi_{\rm uv}} \frac{{\rm d}\phi_2}{M_{\rm Pl}} \frac{\langle \mathcal{N}^{n-1} \rangle (\phi_2)}{v(\phi_2)} \exp\left[\frac{1}{v(\phi_2)} - \frac{1}{v(\phi_1)} \right], \tag{3.46}$$

where $\phi_{\rm end}$ is the value of ϕ at the end of inflation, such that $\langle \mathcal{N}^n \rangle(\phi_{\rm end}) = 0$, and the upper bound of the second integral is set to $\phi_{\rm uv}$ in order to satisfy the second boundary condition, namely $\langle \mathcal{N}^n \rangle'(\phi_{\rm uv}) = 0$. This formula allows one to compute all moments iteratively, for any potential function $v(\phi)$.

Let us now consider the low-diffusion limit. Since v measures the potential energy in Planckian units, $1/v \gg 1$ in the regime of interest, which allows one to perform a saddle-point expansion of the integrals appearing in Eq. (3.46), owing to the large exponential terms. Under the condition $|v''|\, v^2 \ll v'^2$ (which imposes that the slope of the potential is large enough so that the classical drift dominates over quantum diffusion), one obtains [29]

$$\langle \mathcal{N} \rangle (\phi) \simeq \int_{\phi_{\rm end}}^{\phi} \frac{{\rm d}\bar{\phi}}{M_{\rm Pl}^2} \frac{v(\bar{\phi})}{v'(\bar{\phi})} \tag{3.47}$$

$$\langle \delta\mathcal{N}^2 \rangle (\phi) \simeq 2 \int_{\phi_{\rm end}}^{\phi} \frac{{\rm d}\bar{\phi}}{M_{\rm Pl}^4} \frac{v^4(\bar{\phi})}{v'^3(\bar{\phi})} \,. \tag{3.48}$$

At leading order in slow roll where H is almost constant, $k/k_{\rm end} = a_{\rm cl}(k) H_{\rm cl}(k)/(a_{\rm end} H_{\rm end}) \simeq e^{N_{\rm cl}(k) - N_{\rm end}}$, hence the derivative with respect to $\ln(k)$ in Eq. (3.42) is the derivative with respect to $N_{\rm cl}(k) - N_{\rm end} \simeq -\langle \mathcal{N} \rangle [\phi_{\rm cl}(k)]$, which gives rise to

$$\mathcal{P}_\zeta(k) \simeq \frac{\langle \delta\mathcal{N}^2 \rangle' [\phi_{\rm cl}(k)]}{\langle \mathcal{N} \rangle' [\phi_{\rm cl}(k)]} \simeq \frac{2}{M_{\rm Pl}^2} \frac{v^3 [\phi_{\rm cl}(k)]}{v'^2 [\phi_{\rm cl}(k)]} \,. \tag{3.49}$$

In the last equality, we have made use of Eqs. (3.47) and (3.48). In this way, one recovers the standard formula for the power spectrum of curvature perturbations in single-field slow-roll inflation [88, 104]. An important remark is that the validity of this formula relies on assuming quantum diffusion to be low not only at the time when the observed scales are produced, but also at any later time during inflation. While the former condition is known to be satisfied for the scales observed in the CMB, the latter condition is not guaranteed, and is even explicitly violated in models giving rise to large cosmological perturbations on small scales, in particular those leading to primordial black holes. The goal of Chap. 5 is therefore to go beyond those approximations.

Chapter 4

Bell experiments in cosmology

In this chapter, we describe preceding studies on Bell experiments in the context of cosmology. Based on this chapter, we will show our original work in Chap. 6.

4.1 Clauser-Horne-Shimony-Holt (CHSH) scenario

In quantum theories, strong correlations that are impossible classically can be realized. Bell inequalities [64] are used to characterize such a quantum nature. They hold under some classical assumptions and their violations indicate the existence of quantum effects. The most famous class of such inequalities comes from the Clauser-Horne-Shimony-Holt (CHSH) scenario [65], which we briefly review in this section.

What the CHSH scenario tries to test is two assumptions: "realism" and "locality". In this context, "realism" is the assumption that, at each instant in time, the system definitely lies in one of several distinct configurations. The state of the system determines all measurement outcomes exactly, such that all observables possess pre-existing definite values. The principle of locality states that a system cannot be influenced by a spacelike-separated event, and rules out the concept of instantaneous "action at a distance".

In the CHSH scenario, two observers, commonly dubbed Alice and Bob, perform measurements of dichotomic variables $\hat{S}^a$ (for instance, spin variables, where "a" labels the direction of the polarizer) for two subsystems '1' and '2' at separate spatial locations x_1 and x_2, and build the correlator

$$E(a,b) = \left\langle \hat{S}_1^a \hat{S}_2^b \right\rangle . \tag{4.1}$$

From a simple arithmetic calculation, one can show that

$$-1 \leq a, b, a', b' \leq 1 \quad \Rightarrow \quad a(b+b') + a'(b-b') \leq 2 . \tag{4.2}$$

Under the assumptions of "realism" and "locality", the correlator should be calculated as a stochastic average,

$$E(a,b) = \int \mathrm{d}\lambda \, a(\lambda) b(\lambda) P(\lambda) \tag{4.3}$$

where λ is a local hidden variable and $P(\lambda)$ is its probability density function. Multiplying Eq. (4.2) by $P(\lambda)$ and integrating with λ, one obtains

$$B \equiv E(a,b) + E(a,b') + E(a',b) - E(a',b') \leq 2 . \tag{4.4}$$

The violation of this inequality features a quantum signature. In fact, it is known that the Bell operator B can become as large as $B \leq 2\sqrt{2}$ in quantum theory, which is called the Cirel'son bound [105]. Particularly, we refer to the above inequality as a spatial Bell inequality since we will consider a temporal version of it later.

4.2 Continuous variables to dichotomic variables

As is described in the previous section, Bell experiments make use of dichotomic variables such as spin variables. They do not have to be actual spins that represent angular momentum, so one can construct dichotomic variables (called pseudo-spin variables in this context) for a continuous-variable system. Hence, it can be done for adiabatic scalar perturbations in cosmology. Also, since inflation creates highly entangled states (see Sec. 2.3), they are expected to show violations of Bell inequalities. Although there would be theoretical and practical challenges, if violations of Bell inequalities are detected, it becomes direct evidence that the structure of the universe has a quantum origin, which is a big goal. That is why Bell inequalities have also been studied in the context of cosmology [71–75]. In this section, we describe how to construct pseudo-spin operators.

As shown in Eq. (2.98), the Hilbert space for cosmological perturbations is given by a product of bipartite systems each of which contains $\boldsymbol{k}$ and $-\boldsymbol{k}$ modes as two subsystems. Therefore, $\boldsymbol{k}$ and $-\boldsymbol{k}$ correspond to the subscripts '1' and '2' in Eq. (4.1), which is written for a general context. In order to construct dichotomic variables, one can make use of the "position" and "momentum" variables, $Q_{\boldsymbol{k}}$ and $P_{\boldsymbol{k}}$, defined in Eqs. (2.114) and (2.115). Recall that these operators are defined for each mode and do not mix $\boldsymbol{k}$ and $-\boldsymbol{k}$. Following Larsson [106], let us introduce the following pseudo-spin operators,

$$\hat{S}_{x,\boldsymbol{k}}(\ell) = \hat{S}_{+,\boldsymbol{k}}(\ell) + \hat{S}_{-,\boldsymbol{k}}(\ell) \tag{4.5}$$

$$\hat{S}_{y,\boldsymbol{k}}(\ell) = -i\left[\hat{S}_{+,\boldsymbol{k}}(\ell) - \hat{S}_{-,\boldsymbol{k}}(\ell)\right] \tag{4.6}$$

$$\hat{S}_{z,\boldsymbol{k}}(\ell) = \sum_{n=-\infty}^{\infty}(-1)^n \int_{n\ell}^{(n+1)\ell} \mathrm{d}Q_{\boldsymbol{k}} |Q_{\boldsymbol{k}}\rangle\langle Q_{\boldsymbol{k}}| \tag{4.7}$$

with

$$\hat{S}_{+,\boldsymbol{k}}(\ell) = \sum_{n=-\infty}^{\infty} \int_{2n\ell}^{(2n+1)\ell} \mathrm{d}Q_{\boldsymbol{k}}\, |Q_{\boldsymbol{k}}\rangle\langle Q_{\boldsymbol{k}} + \ell| \tag{4.8}$$

and $\hat{S}_{-,\boldsymbol{k}}(\ell) = \hat{S}^{\dagger}_{+,\boldsymbol{k}}(\ell)$. Here, $\hat{S}_{x,\boldsymbol{k}}(\ell)$, $\hat{S}_{y,\boldsymbol{k}}(\ell)$ and $\hat{S}_{z,\boldsymbol{k}}(\ell)$ obey the standard $SU(2)$ commutation relations. Their definition contains a parameter ℓ, which is to be determined by an observer.

In our work shown in Chap. 6, we need only $\hat{S}_{z,\boldsymbol{k}}(\ell)$ given in Eq. (4.7). The reason will be explained in the following section. In practice, measuring $\hat{S}_{z,\boldsymbol{k}}(\ell)$ can be done by measuring $Q_{\boldsymbol{k}}$, identifying in which interval $[n\ell, (n+1)\ell)$ of size ℓ it lies, and returning $(-1)^n$. The variable $\hat{S}_{z,\boldsymbol{k}}(\ell)$ is therefore dichotomic (it can take values $+1$ or -1), as can also be explicitly checked from Eq. (4.7) by verifying that $\hat{S}_{z,\boldsymbol{k}}(\ell)^2 = 1$. In the limit where ℓ is infinite, $\hat{S}_{z,\boldsymbol{k}}(\ell)$ reduces to the sign operator,

$$\hat{S}_{z,\boldsymbol{k}}(\ell \to \infty) = \mathrm{sign}\left(\hat{Q}_{\boldsymbol{k}}\right). \tag{4.9}$$

Let us also mention that there are other ways to define dichotomic variables for continuous systems [107–109], see Refs. [23, 75] for review. Some of those pseudo-spin operators are defined in terms of the Fock space. Compared with them, it is easy to understand experimental protocols to measure the Larsson's spin operator. Its z component particularly has a clear interpretation as described above since it is diagonal with respect to the position variable.

4.3 Obstruction of Bell experiments in cosmology

Using pseudo-spin operators introduced in the previous section, one can calculate the Bell operator shown in Eq. (4.4) for a given state. As demonstrated in Sec. 2.3, cosmological perturbations take two-mode squeezed states. It has been shown that the spatial Bell inequality can be violated in two-mode squeezed states in the large squeezing limit [72]. However, it has been suggested that such violations should not be observable in the context of cosmology in principle [75]. The discussion involves something subtle and complicated since it addresses the measurement problem of quantum mechanics in the context of cosmology. In this section, we describe the essence of that argument.

First, let us stress that, as discussed in Sec. 2.4, a proper operator has a stochastic description when the Wigner function is positive definite, which is the case for squeezed states. Recall that a proper operator is such an operator that its eigenvalues coincide with the values which its Weyl transform takes, where the Weyl transform is defined in Eq. (2.122). On the other hand, according to the discussion in Sec. 4.1, a stochastic description ensures that spatial Bell inequalities are satisfied. Hence, improper operators are needed for violations of spatial Bell inequalities. The Weyl transforms of the Larsson's spin operators given in Eqs. (4.5)-(4.7) can be calculated as

$$\widetilde{S_{x,\boldsymbol{k}}}(Q_{\boldsymbol{k}}, P_{\boldsymbol{k}}) = 2\sum_{n=-\infty}^{+\infty} \cos\left(P_{\boldsymbol{k}}\ell\right)\left[\theta\left(Q_{\boldsymbol{k}} - n\ell - \frac{\ell}{2}\right) - \theta\left(Q_{\boldsymbol{k}} - n\ell - \frac{3}{2}\ell\right)\right] \tag{4.10}$$

$$\widetilde{S_{y,\boldsymbol{k}}}(Q_{\boldsymbol{k}}, P_{\boldsymbol{k}}) = 2\sum_{n=-\infty}^{+\infty} \sin\left(P_{\boldsymbol{k}}\ell\right)\left[\theta\left(Q_{\boldsymbol{k}} - n\ell - \frac{\ell}{2}\right) - \theta\left(Q_{\boldsymbol{k}} - n\ell - \frac{3}{2}\ell\right)\right] \tag{4.11}$$

$$\widetilde{S_{z,\boldsymbol{k}}}(Q_{\boldsymbol{k}}, P_{\boldsymbol{k}}) = \sum_{n=-\infty}^{+\infty} (-1)^n \left[\theta\left(Q_{\boldsymbol{k}} - n\ell\right) - \theta\left(Q_{\boldsymbol{k}} - n\ell - \ell\right)\right], \tag{4.12}$$

where $\theta(\cdot)$ is the Heaviside function. These expressions show that $\hat{S}_{x,\boldsymbol{k}}$ and $\hat{S}_{y,\boldsymbol{k}}$ are improper while $\hat{S}_{z,\boldsymbol{k}}$ is proper. Therefore, measuring $\hat{S}_{x,\boldsymbol{k}}$ or $\hat{S}_{y,\boldsymbol{k}}$ is necessary to detect violations of spatial Bell inequalities.

Next, let us consider if the pseudo-spin operators are observable in cosmology. In laboratory experiments, for example, one can first measure the x-component of the spin, and then repeat the experiment and measure the z-component. However, we are "given" measurements in cosmology. We know $\zeta_{\boldsymbol{k}}$ through the measurements of the CMB temperature anisotropy. From Eqs. (2.129) and (2.130), the "position" operator can be expressed as

$$\hat{Q}_{\boldsymbol{k}} = \frac{z\sqrt{k}}{2}\left(\hat{\zeta}_{\boldsymbol{k}} + \hat{\zeta}_{-\boldsymbol{k}}\right) + \frac{z}{2\sqrt{k}}\left(\hat{\zeta}'_{\boldsymbol{k}} - \hat{\zeta}'_{-\boldsymbol{k}}\right). \tag{4.13}$$

Since the decaying mode is negligible, a measurement of $\hat{\zeta}_{\boldsymbol{k}}$ is a measurement of $\hat{Q}_{\boldsymbol{k}}$. Now the question is whether the pseudo-spin operators can be inferred given a result of

a measurement of $\hat{Q}_{\boldsymbol{k}}$. This can be studied by calculating commutators. One can show that the z-component commutes with $\hat{Q}_{\boldsymbol{k}}$,

$$\left[\hat{S}_{z,\boldsymbol{k}}, \hat{Q}_{\boldsymbol{k}}\right] = 0, \tag{4.14}$$

which indicates that $\hat{S}_{z,\boldsymbol{k}}$ is observable. In fact, we already described a practical manner to infer $\hat{S}_{z,\boldsymbol{k}}$ from a measurement of $\hat{Q}_{\boldsymbol{k}}$ above Eq. (4.9). On the other hand, one can show that the x-component and y-component are incompatible with a measurement of $\hat{Q}_{\boldsymbol{k}}$ because

$$\left[\hat{S}_{x,\boldsymbol{k}}, \hat{Q}_{\boldsymbol{k}}\right] \neq 0\,, \qquad \left[\hat{S}_{y,\boldsymbol{k}}, \hat{Q}_{\boldsymbol{k}}\right] \neq 0\,. \tag{4.15}$$

From the above two paragraphs, we conclude that violations of spatial Bell inequalities cannot be observed in cosmology. Although we discussed the Larsson's spin operators here, a similar argument goes for other sets of pseudo-spin operators as well [75]. Therefore, we are motivated to investigate Bell inequalities about temporal correlators using a single direction of a spin.

4.4 Bell inequalities about temporal correlators

The previous section shows that only one component of the pseudo-spin operators is available in cosmology, so we are motivated to study Bell inequalities which rely on performing measurements at different times instead of at different locations. In this section, we review such class of inequalities in the general context since the fact that it is worth studying such inequalities is not limited to cosmology as described below. A similar discussion is also shown in the introduction of our paper [81].

There are what are called temporal Bell inequalities in the literature [110–112]. In temporal Bell inequalities, Alice performs a projective measurement of $\hat{S}^a$ at time t_1 (so that the state collapses to an eigenstate of $\hat{S}^a$ upon the measurement), then Bob measures $\hat{S}^b$, on the same system, at a later time t_2. They can then construct the correlators $E(a,b) = \langle\{\hat{S}^a(t_1), \hat{S}^b(t_2)\}\rangle/2$, which satisfy the inequality (4.4). Two main differences with spatial Bell inequalities should be highlighted. First, in temporal Bell inequalities, there is no need to have available a bipartite system made of two entangled sub-systems at two different locations, since repeated measurements are performed on the same system. Second, temporal Bell inequalities do not rest on the same assumptions. Although realism is still necessary, locality is now replaced with "non-invasiveness", *i.e.* the ability to perform a measurement without disturbing the state of the system. One's everyday experience of the macroscopic world is that it is both realist and subject to non-invasive measurements, while in quantum mechanics, quantum superposition violates realism and the reduction of the wavefunction (in the Copenhagen interpretation) violates non-invasiveness. This explains why the inequality (4.4) can be violated by quantum systems. Note that temporal Bell inequalities still rely on measuring multiple components of the spin.

Although the assumption of non-invasiveness plays the exact same role for temporally separated systems as locality does for spatially separated systems (spatial scenarios test local hidden-variable theories while temporal scenarios test non-invasive hidden-variable theories), these two types of experiments come with different loopholes. For temporal Bell experiments, the *clumsiness loophole* [79] is the fundamental impossibility to prove that

a physical measurement is actually non-invasive. It is the analog of the *communication loophole* [113] in spatial Bell experiments. However, the communication loophole can be closed by making sure that two measurements are space-like separated, and special relativity ensures that events at one detector cannot influence measurements performed by the other detector. Such a solution to the clumsiness loophole does not exist.[1]

Testing non-invasiveness is still interesting since in alternatives to the Copenhagen interpretation of quantum mechanics, such as in dynamical collapse theories [115–119], the dynamics of projective measurements is altered, and investigating temporal correlations is thus likely to provide ways to distinguish between alternative "interpretations". Multiple-time measurements also enlarge the class of systems, and experimental setups, in which Bell inequality violations can take place.

For instance, if measurements are now performed at three (or more) different times, it is possible to measure a single observable $\hat{S}$ (*i.e.* to fix the label a in the above notations), and upon defining the two-time correlator $E(t_1, t_2) = \langle\{\hat{S}(t_1), \hat{S}(t_2)\}\rangle/2$, realism and non-invasiveness imply the inequality $-3 \leq E(t_1, t_2) + E(t_2, t_3) - E(t_1, t_3) \leq 1$. This is the so-called Leggett-Garg inequality [76] (for a review, see Ref. [77]), which can be generalized to higher-order strings of multiple-time measurements. In contrast to spatial Bell experiments, the Legget-Garg setup does not require to measure several non-commuting observables (*i.e.* spins in different directions for instance) since a single observable does not commute with itself at different times in general, so this is enough to ensure a non-commuting algebra to be present in the problem. This is particularly useful in contexts where only one spin operator can be measured, which is the case in cosmology as described in the previous section. There, too small decaying mode of adiabatic perturbations prevent one from performing experiments involving several, non-commuting spin operators.

Finally, the last class of experiments exists, which mixes features of the two previous classes, and which is in fact what was originally considered by John Bell in 1966 [78] (see Ref. [23] for a recent and insightful resurrection of this work). There, one performs measurements separated both in space and time. More precisely, given a bipartite system made of two subsystems '1' and '2', located at two different locations x_1 and x_2, Alice measures the same dichotomic variable $\hat{S}_1$ on the first sub-system at times t_a and t'_a, while Bob measures $\hat{S}_2$ on the second sub-system at times t_b and t'_b. Here, the two sets of measuring events, $\{(x_1, t_a), (x_1, t'_a)\}$ on one hand, and $\{(x_2, t_b), (x_2, t'_b)\}$ on the other hand, are causally disconnected, and time plays the exact same role as the measurement parameter (*e.g.* the polarizer angle) in the ordinary spatial Bell inequalities. We call this kind of setup "bipartite temporal Bell inequality". The inequality (4.4) is satisfied provided that the assumptions of realism and locality hold (if Alice and/or Bob perform repeated measurements on the same physical realization of the system, or if the two sets of measuring events are not causally disconnected, then one must add non-invasiveness, but this is not compulsory), so the same fundamental properties are tested as in the usual spatial Bell inequality. However, compared to the spatial Bell inequality, this has the advantage of relying on measuring a single spin operator. Let us remind a reader that the subscripts '1' and '2' correspond to '$\boldsymbol{k}$' and '$-\boldsymbol{k}$' in the context of cosmology.

In table 4.1, we summarise the main features of the four classes of Bell inequalities

[1] Let us note that the *freedom of choice* loophole, *i.e.* the ability to ensure that the choice of measurement settings is "free and random", and independent of any physical process that could affect the measurement outcomes, can be closed, or at least pushed back to billions of years ago, by using cosmological sources, see Ref. [114].

Type of inequality	Assumptions	Requires bipartite system	involves single spin measurement only
Spatial Bell	realism and locality	yes	no
Temporal Bell	realism and non-invasiveness	no	no
Legget-Garg	realism and non-invasiveness	no	yes
Bipartite temporal Bell	realism and locality	yes	yes

Table 4.1: Classes of Bell inequality experiments.

discussed above: spatial Bell inequalities, temporal Bell inequalities, Legget-Garg inequalities and bipartite temporal Bell inequalities. In our work shown in Chap. 6, we focus on bipartite temporal Bell inequalities, since they are the only ones that allow us to test realism and locality, while relying on measurements of a single spin operator. In practice, we consider continuous-variable systems that are placed in a two-mode squeezed state.

Part II

Original Works

Chapter 5

Power spectrum in stochastic inflation

In Chap. 3, we described an effective theory for the inflaton fields on superhorizon scales, where the coarse-grained fields obey the Langevin equation. The resultant fluctuations in the duration of inflation among local patches are nothing but curvature perturbations ζ. Hence, in practice, statistics of ζ can be studied by working on the first-passage-time problem of a stochastic process. So far, the first-passage-time problem has been solved for a fixed initial field value $\mathbf{\Phi}$. However, in order to make contact with observations, we need to investigate the first-passage time from an initial condition which rather corresponds to when a given scale k exits the horizon. This would be the final gap between the stochastic-δN formalism and observational predictions, which we work on in this work. In Sec. 5.1, we present our calculation of the power spectrum in a generic inflating setup. In the quasi de-Sitter limit, we show that it boils down to deriving the probability distribution of the field value at a given number of e-folds before the end of inflation, and we explain how this can be computed from the solution of the Fokker-Planck equation and the first-passage-time problem. In Sec. 5.2, we apply our results to the case where quantum diffusion is efficient on small scales only, and we show that even then, it affects the power spectrum on large scales. Some technical aspects are shown in Appendix B.

This chapter is written based on our previous work [80].

5.1 Generic calculation of the power spectrum

5.1.1 Encoding spatial correlations into statistical trees

Since the power spectrum is nothing but the Fourier transform of the two-point correlation function in real space, one must be able to describe the spatial structure of the correlations between the durations of inflation at different points in order to compute the power spectrum. However, since the Langevin equation describes the dynamics of independent patches of the universe, and *a priori* carries no information about their relative spatial positions, one may be concerned that this spatial structure is lost and that only one-point correlation functions can be computed in stochastic inflation. In fact, as we shall now see, the distance between two patches is encoded in the time at which they become statistically independent, such that the two-point function is contained in the one-point dynamics of the Langevin equation.

More explicitly, the situation we consider is depicted in the space-time diagram of

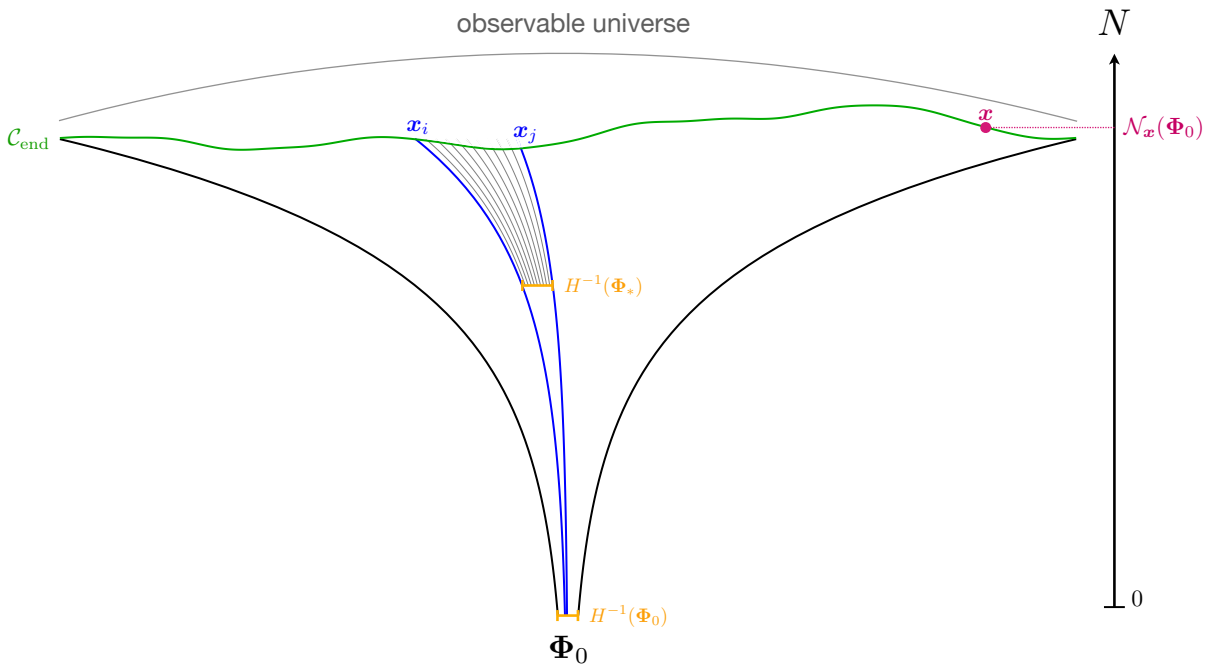

Figure 5.1: Space-time diagram (here in one dimension for display convenience) during inflation. For two comoving points labeled by $\boldsymbol{x}_i$ and $\boldsymbol{x}_j$ on the end-of-inflation surface, there exists a time at which their distance equals the Hubble radius. Prior to this time, they belong to the same Hubble patch and their dynamics is identical. After this time, their evolution becomes statistically independent, and the time that separates this point from the end-of-inflation surface is related to the spatial distance between $\boldsymbol{x}_i$ and $\boldsymbol{x}_j$.

Fig. 5.1. During inflation, there is a point before which the entire observable universe lies within a single Hubble patch. We call $\boldsymbol{\Phi}_0$ the value of the inflationary fields inside that patch (since $\boldsymbol{\Phi}$ is coarse-grained on super-Hubble scales, it is indeed homogeneous within a Hubble patch). Each comoving point on that patch, labeled by its position $\boldsymbol{x}$, crosses the end surface (displayed in green) at a different time, that we denote $\mathcal{N}_{\boldsymbol{x}}(\boldsymbol{\Phi}_0)$ (see the violet point in Fig. 5.1).

Let us consider two points $\boldsymbol{x}_i$ and $\boldsymbol{x}_j$ on the end-of-inflation surface. They are the endpoints of two comoving lines displayed in blue. Prior to the end of inflation, there is a time when the distance between these two lines coincides with the Hubble radius, and we call $\boldsymbol{\Phi}_*$ the value of the fields at that point (since $\boldsymbol{\Phi}$ is uniform across a Hubble patch, it is indeed the same at $\boldsymbol{x}_i$ and $\boldsymbol{x}_j$ at that time). This defines the function

$$\boldsymbol{\Phi}_* \left(\boldsymbol{x}_i, \boldsymbol{x}_j \right) . \tag{5.1}$$

Before that point, the two blue lines lie within the same Hubble patch, hence they share the same history, *i.e.* they are described by the same realization of the Langevin equation. Past that "splitting" point, owing to the Markovian property of the stochastic process we consider, they become statistically independent. If $\overline{N}(\boldsymbol{\Phi}_0)$ denotes the mean value of $\mathcal{N}_{\boldsymbol{x}}(\boldsymbol{\Phi}_0)$ over all endpoints, according to Eq. (3.38), one has

$$\zeta(\boldsymbol{x}_i) = \mathcal{N}_i(\boldsymbol{\Phi}_0) - \overline{N}(\boldsymbol{\Phi}_0) , \tag{5.2}$$

where $\mathcal{N}_i$ is a short-hand notation for $\mathcal{N}_{\boldsymbol{x}_i}$. One can also introduce the physical distance r between the two endpoints. On the splitting patch (displayed in orange and labeled with

$H^{-1}(\boldsymbol{\Phi}_*)$ in Fig. 5.1), let $\boldsymbol{y}$ label the comoving position along the geodesic connecting $\boldsymbol{x}_i$ and $\boldsymbol{x}_j$. Each of such points gives rise to one of the grey lines in Fig. 5.1, and undergoes a number of inflationary e-folds that we denote $\mathcal{N}_{\boldsymbol{y}}[\boldsymbol{\Phi}_*(\boldsymbol{x}_i,\boldsymbol{x}_j)]$. The physical distance between $\boldsymbol{x}_i$ and $\boldsymbol{x}_j$ on the end surface is thus given by

$$r\left(\boldsymbol{x}_i,\boldsymbol{x}_j\right) = \int_0^{H^{-1}[\boldsymbol{\Phi}_*(\boldsymbol{x}_i,\boldsymbol{x}_j)]} e^{\mathcal{N}_{\boldsymbol{y}}[\boldsymbol{\Phi}_*(\boldsymbol{x}_i,\boldsymbol{x}_j)]}\mathrm{d}y\,, \tag{5.3}$$

where we have introduced $\boldsymbol{y} = \boldsymbol{x}_i + y(\boldsymbol{x}_j-\boldsymbol{x}_i)/|\boldsymbol{x}_j-\boldsymbol{x}_i|$. The two-point function of ζ at separation r is then given by the expectation value of the product $\zeta(\boldsymbol{x}_i)\zeta(\boldsymbol{x}_j)$, averaged over all pairs of comoving lines that share the same distance r. The power spectrum is then simply defined as the Fourier transform of that function, such that

$$\langle\zeta(\boldsymbol{x}_i)\zeta(\boldsymbol{x}_j)\rangle_{r(\boldsymbol{x}_i,\boldsymbol{x}_j)=\tilde{r}} = \int_0^\infty \mathcal{P}_\zeta(k)\frac{\sin(k\tilde{r})}{k\tilde{r}}\frac{\mathrm{d}k}{k}. \tag{5.4}$$

A remark is in order regarding the appearance of the cardinal sine function in this expression. In principle, the two-point function of the noise ξ in the Langevin equation (3.21) also depends through a cardinal sine function on the distance (in Hubble units) between the two points at which it is evaluated [25]. Therefore, the realizations of the noise at two distant points are still slightly correlated after they split (*i.e.* after they no longer belong to the same Hubble patch), and are not exactly independent. By neglecting this remaining amount of correlation, one is effectively approximating the cardinal sine function with a Heaviside function (see the remark below Eq. (3.17)). This approximation is well justified since those correlations quickly decay on super-Hubble scales (and given that their details anyway depend on the window function that has been used to coarse-grain the fields), but for consistency, the cardinal sine function in Eq. (5.4) should also be replaced by a Heaviside function. By differentiating both hands of Eq. (5.4) with respect to $\tilde{r}$, one then obtains

$$\mathcal{P}_\zeta(k) = -\left.\frac{\partial}{\partial\ln(\tilde{r})}\langle\zeta(\boldsymbol{x}_i)\zeta(\boldsymbol{x}_j)\rangle_{r(\boldsymbol{x}_i,\boldsymbol{x}_j)=\tilde{r}}\right|_{\tilde{r}=1/k}. \tag{5.5}$$

This formula can be used to extract the power spectrum from a numerical lattice simulation of the Langevin equation.

5.1.2 Using the first-passage-time moments

Let us now try to benefit from the results recalled in Sec. 3.3.1, which provide the statistical moments of the first-passage time through the end surface from a given point in field space. In order to make use of these formulas, it is convenient to introduce $P_r(\boldsymbol{\Phi}_*)$, which is the probability density associated with the field value in the splitting patch, for two comoving lines separated by r on the end surface. The calculation of this function will be discussed below.

Along the line labeled by $\boldsymbol{x}_i$, let us first write $\mathcal{N}_i(\boldsymbol{\Phi}_0)$ as the sum of the number of e-folds realized between the original patch and the splitting patch, which we denote $\mathcal{N}_i[\boldsymbol{\Phi}_0\to\boldsymbol{\Phi}_*(\boldsymbol{x}_i,\boldsymbol{x}_j)]$ (and which is not necessarily a *first*-passage time), and the number of e-folds realized between the splitting patch and the end surface, $\mathcal{N}_i[\boldsymbol{\Phi}_*(\boldsymbol{x}_i,\boldsymbol{x}_j)]$, such that Eq. (5.2) gives rise to

$$\zeta\left(\boldsymbol{x}_i\right) = \mathcal{N}_i\left[\boldsymbol{\Phi}_0\to\boldsymbol{\Phi}_*\left(\boldsymbol{x}_i,\boldsymbol{x}_j\right)\right] + \mathcal{N}_i\left[\boldsymbol{\Phi}_*\left(\boldsymbol{x}_i,\boldsymbol{x}_j\right)\right] - \overline{N}\left(\boldsymbol{\Phi}_0\right)\,. \tag{5.6}$$

Obviously, a similar formula holds for $\zeta(\boldsymbol{x}_j)$, and given that the two branches $\boldsymbol{x}_i$ and $\boldsymbol{x}_j$ share the same common past before the splitting patch, one has $\mathcal{N}_i[\boldsymbol{\Phi}_0 \to \boldsymbol{\Phi}_*(\boldsymbol{x}_i, \boldsymbol{x}_j)] = \mathcal{N}_j[\boldsymbol{\Phi}_0 \to \boldsymbol{\Phi}_*(\boldsymbol{x}_i, \boldsymbol{x}_j)]$. Because of Eq. (5.5), one must cross-correlate Eq. (5.6) with the same expression when $\boldsymbol{x}_i$ is replaced by $\boldsymbol{x}_j$, under the condition that the distance between $\boldsymbol{x}_i$ and $\boldsymbol{x}_j$ is fixed. This gives rise to several terms that we now discuss one by one.

Let us first consider the product term $\mathcal{N}_i(\boldsymbol{\Phi}_*)\mathcal{N}_j(\boldsymbol{\Phi}_*)$ (hereafter, for notational convenience, we drop the arguments of the function $\boldsymbol{\Phi}_*$). Using the chain rule for conditional probabilities, one has

$$\left\langle \mathcal{N}_i\left(\boldsymbol{\Phi}_*\right)\mathcal{N}_j\left(\boldsymbol{\Phi}_*\right)\right\rangle_{r(\boldsymbol{x}_i,\boldsymbol{x}_j)=\tilde{r}} = \int \mathrm{d}\widetilde{\boldsymbol{\Phi}}_* P_{\tilde{r}}\left(\widetilde{\boldsymbol{\Phi}}_*\right) \left\langle \mathcal{N}_i\left(\boldsymbol{\Phi}_*\right)\mathcal{N}_j\left(\boldsymbol{\Phi}_*\right)\right\rangle_{r(\boldsymbol{x}_i,\boldsymbol{x}_j)=\tilde{r},\boldsymbol{\Phi}_*(\boldsymbol{x}_i,\boldsymbol{x}_j)=\widetilde{\boldsymbol{\Phi}}_*} . \quad (5.7)$$

An important remark is that if the distance between $\boldsymbol{x}_i$ and $\boldsymbol{x}_j$ is much larger than the Hubble radius on the end surface (which needs to be the case since the stochastic formalism only allows us to describe long-distance correlations), most lines labeled by $\boldsymbol{y}$ (and displayed in grey in Fig. 5.1) split from the ones ending in $\boldsymbol{x}_i$ and $\boldsymbol{x}_j$ much before the end of inflation. As a consequence, the number of e-folds realized along these lines is almost independent of the one undergone by the lines ending in $\boldsymbol{x}_i$ and $\boldsymbol{x}_j$, hence Eq. (5.3) indicates that the value of r is (almost) uncorrelated with $\mathcal{N}_i\left(\boldsymbol{\Phi}_*\right)$ or $\mathcal{N}_j\left(\boldsymbol{\Phi}_*\right)$. This implies that $\langle\mathcal{N}_i(\boldsymbol{\Phi}_*)\mathcal{N}_j(\boldsymbol{\Phi}_*)\rangle_{r(\boldsymbol{x}_i,\boldsymbol{x}_j)=\tilde{r},\boldsymbol{\Phi}_*(\boldsymbol{x}_i,\boldsymbol{x}_j)=\widetilde{\boldsymbol{\Phi}}_*} = \langle\mathcal{N}_i(\boldsymbol{\Phi}_*)\mathcal{N}_j(\boldsymbol{\Phi}_*)\rangle_{\boldsymbol{\Phi}_*(\boldsymbol{x}_i,\boldsymbol{x}_j)=\widetilde{\boldsymbol{\Phi}}_*} = \langle\mathcal{N}\rangle^2(\widetilde{\boldsymbol{\Phi}}_*)$, and one recovers the first statistical moment of the first-passage time computed in Sec. 3.3.1.

The chain rule of Eq. (5.7) applies more generally to any function of $\boldsymbol{x}_i$ and $\boldsymbol{x}_j$, so the other terms can also be evaluated as integrals over $\boldsymbol{\Phi}_*$ of correlators at fixed r and $\boldsymbol{\Phi}_*$. For the term $\mathcal{N}_i(\boldsymbol{\Phi}_0 \to \boldsymbol{\Phi}_*)\mathcal{N}_j(\boldsymbol{\Phi}_0 \to \boldsymbol{\Phi}_*)$, since r depends only on the post-splitting-patch dynamics, the fact that r is fixed is irrelevant and one has

$$\left\langle \mathcal{N}_i\left(\boldsymbol{\Phi}_0 \to \boldsymbol{\Phi}_*\right)\mathcal{N}_j\left(\boldsymbol{\Phi}_0 \to \boldsymbol{\Phi}_*\right)\right\rangle_{r(\boldsymbol{x}_i,\boldsymbol{x}_j)=\tilde{r},\boldsymbol{\Phi}_*(\boldsymbol{x}_i,\boldsymbol{x}_j)=\widetilde{\boldsymbol{\Phi}}_*} = \left\langle \mathcal{N}^2\left(\boldsymbol{\Phi}_0 \to \widetilde{\boldsymbol{\Phi}}_*\right)\right\rangle \quad (5.8)$$

where we have used that $\mathcal{N}_i(\boldsymbol{\Phi}_0 \to \boldsymbol{\Phi}_*) = \mathcal{N}_j(\boldsymbol{\Phi}_0 \to \boldsymbol{\Phi}_*)$ as mentioned above. Let us stress that contrary to the previous term, this quantity is not a statistical moment of a first passage time, so it cannot be evaluated with the techniques presented in Sec. 3.3.1, but we will see below that it cancels out with other contributions in the final result.

The Markovian nature of the process also implies that $\mathcal{N}_j(\boldsymbol{\Phi}_*)$ and $\mathcal{N}_i(\boldsymbol{\Phi}_0 \to \boldsymbol{\Phi}_*) = \mathcal{N}_j(\boldsymbol{\Phi}_0 \to \boldsymbol{\Phi}_*)$ are independent when $\boldsymbol{\Phi}_*$ is fixed, so

$$\left\langle \mathcal{N}_i\left(\boldsymbol{\Phi}_0 \to \boldsymbol{\Phi}_*\right)\mathcal{N}_j\left(\boldsymbol{\Phi}_*\right)\right\rangle_{r(\boldsymbol{x}_i,\boldsymbol{x}_j)=\tilde{r},\boldsymbol{\Phi}_*(\boldsymbol{x}_i,\boldsymbol{x}_j)=\widetilde{\boldsymbol{\Phi}}_*} = \left\langle \mathcal{N}(\boldsymbol{\Phi}_0 \to \widetilde{\boldsymbol{\Phi}}_*)\right\rangle \langle\mathcal{N}\rangle\left(\widetilde{\boldsymbol{\Phi}}_*\right), \quad (5.9)$$

where the last term is the first moment of the first-passage time.

Those considerations allow one to compute the 9 terms that appear in the expectation value of $\zeta(\boldsymbol{x}_i)\zeta(\boldsymbol{x}_j)$, and after some rearrangements one obtains

$$\begin{aligned}\left\langle \zeta(\boldsymbol{x}_i)\zeta(\boldsymbol{x}_j)\right\rangle_{r(\boldsymbol{x}_i,\boldsymbol{x}_j)=\tilde{r}} = \int \mathrm{d}\boldsymbol{\Phi}_* P_{\tilde{r}}\left(\boldsymbol{\Phi}_*\right) \Big[&\left\langle \mathcal{N}^2\left(\boldsymbol{\Phi}_0 \to \boldsymbol{\Phi}_*\right)\right\rangle + \langle\mathcal{N}\rangle^2\left(\boldsymbol{\Phi}_*\right) + \overline{N}^2\left(\boldsymbol{\Phi}_0\right) \\ &+2\left\langle \mathcal{N}\left(\boldsymbol{\Phi}_0 \to \boldsymbol{\Phi}_*\right)\right\rangle \langle\mathcal{N}\rangle\left(\boldsymbol{\Phi}_*\right) - 2\overline{N}\left(\boldsymbol{\Phi}_0\right)\left\langle \mathcal{N}\left(\boldsymbol{\Phi}_0 \to \boldsymbol{\Phi}_*\right)\right\rangle - 2\overline{N}\left(\boldsymbol{\Phi}_0\right)\langle\mathcal{N}\rangle\left(\boldsymbol{\Phi}_*\right)\Big] \quad (5.10)\end{aligned}$$

This expression can be further simplified by noting that, if one decomposes $\mathcal{N}(\boldsymbol{\Phi}_0) = \mathcal{N}\left(\boldsymbol{\Phi}_0 \to \boldsymbol{\Phi}_*\right) + \mathcal{N}(\boldsymbol{\Phi}_*)$ and takes the stochastic average, one has $\overline{N}\left(\boldsymbol{\Phi}_0\right) = \langle\mathcal{N}(\boldsymbol{\Phi}_0 \to \boldsymbol{\Phi}_*)\rangle + \langle\mathcal{N}\rangle(\boldsymbol{\Phi}_*)$, so by replacing $\overline{N}(\boldsymbol{\Phi}_0)$ in the above expression, it reduces to

$$\left\langle \zeta(\boldsymbol{x}_i)\zeta(\boldsymbol{x}_j)\right\rangle_{r(\boldsymbol{x}_i,\boldsymbol{x}_j)=\tilde{r}} = \int \mathrm{d}\boldsymbol{\Phi}_* P_{\tilde{r}}\left(\boldsymbol{\Phi}_*\right)\left\langle \delta\mathcal{N}^2\left(\boldsymbol{\Phi}_0 \to \boldsymbol{\Phi}_*\right)\right\rangle . \quad (5.11)$$

Finally, let us note that, invoking again the Markovian nature of the process, $\mathcal{N}(\boldsymbol{\Phi}_0 \to \boldsymbol{\Phi}_*)$ and $\mathcal{N}(\boldsymbol{\Phi}_*)$ are two independent variables (when $\boldsymbol{\Phi}_*$ is fixed). Therefore by squaring the relation $\mathcal{N}(\boldsymbol{\Phi}_0) = \mathcal{N}(\boldsymbol{\Phi}_0 \to \boldsymbol{\Phi}_*) + \mathcal{N}(\boldsymbol{\Phi}_*)$ given above, and after taking its stochastic average, one obtains $\langle \delta\mathcal{N}^2(\boldsymbol{\Phi}_0 \to \boldsymbol{\Phi}_*)\rangle = \langle \delta\mathcal{N}^2\rangle(\boldsymbol{\Phi}_0) - \langle \delta\mathcal{N}^2\rangle(\boldsymbol{\Phi}_*)$. Since the first term in the right-hand side of this expression does not depend on $\boldsymbol{\Phi}_*$, it provides a contribution proportional to $\int \mathrm{d}\boldsymbol{\Phi}_* P_{\tilde{r}}(\boldsymbol{\Phi}_*) = 1$ in Eq. (5.11), *i.e.* a term that does not depend on $\tilde{r}$ so Eq. (5.5) gives rise to

$$\mathcal{P}_\zeta(k) = \frac{1}{k}\int \mathrm{d}\boldsymbol{\Phi}_* \left.\frac{\partial P_r(\boldsymbol{\Phi}_*)}{\partial r}\right|_{r=1/k} \left\langle \delta\mathcal{N}^2\right\rangle(\boldsymbol{\Phi}_*) \,. \tag{5.12}$$

This expression has the advantage to directly involve the second moment of the first-passage time, studied in Sec. 3.3.1.

5.1.3 Field value at the splitting patch

The next step in the calculation is to compute the probability associated with the field value at the splitting patch, $P_r(\boldsymbol{\Phi}_*)$, which appears in Eq. (5.12).

An important remark is that if two points are separated by a distance r on the end surface, this distance should be red-shifted (or rather blue-shifted) to previous times using the backward e-fold number, $N_{\rm bw} = N_{\rm end} - N$, *i.e.* the number of e-folds before the end of inflation. Indeed, as argued in Ref. [120], observable quantities should be stated in terms of physical scales as seen by local observers, which requires one to label scales with backward e-folds. Note that since the stochastic noise is turned off at the end of inflation, physical scales on the end surface are directly mapped to scales measured in observations today.

As a consequence, if two comoving lines are separated by a distance r on the end surface, they become independent when

$$e^{N_{\rm bw,*}} = rH(\boldsymbol{\Phi}_*) \,. \tag{5.13}$$

Along each realization of the Langevin equation, one can determine when this condition is satisfied, record the value of $\boldsymbol{\Phi}_*$ at that time, and then reconstruct the probability distribution associated with $\boldsymbol{\Phi}_*$. As will be shown below, in the case of a one-dimensional field phase space (*i.e.* for single-field systems that have reached the slow-roll attractor[1]), the result does not depend on the initial condition $\boldsymbol{\Phi}_0$, because of the Markovian nature of the process. In multiple field systems, however, the distribution $P_r(\boldsymbol{\Phi}_*)$ does *a priori* depend on the choice of $\boldsymbol{\Phi}_0$ (or more generally, on the distribution function associated with $\boldsymbol{\Phi}_0$), which is a fundamental difference.

This prescription allows one to evaluate $P_r(\boldsymbol{\Phi}_*)$ numerically in a straightforward way, so the above considerations provide an explicit procedure to evaluate the power spectrum in stochastic inflation, which was one of the main goals of this paper.

In order to gain further analytical insight, let us notice that in the quasi de-Sitter limit where H is almost a constant, $H(\boldsymbol{\Phi}_*)$ can be simply replaced by $H_{\rm end}$ in Eq. (5.13), which allows one to define

$$N_{\rm bw}(r) = \ln(rH_{\rm end}) = -\ln\left(\frac{k}{k_{\rm end}}\right) \,. \tag{5.14}$$

[1]Single-field setups that violate slow roll for a transient period (and typically enter a phase of ultra slow roll) are usually preceded by a phase of slow roll inflation, in which case the dependence on initial condition is also erased.

In this limit, the probability $P_r(\boldsymbol{\Phi}_*)$ becomes the one associated with the field value at a fixed backward e-fold number,

$$P_r\left(\boldsymbol{\Phi}_*\right) \simeq P_{\rm bw}\left[\boldsymbol{\Phi}_*, N_{\rm bw}(r)\right], \tag{5.15}$$

which we further study in the next section. Combined with Eq. (5.12), it gives rise to

$$\mathcal{P}_\zeta(k) = \int \mathrm{d}\boldsymbol{\Phi}_* \left.\frac{\partial P_{\rm bw}\left(\boldsymbol{\Phi}_*, N_{\rm bw}\right)}{\partial N_{\rm bw}}\right|_{N_{\rm bw}=-\ln(k/k_{\rm end})} \left\langle \delta\mathcal{N}^2 \right\rangle \left(\boldsymbol{\Phi}_*\right) . \tag{5.16}$$

At this stage, it is worth noting that at leading order in the low-diffusion limit, the backward probability is simply a Dirac distribution centered on the classical trajectory, $P_{\rm bw}(\boldsymbol{\Phi}_*, N_{\rm bw}) = \delta[\boldsymbol{\Phi}_* - \boldsymbol{\Phi}_{\rm cl}(k)]$, where the function $\boldsymbol{\Phi}_{\rm cl}(k)$ was introduced in Sec. 3.3.2. By plugging this expression into Eq. (5.16), after integration by parts, one recovers Eq. (3.42), which is a good consistency check.

5.1.4 Backward probability

In this section, we explain how the backward probability can be computed from the solutions of the Fokker-Planck and adjoint Fokker-Planck equations studied in Sec. 3.3. For notational convenience, we use $\mathbb{P}(\cdot)$ to denote the probability (density) associated with the event written in the argument in general. For instance, we have $\mathbb{P}[\boldsymbol{\Phi}(N) = \widetilde{\boldsymbol{\Phi}}|\boldsymbol{\Phi}(N_{\rm in}) = \boldsymbol{\Phi}_{\rm in}] = P(\widetilde{\boldsymbol{\Phi}}, N|\boldsymbol{\Phi}_{\rm in}, N_{\rm in})$, which was introduced in Eq. (3.23), and $\mathbb{P}[\mathcal{N}(\boldsymbol{\Phi}) = \tilde{N}] = P_{\rm FPT}(\tilde{N}, \boldsymbol{\Phi})$, which was introduced in Eq. (3.39).

Let us consider the subset of Langevin realizations originating from the original patch at $\boldsymbol{\Phi}_0$ that realize at least $N_{\rm bw}$ inflationary e-folds. The backward probability $P_{\rm bw}(\boldsymbol{\Phi}_*, N_{\rm bw})$ corresponds to the fraction of those realizations for which the value of the fields $N_{\rm bw}$ e-folds before the end of inflation is $\boldsymbol{\Phi}_*$, so

$$P_{\rm bw}\left(\boldsymbol{\Phi}_*, N_{\rm bw}\right) = \int_{N_{\rm bw}}^{\infty} \mathrm{d}N_{\rm tot} \mathbb{P}\left[\boldsymbol{\Phi}(N_{\rm tot} - N_{\rm bw}) = \boldsymbol{\Phi}_*, \mathcal{N}\left(\boldsymbol{\Phi}_0\right) = N_{\rm tot} | \mathcal{N}\left(\boldsymbol{\Phi}_0\right) > N_{\rm bw}\right] \tag{5.17}$$

where one averages over the value of $\mathcal{N}(\boldsymbol{\Phi}_0)$. Since the integral is performed over $N_{\rm tot} > N_{\rm bw}$, the condition $\mathcal{N}(\boldsymbol{\Phi}_0) = N_{\rm tot}$ guarantees that $\mathcal{N}(\boldsymbol{\Phi}_0) > N_{\rm bw}$ so the integrand of Eq. (5.17) is of the form $\mathbb{P}(A, B|C)$ with $B \Rightarrow C$. Using the chains rule, it can thus be written as $\mathbb{P}(A, B|C) = \mathbb{P}(A, B, C)/\mathbb{P}(C) = \mathbb{P}(A, B)/\mathbb{P}(C)$. Using the chain rule one more time, it is given by $\mathbb{P}(A, B|C) = \mathbb{P}(A|B)\mathbb{P}(B)/\mathbb{P}(C)$, hence

$$P_{\rm bw}\left(\boldsymbol{\Phi}_*, N_{\rm bw}\right) = \frac{\displaystyle\int_{N_{\rm bw}}^{\infty} \mathrm{d}N_{\rm tot} \mathbb{P}\left[\boldsymbol{\Phi}(N_{\rm tot} - N_{\rm bw}) = \boldsymbol{\Phi}_* | \mathcal{N}\left(\boldsymbol{\Phi}_0\right) = N_{\rm tot}\right] P_{\rm FPT}\left(N_{\rm tot}, \boldsymbol{\Phi}_0\right)}{\displaystyle\int_{N_{\rm bw}}^{\infty} \mathrm{d}N_{\rm tot} P_{\rm FPT}\left(N_{\rm tot}, \boldsymbol{\Phi}_0\right)} . \tag{5.18}$$

The first term in the integrand of the numerator is a probability associated with a past event under a future condition, which makes it difficult to apprehend. Instead, it is simpler to use Bayes' theorem and rewrite it in terms of the probability of a future event under a past condition,

$$\begin{aligned}\mathbb{P}\left[\boldsymbol{\Phi}(N_{\rm tot} - N_{\rm bw}) = \boldsymbol{\Phi}_* | \mathcal{N}\left(\boldsymbol{\Phi}_0\right) = N_{\rm tot}\right] = \mathbb{P}\left[\mathcal{N}\left(\boldsymbol{\Phi}_0\right) = N_{\rm tot} | \boldsymbol{\Phi}(N_{\rm tot} - N_{\rm bw}) = \boldsymbol{\Phi}_*\right] \\ \times \frac{\mathbb{P}\left[\boldsymbol{\Phi}(N_{\rm tot} - N_{\rm bw}) = \boldsymbol{\Phi}_*\right]}{P_{\rm FPT}\left(N_{\rm tot}, \boldsymbol{\Phi}_0\right)} .\end{aligned} \tag{5.19}$$

Because of the Markovian property of the process we consider, the probability appearing on the right-hand side in the first line can be written as $\mathbb{P}[\mathcal{N}(\mathbf{\Phi}_0) = N_{\rm tot}|\mathbf{\Phi}(N_{\rm tot} - N_{\rm bw}) = \mathbf{\Phi}_*] = \mathbb{P}[\mathcal{N}(\mathbf{\Phi}_*) = N_{\rm bw}] = P_{\rm FPT}(N_{\rm bw}, \mathbf{\Phi}_*)$, and the probability appearing in the numerator in the second line is nothing but $\mathbb{P}[\mathbf{\Phi}(N_{\rm tot} - N_{\rm bw}) = \mathbf{\Phi}_*] = P(\mathbf{\Phi}_*, N_{\rm tot} - N_{\rm bw}|\mathbf{\Phi}_0, 0)$, where we set the time on the original patch to zero without loss of generality. Combining the above results, one obtains

$$P_{\rm bw}\left(\mathbf{\Phi}_*, N_{\rm bw}\right) = P_{\rm FPT}\left(N_{\rm bw}, \mathbf{\Phi}_*\right) \frac{\displaystyle\int_0^\infty \mathrm{d}N P(\mathbf{\Phi}_*, N|\mathbf{\Phi}_0, 0)}{\displaystyle\int_{N_{\rm bw}}^\infty \mathrm{d}N_{\rm tot} P_{\rm FPT}\left(N_{\rm tot}, \mathbf{\Phi}_0\right)}\,, \tag{5.20}$$

where in the numerator, we have performed the change of integration variable $N = N_{\rm tot} - N_{\rm bw}$. Several remarks are in order regarding this expression. First, one can see that as announced at the beginning of this section, it provides a formula to compute the backward probability from the knowledge of P and $P_{\rm FPT}$ only, *i.e.* from the solutions of the Fokker-Planck and adjoint Fokker-Planck equations. Second, one can check that it is normalized to unity, *i.e.* $\int \mathrm{d}\mathbf{\Phi}_* P_{\rm bw}(\mathbf{\Phi}_*, N_{\rm bw}) = 1$. Third, the term in the denominator corresponds to the probability that at least $N_{\rm bw}$ e-folds are realized starting from $\mathbf{\Phi}_0$. In inflationary models where an arbitrarily large number of e-folds can be realized (as in large-field or plateau potentials, but not in hilltop potentials), by setting $\mathbf{\Phi}_0$ high enough in the potential, this term can therefore be brought to values arbitrarily close to one, in which case it can be discarded. Fourth, for one-dimensional setups, the term in the numerator does not depend on $\mathbf{\Phi}_0$ because of the Markovian nature of the process.[2] This confirms that observable quantities depend on initial conditions for multiple-field systems only.

5.2 Imprint of small-scale diffusion on the large-scale power spectrum

In this section, we apply the results derived in Sec. 5.1 to the case where the scales at which the power spectrum is observed cross out the Hubble radius during inflation at a time when quantum diffusion plays a negligible role. In other words, we assume that the backward probability $P_{\rm bw}[\mathbf{\Phi}_*, N_{\rm bw}(k)]$ takes most of its support at values of $\mathbf{\Phi}_*$ where the potential gradient is the main driver of the field dynamics. This is the case for the scales observed in the CMB in most inflationary models. However, if quantum diffusion plays an important role closer to the end of inflation, which occurs *e.g.* in models producing primordial black holes, the backward probability may be widely spread, and as argued in Sec. 3.3.1, the standard formula does not apply in that case. We, therefore, want to investigate how quantum diffusion at small scales distort the power spectrum at large scales in such scenarios.

[2] To demonstrate this explicitly, let us consider two values for the initial field value, ϕ_{0A} and ϕ_{0B}, with $\phi_{\rm end} < \phi_{0A} < \phi_{0B}$ in a one-dimensional setup. The field distribution initiated from ϕ_{0B}, $P(\phi, N|\phi_{0B}, 0)$, can be expressed in terms of that from ϕ_{0A}, $P(\phi, N|\phi_{0A}, 0)$, as $P(\phi, N|\phi_{0B}, 0) = \int \mathrm{d}\mathcal{N}\, P(\phi, N - \mathcal{N}|\phi_{0A}, 0)\theta(N - \mathcal{N})P_{\rm FPT}(\mathcal{N})$ for $\phi < \phi_{0A}$, where $P_{\rm FPT}(\mathcal{N})$ stands for the first passage time distribution from ϕ_{0B} to ϕ_{0A}. This relation relies on the Markovian property and the fact that the system is one dimensional. By integrating both sides over N, one obtains $\int_0^\infty \mathrm{d}N\, P(\phi, N|\phi_{0B}, 0) = \int_0^\infty \mathrm{d}N\, P(\phi, N|\phi_{0A}, 0)$.

5.2.1 Averaging the classical power spectrum

Let us first note that Eq. (5.20) can be plugged into Eq. (5.16) to derive a compact formula for the power spectrum. In the limit where $\boldsymbol{\Phi}_0$ is taken sufficiently high in the potential and the denominator of Eq. (5.20) can be discarded, the derivative with respect to $N_{\rm bw}$ appearing in Eq. (5.16) only acts on the term $P_{\rm FPT}(N_{\rm bw}, \boldsymbol{\Phi}_*)$ of Eq. (5.20), and according to Eq. (3.39), it gives rise to $\mathcal{L}^\dagger_{\rm FP}(\boldsymbol{\Phi}_*) \cdot P_{\rm FPT}(N_{\rm bw}, \boldsymbol{\Phi}_*)$. By using the definition of the adjoint Fokker-Planck operator in terms of the Fokker-Planck operator, see below Eq. (3.39), one obtains

$$\mathcal{P}_\zeta(k) = \int \mathrm{d}\boldsymbol{\Phi}_* P_{\rm FPT}\left[N_{\rm bw}(k), \boldsymbol{\Phi}_*\right] \int_0^\infty \mathrm{d}N \mathcal{L}_{\rm FP}\left(\boldsymbol{\Phi}_*\right) \cdot \left[\left\langle \delta\mathcal{N}^2 \right\rangle \left(\boldsymbol{\Phi}_*\right) P\left(\boldsymbol{\Phi}_*, N|\boldsymbol{\Phi}_0, 0\right)\right]. \tag{5.21}$$

In this expression, the Fokker-Planck operator, which we recall is a second-order partial differential operator, acts on the product of two terms, namely $\langle\delta\mathcal{N}^2\rangle(\boldsymbol{\Phi}_*)$ and $P(\boldsymbol{\Phi}_*, N|\boldsymbol{\Phi}_0, 0)$. When acting directly on $P(\boldsymbol{\Phi}_*, N|\boldsymbol{\Phi}_0, 0)$, because of Eq. (3.23), it returns $(\partial/\partial N)P(\boldsymbol{\Phi}_*, N|\boldsymbol{\Phi}_0, 0)$, for which the integral over N can be readily performed in Eq. (5.21) and provides a vanishing contribution.[3] This allows one to remove some of the terms appearing in Eq. (5.21). In the regime of low diffusion, the second-order terms (*i.e.* those involving second derivatives with respect to the field values) can be neglected as they account for quantum diffusion, so only the drift term of the Fokker-Planck equation remains (see Eqs. (3.35) and (3.37)), and one finds

$$\mathcal{P}_\zeta(k) \simeq -\int \mathrm{d}\boldsymbol{\Phi}_* P_{\rm bw}\left[\boldsymbol{\Phi}_*, N_{\rm bw}(k)\right] \boldsymbol{F}_{\rm cl}(\boldsymbol{\Phi}_*) \cdot \frac{\partial}{\partial \boldsymbol{\Phi}_*} \left\langle \delta\mathcal{N}^2 \right\rangle \left(\boldsymbol{\Phi}_*\right) \tag{5.22}$$

where we recall that the drift function $\boldsymbol{F}_{\rm cl}$ was introduced in Eq. (3.21), and where the dot stands for a scalar product, namely $\boldsymbol{F}_{\rm cl} \cdot (\partial/\partial\boldsymbol{\Phi}_*) = \sum_i F_{{\rm cl},i}(\partial/\partial\Phi_i)$ where one sums over all the fields contained in the vector $\boldsymbol{\Phi}$. Since $\boldsymbol{F}_{\rm cl}$ is, by definition, $\partial\boldsymbol{\Phi}/\partial N$ along the classical trajectory, one can rewrite the derivative with respect to $\boldsymbol{\Phi}_*$ in Eq. (5.22) as a derivative with respect to N, leading to

$$\mathcal{P}_\zeta(k) \simeq \int \mathrm{d}\boldsymbol{\Phi}_* P_{\rm bw}\left[\boldsymbol{\Phi}_*, N_{\rm bw}(k)\right] \mathcal{P}_{\zeta,{\rm cl}}(\boldsymbol{\Phi}_*). \tag{5.23}$$

In this expression, the classical power spectrum $\mathcal{P}_{\zeta,{\rm cl}}$ corresponds to Eq. (3.42), obtained in the low-diffusion limit. The physical interpretation of Eq. (5.23) is rather clear: it corresponds to the standard formula for the power spectrum evaluated at $\boldsymbol{\Phi}_*$, and averaged over all possible values of $\boldsymbol{\Phi}_*$ reached $N_{\rm bw}(k)$ e-folds before the end of inflation. Let us however stress that, although intuitive, this formula only holds when quantum diffusion is low at the scale one considers: in general, the power spectrum does *not* result from an averaging procedure of the type of Eq. (5.23), and one should rather use Eq. (5.21), which features a more involved structure.

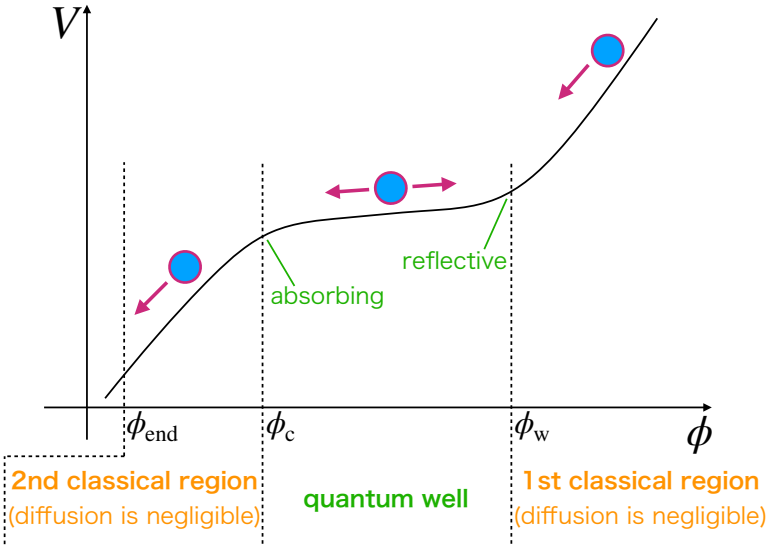

Figure 5.2: Sketch of a single-field potential studied in Sec. 5.2.2, where quantum diffusion is only effective inside a "quantum well", that is surrounded by two regions where the field is only driven by the potential gradient.

5.2.2 A quantum well between two classical regions

For explicitness, let us restrict the analysis to single-field slow-roll setups, for which the Langevin equation (3.21) reads

$$\frac{\mathrm{d}\phi}{\mathrm{d}N} = -M_{\rm Pl}^2\frac{v'}{v} + M_{\rm Pl}\sqrt{2v}\,\xi(N) \tag{5.24}$$

where ξ is a white Gaussian noise with vanishing mean and unit variance. The potential we consider is depicted in Fig. 5.2, where quantum diffusion is only effective inside the region comprised between $\phi_{\rm c}$ and $\phi_{\rm w}$ that we call the "quantum well". This quantum well is surrounded by two other regions where we assume that the stochastic noise plays a negligible role compared to the potential gradient and can therefore be neglected. This corresponds for instance to models with a flat inflection point close to the end of inflation [121, 122], where large perturbations (that possibly later collapse into primordial black holes) are produced within the well, while the CMB scales emerge in the first classical region, at $\phi > \phi_{\rm w}$.

Let us introduce a few notations. For $\phi > \phi_{\rm w}$, let $N_{\rm cl,1}(\phi)$ be the number of e-folds that is classically realized from ϕ to $\phi_{\rm w}$, and similarly, for $\phi < \phi_{\rm c}$, let $N_{\rm cl,2}(\phi)$ denote the number of e-folds that is classically realized from ϕ to $\phi_{\rm end}$. In practice, they are given by Eq. (3.47), where, for $N_{\rm cl,1}(\phi)$, the lower bound of the integral has to be set to $\phi_{\rm w}$. These functions are inverted as $\phi_{\rm cl,1}(N)$ and $\phi_{\rm cl,2}(N)$, which return the field

[3]The lower bound is $P(\boldsymbol{\Phi}_*, 0|\boldsymbol{\Phi}_0, 0) = \delta(\boldsymbol{\Phi}_* - \boldsymbol{\Phi}_0)$, so the term $P_{\rm FPT}[N_{\rm bw}(k), \boldsymbol{\Phi}_*]$ has to be evaluated at $\boldsymbol{\Phi}_* = \boldsymbol{\Phi}_0$ where it vanishes for finite $N_{\rm bw}$ since $\boldsymbol{\Phi}_0$ has been set asymptotically high up in the potential. The upper bound $P(\boldsymbol{\Phi}_*, \infty|\boldsymbol{\Phi}_0, 0)$ vanishes since all realizations exit the inflating domain after a finite number of e-folds.

value N e-folds before reaching $\phi_{\rm w}$ and $\phi_{\rm end}$ respectively. In addition, for $\phi_{\rm c} < \phi < \phi_{\rm w}$, the distribution associated with the time of first passage through $\phi_{\rm c}$ is noted $P^{\rm well}_{\rm FPT}(\mathcal{N}, \phi)$. Let us note that since the field can only decrease at $\phi < \phi_{\rm c}$, it can never return into the well once it has escaped from it, and likewise, since the field can only decrease at $\phi > \phi_{\rm w}$, it can never exit the well from above. In practice, this can be modeled by setting an absorbing boundary at $\phi_{\rm c}$ and a reflective boundary at $\phi_{\rm w}$. Finally, the probability associated with the field value after it has spent N e-folds inside the well is noted $P^{\rm well}(\phi, N) = P(\phi, N|\phi_{\rm w}, 0)$.

In Sec. 5.2.3, the calculation will be specified to the case where the quantum well is exactly flat, but the present considerations are still generic, the only assumption is that the stochastic noise can be neglected outside the well.

Backward probability

Let us first evaluate the backward probability in this model. We assume that ϕ_0 is set sufficiently high up in the potential such that the denominator of Eq. (5.20) can be discarded. In practice, this is guaranteed if one considers scales such that $N_{\rm bw}(k) \leq N_{\rm cl,2}(\phi_{\rm c}) + N_{\rm cl,1}(\phi_0)$. Since field space is one dimensional, we therefore expect the result not to depend on ϕ_0, see footnote 2.

If $N_{\rm bw} \leq N_{\rm cl,2}(\phi_{\rm c})$, the field is necessarily in the second deterministic region $N_{\rm bw}$ e-folds before the end of inflation, and the backward probability is simply

$$P_{\rm bw}(\phi_*, N_{\rm bw}) = \delta\left[\phi_* - \phi_{\rm cl,2}(N_{\rm bw})\right] \quad \text{for} \quad \phi_{\rm end} \leq \phi_* \leq \phi_{\rm c}\,. \tag{5.25}$$

If $N_{\rm bw} \geq N_{\rm cl,2}(\phi_{\rm c})$, the field is either in the quantum well or in the first deterministic region $N_{\rm bw}$ e-folds before the end of inflation. The solution of the Fokker-Planck equation, for $\phi > \phi_{\rm c}$, is given by

$$P(\phi, N|\phi_0, 0) = \begin{cases} P^{\rm well}\left[\phi, N - N_{\rm cl,1}\left(\phi_0\right)\right]\theta\left[N - N_{\rm cl,1}(\phi_0)\right] & \text{for} \quad \phi_{\rm c} \leq \phi \leq \phi_{\rm w} \\ \delta\left[\phi - \phi_{\rm cl,1}\left[N_{\rm cl,1}(\phi_0) - N\right]\right]\theta\left[N_{\rm cl,1}(\phi_0) - N\right] & \text{for} \quad \phi \geq \phi_{\rm w} \end{cases}, \tag{5.26}$$

where θ is the Heaviside function, and we do not give the solution for $\phi < \phi_{\rm c}$ since we will not use it. In order to evaluate the backward probability with Eq. (5.20), on the one hand, one needs to integrate this probability over N, giving rise to[4]

$$\int_0^\infty {\rm d}N\, P(\phi_*, N|\phi_0, 0) = \begin{cases} \int_0^\infty {\rm d}N\, P^{\rm well}(\phi_*, N) & \text{for} \quad \phi_{\rm c} \leq \phi_* \leq \phi_{\rm w} \\ N'_{\rm cl,1}\left(\phi_*\right) & \text{for} \quad \phi_* > \phi_{\rm w} \end{cases}, \tag{5.27}$$

where the prime represents the derivative with respect to ϕ. On the other hand, Eq. (5.20) involves the probability density function of the first-passage time $P_{\rm FPT}(N, \phi_*)$, which is given by

$$P_{\rm FPT}(N, \phi_*) = \begin{cases} P^{\rm well}_{\rm FPT}\left[N - N_{\rm cl,2}(\phi_{\rm c}), \phi_*\right] & \text{for} \quad \phi_{\rm c} \leq \phi_* \leq \phi_{\rm w} \\ P^{\rm well}_{\rm FPT}\left[N - N_{\rm cl,1}(\phi_*) - N_{\rm cl,2}(\phi_{\rm c}), \phi_{\rm w}\right]\theta\left[N - N_{\rm cl,1}(\phi_*) - N_{\rm cl,2}(\phi_{\rm c})\right] & \text{for} \quad \phi_* \geq \phi_{\rm w} \end{cases}. \tag{5.28}$$

[4]Note that the delta function about ϕ in the second branch of Eq. (5.26) can be rewritten as a delta function about N with a prefactor $\sim |{\rm d}\phi_{\rm cl,1}/{\rm d}N|^{-1}$.

By plugging Eqs. (5.27) and (5.28) into Eq. (5.20), it can thus be computed for $N_{\rm bw} \geq N_{\rm cl,2}(\phi_{\rm c})$, and combining the result with Eq. (5.25), one obtains

$$P_{\rm bw}\left(\phi_*, N_{\rm bw}\right) = \begin{cases} \delta\left[\phi_* - \phi_{\rm cl,2}(N_{\rm bw})\right]\theta\left[N_{\rm cl,2}(\phi_{\rm c}) - N_{\rm bw}\right] & \text{for} \quad \phi_{\rm end} \leq \phi_* \leq \phi_{\rm c} \\ P_{\rm FPT}^{\rm well}\left[N_{\rm bw} - N_{\rm cl,2}(\phi_{\rm c}), \phi_*\right] \int_0^\infty {\rm d}N\, P^{\rm well}(\phi_*, N)\theta\left[N_{\rm bw} - N_{\rm cl,2}(\phi_{\rm c})\right] & \text{for} \quad \phi_{\rm c} \leq \phi_* \leq \phi_{\rm w} \\ N'_{\rm cl,1}\left(\phi_*\right) P_{\rm FPT}^{\rm well}\left[N_{\rm bw} - N_{\rm cl,1+2}(\phi_*), \phi_{\rm w}\right]\theta\left[N_{\rm bw} - N_{\rm cl,1+2}(\phi_*)\right] & \text{for} \quad \phi_* \geq \phi_{\rm w} \end{cases}, \tag{5.29}$$

where we have defined $N_{\rm cl,1+2}(\phi_*) \equiv N_{\rm cl,1}(\phi_*) + N_{\rm cl,2}(\phi_{\rm c})$.

Power spectrum

In order to evaluate the power spectrum (5.16), one also needs to compute $\langle \delta\mathcal{N}^2 \rangle(\phi_*)$. As explained above, the boundaries placed at $\phi_{\rm c}$ and $\phi_{\rm w}$ are one-way boundaries (the field can cross them once only and only from above), so the number of e-folds realized in each of the three regions are independent random variables (invoking again the Markovian nature of the process). As a consequence, one has

$$\left\langle \delta\mathcal{N}^2 \right\rangle\left(\phi_*\right) = \begin{cases} \left\langle \delta N_{\rm cl,2}^2 \right\rangle\left(\phi_*\right) & \text{for} \quad \phi_* < \phi_{\rm c} \\ \left\langle \delta N_{\rm cl,2}^2 \right\rangle\left(\phi_{\rm c}\right) + \left\langle \delta\mathcal{N}_{\rm well}^2 \right\rangle\left(\phi_*\right) & \text{for} \quad \phi_{\rm c} < \phi_* < \phi_{\rm w} \\ \left\langle \delta N_{\rm cl,2}^2 \right\rangle\left(\phi_{\rm c}\right) + \left\langle \delta\mathcal{N}_{\rm well}^2 \right\rangle\left(\phi_{\rm w}\right) + \left\langle \delta N_{\rm cl,1}^2 \right\rangle\left(\phi_*\right) & \text{for} \quad \phi_* > \phi_{\rm w} \end{cases}, \tag{5.30}$$

with $\langle \delta N_{\rm cl,1}^2 \rangle$ and $\langle \delta N_{\rm cl,2}^2 \rangle$ given by Eq. (3.48), where, in the case of $\langle \delta N_{\rm cl,1}^2 \rangle$, the lower bound of the integral needs to be replaced with $\phi_{\rm w}$.

If the scale k is such that $N_{\rm bw}(k) < N_{\rm cl,2}(\phi_{\rm c})$, only the first branch ($\phi_* \leq \phi_{\rm c}$) of Eq. (5.29) contributes to the integral of Eq. (5.16). By acting $\partial/\partial N_{\rm bw}$ onto $P_{\rm bw}$ given in Eq. (5.29), one obtains $-\delta'[\phi_* - \phi_{\rm cl,2}(N_{\rm bw})]/N'_{\rm cl,2}(\phi_*)$. Plugging the result into Eq. (5.16), and making use of Eq. (5.30), after integration by parts one obtains $\mathcal{P}_\zeta(k) = \langle \delta N_{\rm cl,2}^2 \rangle'[\phi_{\rm cl,2}(N_{\rm bw})]/N'_{\rm cl,2}[\phi_{\rm cl,2}(N_{\rm bw})]$. Using Eqs. (3.47) and (3.48), this gives rise to Eq. (3.49), so one recovers the standard formula for the power spectrum in the low-diffusion limit, which is a good consistency check.

If the scale k is such that $N_{\rm bw}(k) > N_{\rm cl,2}(\phi_{\rm c})$, the second ($\phi_{\rm c} < \phi_* < \phi_{\rm w}$) and third ($\phi > \phi_{\rm w}$) branches of Eq. (5.29) contribute to the integral of Eq. (5.16). We denote their contributions by $\mathcal{P}_\zeta^{(2)}$ and $\mathcal{P}_\zeta^{(3)}$ respectively. We cannot say much about $\mathcal{P}_\zeta^{(2)}$ without specifying the shape of the inflationary potential inside the quantum well (this will be done in Sec. 5.2.3), so let us focus on $\mathcal{P}_\zeta^{(3)}$. When acting $\partial/\partial N_{\rm bw}$ on the third branch of Eq. (5.29), one obtains two terms, one where $\partial/\partial N_{\rm bw}$ acts on $P_{\rm FPT}^{\rm well}$ and one where $\partial/\partial N_{\rm bw}$ acts on the Heaviside function. The second term is proportional to $\delta[N_{\rm bw} - N_{\rm cl,1+2}(\phi_*)]$ so it involves $P_{\rm FPT}^{\rm well}(0, \phi_{\rm w})$, which vanishes (the probability to cross the entire well in no time at all is necessarily zero). Only remains the first term, and by plugging the result into Eq. (5.16), one obtains

$$\mathcal{P}_\zeta^{(3)}(k) = \int_{\phi_{\rm w}}^{\phi_{\rm cl,1}[N_{\rm bw} - N_{\rm cl,2}(\phi_{\rm c})]} {\rm d}\phi_* N'_{\rm cl,1}(\phi_*) \frac{\partial P_{\rm FPT}^{\rm well}\left[N_{\rm bw} - N_{\rm cl,1+2}(\phi_*), \phi_{\rm w}\right]}{\partial N_{\rm bw}} \left\langle \delta\mathcal{N}^2 \right\rangle\left(\phi_*\right). \tag{5.31}$$

Let us then perform a change of integration variable and label the field value ϕ_* via the corresponding classical e-fold number, $N_{\rm cl} = N_{\rm cl,1+2}(\phi_*)$. This allows us to rewrite the

above expression as

$$\mathcal{P}_\zeta^{(3)}(k) = \int_{N_{\rm cl,2}(\phi_{\rm c})}^{N_{\rm bw}} {\rm d}N_{\rm cl} \frac{\partial P_{\rm FPT}^{\rm well}\left(N_{\rm bw} - N_{\rm cl}, \phi_{\rm w}\right)}{\partial N_{\rm bw}} \left\langle \delta\mathcal{N}^2 \right\rangle \left(\phi_{\rm cl,1}\left[N_{\rm cl} - N_{\rm cl,2}(\phi_{\rm c})\right]\right). \quad (5.32)$$

An important remark is that since $P_{\rm FPT}^{\rm well}$ depends on $N_{\rm bw}$ only through the combination $N_{\rm bw} - N_{\rm cl}$, acting $\partial/\partial N_{\rm bw}$ on it is equivalent to acting $-\partial/\partial N_{\rm cl}$. This allows one to integrate by parts, leading to

$$\begin{aligned}\mathcal{P}_\zeta^{(3)}(k) &= P_{\rm FPT}^{\rm well}\left[N_{\rm bw} - N_{\rm cl,2}(\phi_{\rm c}), \phi_{\rm w}\right] \left\langle \delta\mathcal{N}^2 \right\rangle (\phi_{\rm w}) \\ &+ \int_{N_{\rm cl,2}(\phi_{\rm c})}^{N_{\rm bw}} {\rm d}N_{\rm cl} P_{\rm FPT}^{\rm well}\left(N_{\rm bw} - N_{\rm cl}, \phi_{\rm w}\right) \phi'_{\rm cl,1}\left[N_{\rm cl} - N_{\rm cl,2}(\phi_{\rm c})\right] \left\langle \delta\mathcal{N}^2 \right\rangle' \left(\phi_{\rm cl,1}\left[N_{\rm cl} - N_{\rm cl,2}(\phi_{\rm c})\right]\right)\end{aligned} \quad (5.33)$$

where we have used again that $P_{\rm FPT}^{\rm well}(0, \phi_{\rm w}) = 0$. In this expression, making use of Eq. (5.30), one has $\langle \delta\mathcal{N}^2 \rangle' = \langle \delta N_{\rm cl,1}^2 \rangle'$, and performing the inverse change of integration $N_{\rm cl} \to \phi_* = \phi_{\rm cl,1}[N_{\rm cl} - N_{\rm cl,2}(\phi_{\rm c})]$, one obtains

$$\begin{aligned}\mathcal{P}_\zeta^{(3)}(k) &= P_{\rm FPT}^{\rm well}\left[N_{\rm bw} - N_{\rm cl,2}(\phi_{\rm c}), \phi_{\rm w}\right] \left\langle \delta\mathcal{N}^2 \right\rangle (\phi_{\rm w}) \\ &+ \int_{\phi_{\rm w}}^{\phi_{\rm cl,1}[N_{\rm bw} - N_{\rm cl,2}(\phi_{\rm c})]} {\rm d}\phi_* P_{\rm FPT}^{\rm well}\left[N_{\rm bw} - N_{\rm cl,1+2}(\phi_*), \phi_{\rm w}\right] \left\langle \delta N_{\rm cl,1}^2 \right\rangle' (\phi_*).\end{aligned} \quad (5.34)$$

Let us note that, looking at the third branch of Eq. (5.29), the second term in the above expression can be written as $\int {\rm d}\phi_* P_{\rm bw}(\phi_*, N_{\rm bw}) \mathcal{P}_{\zeta,{\rm cl}}(\phi_*)$ where the classical power spectrum $\mathcal{P}_{\zeta,{\rm cl}} = \langle \delta N_{\rm cl}^2 \rangle' / N'_{\rm cl}$ is given in Eq. (3.49). One therefore recovers the standard power spectrum averaged with the backward probability, see Eq. (5.23), but let us stress that this is not the only contribution: there is also the first integrated term of Eq. (5.34), and $\mathcal{P}_\zeta^{(2)}$, which we have not computed yet and to which we now turn our attention. These additional contributions correspond to realizations where, $N_{\rm bw}(k)$ e-folds before the end of inflation, the field is found inside the quantum well.

5.2.3 Case of a flat quantum well

In this section, in order to derive explicit results, we assume for simplicity that the quantum well is exactly flat. One may be concerned that, if the potential is exactly flat, inflation proceeds in the ultra-slow-roll regime and the slow-roll approximation may not be valid. This, however, is not the case if the approach to the flat region is sufficiently smooth, and in practice, as shown in Refs. [54, 55], a flat well provides a good approximation to several potentials featuring flat or quasi-flat points, for which the width of the equivalent flat well has to be set by the criterion $|v''|\, v^2 \sim v'^2$ mentioned above. This toy model is therefore of practical interest.

By rescaling the field variable as $x = (\phi - \phi_{\rm c})/(\phi_{\rm w} - \phi_{\rm c})$ inside the well, where x varies between 0 and 1, the Langevin equation (5.24) takes the simple form

$$\frac{{\rm d}x}{{\rm d}N} = \frac{\sqrt{2}}{\mu}\xi(N), \quad \text{where} \quad \mu^2 = \frac{\left(\phi_{\rm w} - \phi_{\rm c}\right)^2}{M_{\rm Pl}^2 v_{\rm well}} \quad (5.35)$$

is the ratio between the squared width of the potential well and its height, in Planckian units. In Appendix B, we show that the solution to the Fokker-Planck and adjoint

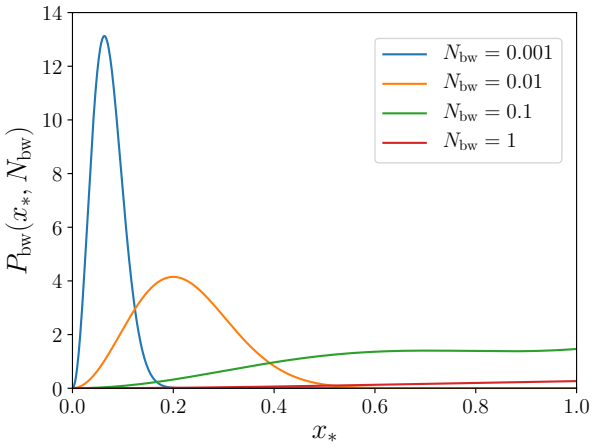

Figure 5.3: Backward probability in a flat potential with an absorbing wall at $x = 0$ and a reflective wall at $x = 1$, computed by means of Eq. (5.40), with $\mu = 1$ and for a few values of $N_{\rm bw}$, assuming that $N_{\rm cl,2}(\phi_{\rm c}) = 0$ (otherwise the value of $N_{\rm bw}$ is simply shifted by $N_{\rm cl,2}(\phi_{\rm c})$) .

Fokker-Planck equations are given by

$$P^{\rm well}(x, N|x_{\rm in}, 0) = \frac{1}{2}\vartheta_2\left(-\frac{\pi}{2}(x - x_{\rm in}), e^{-\frac{\pi^2 N}{\mu^2}}\right) + \frac{1}{2}\vartheta_2\left(-\frac{\pi}{2}(x + x_{\rm in}), e^{-\frac{\pi^2 N}{\mu^2}}\right) \tag{5.36}$$

$$P^{\rm well}_{\rm FPT}(x, N) = -\frac{\pi}{2\mu^2}\vartheta_2'\left(\frac{\pi}{2}x, e^{-\frac{\pi^2 N}{\mu^2}}\right) \tag{5.37}$$

where ϑ_2 is the second elliptic theta function defined in Eq. (A.2), and ϑ_2' denotes its derivative with respect to its first argument. Note that the expression for $P^{\rm well}_{\rm FPT}$ was already obtained in Ref. [54], see Eq. (4.11) of that reference, but in Appendix B it is derived with different techniques (namely the "method of images", while in Ref. [54] the result is obtained by solving for the characteristic function). In a flat potential, the integrals appearing in Eq. (3.46) can also be performed exactly, and for the two first moments, one obtains

$$\langle \mathcal{N}_{\rm well} \rangle (x) = \frac{\mu^2}{2}\left[1 - (1 - x)^2\right] , \tag{5.38}$$

$$\langle \delta\mathcal{N}^2_{\rm well} \rangle (x) = \frac{\mu^4}{6}\left[1 - (1 - x)^4\right] . \tag{5.39}$$

These expressions allow one to further specify the second and third branches of the backward probability in Eq. (5.29). The second branch requires one to integrate Eq. (5.36) over N when $x_{\rm in} = 1$. This is done in details at the end of Appendix B, where it is first noted that by setting $x_{\rm in} = 1$ in Eq. (5.36), one obtains $P^{\rm well}(x, N) = \vartheta_1(\pi x/2, e^{-\pi^2 N/\mu^2})$, which then gives rise to $\int_0^\infty P^{\rm well}(x, N){\rm d}N = \mu^2 x$. When $N_{\rm bw} > N_{\rm cl,2}(\phi_{\rm c})$, the backward probability (5.29) thus reads

$$P_{\rm bw}(\phi_* N_{\rm bw}) = \begin{cases} -\frac{\pi x_*}{2(\phi_{\rm w} - \phi_{\rm c})}\vartheta_2'\left(\frac{\pi}{2}x_*, e^{-\frac{\pi^2}{\mu^2}\left[N_{\rm bw} - N_{\rm cl,2}(\phi_{\rm c})\right]}\right) & \text{for} \quad \phi_{\rm c} < \phi_* < \phi_{\rm w} \\ -N'_{\rm cl,1}(\phi_*)\,\frac{\pi}{2\mu^2}\vartheta_2'\left(\frac{\pi}{2}, e^{-\frac{\pi^2}{\mu^2}\left[N_{\rm bw} - N_{\rm cl,1+2}(\phi_*)\right]}\right)\theta\left[N_{\rm bw} - N_{\rm cl,1+2}(\phi_*)\right] & \text{for} \quad \phi_* > \phi_{\rm w} \end{cases}$$

(5.40)

and is displayed in Fig. 5.3 when ϕ_* lies within the well (outside the well, the distribution depends on the inflationary potential at $\phi > \phi_{\rm w}$, which we have not specified yet) and for a few values of $N_{\rm bw}$. When $N_{\rm bw}$ is small, the distribution is peaked close to the absorbing boundary, and is in fact similar to the one obtained in Appendix B.1 without setting a reflective boundary at $x = 1$, see Fig. B.1. This is because, for small values of $N_{\rm bw}$, the probability to bounce against the reflective wall during the last $N_{\rm bw}$ e-folds spent in the well is low. Formally, one can indeed show that by expanding Eq. (5.40) in the limit $x_* \ll 1$, one recovers Eq. (B.12). When $N_{\rm bw}$ increases, the backward distribution becomes more widely spread, and centered over larger field values. Let us also note that by integrating Eq. (5.40) over ϕ_*, one can check explicitly that it is properly normalized, and that the probability to find the field inside the well $N_{\rm bw}$ e-folds before the end of inflation is given by

$$p_{\rm well}\left(N_{\rm bw}\right) = \frac{4}{\pi}\sum_{n=0}^{\infty}\frac{(-1)^n}{2n+1}e^{-\left(n+\frac{1}{2}\right)^2\frac{\pi^2}{\mu^2}\left[N_{\rm bw}-N_{\rm cl,2}(\phi_{\rm c})\right]}\,. \tag{5.41}$$

When $N_{\rm bw} = N_{\rm cl,2}(\phi_{\rm c})$, this probability equals one as expected, and then it decreases when $N_{\rm bw}$ increases.

Let us now compute the power spectrum. The contribution coming from the branch $\phi_{\rm c} < \phi_* < \phi_{\rm w}$, denoted $\mathcal{P}_\zeta^{(2)}$ in Sec. 5.2.2, can be obtained by plugging Eqs. (5.40) and (5.39) into Eq. (5.16). It is however more convenient to use Eq. (5.21) directly, where the Fokker-Planck operator can be read off from the right-hand side of Eq. (B.2), namely $\mathcal{L}_{\rm FP} = \partial^2/\partial x^2$. This gives rise to

$$\begin{aligned}\mathcal{P}_\zeta^{(2)}(k) = {}& \frac{\pi\mu^2}{3}\int_0^1 {\rm d}x\,(1-x)^2\,(5x-2)\,\vartheta_2'\left(\frac{\pi}{2}x, e^{-\frac{\pi^2}{\mu^2}N_{\rm bw}(k)}\right)\\ &+\frac{\pi\mu^2}{12}\vartheta_2'\left(\frac{\pi}{2}, e^{-\frac{\pi^2}{\mu^2}\left[N_{\rm bw}(k)-N_{\rm cl,2}(\phi_{\rm c})\right]}\right)\,.\end{aligned} \tag{5.42}$$

The integral in the first line can be performed by expanding the second elliptic function according to its definition (A.2), and by integrating each term individually. Making use of Eqs. (5.37) and(5.39), one can also show that the term in the second line exactly cancels out with the first term in Eq. (5.34). Furthermore, the integral term of $\mathcal{P}_\zeta^{(3)}$ can be evaluated by plugging Eqs. (5.37) and (5.39) into Eq. (5.34), and after performing the change of variable $\phi_* \to N_{\rm bw} - N_{\rm cl,2}(\phi_{\rm c}) - N_{\rm cl,1}(\phi_*)$ in the integral, the sum of $\mathcal{P}_\zeta^{(2)}$ and $\mathcal{P}_\zeta^{(3)}$ reads

$$\begin{aligned}\mathcal{P}_\zeta(k) = {}& \frac{4\mu^2}{3}\vartheta_2\left(0, e^{-\frac{\pi^2}{\mu^2}\left[N_{\rm bw}(k)-N_{\rm cl,2}(\phi_{\rm c})\right]}\right)\\ &+8\frac{\mu^2}{\pi^3}\sum_{n=0}^{\infty}\frac{e^{-\left(n+\frac{1}{2}\right)^2\frac{\pi^2}{\mu^2}\left[N_{\rm bw}(k)-N_{\rm cl,2}(\phi_{\rm c})\right]}}{\left(n+\frac{1}{2}\right)^2}\left[5\frac{(-1)^n}{\left(n+\frac{1}{2}\right)}-4\pi\right]\\ &-\frac{1}{2\pi}\int_e^{-\frac{\pi^2}{\mu^2}\left[N_{\rm bw}(k)-N_{\rm cl,2}(\phi_{\rm c})\right]}\frac{{\rm d}q}{q}\vartheta_2'\left(\frac{\pi}{2}, q\right)\mathcal{P}_{\zeta,{\rm cl}}\,.\end{aligned} \tag{5.43}$$

This expression applies for scales k such that $N_{\rm bw}(k) > N_{\rm cl,2}(\phi_{\rm c})$, and when $N_{\rm bw}(k) < N_{\rm cl,2}(\phi_{\rm c})$, we recall that Eq. (3.49) applies, see the discussion below Eq. (5.30). In the

last term, $\mathcal{P}_{\zeta,\mathrm{cl}} = \langle \delta N_{\mathrm{cl}}^2 \rangle' / N_{\mathrm{cl}}'$ corresponds to the standard formula for the power spectrum, see Eq. (3.49). It needs to be evaluated at the value ϕ_* related to q through the change of variables we just mentioned. Note that this last term can also be written as $\int_{\phi_{\mathrm{w}}}^{\infty} \mathrm{d}\phi_* P_{\mathrm{bw}}(\phi_*, N_{\mathrm{bw}}) \mathcal{P}_{\zeta,\mathrm{cl}}(\phi_*)$, so it corresponds to the standard power spectrum averaged over the first classical part of the inflationary potential with the backward probability, see Eq. (5.23). This, however, is not the only contribution, and the power spectrum receives correction from the quantum well directly, in the form of the terms displayed in the first two lines. One notices that if, $N_{\mathrm{bw}}(k)$ e-folds before the end of inflation, the probability to find the field inside the well is low, *i.e.* if $p_{\mathrm{well}}(N_{\mathrm{bw}}) \ll 1$, where $p_{\mathrm{well}}(N_{\mathrm{bw}})$ is given in Eq. (5.41), then the correction coming from those terms is small too. This happens when the number of e-folds elapsed before the second classical part is much larger than the mean number of e-folds spent in the well, given in Eq. (5.38). In the limit where this is the case, *i.e.* when $N_{\mathrm{bw}} - N_{\mathrm{cl},2}(\phi_{\mathrm{c}}) \gg \mu^2$, the terms with $n = 0$ and $n = 1$ dominate in the infinite sums appearing in those corrective terms, which thus provide a contribution approximated by

$$\Delta\mathcal{P}_{\zeta}(k) \simeq \underbrace{\frac{960 - 384\pi + 8\pi^3}{3\pi^3}}_{\simeq 0.02} \mu^2 e^{-\frac{\pi^2}{4\mu^2}\left[N_{\mathrm{bw}}(k) - N_{\mathrm{cl},2}(\phi_{\mathrm{c}})\right]} . \tag{5.44}$$

In practice, the amplitude of the correction coming from the direct contribution of the well can thus be assessed by comparing this value to the amplitude of the power spectrum observed in the CMB, $\mathcal{P}_{\zeta} \simeq 2.1 \times 10^{-9}$.

Quadratic potential

In order to illustrate our analytical result (5.43) with numerical computations, one needs to specify the potential outside the well (so one can evaluate $\mathcal{P}_{\zeta,\mathrm{cl}}$ appearing in the last term). For simplicity, let us consider the case of a quadratic potential interrupted by a flat quantum well,

$$V(\phi) = \begin{cases} \frac{1}{2} m^2 \phi_{\mathrm{w}}^2 & \text{for} \quad \phi_{\mathrm{end}} \leq \phi \leq \phi_{\mathrm{w}} \\ \frac{1}{2} m^2 \phi^2 & \text{for} \quad \phi \geq \phi_{\mathrm{w}} \end{cases} . \tag{5.45}$$

We also assume that there is no second classical phase, so $\phi_{\mathrm{c}} = \phi_{\mathrm{end}}$ (otherwise $\ln(k)$ is simply shifted by a constant). From Eq. (3.47), in the classical branch, one has $N_{\mathrm{cl},1}(\phi_*) = (\phi_*^2 - \phi_{\mathrm{w}}^2)/(4M_{\mathrm{Pl}}^2)$, and from Eq. (3.49), $\mathcal{P}_{\zeta,\mathrm{cl}}(\phi_*) = m^2\phi_*^4/(96\pi^2 M_{\mathrm{Pl}}^6)$.

The model contains three parameters, namely m, μ and ϕ_{w}. Let us fix two of them such that we only have one parameter to vary. In order to allow for a direct comparison with the standard case, where no quantum well is considered, we take for m the standard value

$$m \simeq 6.98 \times 10^{-6} M_{\mathrm{Pl}} \frac{2 \times 50 + 1}{2N_{\mathrm{bw}}(k_{\mathrm{p}}) + 1} , \tag{5.46}$$

which leads to the correct normalization of the amplitude of the power spectrum at CMB scales if the pivot scale of the CMB, $k_{\mathrm{p}} = 0.05\,\mathrm{Mpc}^{-1}$, exits the Hubble radius $N_{\mathrm{bw}}(k_{\mathrm{p}})$ e-folds before the end of inflation [123]. Furthermore, since the mean number of e-folds elapsed from $\phi_* > \phi_{\mathrm{w}}$ to the end of inflation is given by

$$\langle \mathcal{N}(\phi_*) \rangle = N_{\mathrm{cl},1}(\phi_*) + \langle \mathcal{N}(\phi_{\mathrm{w}}) \rangle = \frac{\phi_*^2 - \phi_{\mathrm{w}}^2}{4M_{\mathrm{Pl}}^2} + \frac{\mu^2}{2} , \tag{5.47}$$

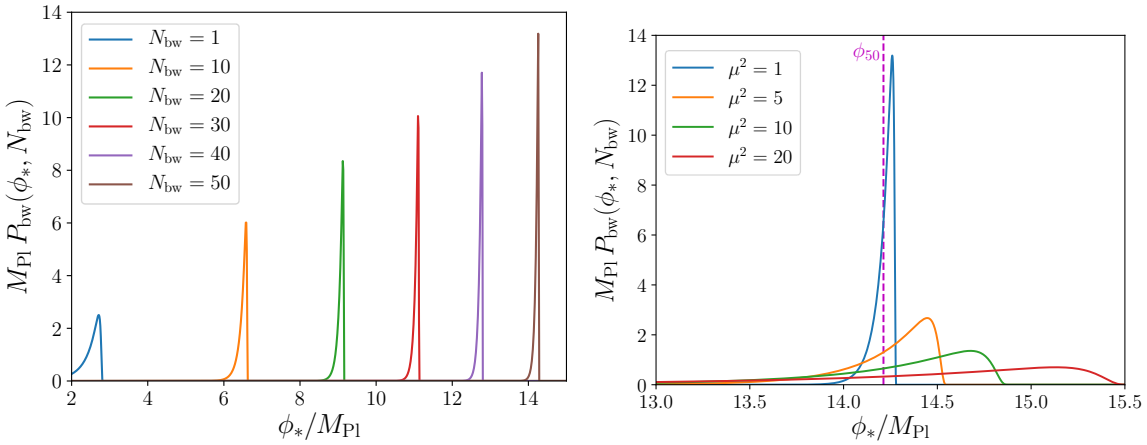

Figure 5.4: Backward probability outside the flat well in the quadratic potential (5.45), where m and $\phi_{\rm w}$ are set according to the discussion around Eq. (5.48). In the left panel, we take $\mu = 1$ (which corresponds to $\phi_{\rm w} = 2M_{\rm Pl}$) and the result is shown for several values of $N_{\rm bw}$ (the backward probability inside the well for that same value of μ is shown in Fig. 5.3). When $N_{\rm bw} = 1$, the probability to lie in the quantum well is $p_{\rm well} \simeq 0.11$, see Eq. (5.41), and this probability is negligible for the other values of $N_{\rm bw} = 1$. In the right panel, we set $N_{\rm bw} = 50$ and let μ vary. The magenta dashed line shows such a field value ϕ_{50} from which the mean number of e-folds is 50, *i.e.* such that $\langle \mathcal{N} \rangle(\phi_{50}) = 50$.

let us choose $\phi_{\rm w}$ such that this also matches the standard formula $N(\phi_*) = (\phi_*^2 - \phi_{\rm end}^2)/(4M_{\rm Pl}^2)$ where $\phi_{\rm end} = \sqrt{2}M_{\rm Pl}$ [123], which leads to

$$\phi_{\rm w} = \sqrt{2\,(\mu^2+1)}M_{\rm Pl}\,. \tag{5.48}$$

This fixes m and $\phi_{\rm w}$, and we can keep μ as the only free parameter. When $\mu = 0$, $\phi_{\rm w} = \phi_{\rm c} = \phi_{\rm end}$ and one recovers standard quadratic inflation, while $\mu > 0$ should yield finite stochastic corrections to the power spectrum at all scales. Note that quadratic inflation is known to yield a tensor-to-scalar ratio that is in strong tension with the latest observations [12], but here it is used only as a toy example to illustrate the impact of quantum diffusion at small scales on scalar fluctuations (more precisely on the amplitude and spectral tilt of the scalar power spectrum) at large scales.

In Fig. 5.4, we first display the backward probability outside the well, in the first classical region. In the left panel, we set $\mu = 1$ [so $\phi_{\rm w} = 2M_{\rm Pl}$ because of Eq. (5.48)], and we recall that the backward probability inside the well for that value of μ was shown in Fig. 5.3. When $N_{\rm bw}$ increases, the distribution becomes more peaked and centered around larger values of ϕ_*. This is because the velocity of the inflaton measured in terms of e-folds, $|{\rm d}\phi/{\rm d}N| \propto 1/\phi$, is larger for smaller ϕ. In the right panel, we set $N_{\rm bw} = 50$ and let μ vary. Because of the choice made in Eq. (5.48), the value of ϕ_* from which the mean number e-folds equals 50 is the same for all curves, and one can see that as μ decreases, the backward probability becomes more and more peaked around this value. It is also interesting to note that the backward distribution is rather skewed, and has a heavier tail at small values of ϕ_* (*i.e.* towards the location of the flat well) than at large values of ϕ_*.

The amplitude of the power spectrum at the CMB pivot scale is then displayed as a function of μ in Fig. 5.5, for $N_{\rm bw}(k_{\rm p}) = 50$ and $N_{\rm bw}(k_{\rm p}) = 60$. In the left panel, the

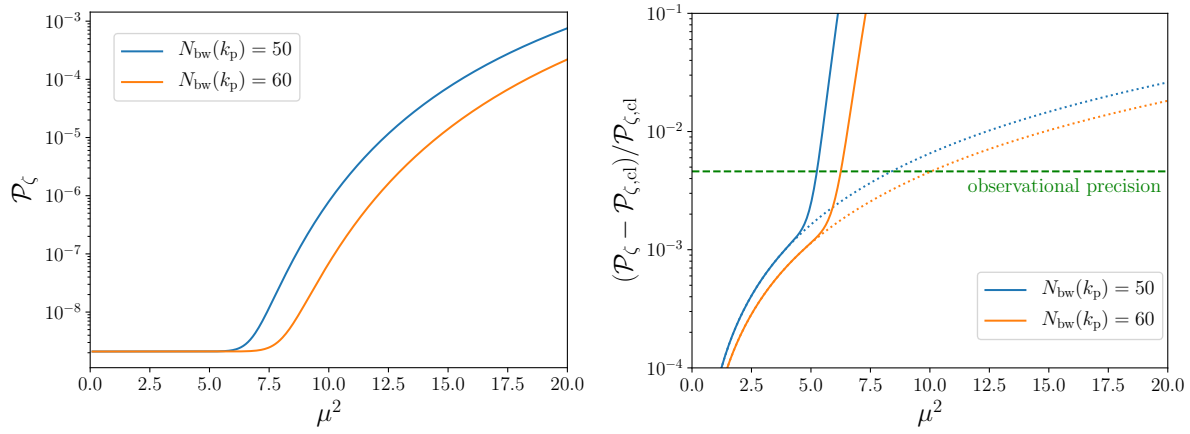

Figure 5.5: Power spectrum of curvature perturbations at the CMB pivot scale $k_{\rm p}$, in a quadratic potential with a flat quantum well near the end of inflation, see Eq. (5.45), where m and $\phi_{\rm w}$ are set according to the discussion around Eq. (5.48). The result is shown as a function of μ, for $N_{\rm bw}(k_{\rm p}) = 50$ and $N_{\rm bw}(k_{\rm p}) = 60$. In the left panel, the absolute value of the power spectrum is displayed, while the right panel shows the relative correction to the value $\mathcal{P}_{\zeta,\rm cl} = 2.1\times10^{-9}$, to which the power spectrum is normalized in the limit $\mu \to 0$. The solid lines represent the full expression while the dotted lines stand for the classical power spectrum averaged with the backward probability, *i.e.* they correspond to the last line in Eq. (5.43). The green dashed line indicates the 68% observational precision [124] on the power spectrum amplitude.

absolute value of the power spectrum is shown. One can check that when $\mu \to 0$, the power spectrum approaches the observed value $\mathcal{P}_{\zeta,\rm cl} = 2.1 \times 10^{-9}$, which is guaranteed by our choice for m. When $\mu^2 \gtrsim 6$, a substantial enhancement of the power spectrum at CMB scales is observed compared to the standard case. The correction is larger for smaller values of $N_{\rm bw}(k_{\rm p})$ (the actual value of $N_{\rm bw}(k_{\rm p})$ depends on the reheating dynamics [125, 126]), given that, when $N_{\rm bw}(k_{\rm p})$ decreases, the pivot scale crosses out the Hubble radius closer to the quantum well.

In order to compare the amplitude of the stochastic corrections with observational precision, in the right panel, we show the relative difference between the full power spectrum and its classical counterpart, and we superimpose the 68% observational precision from the Planck satellite measurement [124]. This confirms that, for $\mu^2 \gtrsim 6$, the effect is within the reach of current experiments. Interestingly, $\mu^2 \sim 6$ also corresponds to the point where the classical power spectrum averaged with the backward probability, *i.e.* the term in the last line of Eq. (5.43) (see also Eq. (5.23)), stops providing an accurate approximation to the full result. This means that, when $\mu^2 \gtrsim 6$, the quantum well does not only "blur" the relationship between k and ϕ_* at large scales, it also directly contributes to the power spectrum amplitude at the pivot scale.

Let us also note that the averaged classical power spectrum, *i.e.* the last term in Eq. (5.43), can be approximated as follows. In the regime where it provides a good description of the full result, $p_{\rm well}$ has to be small, hence, from Eq. (5.41), the lower bound in the integral of the averaged power spectrum is small too. We thus assume that it can be taken to 0, which amounts to neglecting corrections suppressed by $e^{-\pi^2 N_{\rm bw}/\mu^2}$, which are of the same order as the first terms of Eq. (5.43) that we also neglect (the fact

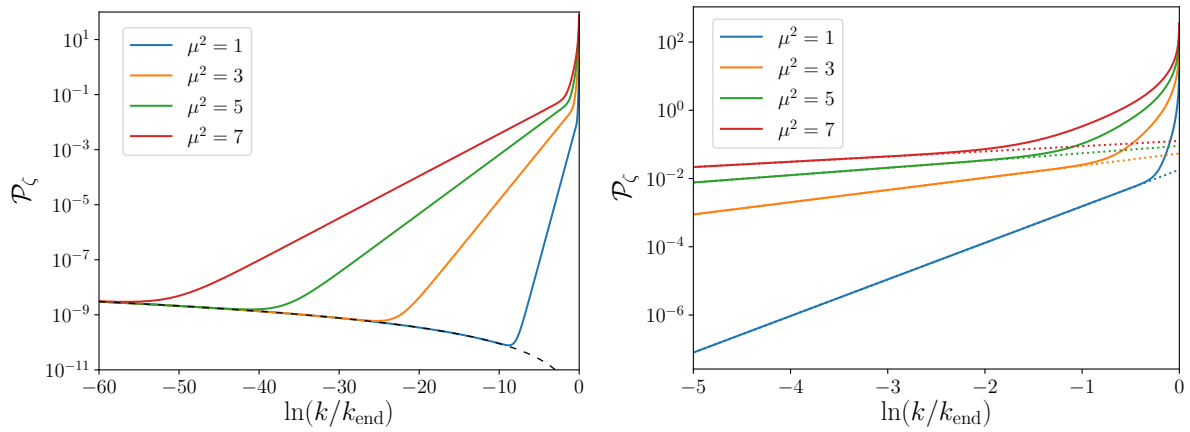

Figure 5.6: Power spectrum of curvature perturbations in the same situation as in Fig. 5.5, as a function of the wavenumber k, for $N_{\rm bw}(k_{\rm p}) = 50$. In the left panel, the black dashed line stands for the classical result, see Eq. (3.49). The right panel zooms in on the region close to $k_{\rm end}$. The dotted lines stand for the sum of Eqs. (5.49) and (5.44), which provides a good approximation to the full result when $N_{\rm bw}(k) \gg \mu^2/\pi^2$.

that the function $\vartheta_2'(\pi/2, q)$ approaches 0 when $q \to 0$ makes the approximation even better). Making use of the expressions given above for $\mathcal{P}_{\zeta,\rm cl}(\phi_*)$ and for $N_{\rm cl,1}(\phi_*)$, the classical power spectrum as a function of q is given by $\mathcal{P}_{\zeta,\rm cl} = m^2/(6\pi^2 M_{\rm Pl}^2)[N_{\rm bw}(k) + (\mu^2+1)/2+\mu^2\ln(q)/\pi^2]^2$. The integral over q can thus be performed exactly, by expanding the elliptic theta function according to its definition (A.2) and by integrating each term individually, before resumming them. One obtains

$$\mathcal{P}_\zeta(k) \simeq \frac{m^2}{6\pi^2 M_{\rm Pl}^2}\left\{\left[N_{\rm bw}(k) + \frac{1}{2}\right]^2 + \frac{\mu^4}{6}\right\}. \tag{5.49}$$

This provides an excellent approximation to the dotted lines in Fig. 5.5 (where we do not display Eq. (5.49) since the difference would not be seen by eye). This formula confirms that, when $\mu \to 0$, one recovers the standard result $\mathcal{P}_\zeta(k) \simeq \mathcal{P}_{\zeta,\rm cl}(k)$. The standard result is also recovered at large values of $N_{\rm bw}(k)$, *i.e.* at large scales.

A shift in the overall amplitude of the power spectrum can however be easily absorbed by a change in the normalization of m, hence it is not clear how the presence of those corrections would be detected experimentally. Nonetheless, we also have at our disposal high-accuracy measurements of the scale dependence of the power spectrum, in particular via its spectral index

$$n_{\rm S} = 1 + \frac{{\rm d}\ln\mathcal{P}_\zeta}{{\rm d}\ln k} \simeq 1 - \frac{{\rm d}\ln\mathcal{P}_\zeta}{{\rm d}N_{\rm bw}(k)} \tag{5.50}$$

where in the second expression, we have made use of Eq. (5.14), which is valid at leading order in slow roll only. This is why, in Fig. 5.6, we show the power spectrum as a function of k for several values of μ^2. The right panel zooms in on the region close to $k_{\rm end}$. One can see that the power spectrum is roughly divided into three regions. At small values of k, the probability to find the field inside the well $N_{\rm bw}(k)$ e-folds before the end of inflation is low, so the power spectrum is well approximated by the average of

the classical power spectrum with the backward probability. In this regime, Eq. (5.49) provides a good approximation to the full result, and from Eq. (5.50), the spectral index receives a perturbatively small correction,

$$n_{\rm S} - 1 \simeq -\frac{2}{N_{\rm bw} + \frac{1}{2}} \left[1 - \frac{\mu^4}{\mu^4 + 6\left(N_{\rm bw} + \frac{1}{2}\right)^2} \right], \tag{5.51}$$

where the first term corresponds to the standard result. At intermediate scales, this formula breaks down (as we have seen in Fig. 5.5), but one can still approximate the full result by keeping the leading-order term when expanding Eq. (5.43) in powers of $e^{-\pi^2 N_{\rm bw}(k)/\mu^2}$, which leads to Eq. (5.44). The sum of the contributions (5.49) and (5.44) is displayed with the dotted lines in the right panel of Fig. 5.6, where one can check that it indeed provides an excellent approximation to the full result when $N_{\rm bw}(k) \gg \mu^2/\pi^2$. In this intermediate regime, the spectral index is given by

$$n_{\rm S} - 1 \simeq \frac{\pi^2}{4\mu^2}\,. \tag{5.52}$$

In particular, one can see that the power spectrum is blue, *i.e.* its amplitude increases with k, which is ruled out by current measurements. This means that the scales observed in the CMB cannot be in the intermediate region, and this places strong constraints on μ. In the present toy model, this gives rise to $\mu^2 \lesssim 6$ as explained above, but this time, the effect cannot be simply re-absorbed by a change in the normalization of the parameters of the model, since the problem comes from the color of the spectrum. Finally, when $N_{\rm bw}(k) \lesssim \mu^2/\pi^2$, even this approximation breaks down, and one has to make use of the full result (5.43).

Let us stress that at both intermediate and small scales, the power spectrum is found to be very blue (and even bluer at small scales than at intermediate scales). The fact that quantum diffusion breaks the quasi scale invariance of near de Sitter expansion is related to the presence of the end-of-inflation surface, which acts as an absorbing wall in field space and strongly breaks field-translation invariance. This is a nontrivial result, and indicates that a large enhancement of the power spectrum can arise at small scales without violating slow roll, which is otherwise often presented as a necessary condition to produce primordial black holes.

One may be concerned that as k approaches $k_{\rm end}$, the power spectrum seems to diverge in Fig. 5.6. This is however an artifact of the simple toy model we have considered in this discussion, where the slope of the potential is discontinuous as one approaches $\phi_{\rm c} = \phi_{\rm end}$, where inflation is ended abruptly. One may expect that, if the transition at the end of inflation was rather described by a smooth potential, the power spectrum would approach a finite value, the details of which depend on how inflation ends. Moreover, as pointed out in Sec. 5.1.1, the present calculation of the power spectrum in the stochastic-δN formalism neglects the presence of correlations between nearby patches. While this is a valid approximation at large scales, it becomes inaccurate for scales immediately above the Hubble radius, which indicates that the result may not be trusted for wavenumbers k near $k_{\rm end}$.

Before concluding this section, let us stress that the intermediate regime, where the averaged classical power spectrum fails to reproduce the full result and Eq. (5.44) provides a reliable approximation, lies in the domain of parameter space where $N_{\rm bw}(k) \gg \mu^2/\pi^2$, *i.e.* is such that the probability to find the field in the well $N_{\rm bw}$ e-folds before the end

of inflation is exponentially suppressed, see Eq. (5.41). If $p_{\rm well}(N_{\rm bw})$ is small, one may be surprised that the averaged classical formula breaks down, but the reason is that the power spectrum inside the quantum well can be much larger than the one at large-field values, as can be seen when comparing Eqs. (5.49) and (5.44). This means that, although there are very few Hubble patches on the end-of-inflation surface for which ϕ_* lies inside the quantum well, those patches feature a very large power spectrum at the scale of interest, so large that it compensates for their sparse statistics. In such a case, one might expect a signal to arise in the statistics of very hot or very cold spots, that we may not be able to describe with the power spectrum only. This also allows us to stress that, even if $p_{\rm well}(N_{\rm bw})$ is small, the corrections induced by quantum diffusion at small scales on the large-scale power spectrum can be more involved than a simple re-averaging of the power spectrum, which shows the usefulness of the formalism we have developed in this work.

5.3 Discussion

Let us summarise our main results and draw a few conclusions of this chapter. In this work, we have derived the formalism required to compute the power spectrum of curvature perturbations in stochastic inflation. This relies on deriving the distribution of the first-passage time from a given position in field space, which had already been studied in previous works [29, 54, 55], but here, we have also accounted for the fact that the value of the fields driving inflation at the time when a given scale exits the Hubble radius is different for each realization of the stochastic process.

The most generic formulae are given by Eqs. (5.5) and (5.12), which can be used in numerical lattice simulations. In the quasi de-Sitter limit, a given scale emerges from the Hubble radius at a fixed number of e-folds before the end of inflation, and this reduces to Eq. (5.16). This formula features the backward probability distribution, *i.e.* the distribution of the field value at a given number of e-folds before the end of inflation. This is because we have computed the power spectrum in physical scales, as seen by a local observer. We have explained how to compute the backward probability in Sec. 5.1.4 in terms of the solutions of the Fokker-Planck and adjoint Fokker-Planck equations, see Eq. (5.20).

We have then studied in more detail the possible corrections arising at CMB scales from quantum diffusion occurring at small scales (*i.e.* at scales that cross out the Hubble radius close to the end of inflation). We have found that, in some regimes, the full power spectrum is well approximated by the standard result if averaged with the backward distribution. We have however stressed that this is not always the case, and that this approximation can break down even in regimes where the probability to find the fields inside the stochastically dominated region 50 e-folds before the end of inflation is small. This shows that, in general, quantum diffusion at small scales does not only blur the classical relationship between wavenumbers and field values, and that it can go beyond a simple re-averaging of the standard formulas (which otherwise yield small corrections for quasi scale-invariant power spectra, *i.e.* corrections that are proportional to the spectral running).

Finally, for illustration, we have considered the case of a single-field quadratic potential containing a flat potential well near the end of inflation. The amplitude of the stochastic corrections in that case is controlled by the parameter denoted μ^2, see Eq. (5.35), which corresponds to the squared width of the well divided by its potential height, in Planckian

units. We have found that when $\mu^2 \gtrsim 6$, the corrections coming from the quantum well are so large that they make the power spectrum blue (*i.e.* the spectral index is larger than one), which is excluded by CMB measurements. Let us stress that for $\mu^2 = 6$, the scale that crosses out the Hubble radius 50 e-folds before the end of inflation has probability $p_{\rm well} \simeq 1.5 \times 10^{-9}$ to do so when the field is inside the quantum well. The CMB therefore scans regions of the inflationary potential that are very far from the quantum well, but yet, the contribution from the well to the observed power spectrum is substantial.

This shows that, for models featuring large quantum diffusion at small scales, it is important to employ the formalism developed in this work to compute the power spectrum at large scales, even if CMB scales seem a priori (and, we argue, wrongly) immune to physics at much smaller scales. This is typically the case in models leading to primordial black holes. This also indicates that CMB measurements have the ability to constrain the shape of the inflationary potential in the entire range from the point where CMB scales are generated down to the end of inflation.

We also found that, at small scales where quantum diffusion dominates, the power spectrum becomes very blue tilted. Contrary to the standard lore, slow-roll violations are therefore not necessary to enhance perturbations at small scales and produce primordial black holes.

Let us also mention that the constraint $\mu^2 \lesssim 6$ may not seem very competitive since it was shown in Ref. [54] that $\mu^2 \gtrsim 1$ leads to an overproduction of primordial black holes anyway. However, primordial black holes arising from scales that emerge close to the end of inflation are often very light, and can Hawking evaporate before big-bang nucleosynthesis, in which case they cannot be constrained without making further assumptions (with the exception of via the stochastic gravitational wave background that is emitted in the transient phase during which they dominate the universe content [127]). More precisely, if inflation proceeds at an energy density of 10^{16}GeV (which is the largest value that is compatible with current upper bounds on the tensor-to-scalar ratio in single-field slow-roll models), the Hubble mass at the end of inflation is of the order of 10 g, and the mass that would evaporate at big-bang nucleosynthesis, 10^9 g, crosses out the Hubble radius around 10 e-folds before the end of inflation if black holes form during a radiation era, and around 6 e-folds if they form in a matter era. From Eq. (5.38), the mean number of e-folds spent in the quantum well is $\mu^2/2$, so it means that the (potentially overproduced) black holes evaporate before big-bang nucleosynthesis and can therefore not be excluded as soon as $\mu^2 \lesssim 20$ (if black holes form in a radiation era) or $\mu^2 \lesssim 12$ (if black holes form in a matter era). The constraint $\mu^2 \lesssim 6$ is therefore competitive. Furthermore, we have found that inside the quantum well, the power spectrum is blue-tilted. In such cases, it has recently been shown [128] that the mass distribution of primordial black holes peaks at the smallest masses, which are the ones that Hawking-evaporate first. In this case, the overproduction problem may be even easier to evade, and our constraint becomes even more important. Let us also mention the possibility of having multiple quantum wells, each compatible with primordial black holes constraints, but collectively leading to a large μ^2. Such models have recently been proposed in the context of the swampland conjectures [129–132], and primordial black holes arising from multi-staged inflation have been studied in Ref. [133].

The formalism we have developed also opens up quite a few prospects. First, while the concrete example we have considered in Secs. 5.2.2 and 5.2.3 is the one of a single-field, slow-roll toy model, the formalism we have developed in Sec. 5.1 applies to any inflationary setup. In particular, we have shown that the dependence on the (probability

distribution of the) initial condition $\mathbf{\Phi}_0$ drops only in single-field models in the presence of a dynamical attractor such as slow roll, but remains otherwise. It would be interesting to study the role played by initial conditions in multiple-field models.

Second, most analytical expressions we have derived are valid in the quasi de-Sitter limit, since they assume that a given scale crosses out the Hubble radius at a fixed number of e-folds before the end of inflation (hence that H is almost constant). Otherwise, analytical calculations seem difficult to carry out. However, fully numerical approaches can still be designed, making use of the exact formula (5.5) or with Eq. (5.12). This may be required to compute slow-roll corrections at next-to-leading order. Lattice simulations could also include the finite spatial correlation between the noise realizations in two separate Hubble patches.

Third, the power spectrum we have computed in this work is the statistical expectation value of the power spectrum inside a given observable universe, but it should be possible to extend our formalism to compute higher moments, such as the stochastic variance of the power spectrum for instance. This would lead to a calculation of cosmic variance that includes quantum diffusion effects. One may also want to resolve the full distribution function associated with the power spectrum. In the toy-model example mentioned above, indeed, a very small fraction of the Hubble patches on the end-of-inflation surface receive a direct contribution from the quantum well, but this contribution is so large that it leads to a substantial enhancement of the mean power spectrum. Instead of the mean power spectrum, a more relevant calculation may therefore be the probability that such a patch lies inside our observable universe, or the density of the hot (or cold) spots associated with such rare patches.

More generally, note that, in this work, as a first step, we have only performed the calculation of the power spectrum of curvature perturbations ζ at a given scale k, leaving the investigation of the full statistics of ζ_k, and possibly, of joint distributions between the curvature perturbations at several scales, for future works. The reason is that the main application we have considered is the imprint left by quantum diffusion at small scales on large-scales observables such as the CMB. Since, at large scales, non-Gaussianities have not been detected yet, the power spectrum is the only observable we have at our disposal, which explains why we focused on the power spectrum. We however think that the tools we have developed here laid the ground for such extensions to be carried out in the future.

Chapter 6

Bipartite temporal Bell inequalities for two-mode squeezed states

In this chapter, we test for violations of bipartite temporal Bell inequalities for two-mode squeezed states. Although the motivations and basics of this work are described in Part I in detail, let us state what we compute briefly and explicitly here.

Suppose that, given a bipartite system composed of two subsystems '1' and '2', Alice measures a dichotomic variable $\hat{S}_1$ on the first subsystem at times t_a and t'_a while Bob measures $\hat{S}_2$ on the second subsystem at t_b and t'_b. For a two-time correlator $E\left(t_a, t_b\right)$, whose explicit form is shown in Eq. (6.11), an inequality with the same form as (4.4),

$$B \equiv E(t_a, t_b) + E(t_a, t'_b) + E(t'_a, b) - E(t'_a, t'_b) \leq 2\,, \tag{6.1}$$

is satisfied under the assumptions of realism and locality. We call this setup "bipartite temporal Bell inequality" (see Sec. 4.4 for an overview of various classes of Bell inequalities). We intend to test this inequality for two-mode squeezed states, whose time evolution is described by a unitary operator $\hat{U}(t) = \hat{U}_{\mathrm{S}}(t)\hat{R}(t)$ composed of the squeezing operator

$$\hat{U}_{\mathrm{S}}(t) = \exp\left(re^{-2i\varphi}\hat{c}_1^\dagger\hat{c}_2^\dagger - re^{2i\varphi}\hat{c}_1\hat{c}_2\right)\,, \tag{6.2}$$

and the rotation operator

$$\hat{R}(t) = \exp\left(i\theta\hat{c}_1^\dagger\hat{c}_1 + i\theta\hat{c}_2^\dagger\hat{c}_2\right) = e^{i\theta\hat{n}_1}e^{i\theta\hat{n}_2} \tag{6.3}$$

(see also Eqs. (2.95)-(2.97)). Here, $\hat{c}_i$ and $\hat{c}_i^\dagger$ denote the annihilation operator and the creation operator in the subsystem $i = 1, 2$. They satisfy the commutation relations $\left[\hat{c}_i, \hat{c}_j^\dagger\right] = \delta_{ij}$, and $\hat{n}_i = \hat{c}_i^\dagger\hat{c}_i$ is the number of particles operator. Two-mode squeezed states describe bipartite continuous systems, and the investigation of Bell inequalities first requires to build dichotomic observables for such systems. We thus use the z-component of the Larsson's spin operator [106],

$$\hat{S}_i(\ell) = \sum_{n=-\infty}^{\infty}(-1)^n\int_{n\ell}^{(n+1)\ell}\mathrm{d}Q_i\,|Q_i\rangle\langle Q_i| \tag{6.4}$$

as the dichotomic variables (see also Eq. (4.7)), where $|Q\rangle_i$ is an eigenstate of the position operator for the subsystem i,

$$\hat{Q}_i = \frac{1}{\sqrt{2}}\left(\hat{c}_i + \hat{c}_i^\dagger\right)\,. \tag{6.5}$$

Several comments are in order. First, two-mode squeezed states arise commonly from a quadratic Hamiltonian including quantum optical setups and are characterized by three parameters: the squeezing amplitude r, the squeezing angle φ and the rotation angle θ. As mentioned in Sec. 2.3, θ is often discarded in the literature since it is irrelevant for a state at a fixed time. However, it appears in two-time correlators, so we take it into account properly. In fact, we will see that it plays an important role in violations of bipartite temporal Bell inequalities. Second, bipartite temporal Bell inequalities have the advantage that realism and locality can be tested by using only one direction of a spin. This means that they are applicable to continuous-variable systems where only the position variable can be measured. Third, although this study is carried out in a general context, it is particularly relevant for cosmology as discussed in Part I. Cosmological perturbations take two-mode squeezed states where the '1' and '2' subsystems are realized as '$\boldsymbol{k}$' and '$-\boldsymbol{k}$' modes. Due to the negligible decaying mode, only the position variable can be measured. Therefore, in contrast with spatial Bell inequalities, bipartite temporal Bell inequalities could be tested in cosmology in principle. This has the potential to provide direct evidence that the structure of the universe has a quantum origin.

This chapter is written based on our previous work [81].

6.1 Two-time correlators

In this section, we discuss two-time correlators, $E(t_a, t_b)$, which are pieces included in bipartite temporal Bell inequalities. In Sec. 6.1.1, we show that two-time correlators are expressed using an anti-commutator in terms of projective measurements. In Sec. 6.1.2, we derive a formula to calculate the correlators. Some technical parts are shown in Appendix C.

6.1.1 Projective measurements

The investigation of temporal Bell inequalities requires one to define quantum expectation values of projective measurements. Indeed, in spatial Bell inequalities, the two operators $\hat{S}_1^a$ and $\hat{S}_2^b$ commute (since they act on two separate subsystems), hence $\hat{S}_1^a\hat{S}_2^b$ is Hermitian and the correlator is simply given by $E(a,b) = \langle\hat{S}_1^a\hat{S}_2^b\rangle$. However, in temporal Bell inequalities, one has to work in the Heisenberg picture and consider the time-evolved operators

$$\hat{S}_1(t_a) = \hat{U}^\dagger(t_a)\hat{S}_1\hat{U}(t_a) \qquad \text{and} \qquad \hat{S}_2(t_b) = \hat{U}^\dagger(t_b)\hat{S}_2\hat{U}(t_b) \tag{6.6}$$

where $\hat{U}(t)$ is the unitary time evolution operator. Although $\hat{S}_1$ and $\hat{S}_2$ commute, it is not the case in general for $\hat{S}_1(t_a)$ and $\hat{S}_2(t_b)$, hence $\hat{S}_1(t_a)\hat{S}_2(t_b)$ is not Hermitian, and taking its expectation value would not give a real result. One must instead define quantum expectation values of projective measurements, which is done here following the prescription of Ref. [112]. For explicitness, let us assume that $t_a \leq t_b$ although we will see that our final result also applies to the opposite situation. For the dichotomic variable $\hat{S}_1(t_a)$, with possible outcomes ±1, the projection operators onto the $+1$-eigenspace and the -1-eigenspace are respectively given by

$$\hat{P}_1^{(1)} = \frac{1}{2}\left[1 + \hat{S}_1\left(t_a\right)\right] \qquad \text{and} \qquad \hat{P}_{-1}^{(1)} = \frac{1}{2}\left[1 - \hat{S}_1\left(t_a\right)\right], \tag{6.7}$$

and similar expressions for $\hat{P}_1^{(2)}$ and $\hat{P}_{-1}^{(2)}$, the projection operators onto the $+1$-eigenspace and the -1-eigenspace of $\hat{S}_1(t_b)$. Let us denote by r and s the outcomes of the first and second measurements respectively. We denote by $P(r,s)$ the joint probability for Alice to get the outcome r and for Bob to get the outcome s, which can be expressed as the probability that Alice observes the outcome r, multiplied by the probability that Bob gets the outcome s upon measuring the state of the system after it has collapsed due to Alice's measurement. According to the projection postulate, after performing the measurement of $\hat{S}_1(t_a)$ on the state $|\psi\rangle$, if the outcome of the measurement is $r=+1$, the state becomes $\hat{P}_1^{(1)}|\psi\rangle$, while if the outcome of the measurement is $r=-1$, the state becomes $\hat{P}_{-1}^{(1)}|\psi\rangle$. After the first measurement, $|\psi\rangle$ thus becomes $\hat{P}_r^{(1)}|\psi\rangle$, so according to the Born rule, the joint probability is given by

$$
\begin{aligned}
P(r,s) &= \left\langle \psi \right| \hat{P}_r^{(1)} \hat{P}_s^{(2)} \hat{P}_r^{(1)} \left| \psi \right\rangle && (6.8)\\
&= \frac{1}{4} + \frac{r}{4} \left\langle \psi \right| \hat{S}_1\left(t_a\right) \left| \psi \right\rangle + \frac{s}{8} \left\langle \psi \right| \hat{S}_2\left(t_b\right) \left| \psi \right\rangle + \frac{rs}{8} \left\langle \psi \right| \left\{ \hat{S}_1\left(t_a\right), \hat{S}_2\left(t_b\right) \right\} \left| \psi \right\rangle \\
&\quad + \frac{s}{8} \left\langle \psi \right| \hat{S}_1\left(t_a\right) \hat{S}_2\left(t_b\right) \hat{S}_1\left(t_a\right) \left| \psi \right\rangle , && (6.9)
\end{aligned}
$$

where we have used that, since $\hat{S}_1\left(t_a\right)$ is a spin operator, $\hat{S}_1^2\left(t_a\right) = 1$, and that $r^2 = 1$, and where $\{\cdot,\cdot\}$ denotes the anti-commutator. We now introduce the correlator

$$
E\left(t_a, t_b\right) = \sum_{r,s} rsP(r,s) = P(+1,+1) - P(+1,-1) - P(-1,+1) + P(-1,-1) . \quad (6.10)
$$

Plugging Eq. (6.9) into that formula, one obtains

$$
E\left(t_a, t_b\right) = \frac{1}{2} \left\langle \psi \right| \left\{ \hat{S}_1\left(t_a\right), \hat{S}_2\left(t_b\right) \right\} \left| \psi \right\rangle , \quad (6.11)
$$

One can check that, by construction, this correlator is real since taking the anticommutator guarantees that the operator $\left\{ \hat{S}_1\left(t_a\right), \hat{S}_2\left(t_b\right) \right\}$ is Hermitian. Let us also note that although we assumed $t_a \leq t_b$, the result is perfectly symmetric in t_a and t_b so the correlator does not depend on who between Alice and Bob measures first.

6.1.2 Correlator

Plugging Eq. (6.4) into Eq. (6.11), one obtains for the two-time correlator

$$
\begin{aligned}
E(t_a,t_b) &\equiv \frac{1}{2} \left\langle 0,0 \right| \left\{ \hat{S}_1(t_a), \hat{S}_2(t_b) \right\} \left| 0,0 \right\rangle && (6.12)\\
&= \Re\mathrm{e} \left\langle 0,0 \right| \hat{U}^\dagger(t_a) \hat{S}_1 \hat{U}(t_a) \hat{U}^\dagger(t_b) \hat{S}_2 \hat{U}(t_b) \left| 0,0 \right\rangle && (6.13)\\
&= \sum_{n=-\infty}^{\infty} \sum_{m=-\infty}^{\infty} (-1)^{n+m} \int_{n\ell}^{(n+1)\ell} \mathrm{d}\tilde{Q}_1 \int_{m\ell}^{(m+1)\ell} \mathrm{d}\bar{Q}_2 \\
&\quad \Re\mathrm{e} \left[\left\langle 0,0 \right| \hat{U}^\dagger(t_a) \left| \tilde{Q}_1 \right\rangle \left\langle \tilde{Q}_1 \right| \hat{U}(t_a) \hat{U}^\dagger(t_b) \left| \bar{Q}_2 \right\rangle \left\langle \bar{Q}_2 \right| \hat{U}(t_b) \left| 0,0 \right\rangle \right] . && (6.14)
\end{aligned}
$$

By introducing the closure relation $\hat{1} = \int_{-\infty}^{\infty} \mathrm{d}\tilde{Q}_2 \left| \tilde{Q}_2 \right\rangle \left\langle \tilde{Q}_2 \right|$ between the first and the second correlators in the argument of the real part, and $\hat{1} = \int_{-\infty}^{\infty} \mathrm{d}\bar{Q}_1 \left| \bar{Q}_1 \right\rangle \left\langle \bar{Q}_1 \right|$ between

the second and the third correlators, one obtains

$$E(t_a,t_b) = \sum_{n=-\infty}^{\infty}\sum_{m=-\infty}^{\infty}(-1)^{n+m}\int_{n\ell}^{(n+1)\ell}\mathrm{d}\tilde{Q}_1\int_{m\ell}^{(m+1)\ell}\mathrm{d}\bar{Q}_2\int_{-\infty}^{\infty}\mathrm{d}\tilde{Q}_2\int_{-\infty}^{\infty}\mathrm{d}\bar{Q}_1$$
$$\Re\mathrm{e}\left[\Psi^*_{2\mathrm{sq}}(\tilde{Q}_1,\tilde{Q}_2;t_a)\Psi_{2\mathrm{sq}}(\bar{Q}_1,\bar{Q}_2;t_b)\left\langle\tilde{Q}_1,\tilde{Q}_2\right|\hat{U}(t_a)\hat{U}^\dagger(t_b)\left|\bar{Q}_1,\bar{Q}_2\right\rangle\right] \quad (6.15)$$

In this expression, the wavefunction in position space is given by Eq. (C.28), as derived from Eq. (2.107) in Appendix C.1. It has a Gaussian structure. The correlator $\left\langle\tilde{Q}_1,\tilde{Q}_2\right|\hat{U}(t_a)\hat{U}^\dagger(t_b)\left|\bar{Q}_1,\bar{Q}_2\right\rangle$ is calculated in Appendix C.2, where it is shown to be also of the Gaussian form, see Eq. (C.64). Combining these two results, one obtains

$$\Psi^*_{2\mathrm{sq}}(\tilde{Q}_1,\tilde{Q}_2;t_a)\Psi_{2\mathrm{sq}}(\bar{Q}_1,\bar{Q}_2;t_b)\left\langle\tilde{Q}_1,\tilde{Q}_2\right|\hat{U}(t_a)\hat{U}^\dagger(t_b)\left|\bar{Q}_1,\bar{Q}_2\right\rangle = \mathcal{A}\exp\left(\frac{1}{2}X^{\mathrm{T}}\Lambda X\right) \quad (6.16)$$

where $X^{\mathrm{T}} = \left[\bar{Q}_1,\bar{Q}_2,\tilde{Q}_1,\tilde{Q}_2\right]$,

$$\mathcal{A} = \left(\pi^2\cosh^2 r_a\cosh^2 r_b\sqrt{1-e^{4i\varphi_a}\tanh^2 r_a}\sqrt{1-e^{-4i\varphi_b}\tanh^2 r_b}\sqrt{\det M}\right)^{-1}, \quad (6.17)$$

with $\det M$ given in Eq. (C.52), and

$$\Lambda = \begin{bmatrix} \mathcal{D}_1 & \mathcal{D}_2 & D_3 & D_4 \\ \mathcal{D}_2 & \mathcal{D}_1 & D_4 & D_3 \\ D_3 & D_4 & \bar{\mathcal{D}}_1 & \bar{\mathcal{D}}_2 \\ D_4 & D_3 & \bar{\mathcal{D}}_2 & \bar{\mathcal{D}}_1 \end{bmatrix}. \quad (6.18)$$

In this last expression, we have introduced

$$\mathcal{D}_1 = \frac{1}{2} + A(r_b,\varphi_b) - D_1, \quad \bar{\mathcal{D}}_1 = \frac{1}{2} + A^*(r_a,\varphi_a) - \bar{D}_1 \quad (6.19)$$
$$\mathcal{D}_2 = B(r_b,\varphi_b) - D_2, \quad \bar{\mathcal{D}}_2 = B^*(r_a,\varphi_a) - \bar{D}_2, \quad (6.20)$$

where A and B are given in Eq. (C.29), and D_1, D_2, $\bar{D}_1$ and $\bar{D}_2$ by Eqs. (C.60) and (C.61).

The Gaussian integral over $\bar{Q}_1$ and $\tilde{Q}_2$ in Eq. (6.15) can then be performed, and one obtains

$$E(t_a,t_b) = \Re\mathrm{e}\left[\frac{2\pi\mathcal{A}}{\sqrt{\mathcal{D}_1\bar{\mathcal{D}}_1 - D_4^2}}\sum_{n,m=-\infty}^{\infty}(-1)^{n+m}\int_{n\ell}^{(n+1)\ell}\mathrm{d}Y_1\int_{m\ell}^{(m+1)\ell}\mathrm{d}Y_2\exp\left(\frac{1}{2}Y^{\mathrm{T}}\Xi Y\right)\right], \quad (6.21)$$

where

$$\Xi_{11} = \mathcal{D}_1 - \frac{\bar{\mathcal{D}}_1\mathcal{D}_2^2 + \mathcal{D}_1 D_3^2 - 2\mathcal{D}_2 D_3 D_4}{\mathcal{D}_1\bar{\mathcal{D}}_1 - D_4^2}, \quad (6.22)$$
$$\Xi_{22} = \bar{\mathcal{D}}_1 - \frac{\mathcal{D}_1\bar{\mathcal{D}}_2^2 + \bar{\mathcal{D}}_1 D_3^2 - 2\bar{\mathcal{D}}_2 D_3 D_4}{\mathcal{D}_1\bar{\mathcal{D}}_1 - D_4^2}, \quad (6.23)$$
$$\Xi_{12} = \Xi_{21} = D_4 - \frac{\bar{\mathcal{D}}_1\mathcal{D}_2 D_3 + \mathcal{D}_1\bar{\mathcal{D}}_2 D_3 - \mathcal{D}_2\bar{\mathcal{D}}_2 D_4 - D_3^2 D_4}{\mathcal{D}_1\bar{\mathcal{D}}_1 - D_4^2}. \quad (6.24)$$

A few comments are in order regarding this formula. First, in Appendix D.1, we study the conditions under which the Gaussian integrals in Eq. (6.21) are convergent, and we find that it is the case if

$$\Re\mathrm{e}\,(\Xi_{11})<0,\quad \Re\mathrm{e}\,(\Xi_{22})<0,\quad \Re\mathrm{e}\left(\Xi_{11}-\frac{\Xi_{12}^2}{\Xi_{22}}\right)<0,\quad \Re\mathrm{e}\left(\Xi_{22}-\frac{\Xi_{12}^2}{\Xi_{11}}\right)<0, \tag{6.25}$$

see Eq. (D.17). In practice, we have checked that these conditions are always satisfied in all physical configurations we have studied, but let us stress that all formulas derived below assume that Eq. (6.25) holds. Second, as explained in footnote 2 in Appendix C.2, in order to solve the sign ambiguity in the term $\sqrt{\det M}$ that appears in Eq. (6.17) for $\mathcal{A}$, one needs to solve an eigenvalue problem for M, which is a 12×12 matrix. However, one can show that the following identity holds for any r_a, r_b, φ_a, φ_b, θ_a and θ_b,

$$\frac{\mathcal{A}}{\sqrt{\mathcal{D}_1\bar{\mathcal{D}}_1-D_4^2}}=\frac{\sqrt{\Xi_{11}\Xi_{22}-\Xi_{12}^2}}{4\pi^2}\,, \tag{6.26}$$

which simplifies the prefactor in Eq. (6.21) and allows us to avoid dealing with the eigenvalue problem.[1] Finally, let us point out that although $E(t_a,t_b)$ a priori depends on 6 parameters, r_a, r_b, φ_a, φ_b, θ_a and θ_b, only the difference between the rotation angles is involved, namely $\Delta\theta\equiv\theta_a-\theta_b$, see the formulas obtained in Appendix C.2. This is because, as mentioned above, the rotation angle only appears in the time evolution from t_a and t_b. As a consequence, $E(t_a,t_b)$ depends on 5 parameters only.

6.2 Analytical limits

Before evaluating Eq. (6.21) numerically, and exploring whether or not there are configurations where the Bell inequality (4.4) can be violated, let us first study some limiting cases analytically. This will be useful to design a strategy for the numerical exploration of Sec. 6.3, which is otherwise tedious given the large dimensionality of parameter space. Indeed, at each time t_a, t_a', t_b, t_b', one must specify a squeezing amplitude, a squeezing angle and a rotation angle. Because of the above remark on the rotation angles, only the combinations $\Delta\theta_{ab}$, $\Delta\theta_{ab'}$, $\Delta\theta_{a'b}$ and $\Delta\theta_{a'b'}$ are involved, which are related through

[1] Contrary to $\sqrt{\det M}$, $\sqrt{\det\Xi}$ does not require solving an eigenvalue problem. Indeed, since Ξ is a 2×2 matrix, it has two eigenvalues with a negative real sign (see below), which can be written as $d_\pm=-\rho_\pm e^{i\alpha_\pm}$, with $\rho_\pm>0$ and $-\pi/2<\alpha_\pm<\pi/2$. This means that $\det\Xi=d_+d_-=\rho_+\rho_-e^{i(\alpha_++\alpha_-)}$. Since $-\pi<\alpha_++\alpha_-<\pi$, the phase of $\det\Xi$ never crosses the branch cut of the square root function and thus it leaves no sign ambiguity. Notice that, strictly speaking, in order to ensure that the eigenvalues of Ξ have a negative real part, one needs to impose a stronger condition than Eq. (6.25), where the last two inequalities are replaced with $\Re\mathrm{e}\,(\Xi_{11})\,\Re\mathrm{e}\,(\Xi_{22})-\Re\mathrm{e}\,(\Xi_{12})^2>0$. This is the analog of Eq. (D.18), while Eq. (6.25) is the analog of Eq. (D.17). Furthermore, in order to ensure that Ξ can be diagonalized by an orthogonal matrix, one has to verify that Ξ is normal *i.e.* $\Xi\Xi^\dagger=\Xi^\dagger\Xi$, see also footnote 2. From Eq. (6.30), one can check that this is the case when $r_a=r_b$ in the large-squeezing limit. Otherwise, one can nevertheless find an invertible matrix that transforms Ξ into a diagonal matrix in the following way. If one writes $\Xi=-A+iB$, as long as $=-\Re\mathrm{e}\,(\Xi)$ is positive definite, $\sqrt{A}$ is well-defined. Since $\sqrt{A}^{-1}B\sqrt{A}^{-1}$ is real and symmetric, it can be diagonalized by an orthogonal matrix O. Then, one can construct an invertible matrix $V\equiv\sqrt{A}^{-1}O$, so that $V^{\mathrm{T}}\Xi V$ is diagonal. Although its diagonal elements are not the eigenvalues of Ξ anymore, this "diagonalization" makes it possible to perform the Gaussian integral analytically. In any case, the procedure is straightforward since one only needs to compute the eigenvalues of a 2×2 matrix.

the Chasles relation $\Delta\theta_{ab} - \Delta\theta_{a'b} + \Delta\theta_{a'b'} - \Delta\theta_{ab'} = 0$. This still leaves us with 11 parameters to explore, and at each point in parameter space, each correlator appearing in Eq. (4.4) is given by a double infinite sum of double integrals. Even though one of the two integrals can be performed analytically, see Eq. (6.35) in Sec. 6.3 below, this remains computationally heavy, which justifies the need for further analytical insight.

6.2.1 Large-ℓ limit

In the limit where ℓ is large, as mentioned above the spin operator (6.4) becomes the sign operator, see Eq. (4.9). In this regime, only four terms in the sum (6.21) remain, namely those for $(n, m) = (0, 0)$, $(-1, 0)$, $(0, -1)$ and $(-1, -1)$. By performing the change of integration variable $Y_1 \to -Y_1$ and $Y_2 \to -Y_2$, one can see that the integrals for $(n, m) = (0, 0)$ and $(n, m) = (-1, -1)$ are the same, and that the integrals for $(n, m) = (-1, 0)$ and $(n, m) = (0, -1)$ are the same. This gives rise to

$$E(t_a, t_b) = \Re\mathrm{e}\left[\frac{4\pi\mathcal{A}}{\sqrt{\mathcal{D}_1\bar{\mathcal{D}}_1 - D_4^2}}\left(\int_0^\infty \mathrm{d}Y_1 \int_0^\infty \mathrm{d}Y_2 - \int_{-\infty}^0 \mathrm{d}Y_1 \int_0^\infty \mathrm{d}Y_2\right) \exp\left(\frac{1}{2}Y^{\mathrm{T}}\Xi Y\right)\right]. \tag{6.27}$$

In Appendix D.1, it is shown how the two integrals appearing in Eq. (6.27) can be expressed in terms of the arc tan function, see Eqs. (D.14) and (D.16). Making use of Eq. (6.26), this leads to

$$E(t_a, t_b) \underset{\ell\to\infty}{\longrightarrow} \frac{2}{\pi}\Re\mathrm{e}\left[\arctan\left(\frac{\Xi_{12}}{\sqrt{\Xi_{11}\Xi_{22} - \Xi_{12}^2}}\right)\right]. \tag{6.28}$$

This formula (6.28) is compared with a full numerical computation of Eq. (6.21) in Fig. 6.1, where one can check that it correctly reproduces the asymptotic value of $E(t_a, t_b)$ when $\ell \to \infty$.

6.2.2 Small-ℓ limit

In the small-ℓ limit, conversely, an infinitely large number of terms in the sum over n and m in Eq. (6.21) substantially contribute to the result. However, the range of the integrals appearing in Eq. (6.21) becomes very small in that limit, so one can Taylor expand the integrand in each range and perform the integral analytically. This procedure is nonetheless delicate and in Appendix D.2, it is performed in detail, making use of elliptic theta functions to carefully resum and expand the different contributions. Plugging Eqs. (D.36) and (6.26) into Eq. (6.21), one obtains

$$E(t_a, t_b) \underset{\ell\ll e^r}{\longrightarrow} \frac{8}{\pi^2}\Re\mathrm{e}\left(e^{p_+} - e^{p_-}\right), \qquad \text{where} \qquad p_\pm \equiv \frac{\pi^2\left(\Xi_{11} + \Xi_{22} \pm 2\Xi_{12}\right)}{2\left(\Xi_{11}\Xi_{22} - \Xi_{12}^2\right)\ell^2}. \tag{6.29}$$

Notice that the expansion performed in Appendix D.2 requires that $\Re\mathrm{e}\left(\Xi_{11} - \Xi_{12}^2/\Xi_{22}\right) < 0$, see Eq. (A.27), which here is guaranteed by Eq. (6.25). Note also that "$\ell \ll e^r$" is a shorthand notation for $\ell \ll \min(e^{r_a}, e^{r_b})$. The formula (6.29) is again compared with the full numerical computation of Eq. (6.21) in Fig. 6.1, where one can check that it gives a very good fit to the full result, up to values of ℓ of order e^r.

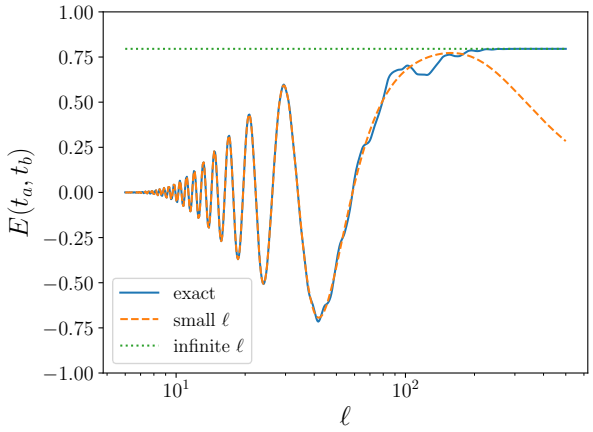

Figure 6.1: The correlation function $E(t_a, t_b)$ for $r_a = r_b = 5, \varphi_a = -0.2, \varphi_b = 0.2, \Delta\theta = 0.5$, as a function of ℓ. The blue line corresponds to the numerical computation of Eq. (6.21), the dashed orange line to the small-ℓ approximation (6.29), and the dotted green line to the large-ℓ approximation (6.28). One can check that these two approximations give good fits to the full result in their respective domains of validity, $\ell \ll e^r$ and $\ell \gg e^r$.

6.2.3 Large-squeezing limit

Another limit of interest is when the squeezing amplitude of the state is large. A large amount of squeezing is associated with a large entanglement entropy and a large quantum discord between the two subsystems [20], *i.e.* to the presence of genuine quantum correlations. In Ref. [72], it was shown that the usual Bell inequalities can be violated by two-mode squeezed states provided the squeezing amplitude is large enough (namely $r \gtrsim 1.2$), so one might expect that bipartite temporal Bell inequalities also require a minimum amount of squeezing.

Note that since the squeezing amplitude r always appears in the form of e^r, the large-squeezing regime corresponds to $e^r \gg 1$ (hence the value $r = 5$, which is used in most numerical applications below, falls in that regime). For convenience, we thus introduce the notation $u \equiv e^{-r}$, so the large-squeezing limit stands for u_a, $u_b \ll 1$. In this regime, from Eqs. (6.22)-(6.24), one obtains

$$\Xi_{11} \simeq -2\frac{u_b^2}{\mathcal{X}}, \qquad \Xi_{22} \simeq -2\frac{u_a^2}{\mathcal{X}}, \qquad \Xi_{12} \simeq e^{i\Delta\theta}\left(e^{2i\varphi_a} + e^{-2i\varphi_b}\right)\frac{u_a u_b}{\mathcal{X}}, \tag{6.30}$$

where

$$\mathcal{X} = \frac{1}{8}\left[4 - e^{2i\Delta\theta}\left(e^{2i\varphi_a} + e^{-2i\varphi_b}\right)^2\right]. \tag{6.31}$$

One can easily check that $\Re\mathrm{e}\,(\mathcal{X}) \geq 0$, so $\Re\mathrm{e}\,(\Xi_{11}) < 0$ and $\Re\mathrm{e}\,(\Xi_{22}) < 0$, and the two first conditions of Eq. (6.25) are satisfied. Moreover, since $\Xi_{11} - \Xi_{12}^2/\Xi_{22} = -4u_b^2$, $\Xi_{22} - \Xi_{12}^2/\Xi_{11} = -4u_a^2$, they are real and negative, which shows that the two last conditions of Eq. (6.25) are satisfied too.

6.2.4 Large-ℓ, large-squeezing limit

Let us now combine the two limits studied in Secs. 6.2.1 and 6.2.3, and investigate the large-ℓ, large-squeezing limit. By plugging Eqs. (6.30) and (6.31) into Eq. (6.28), one

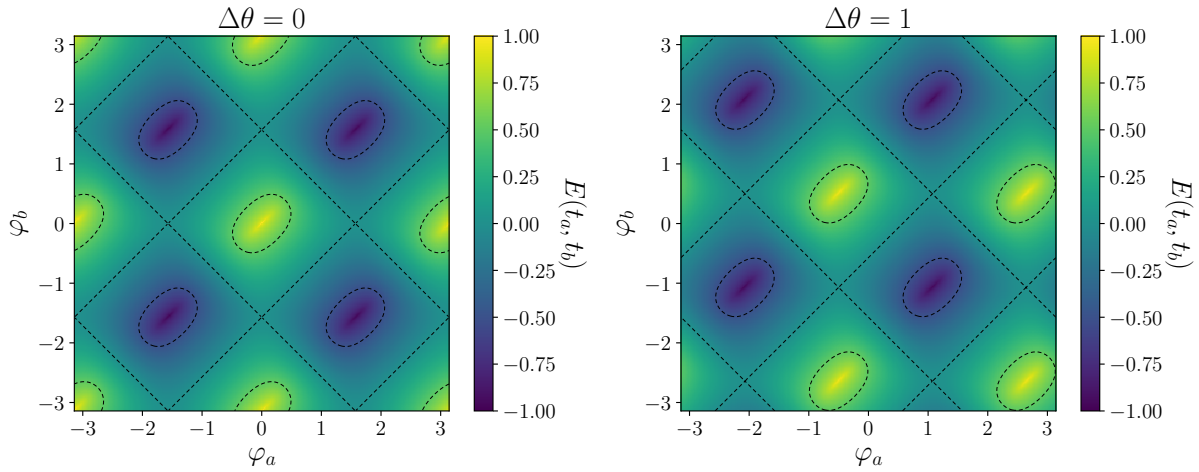

Figure 6.2: The correlation function $E(t_a, t_b)$ in the large-ℓ, large-squeezing limits, *i.e.* ℓ, r_a, $r_b \to \infty$, as a function of φ_a and φ_b, computed with Eq. (6.32). The black dashed lines are contour lines for $E(t_a, t_b) = 0.5, 0$ and -0.5 and are guides for the eye. In the left panel, $\Delta\theta = 0$, while $\Delta\theta = 1$ in the right panel. These two figures are simply related by a translation: when going from the left to the right panel, φ_a is shifted by $-\Delta\theta/2$ and φ_b by $\Delta\theta/2$.

obtains

$$E(t_a, t_b) \xrightarrow[\ell, r_a, r_b \to \infty]{} \frac{2}{\pi} \Re\mathrm{e} \left\{ \arctan \left[\frac{e^{i\Delta\theta} \left(e^{2i\varphi_a} + e^{-2i\varphi_b} \right)}{\sqrt{4 - e^{2i\Delta\theta} \left(e^{2i\varphi_a} + e^{-2i\varphi_b} \right)^2}} \right] \right\} . \tag{6.32}$$

This formula is displayed in Fig. 6.2, as a function of φ_a and φ_b, for $\Delta\theta = 0$ (left panel) and $\Delta\theta = 1$ (right panel). The black dashed lines are contour lines for $E(t_a, t_b) = 0.5, 0$ and -0.5, and are guide for the eye. As can be seen from Eq. (6.32), when $\Delta\theta$ varies the map is simply modified by a translation, where φ_a is shifted by $-\Delta\theta/2$ and φ_b by $\Delta\theta/2$.

The correlation is maximal, *i.e.* $E(t_a, t_b) = \pm 1$, when the denominator of the argument of the arc tan function in Eq. (6.32) vanishes. This happens when $\varphi_a = (n\pi - \Delta\theta)/2$ and $\varphi_b = (m\pi + \Delta\theta)/2$, where n and m are two integers of the same parity. More precisely, $E(t_a, t_b) = 1$ when n and m are even, and $E(t_a, t_b) = -1$ when n and m are odd.

In Fig. 6.3 we show three slices from the maps displayed in Fig. 6.2, where $E(t_a, t_b)$ is plotted as a function of φ_a for different choices of φ_b and $\Delta\theta = 0$. The blue line corresponds to $\varphi_b = \varphi_a$, and one can see that $E(t_a, t_b)$ is a piecewise affine function of φ_a. Indeed, more generally, the lines $\varphi_b = \varphi_a + \Delta\theta + n\pi$ ($n \in \mathbb{Z}$) connect all the points where $E(t_a, t_b) = \pm 1$, and along these lines one has

$$E(t_a, t_b) = (-1)^m \times \begin{cases} -\frac{2}{\pi} (\varphi_a + \varphi_b - 2n\pi) + 1 & \text{for} \quad 2n\pi < \varphi_a + \varphi_b \leq (2n+1)\pi \\ \frac{2}{\pi} (\varphi_a + \varphi_b - 2n\pi) + 1 & \text{for} \quad (2n-1)\pi < \varphi_a + \varphi_b \leq 2n\pi \end{cases} \tag{6.33}$$

The orange line corresponds to $\varphi_b = -\varphi_a$, where one notices the existence of cusps at the points where $E(t_a, t_b) = \pm 1$. Around the cusps, $E(t_a, t_b)$ indeed behaves as

$$E(t_a, t_b) \simeq \pm 1 \pm \frac{2\sqrt{2\,(\varphi_a - \varphi_{a,\mathrm{cusp}})}}{\pi} , \tag{6.34}$$

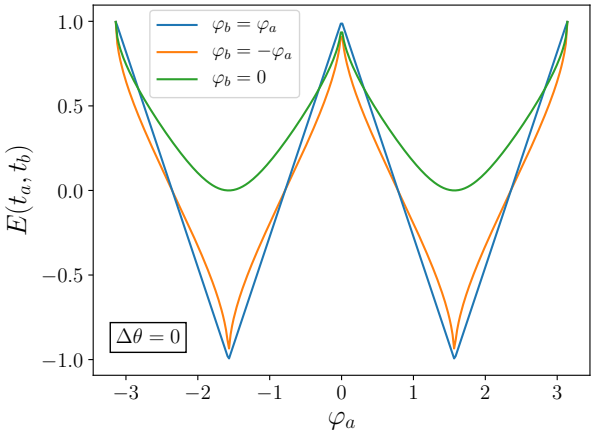

Figure 6.3: The correlation function $E(t_a, t_b)$ in the large-ℓ, large-squeezing limits, *i.e.* ℓ, r_a, $r_b \to \infty$, as computed in Eq. (6.32), as a function of φ_a for $\Delta\theta = 0$ and $\varphi_b = \varphi_a$ (blue line), $\varphi_b = -\varphi_a$ (orange line), and $\varphi_b = 0$ (green line). These are slices from the left panel of Fig. 6.2. For $\varphi_b = \varphi_a$, $E(t_a, t_b)$ is a piecewise affine function of φ_a, see Eq. (6.33). For $\varphi_b = -\varphi_a$, the derivative of $E(t_a, t_b)$ diverges at the points where $E(t_a, t_b) = \pm 1$, see Eq. (6.34).

where $\varphi_{a,\text{cusp}}$ indicates the location of a cusp point. Finally, the green line stands for a fixed value of φ_b, namely $\varphi_b = 0$.

6.3 Numerical exploration

Beyond the limits studied in the previous section, one has to compute Eq. (6.21) numerically. It is useful to notice that one of the two integrals appearing in Eq. (6.21) can be performed in terms of the complementary error function $\text{erfc}(z) \equiv 1 - \text{erf}(z)$, where the error function $\text{erf}(z)$ is defined below Eq. (D.2). For $\Xi_{22} \neq 0$, one has

$$E(t_a, t_b) = \Re\text{e}\left\{ -\frac{\sqrt{\Xi_{11}\Xi_{22} - \Xi_{12}^2}}{2\sqrt{2\pi}\sqrt{-\Xi_{22}}} \sum_{n=-\infty}^{\infty} \sum_{m=-\infty}^{\infty} (-1)^{n+m} \int_{n\ell}^{(n+1)\ell} \mathrm{d}Y_1 \right.$$
$$\left(\text{erfc}\left\{ \sqrt{-\frac{\Xi_{22}}{2}} \left[(m+1)\ell + \frac{\Xi_{12}}{\Xi_{22}} Y_1 \right] \right\} - \text{erfc}\left[\sqrt{-\frac{\Xi_{22}}{2}} \left(m\ell + \frac{\Xi_{12}}{\Xi_{22}} Y_1 \right) \right] \right)$$
$$\left. \exp\left[\frac{1}{2} \left(\Xi_{11} - \frac{\Xi_{12}^2}{\Xi_{22}} \right) Y_1^2 \right] \right\} \tag{6.35}$$

where Eq. (6.26) has been used to simplify the prefactor.

This expression can be further simplified (for the sake of numerical computation) by noticing that Eq. (6.21) is of the form $\sum_{n=-\infty}^{\infty} \sum_{m=-\infty}^{\infty} a_{n,m}$ where, by performing the change of integration variable $Y_1 \to -Y_1$ and $Y_2 \to -Y_2$, one has $a_{-n-1,-m-1} = a_{n,m}$. One can use this relation to restrict the sum over positive values of m only, and replace $\sum_{m=-\infty}^{\infty}$ with $2\sum_{m=0}^{\infty}$. The sum over m can then be re-ordered since the complementary error functions are absolutely convergent as long as $\Re\text{e}(\Xi_{22}) < 0$, which is required according

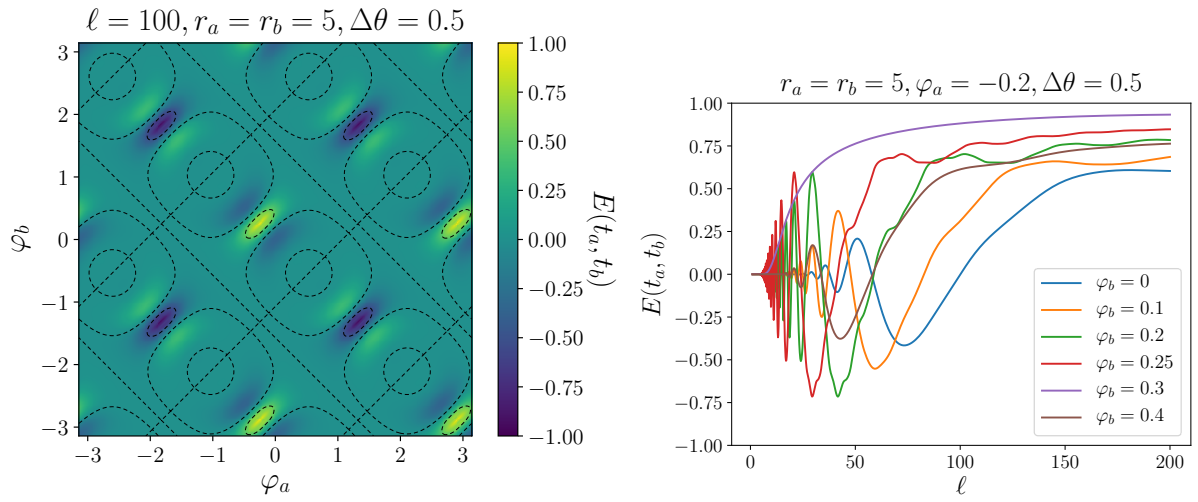

Figure 6.4: Left panel: $E(t_a, t_b)$ for $\ell = 100$, $r_a = r_b = 5$ and $\Delta\theta = 0.5$, as a function of φ_a and φ_b. The black dashed lines are contours for $E(t_a, t_b) = 0.5$, 0 and -0.5. Right panel: $E(t_a, t_b)$ as a function of ℓ for $r_a = r_b = 5$, $\varphi_a = -0.2$, $\Delta\theta = 0.5$. Different colours label different values of φ_b.

to Eq. (6.25). This gives rise to

$$E(t_a, t_b) = \Re\mathrm{e}\Bigg\{ \frac{\sqrt{\Xi_{11}\Xi_{22} - \Xi_{12}^2}}{\sqrt{2\pi}\sqrt{-\Xi_{22}}} \sum_{n=-\infty}^{\infty} (-1)^n \int_{n\ell}^{(n+1)\ell} \mathrm{d}Y \Bigg\{ 2\sum_{m=0}^{\infty} (-1)^m \mathrm{erfc}\left[\sqrt{\frac{-\Xi_{22}}{2}} \left(m\ell + \frac{\Xi_{12}}{\Xi_{22}} Y \right) \right] - \mathrm{erfc}\left(\frac{-\Xi_{12}}{\sqrt{-2\Xi_{22}}} Y \right) \Bigg\} \exp\left[\frac{1}{2} \left(\Xi_{11} - \frac{\Xi_{12}^2}{\Xi_{22}} \right) Y^2 \right] \Bigg\}. \tag{6.36}$$

This expression is helpful to compute $E(t_a, t_b)$ numerically, and in practice, we truncate the sums over n and m at an order above which we check that the dependence of the result on the truncation order becomes negligible.

In the left panel of Fig. 6.4, the correlation function is displayed for $r_a = r_b = 5$, $\Delta\theta = 0.5$ and $\ell = 100$, as a function of φ_a and φ_b. From Fig. 6.1, one can check that $\ell = 100$ is too large for the small-ℓ approximation developed in Sec. 6.2.2 to apply, since it requires $\ell \ll e^r$, and too small for the large-ℓ approximation developed in Sec. 6.2.1 to apply, since it requires $\ell \gg e^r$. This value of ℓ is therefore "intermediate" in that sense. This is further confirmed by noting the difference between the left panel of Fig. 6.4 and Fig. 6.2, which displays the large-ℓ (and large squeezing, which here applies since $r = 5$) limit. For intermediate ℓ, one notices in the left panel of Fig. 6.4 the presence of local maximums and local minimums, which do not exist in the limit where ℓ is infinite. As we will see below, those local extremums are crucial to obtain violations of bipartite temporal Bell inequalities.

In order to better depict the role played by the parameter ℓ, which in principle is left to the free choice of the observer, in the right panel of Fig. 6.4 we show the correlation function $E(t_a, t_b)$ as a function of ℓ, for $r_a = r_b = 5$, $\varphi_a = -0.2$ and $\Delta\theta = 0.5$, for a few values of φ_b. This confirms the tendency observed in Fig. 6.1: when $\ell \ll e^r$, *i.e.* in

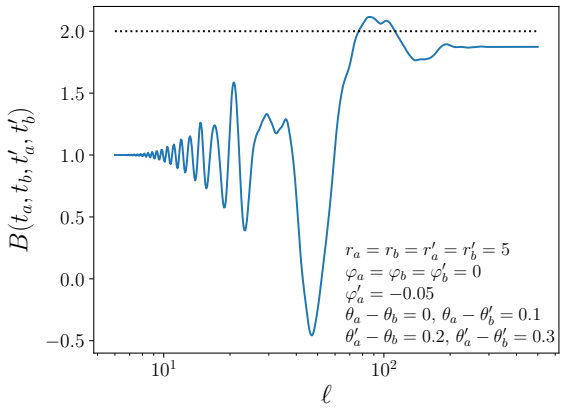

Figure 6.5: Expectation value of the Bell operator $B(t_a, t_b, t'_a, t'_b)$ as a function of ℓ, where the parameters specifying the state of the systems at times t_a, t_b, t'_a and t'_b have been fixed to the values given in the figure. The black dotted line stands for $B = 2$, above which a violation occurs. On can see that the maximal violation is obtained around intermediate values of ℓ (namely, according to the above discussion, around $\ell \sim e^r$).

the small-ℓ regime, there are oscillations, the amplitude and frequency of which strongly depend on the squeezing and rotation angles, while when $\ell \gg e^r$, one asymptotes the infinite-ℓ result. One should note that the case $\varphi_b = \varphi_a + \Delta\theta$ is an exception since no oscillation appears at small values of ℓ in that configuration (this corresponds to the violet curve, $\varphi_b = 0.3$, in the right panel of Fig. 6.4). This is because, in the large-squeezing limit, all components of Ξ are real, as can be seen from Eqs. (6.30)-(6.31), while the oscillations come from evaluating exponential functions with complex arguments.

Now that we have made clear how to compute the correlation function $E(t_a, t_b)$, the result can be plugged into Eq. (4.4) and one can test for violations of bipartite temporal Bell inequalities. As explained at the beginning of Sec. 6.2, 11 parameters are required to specify the state of the systems at times t_a, t_b, t'_a and t'_b, given that only the changes in the rotation angles matter, and not their individual values. One should also add the spin operator parameter ℓ, which the observer can in principle set in a free way. This leaves us with 12 parameters. We have not performed a comprehensive analysis of this whole, high-dimensional parameter space but have instead considered some two-dimensional slices, which is enough to prove that indeed, bipartite temporal Bell inequalities can be violated by two-mode squeezed states.

Our strategy is that since we are searching for violations of the Bell inequality, $B > 2$, it seems reasonable to focus on parameters that make the first correlator appearing in B, $E(t_a, t_b)$, close to unity. We already know that $E(t_a, t_b)$ is close to one when $(\varphi_a, \varphi_b) = (-\Delta\theta/2, \Delta\theta/2)$, for a given $\Delta\theta$, in the large squeezing regime (see Sec. 6.2.4). This is why in the following, we set $\theta_a - \theta_b = 0$ and $\varphi_a = \varphi_b = 0$. In Fig. 6.5, we display the expectation value of the Bell operator as a function of ℓ, where the other parameters have been fixed according to that strategy. One can see that a violation is obtained when ℓ is "intermediate" in the sense discussed above, *i.e.* when $\ell \sim e^r$.[2] We will therefore focus

[2]One might be concerned that the plot shown in Fig. 6.5 does not look smooth in the intermediate region of ℓ. However, we tuned internal parameters in the numerical computation very carefully. Other

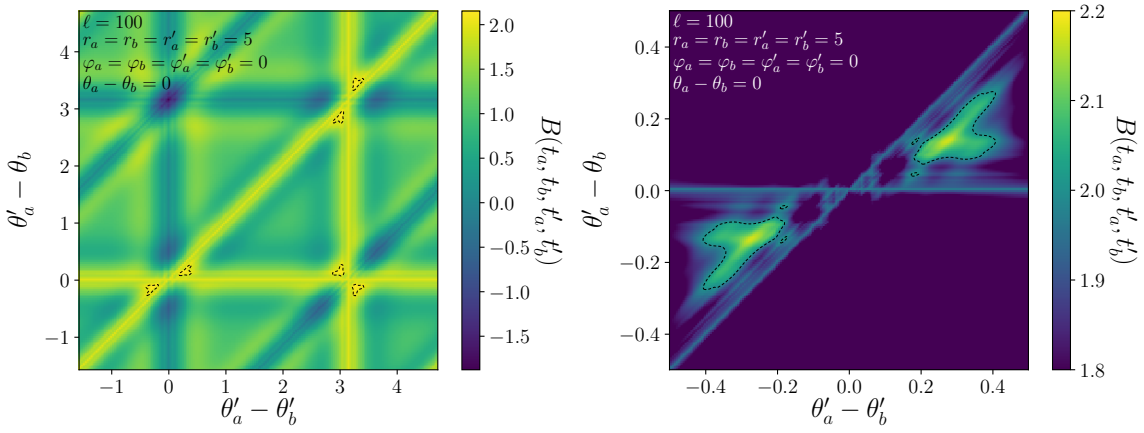

Figure 6.6: Expectation value of the Bell operator $B(t_a, t_b, t'_a, t'_b)$, for $\ell = 100$, $r_a = r_b = r'_a = r'_b = 5$, $\varphi_a = \varphi_b = \varphi_{a'} = \varphi_{b'} = 0$ and $\theta_a - \theta_b = 0$, as a function of $\theta'_a - \theta'_b$ and $\theta'_a - \theta_b$. The black dashed lines are contours for $B = 2$, so violation occurs inside the contours. In the left panel, the full $2\pi \times 2\pi$ parameter space is displayed while the right panel zooms in the region $(\theta'_a - \theta'_b, \theta'_a - \theta_b) = (0, 0)$ where violation islands exist. The maximum value of B across the entire map is $\simeq 2.18$.

on such intermediate values of ℓ below.

In Fig. 6.6, the expectation value of the Bell operator is shown in the case that all squeezing parameters are frozen ($r_a = r_b = r'_a = r'_b = 5$ and $\varphi_a = \varphi_b = \varphi_{a'} = \varphi_{b'} = 0$) and only the rotation angles vary. This is because, in experiments where measurements are performed at a single time, the rotation angle only determines an overall, irrelevant phase of the wavefunction. This is why most analyses of the two-mode squeezed states discard it. As argued above, for multiple-time measurements this is not the case anymore, and we would like to determine how important the rotation angle becomes. The black lines in Fig. 6.6 are contours of $B = 2$, above which the bipartite temporal Bell inequality is violated. As one can see, there are islands in parameters space, inside the contours, where the inequality is indeed violated, and the rotation angles play a crucial role in determining whether or not this is the case. These islands are located around the three points $(\theta'_a - \theta'_b, \theta'_a - \theta_b) = (0, 0), (\pi, 0)$ and (π, π), and the right panel of Fig. 6.6 zooms in one of these points (the detailed structure of the map is similar at each of these points). At those points exactly, one can check that each correlator E involved in Eq. (4.4) is close to ± 1, but they cancel each other out in such a way that no violation occurs. One therefore has to move slightly away from those points, and in the right panel of Fig. 6.6 one can see that smaller, secondary islands actually exist. The structure of the violation map is therefore rather involved.

We have checked that no violation occurs in the infinite-ℓ limit. At finite ℓ, as explained above (see the discussion around the right panel of Fig. 6.4), oscillatory features appear in each correlation function E, around points where $E \simeq \pm 1$ and this leads to the violations. Bipartite temporal Bell inequality violations seem therefore to require $\ell \lesssim e^r$.

than that, let us give a comment to support the validity of this result. The smaller ℓ we take, the more expensive the computation of Eq. (6.36) becomes. This is because we need to take terms with large n and m, and assess a lot of error functions for small ℓ. Nevertheless, as can be seen Fig. 6.1, our numerical calculation matches the analytical expression for small-ℓ limit. It is easier to implement correct numerical calculation for intermediate ℓ.

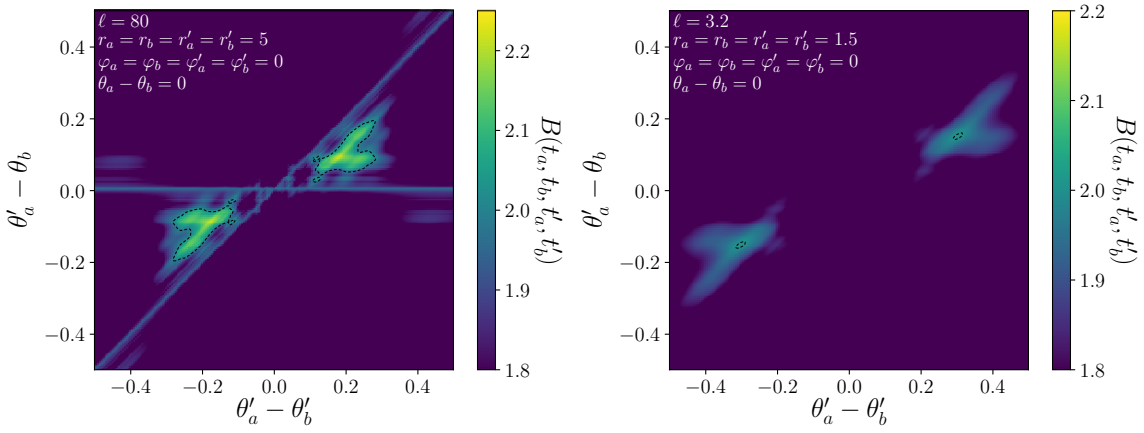

Figure 6.7: Expectation value of the Bell operator $B(t_a, t_b, t'_a, t'_b)$ as a function of $\theta'_a - \theta'_b$ and $\theta'_a - \theta_b$. Left panel: $\ell = 100$, $r_a = r_b = r'_a = r'_b = 5$, $\varphi_a = \varphi_b = \varphi_{a'} = \varphi_{b'} = 0$ and $\theta_a - \theta_b = 0$. The maximum value of B across the entire map is $\simeq 2.22$. Right panel: $\ell = 3.2$ (optimised to get maximal violation), $r_a = r_b = r'_a = r'_b = 1.5$, $\varphi_a = \varphi_b = \varphi_{a'} = \varphi_{b'} = 0$, and $\theta_a - \theta_b = 0$. The maximum value of B across the entire map is $\simeq 2.00$ up to numerical precision. In both panels, the black dashed lines are contours for $B = 2$.

In order to better see the role played by ℓ, in the left panel of Fig. 6.7, the same map as in the right panel of Fig. 6.6 is displayed but with $\ell = 80$. The violation islands still exist. While they are smaller, they are also higher (the maximal value of B in Fig. 6.6 is found to be $B_{\max} \simeq 2.18$ while in the left panel of Fig. 6.7, it is $B_{\max} \simeq 2.22$, and we recall that the Cirel'son bound [105] is given by $B \leq 2\sqrt{2} \simeq 2.83$). We have also tried to decrease the squeezing amplitude starting from the configuration displayed in these figures, allowing us to choose the value of ℓ that leads to the maximal violation. In the right panel of Fig. 6.7, we show the result for $r = 1.5$, where the violation is maximal for $\ell \simeq 3.2$. There, the islands have almost disappeared, and the maximal value one obtains is $B_{\max} \simeq 2.00$ up to numerical precision. In these slices, Bell inequality violations seem therefore to require $r \gtrsim 1.5$.

Finally, in order to study how the temporal Bell inequality violation depends on the squeezing amplitudes and angles, in Fig. 6.8, we make the parameters r'_a and r'_b (left panel), and φ'_a and φ'_b (right panel), vary, starting from close to the maximal violation point of Fig. 6.6. One can see that some amount of fine tuning in these parameters is also necessary to achieve violation.

6.4 Discussion

In this chapter, we have studied bipartite temporal Bell inequalities with two-mode squeezed states. Such inequalities have the ability to test for realism and locality while requiring position measurements only. This is particularly useful for experimental setups in which momentum observables cannot be directly accessed, as for instance in the cosmological context. Two-mode squeezed states are continuous, entangled Gaussian states, so we had to introduce a dichotomic, spin-like observable for continuous systems, which we did via Eq. (6.4). This operator turns the position into $+1$ or -1, depending on which interval of size ℓ it falls. We have shown how to compute the bipartite two-point function

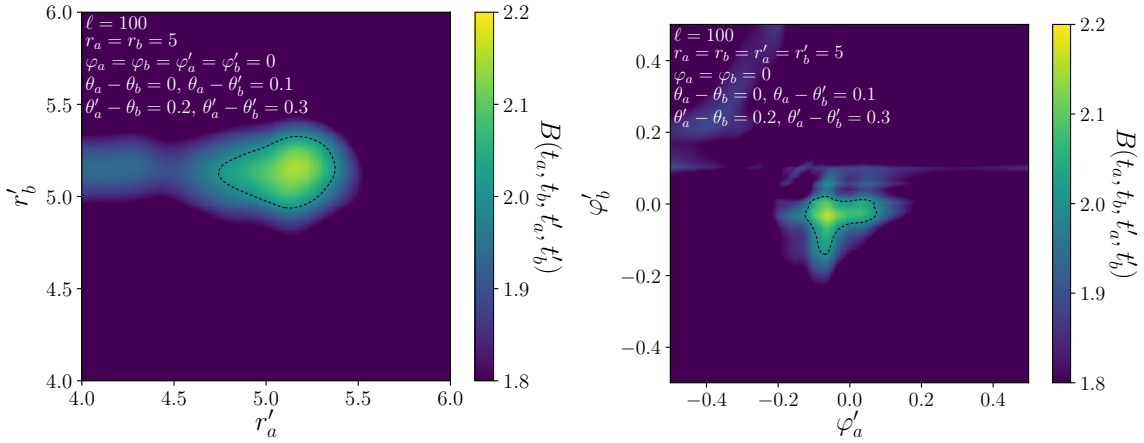

Figure 6.8: Expectation value of the Bell operator $B(t_a, t_b, t'_a, t'_b)$ as a function of r'_a and r'_b (left panel), and φ'_a and φ'_b (right panel), around the violations islands of Fig. 6.6.

of that operator, and have studied various analytical limits that were useful to guide our numerical exploration, which is otherwise tedious due to the high dimensionality of the problem. We have then exhibited configurations where the Bell inequality is violated, confirming that two-mode squeezed states have the ability to violate bipartite temporal Bell inequalities. This is clearly the main result of this work. Bell inequality violations found here could be detected in cosmology in principle, which would provide a direct evidence that the structure of the universe comes from quantum fluctuations.

When ℓ is infinite, the pseudo-spin operator becomes the sign operator, which returns $+1$ is the position is positive and -1 otherwise, and we could not find configurations leading to successful violations in that case. Optimizing the value of ℓ, which is in principle left to the observer to freely chose, seems therefore to be crucial. We have also highlighted the role played by the rotation angle. Two-mode squeezed states are characterized by three parameters: the squeezing amplitude, the squeezing angle and the rotation angle; but in single-time measurements, the rotation angle simply sets an overall phase in the wave-function of the two-mode squeezed state, and is thus irrelevant. It is therefore discarded in most analyses of two-mode squeezed states. However, we have shown that it plays a crucial role in the present context, where measurements are performed at different times, between which the rotation angle is liable to evolve, and the phase difference between the various measurements becomes an important parameter to determine whether or not Bell inequalities are violated. Let us also stress that the dynamics of the rotation angle is set by the Hamiltonian of the system, so probing the part of the Hamiltonian that drives the rotation angle is only possible if multiple-time measurements are performed. This work therefore lays the ground for more thorough investigations of physical systems leading to squeezed states. In fact, in one-mode squeezed states as well, the rotation angle becomes relevant for multiple-time measurements. Such effects will be able to be investigated in the context of Leggett-Garg inequalities for one-mode squeezed states. The study on how quantum decoherence reduces Bell inequality violations in these contexts is also left for future work.

Finally, let us comment on how to observe Bell inequality violations in cosmology. Bipartite temporal Bell inequalities are free from a fundamental problem of Bell experiments in cosmology as discussed in Chap. 4, but it will be still chanllenging to perform

such Bell experiments in practice. At least, one needs to measure two-time correlators of scalar perturbations. A combination of the CMB anisotropy and the LSS is a candidate of two-time measurements. Another possibility is that we might be able to extract information involving finite duration of time from CMB observations since the last scattering surface should have a finite thickness. The Canadian Intensity Hydrogen Mapping Experiment (CHIME, see *e.g.* Ref. [134]) might also be helpful since it probes the history of the spatial distribution of neutral hydrogen.

Conclusion

In this thesis, we have discussed cosmological inflation and adiabatic scalar perturbations generated during inflation. In Part I, we have reviewed the basics of inflationary cosmology, the stochastic inflation and Bell experiments in cosmology. In Part II, we have presented our original works where we studied cosmological perturbations from two perspectives: stochastic picture (Chap. 5) and quantum aspects (Chap. 6). The detailed consequences and implications of each work are shown in the last section of each chapter *i.e.* Sec. 5.3 and Sec. 6.4.

In Chap. 5, we have computed the amplitude of curvature perturbations for a given length scale in the stochastic-δN formalism. This consists of two steps: computing the statistics of the first-passage time from a given field value, which has already been done in the literature, and deriving the distribution of the field value at the time when a given scale exits the horizon. In the quasi de-Sitter limit, a given physical scale exits the horizon at a fixed number of e-folds before the end of inflation. It leads us to the use of the backward probability distribution, which is the probability density function of the field value at a fixed number of e-folds before inflation ends. We have then found that the power spectrum is expressed by using the backward distribution as Eq. (5.16) and the backward distribution can be evaluated by solving the Fokker-Planck and the adjoint Fokker-Planck equations through Eq. (5.20). This is one of the main results of this thesis. Then, we have applied our formalism to study the effects of quantum diffusion near the end of inflation, which arises in models leading to primordial black hole formation, on large-scale perturbations. The correction occurs because the classical relation between a scale and a field value is distorted. Particularly, we have found that the direct contribution from patches that stay in a flat region of a potential for a long time can ruin the agreement with the CMB observations, making the scalar spectral index blue (see Fig. 5.6). This indicates that the CMB measurements are capable of constraining the entire inflationary potential.

Since the stochastic-δN formalism has been studied in the literature, let us stress what is new in our work again. In the preceding works, the first-passage time from a given field value is investigated. To compare it with observations, we need to extract information about a given scale. In the low-diffusion limit, there is a one-to-one correspondence between a scale and a field value. However, the background trajectory does not make sense in the presence of a significant amount of diffusion. We have then solved the first-passage-time problem associated with a given scale taking into account the spatial structure involved in the stochastic inflation. Therefore, we have filled the final gap between the stochastic-δN formalism and observational predictions for the first time. In fact, it has been done for one object: power spectrum. The tools we have developed will provide the ground for extensions to other objects. Our study has also implied that very hot or cold spots can arise in the CMB due to quantum diffusion. This situation would be characterized more appropriately by higher-order correlations or the probability that

such a patch lies in the observable universe, rather than the power spectrum. This means that our study has opened up a lot of prospects to study.

In Chap. 6, we have studied bipartite temporal Bell inequalities for two-mode squeezed states. This class of inequalities can be used to test for realism and locality relying on position measurements only, and their violations indicate a quantum signature. Since two-mode squeezed states are continuous-variable systems, we had to introduce a dichotomic variable, which we took the z-component of the Larsson's spin operator. First, we have derived a formula to compute two-time correlators (Eq. (6.21)), which are pieces appearing in bipartite temporal Bell inequalities, from quantum mechanical calculations. Next, we have obtained some analytical expressions for their asymptotic behaviors, which are helpful to search for Bell inequality violations considering the huge parameter space at hand. Finally, we have performed numerical calculations and showed configurations where bipartite temporal Bell inequalities are violated (see *e.g.* Fig. 6.6). This is another main result of this thesis. This study has been carried out keeping on highlighting the rotation angle of squeezed states. It is often discarded since it merely determines the overall phase of the wavefunction, but in multiple-time measurements, it becomes relevant and plays a crucial role in Bell inequality violations. Two-mode squeezed states are realized in cosmological perturbations as well as in quantum optical systems. Since bipartite temporal Bell inequalities can be tested relying on the position measurements only, this study overcomes a fundamental obstacle of Bell experiments in cosmology where the decaying mode is too tiny to observe. It implies that Bell inequality violations could be found in cosmology in principle, which would provide direct evidence that the structure of the universe is of quantum origin.

Acknowledgements

First of all, I would like to thank my supervisor Masahiro Kawasaki for his advice during my Ph.D. course. Thanks to him, I could have fun working on cosmology. I would also like to express my deep gratitude to my collaborator, Vincent Vennin. He kindly accepted the collaboration with me and supported our research with his notable intuition in physics. This thesis is thankfully judged by Jun'ichi Yokoyama, Hideyuki Tagoshi, Kipp Cannon, Izumi Tsutsui and Shinji Miyoki. I am also grateful to the members of ICRR theory group for fruitful discussions. Finally, I would like to deeply appreciate my family for their support.

Appendix A

Elliptic theta functions

In this appendix, we summarize definitions and properties of the elliptic theta functions [135], which are used in this thesis extensively. They are defined as

$$\vartheta_1(z,q) = -iq^{1/4}e^{iz}\sum_{n=-\infty}^{\infty}(-1)^n q^{n(n+1)}e^{2inz} = 2\sum_{n=0}^{\infty}(-1)^n q^{(n+1/2)^2}\sin\left((2n+1)z\right) \tag{A.1}$$

$$\vartheta_2(z,q) = q^{1/4}e^{iz}\sum_{n=-\infty}^{\infty} q^{n(n+1)}e^{2inz} = 2\sum_{n=0}^{\infty} q^{(n+1/2)^2}\cos\left((2n+1)z\right) \tag{A.2}$$

$$\vartheta_3(z,q) = \sum_{n=-\infty}^{\infty} q^{n^2}e^{2inz} = 1 + 2\sum_{n=1}^{\infty} q^{n^2}\cos\left(2nz\right) \tag{A.3}$$

$$\vartheta_4(z,q) = \sum_{n=-\infty}^{\infty}(-1)^n q^{n^2}e^{2inz} = 1 + 2\sum_{n=1}^{\infty}(-1)^n q^{n^2}\cos\left(2nz\right) \tag{A.4}$$

with $z, q \in \mathbb{C}$ and $|q| < 1$. Here, $q \equiv e^{i\pi\tau}$ is called the nome and it is also written in terms of such τ that $\tau \in \mathbb{C}$, $\Im\mathrm{m}\,(\tau) > 0$. The above definitions include $q^{1/4}$, which has branch cuts. It actually means $q^{1/4} = e^{i\pi\tau/4}$, so τ resolves issues of branch cuts.

The elliptic theta functions have the following periodic properties,

$$\vartheta_1(z+\pi,q) = -\vartheta_1(z,q) \qquad \vartheta_1\left(z+\frac{\pi}{2},q\right) = \vartheta_2(z,q) \tag{A.5}$$

$$\vartheta_2(z+\pi,q) = -\vartheta_2(z,q) \qquad \vartheta_2\left(z+\frac{\pi}{2},q\right) = -\vartheta_1(z,q) \tag{A.6}$$

$$\vartheta_3(z+\pi,q) = \vartheta_3(z,q) \qquad \vartheta_3\left(z+\frac{\pi}{2},q\right) = \vartheta_4(z,q) \tag{A.7}$$

$$\vartheta_4(z+\pi,q) = \vartheta_4(z,q) \qquad \vartheta_4\left(z+\frac{\pi}{2},q\right) = \vartheta_3(z,q)\,, \tag{A.8}$$

and for $q = e^{i\pi\tau}$,

$$\vartheta_1(z+\pi\tau,q) = -q^{-1}e^{-2iz}\vartheta_1(z,q) \qquad \vartheta_1\left(z+\frac{\pi}{2}\tau,q\right) = iq^{-1/4}e^{-iz}\vartheta_4(z,q) \tag{A.9}$$

$$\vartheta_2(z+\pi\tau,q) = q^{-1}e^{-2iz}\vartheta_2(z,q) \qquad \vartheta_2\left(z+\frac{\pi}{2}\tau,q\right) = q^{-1/4}e^{-iz}\vartheta_3(z,q) \tag{A.10}$$

$$\vartheta_3(z+\pi\tau,q) = q^{-1}e^{-2iz}\vartheta_3(z,q) \qquad \vartheta_3\left(z+\frac{\pi}{2}\tau,q\right) = q^{-1/4}e^{-iz}\vartheta_2(z,q) \tag{A.11}$$

$$\vartheta_4(z+\pi\tau,q) = -q^{-1}e^{-2iz}\vartheta_4(z,q) \qquad \vartheta_4\left(z+\frac{\pi}{2}\tau,q\right) = iq^{-1/4}e^{-iz}\vartheta_1(z,q)\,. \tag{A.12}$$

Also, they have the following parity

$$\vartheta_1(-z,q) = -\vartheta_1(z,q) \tag{A.13}$$
$$\vartheta_j(-z,q) = \vartheta_j(z,q) \quad \text{for} \quad j=2,3,4\,. \tag{A.14}$$

By applying the Poisson summation formula

$$\sum_{n=-\infty}^{\infty} f(n) = \sum_{m=-\infty}^{\infty} \tilde{f}(2\pi m) \left(\equiv \sum_{m=-\infty}^{\infty} \int_{-\infty}^{\infty} \mathrm{d}x\, f(x) e^{-2\pi i m x} \right) \tag{A.15}$$

to the elliptic theta functions, we obtain the following identities called the Jacobi identities,

$$\vartheta_1\left(z, e^{i\pi\tau}\right) = -i\,(-i\tau)^{-1/2} \exp\left(-\frac{iz^2}{\pi\tau}\right) \vartheta_1\left(-\frac{z}{\tau}, e^{-i\pi/\tau}\right) \tag{A.16}$$
$$\vartheta_2\left(z, e^{i\pi\tau}\right) = (-i\tau)^{-1/2} \exp\left(-\frac{iz^2}{\pi\tau}\right) \vartheta_4\left(-\frac{z}{\tau}, e^{-i\pi/\tau}\right) \tag{A.17}$$
$$\vartheta_3\left(z, e^{i\pi\tau}\right) = (-i\tau)^{-1/2} \exp\left(-\frac{iz^2}{\pi\tau}\right) \vartheta_3\left(-\frac{z}{\tau}, e^{-i\pi/\tau}\right) \tag{A.18}$$
$$\vartheta_4\left(z, e^{i\pi\tau}\right) = (-i\tau)^{-1/2} \exp\left(-\frac{iz^2}{\pi\tau}\right) \vartheta_2\left(-\frac{z}{\tau}, e^{-i\pi/\tau}\right)\,. \tag{A.19}$$

From the definition, it is straightforward to derive the following approximate expressions for $|q| \ll 1$,

$$\vartheta_1(z,q) \simeq 2q^{1/4}\sin(z) \tag{A.20}$$
$$\vartheta_2(z,q) \simeq 2q^{1/4}\cos(z) \tag{A.21}$$
$$\vartheta_3(z,q) \simeq 1 + 2q\cos(2z) \tag{A.22}$$
$$\vartheta_4(z,q) \simeq 1 - 2q\cos(2z)\,. \tag{A.23}$$

The approximation formulae for small τ are obtained by applying Eqs. (A.20)-(A.23) to the right-hand side of Eqs. (A.16)-(A.19). However, in the right-hand side of Eqs. (A.16)-(A.19), the first argument of the elliptic theta functions diverge for $\tau \to 0$ except for $z = 0$. Therefore, the following approximate expressions for $\Re\mathrm{e}\,(\alpha) > 0$ and $|\alpha| \ll 1$ are valid around $z \simeq 0$,

$$\vartheta_1\left(z, e^{-\alpha}\right) \simeq 2\sqrt{\frac{\pi}{\alpha}} \exp\left(-\frac{\pi^2 + 4z^2}{4\alpha}\right) \sinh\left(\frac{\pi z}{\alpha}\right) \tag{A.24}$$
$$\vartheta_2\left(z, e^{-\alpha}\right) \simeq \sqrt{\frac{\pi}{\alpha}} \exp\left(-\frac{z^2}{\alpha}\right) \tag{A.25}$$
$$\vartheta_3\left(z, e^{-\alpha}\right) \simeq \sqrt{\frac{\pi}{\alpha}} \exp\left(-\frac{z^2}{\alpha}\right) \tag{A.26}$$
$$\vartheta_4\left(z, e^{-\alpha}\right) \simeq 2\sqrt{\frac{\pi}{\alpha}} \exp\left(-\frac{\pi^2 + 4z^2}{4\alpha}\right) \cosh\left(\frac{\pi z}{\alpha}\right) \tag{A.27}$$

These expressions should be understood together with the periodicity shown in Eqs. (A.5)-(A.8).

Appendix B

Solutions to the Fokker-Planck and adjoint Fokker-Planck equations in a flat potential well

In this appendix, we derive the solution of the Fokker-Planck equation for the distribution function of the field, $P^{\rm well}(\phi, N)$, and of the adjoint Fokker-Planck equation for the distribution function of first passage times, $P_{\rm FPT}(\mathcal{N}, \phi)$, in a flat potential well. Following the discussion presented in Sec. 5.2.3, we label the field with the variable x introduced in Eq. (5.35), in terms of which the Langevin equation reads

$$\frac{\mathrm{d}x}{\mathrm{d}N} = \frac{\sqrt{2}}{\mu}\xi(N)\,. \tag{B.1}$$

Inside the well, the variable x varies between 0, where an absorbing boundary is located, and 1, where a reflective boundary is placed. The Fokker-Planck equation associated with Eq. (B.1) is given by [99]

$$\frac{\partial}{\partial N}P^{\rm well}(x, N|x_{\rm in}, 0) = \frac{1}{\mu^2}\frac{\partial^2}{\partial x^2}P^{\rm well}(x, N|x_{\rm in}, 0)\,. \tag{B.2}$$

This result does not depend on the discretization scheme the Langevin equation is interpreted with, see Sec. 3.2.

B.1 Flat well with one absorbing wall

As a warm-up, let us first consider the case where only the absorbing boundary at $x = 0$ is considered. This boundary condition imposes that $P^{\rm well}(x, N|x_{\rm in}, 0) = 0$ when $x = 0$, and we set the initial condition at $x_{\rm in}$ when $N = 0$, *i.e.* $P^{\rm well}(x, 0|x_{\rm in}, 0) = \delta(x - x_{\rm in})$. A first remark is that Eq. (B.2) describes free Brownian motion with diffusivity $2/\mu^2$, hence it accepts Gaussian solutions of the form

$$f_{\bar{x},\bar{N}}(x, N) = \frac{\mu}{2\sqrt{\pi\left(N - \bar{N}\right)}}e^{-\frac{\mu^2}{4}\frac{(x-\bar{x})^2}{N-\bar{N}}}\,, \tag{B.3}$$

where $\bar{x}$ and $\bar{N}$ are two integration constants. Since the Fokker-Planck operator is linear and second order, those functions form a basis on which all solutions can be expanded.

In practice, the coefficients in these expansions are set in order to satisfy the boundary conditions. Let us note that in the absence of any boundary condition, the solution would be simply given by $P^{\rm well}(x,N|x_{\rm in},0) = f_{x_{\rm in},0}(x,N)$. However, this solution does not satisfy the boundary condition at $x=0$. This can be fixed by subtracting the same solution, but centered at the symmetric point $-x_{\rm in}$, which gives rise to $P^{\rm well}(x,N|x_{\rm in},0) = f_{x_{\rm in},0}(x,N) - f_{-x_{\rm in},0}(x,N)$, or more explicitly,

$$P^{\rm well}(x,N|x_{\rm in},0) = \frac{\mu}{2\sqrt{\pi N}}\left[e^{-\frac{\mu^2}{4}\frac{(x-x_{\rm in})^2}{N}} - e^{-\frac{\mu^2}{4}\frac{(x+x_{\rm in})^2}{N}}\right]\theta(x)\,. \tag{B.4}$$

By construction, this function satisfies the Fokker-Planck equation, it vanishes at $x=0$, and it is such that $P^{\rm well}(x,0|x_{\rm in},0) = [\delta(x-x_{\rm in})-\delta(x+x_{\rm in})]\theta(x) = \delta(x-x_{\rm in})$. It has been obtained by subtracting the mirrored image of the solution obtained without boundary conditions (where the "mirror" is thought of as sitting at the location of the absorbing boundary), and for that reason, this technique is often referred to as the "method of images".

The distribution associated with the first-passage-time through the absorbing boundary can then be obtained as follows. On the one hand, from the solution of the Fokker-Planck equation, one can compute the survival probability $S(N)$, which corresponds to the probability that the field is still within the well at time N,

$$S(N) = \int_0^\infty P^{\rm well}(x,N|x_{\rm in},0){\rm d}x\,. \tag{B.5}$$

On the other hand, the probability to have already escaped from the well at time N is given by

$$\int_0^N P_{\rm FPT}(\mathcal{N},x_{\rm in}){\rm d}\mathcal{N} = 1 - S(N)\,. \tag{B.6}$$

By differentiating both expressions with respect to N, one obtains

$$P_{\rm FPT}(N,x_{\rm in}) = -\frac{\partial}{\partial N}\int_0^\infty P^{\rm well}(x,N|x_{\rm in},0){\rm d}x\,. \tag{B.7}$$

One can then use the fact that $P^{\rm well}$ satisfies the Fokker-Planck equation (B.2), which leads to

$$P_{\rm FPT}(N,x_{\rm in}) = \frac{1}{\mu^2}\,\frac{\partial}{\partial x}P^{\rm well}(x,N|x_{\rm in},0)\Big|_{x=0}\,. \tag{B.8}$$

Making use of Eq. (B.4), one finally obtains a Levy distribution,

$$P_{\rm FPT}(N,x_{\rm in}) = \frac{\mu x_{\rm in}}{2\sqrt{\pi}N^{3/2}}e^{-\frac{\mu^2 x_{\rm in}^2}{4N}}\,. \tag{B.9}$$

In passing, let us compute the backward probability distribution in this semi-infinite well. This can be done by plugging Eqs. (B.4) and (B.9) into Eq. (5.20). The integral of $P_{\rm FPT}(N,\phi_0)$ over N can be performed by means of the error function,

$$\int_{N_{\rm bw}}^\infty {\rm d}N\, P_{\rm FPT}\left(N,x_0\right) = {\rm erf}\left(\frac{x_0\mu}{2\sqrt{N_{\rm bw}}}\right)\,. \tag{B.10}$$

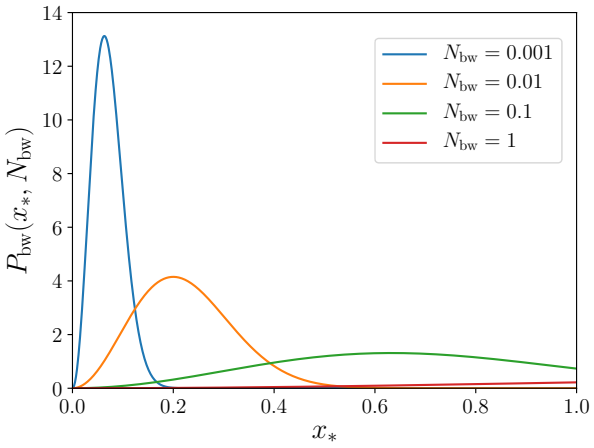

Figure B.1: Backward probability distribution for a flat potential with an absorbing boundary at $x = 0$ and in the $x_0 \to \infty$ limit, computed with Eq. (B.12), for $\mu = 1$ and with four different values of $N_{\rm bw}$.

This approaches one when $x_0 \to \infty$, in agreement with the discussion below Eq. (5.20). The integral of $P^{\rm well}(x, N|x_0, 0)$ over N also takes a simple form, and combining the above results, one obtains

$$P_{\rm bw}\left(x_*, N_{\rm bw}\right) = \frac{\mu^3 x_* \min(x_*, x_0)}{2\sqrt{\pi} N_{\rm bw}^{3/2}} \frac{e^{-\frac{\mu^2 x^2}{4N_{\rm bw}}}}{\operatorname{erf}\left(\frac{x_0 \mu}{2\sqrt{N_{\rm bw}}}\right)} . \tag{B.11}$$

One can check explicitly that this distribution is properly normalized, and that it vanishes when $x_* = 0$. In the limit where x_0 is sent to infinity, it reduces to

$$P_{\rm bw}\left(x, N_{\rm bw}\right) = \frac{\mu^3 x_*^2}{2\sqrt{\pi} N_{\rm bw}^{3/2}} e^{-\frac{\mu^2 x_*^2}{4N_{\rm bw}}} . \tag{B.12}$$

This distribution is displayed in Fig. B.1 for $\mu = 1$ and for a few values of $N_{\rm bw}$. One can check that, for small values of $N_{\rm bw}$, the distribution is peaked close to $x = 0$, while it is more widely spread and centered around larger values of x for larger values of $N_{\rm bw}$.

B.2 Flat well with one absorbing wall and one reflective wall

Let us now study the setup of interest for Sec. 5.2.3, where, on top of the absorbing boundary at $x = 0$, one places a reflective boundary at $x = 1$. Compared to the situation studied in Sec. B.1, the equations are slightly more involved, but the calculational techniques are the same, which is why it was useful to first study the simple case where only the absorbing boundary is accounted for.

The method of images can be employed by introducing the image sources at locations

$$\bar{x}_n = n + \frac{1}{2} + (-1)^n \left(x_{\rm in} - \frac{1}{2}\right) . \tag{B.13}$$

When $n = 0$, one has $\bar{x}_n = x_{\rm in}$, so one initiates this set of image sources at the initial location of the field. Then, when mirrored through the absorbing wall, one has $\bar{x}_n \to -\bar{x}_n = \bar{x}_{-n-1}$, and when mirrored through the reflective wall, one has $\bar{x}_n \to 2 - \bar{x}_n = \bar{x}_{-n+1}$. Therefore, the values $\bar{x}_n$ indeed correspond to all possible image sources of $x_{\rm in}$ after an arbitrary number of reflections against the absorbing and reflective walls. The solution to the Fokker-Planck equation should be constructed as a sum of free solutions centered on each of these images, with a sign that remains the same when going through the reflective wall and that flips when going through the absorbing wall. Starting from $x_{\rm in}$, schematically, one has

$$\underbrace{x_{\rm in}}_{+} \xrightarrow{R} \underbrace{\bar{x}_1}_{+} \xrightarrow{A} \underbrace{\bar{x}_{-2}}_{-} \xrightarrow{R} \underbrace{\bar{x}_3}_{-} \xrightarrow{A} \underbrace{\bar{x}_{-4}}_{+} \xrightarrow{R} \underbrace{\bar{x}_5}_{+} \longrightarrow \cdots \tag{B.14}$$

$$\underbrace{x_{\rm in}}_{+} \xrightarrow{A} \underbrace{x_{-1}}_{-} \xrightarrow{R} \underbrace{\bar{x}_2}_{-} \xrightarrow{A} \underbrace{\bar{x}_{-3}}_{+} \xrightarrow{R} \underbrace{\bar{x}_4}_{+} \xrightarrow{A} \underbrace{\bar{x}_{-5}}_{-} \longrightarrow \cdots \tag{B.15}$$

where A and R mean reflection against the absorbing and reflective walls respectively, and the sign associated with each image source is displayed below it. One can see that it is given by $(-1)^{\lfloor n/2 \rfloor}$, where $\lfloor \cdot \rfloor$ denotes the floor integer part. One thus has

$$P^{\rm well}(x, N|x_{\rm in}, 0) = \theta(x)\theta(1-x) \sum_{n=-\infty}^{\infty} (-1)^{\lfloor \frac{n}{2} \rfloor} f_{\bar{x}_n, 0}\left(x, N\right) . \tag{B.16}$$

Hereafter, we will drop the Heaviside functions and remember that the above expression applies within the well only. It can be decomposed into two sums, one where $n = 2m$ is even and one where $n = 2m+1$ is odd. In both cases, $\lfloor n/2 \rfloor = m$, and making use of Eq. (B.3), this gives rise to

$$P^{\rm well}(x, N|x_{\rm in}, 0) = \frac{\mu}{2\sqrt{\pi N}} \left[\sum_{m=-\infty}^{\infty} (-1)^m e^{-\frac{\mu^2 (x - \bar{x}_{2m})^2}{4N}} + \sum_{m=-\infty}^{\infty} (-1)^m e^{-\frac{\mu^2 (x - \bar{x}_{2m+1})^2}{4N}} \right] . \tag{B.17}$$

If one replaces the locations of the image sources by their expression (B.13), one obtains

$$P^{\rm well}(x, N|x_{\rm in}, 0) = \frac{\mu}{2\sqrt{\pi N}} \sum_{m=-\infty}^{\infty} (-1)^m e^{-\frac{\mu^2}{4N}(x - x_{\rm in} - 2m)^2} - \{x_{\rm in} \to -x_{\rm in}\} . \tag{B.18}$$

By expanding the square in the argument of the exponential function, one notices that the result can be written in terms of the fourth elliptic theta function ϑ_4,

$$P^{\rm well}(x, N|x_{\rm in}, 0) = \frac{\mu}{2\sqrt{\pi N}} e^{-\frac{\mu^2}{4N}(x - x_{\rm in})^2} \vartheta_4 \left[\frac{i\mu^2}{2N} \left(x - x_{\rm in}\right), e^{-\frac{\mu^2}{N}} \right] - \{x_{\rm in} \to -x_{\rm in}\} \tag{B.19}$$

where ϑ_4 is defined in Eq. (A.4). The next step is to notice that this expression can be further simplified by making use of the Jacobi identity (A.19), where ϑ_2 is defined in Eq. (A.2). This allows one to rewrite Eq. (B.19) as

$$P^{\rm well}(x, N|x_{\rm in}, 0) = \frac{1}{2}\vartheta_2 \left[-\frac{\pi}{2} \left(x - x_{\rm in}\right), e^{-\frac{\pi^2 N}{\mu^2}} \right] - \frac{1}{2}\vartheta_2 \left[-\frac{\pi}{2} \left(x + x_{\rm in}\right), e^{-\frac{\pi^2 N}{\mu^2}} \right] . \tag{B.20}$$

This expression also allows one to compute the distribution of first passage times, making use of Eq. (B.8). The result is given in terms of the ϑ_2' function, which denotes the

derivative of ϑ_2 with respect to its first argument. Since ϑ_2 is an even function of its first argument, ϑ_2' is an odd function, so the two terms in Eq. (B.20) provide the same contribution and one obtains

$$P_{\rm FPT}^{\rm well}(x,N) = -\frac{\pi}{2\mu^2}\vartheta_2'\left(\frac{\pi}{2}x, e^{-\frac{\pi^2 N}{\mu^2}}\right) . \tag{B.21}$$

This matches Eq. (4.11) of Ref. [54], although here it is derived using different techniques.

Finally, let us note that in order to evaluate the backward probability with Eq. (5.20), one needs to integrate Eq. (B.20) over N when setting $x_{\rm in} = 1$. A first remark is that, from Eq. (A.6), one can easily show that $\vartheta_2(z \pm \pi/2, q) = \pm\vartheta_1(-z, q)$. As a consequence, one has

$$P^{\rm well}(x, N|1, 0) = \vartheta_1\left(\frac{\pi}{2}x, e^{-\frac{\pi^2 N}{\mu^2}}\right) . \tag{B.22}$$

After performing the change of integration variable $e^{-\pi^2 N/\mu^2} = q$, and denoting $z = \pi x/2$, one thus has to compute

$$\int_0^\infty P^{\rm well}(x,N){\rm d}N = \frac{\mu^2}{\pi^2}\int_0^1 \frac{{\rm d}q}{q}\vartheta_1\left(z,q\right) . \tag{B.23}$$

By expanding the ϑ_1 function according to its definition given in Eq. (A.1), each term can be integrated exactly, and this gives rise to

$$\int_0^1 \frac{{\rm d}q}{q}\vartheta_1\left(\frac{\pi}{2}x, q\right) = 8\sum_{n=0}^{\infty}(-1)^n\frac{\sin\left[(2n+1)\,z\right]}{(2n+1)^2} \equiv F(z)\,, \tag{B.24}$$

which defines the function $F(z)$. By differentiating this function, one obtains

$$F'(z) = 8\sum_{n=0}^{\infty}(-1)^n\frac{\cos\left[(2n+1)\,z\right]}{(2n+1)} \tag{B.25}$$

$$= 4\left[\underbrace{\sum_{n=0}^{\infty}\frac{(-1)^n}{2n+1}e^{(2n+1)iz}}_{\arctan(e^{iz})} + \underbrace{\sum_{n=0}^{\infty}\frac{(-1)^n}{2n+1}e^{-(2n+1)iz}}_{\arctan(e^{-iz})}\right] , \tag{B.26}$$

where we one recognizes the Taylor expansion of the arctan function. The next step is to make use of the identity $\arctan(Z)+\arctan(1/Z) = \pi/2$, which is valid when the argument of Z is comprised between 0 and $\pi/2$, which is the case here since $Z = e^{iz} = e^{i\pi x/2}$ and $0 \leq x \leq 1$. This gives rise to $F'(z) = 2\pi$. Furthermore, when $z = 0$, $\theta_1(z,q) = 0$ so $F(0) = 0$ and one obtains $F(z) = 2\pi z$. Combining the above results, one is led to

$$\int_0^\infty P^{\rm well}(x,N){\rm d}N = \mu^2 x\,, \tag{B.27}$$

which we use in the main text below Eq. (5.39).

Appendix C

Quantum mechanical calculations

C.1 Wavefunction of the two-mode squeezed state

In this appendix, we provide a derivation of the expression (2.107) for the two-mode squeezed state. From the expression of the rotation operator in terms of the number of particles operators, Eq. (6.3), it is clear that the vacuum state is invariant under rotations, *i.e.* $\hat{R}(t)\,|0,0\rangle = |0,0\rangle$. The two-mode squeezed state is thus given by $|\Psi_{2\text{sq}}(t)\rangle = \hat{U}_{\text{S}}(t)\hat{R}(t)\,|0,0\rangle = \hat{U}_{\text{S}}(t)\,|0,0\rangle$, where the squeezing operator is given by Eq. (6.2). We rewrite this expression as

$$\hat{U}_{\text{S}}(t) = e^{\alpha^* \hat{A}^\dagger - \alpha \hat{A}}\,, \tag{C.1}$$

with $\alpha = re^{2i\varphi}$ and $\hat{A} = \hat{c}_1\hat{c}_2$. The idea is to make use of operator ordering theorems to rewrite Eq. (C.1) as a product of exponentials that can be easily applied onto the vacuum state, following similar lines as those presented in section 3.3 of Ref. [136].

Our first step is to study the algebra generated by the operators appearing in Eq. (C.1), $\hat{A}$ and $\hat{A}^\dagger$. Introducing the Hermitian operator $\hat{B} \equiv \hat{c}_1\hat{c}_1^\dagger + \hat{c}_2^\dagger\hat{c}_2 = \hat{B}^\dagger$, one can first check that $\hat{A}$, $\hat{A}^\dagger$ and B form a closed algebra, with

$$\left[\hat{A}, \hat{A}^\dagger\right] = B\,, \qquad \left[\hat{A}, \hat{B}\right] = 2\hat{A}\,, \qquad \left[\hat{A}^\dagger, \hat{B}\right] = -2\hat{A}^\dagger\,. \tag{C.2}$$

All commutators within this algebra can be computed with these formulas using iterative methods. In particular, one finds

$$\left[\hat{A}^n, \hat{B}\right] = 2n\hat{A}^n \tag{C.3}$$

$$\left[\left(\hat{A}^\dagger\right)^n, \hat{B}\right] = -2n\left(\hat{A}^\dagger\right)^n \tag{C.4}$$

$$\left[\hat{A}^n, \hat{A}^\dagger\right] = n\hat{A}^{n-1}\hat{B} - n(n-1)\hat{A}^{n-1} \tag{C.5}$$

$$\left[\left(\hat{A}^\dagger\right)^n, \hat{A}\right] = -n\hat{B}\left(\hat{A}^\dagger\right)^{n-1} + n\,(n-1)\left(\hat{A}^\dagger\right)^{n-1} \tag{C.6}$$

$$\left[\hat{A}, \hat{B}^n\right] = \hat{A}\left[\hat{B}^n - \left(\hat{B}-2\right)^n\right] = \left[\left(\hat{B}+2\right)^n - \hat{B}^n\right]\hat{A} \tag{C.7}$$

$$\left[\hat{A}^\dagger, \hat{B}^n\right] = \hat{A}^\dagger\left[\hat{B}^n - \left(\hat{B}+2\right)^n\right] = \left[\left(\hat{B}-2\right)^n - \hat{B}^n\right]\hat{A}^\dagger \tag{C.8}$$

for any integer number n. From here, commutators involving exponentials can be readily derived. Making use of Eqs. (C.4), (C.7) and (C.6), one respectively finds three formulas

that will turn out to be useful below, namely

$$\left[e^{z\hat{A}^\dagger}, \hat{B}\right] = -2z\hat{A}^\dagger e^{z\hat{A}^\dagger} \tag{C.9}$$

$$\left[e^{z\hat{B}}, \hat{A}\right] = \left(e^{-2z} - 1\right)\hat{A}e^{z\hat{B}} \tag{C.10}$$

$$\left[e^{z\hat{A}^\dagger}, \hat{A}\right] = \left(z^2\hat{A}^\dagger - z\hat{B}\right)e^{z\hat{A}^\dagger} \tag{C.11}$$

for any complex number z.

Our second step is to introduce the function

$$F(x) = e^{x\left(\alpha^*\hat{A}^\dagger - \alpha\hat{A}\right)}, \tag{C.12}$$

such that $\hat{U}_{\rm S} = F(1)$, and to study that function. The goal is to rewrite $F(x)$ as a product of exponentials. These exponentials must involve elements of the algebra only, which allow us to introduce the ansatz

$$F(x) = e^{f(x)\hat{A}^\dagger}e^{g(x)\hat{B}}e^{h(x)\hat{A}} \tag{C.13}$$

where f, g and h are three functions to determine. This can be done by differentiating F with respect to x. Making use of Eq. (C.12), one has

$$F'(x) = \left(\alpha^*\hat{A}^\dagger - \alpha\hat{A}\right)F(x), \tag{C.14}$$

while Eq. (C.13) gives rise to three terms, namely

$$F'(x) = f'(x)\hat{A}^\dagger e^{f(x)\hat{A}^\dagger}e^{g(x)\hat{B}}e^{h(x)\hat{A}} + g'(x)e^{f(x)\hat{A}^\dagger}\hat{B}e^{g(x)\hat{B}}e^{h(x)\hat{A}} + h'(x)e^{f(x)\hat{A}^\dagger}e^{g(x)\hat{B}}\hat{A}e^{h(x)\hat{A}}. \tag{C.15}$$

In this expression, the first term is simply given by $f'(x)\hat{A}^\dagger F(x)$. For the second term, making use of Eq. (C.9) to rewrite $e^{f(x)\hat{A}^\dagger}\hat{B} = \hat{B}e^{f(x)\hat{A}^\dagger} - 2f(x)\hat{A}^\dagger e^{f(x)\hat{A}^\dagger}$, one finds that it is given by $g'(x)[\hat{B} - 2f(x)\hat{A}^\dagger]F(x)$. The third term can be computed similarly by first making use of Eq. (C.10) and then of Eq. (C.11), and one obtains $h'(x)e^{-2g(x)}[f^2(x)\hat{A}^\dagger + \hat{A} - f(x)\hat{B}]F(x)$. Combining these results together, one obtains

$$\begin{aligned} F'(x) = \Big\{&h'(x)e^{-2g(x)}\hat{A} + \left[f'(x) - 2f(x)g'(x) + h'(x)e^{-2g(x)}f^2(x)\right]\hat{A}^\dagger \\ &+ \left[g'(x) - h'(x)f(x)e^{-2g(x)}\right]\hat{B}\Big\}F(x). \end{aligned} \tag{C.16}$$

By identifying Eqs. (C.14) and (C.16), one obtains three coupled differential equations for the functions f, g and h, namely

$$f' - 2fg' + h'f^2e^{-2g} = \alpha^*, \tag{C.17}$$

$$h'e^{-2g} = -\alpha, \tag{C.18}$$

$$g' - fh'e^{-2g} = 0. \tag{C.19}$$

This system must be solved with the boundary conditions $f(0) = g(0) = h(0) = 0$ that simply follow from identifying Eqs. (C.12) and (C.13) when $x = 0$. This can be done as follows. Plugging Eq. (C.19) into Eq. (C.18), one obtains $g' = -\alpha f$, and plugging that

relation together with Eq. (C.19) into Eq. (C.17) gives rise to $f' + \alpha f^2 = \alpha^*$. This can be readily integrated, and imposing that $f(0) = 0$, one obtains

$$f(x) = \sqrt{\frac{\alpha^*}{\alpha}} \tanh\left(|\alpha| x\right) . \tag{C.20}$$

From here, the relation $g' = -\alpha f$ can also be integrated, and imposing that $g(0) = 0$ leads to

$$g(x) = -\ln\left[\cosh\left(|\alpha| x\right)\right] . \tag{C.21}$$

Finally, Eq. (C.19) gives rise to $h' = -\alpha e^{2g}$, which can be integrated as

$$h(x) = -\sqrt{\frac{\alpha}{\alpha^*}} \tanh\left(|\alpha| x\right) \tag{C.22}$$

where we have used that $h(0) = 0$. Evaluating the three functions f, g and h when $x = 1$, and expressing α in terms of r and φ, one obtains for the squeezing operator

$$\hat{U}_{\rm S} = \exp\left[e^{-2i\varphi} \tanh(r) \hat{A}^\dagger\right] \exp\left[-\ln\left(\cosh r\right) \hat{B}\right] \exp\left[-e^{2i\varphi} \tanh(r) \hat{A}\right] , \tag{C.23}$$

which is the operator ordered expression we were seeking.

We can now apply the squeezing operator onto the vacuum state. Recalling that $\hat{A} = \hat{c}_1 \hat{c}_2$ and $\hat{B} \equiv \hat{c}_1 \hat{c}_1^\dagger + \hat{c}_2^\dagger \hat{c}_2$, one can see that $\hat{A}$ annihilates the vacuum state, while $\hat{B}$ leaves it invariant, $\hat{B} \left|0,0\right\rangle = \left|0,0\right\rangle$. When applied to the vacuum state, the last exponential term in Eq. (C.23) has therefore no effect, while the second term adds a prefactor $1/\cosh(r)$. Taylor expanding the first exponential term, one then obtains

$$\left|\Psi_{\rm 2sq}\right\rangle = \frac{1}{\cosh(r)} \sum_{n=0}^{\infty} e^{-2in\varphi} \tanh^n(r) \left|n,n\right\rangle , \tag{C.24}$$

which coincides with Eq. (2.107) given in the main text.

This two-mode squeezed state can finally be expressed in position space, and the wavefunction is given by

$$\Psi_{\rm 2sq}\left(Q_1,Q_2\right) = \left\langle Q_1,Q_2\right| \left.\Psi_{\rm 2sq}\right\rangle = \frac{1}{\cosh(r)} \sum_{n=0}^{\infty} e^{-2in\varphi} \tanh^n(r) \left\langle Q_1\right| \left.n\right\rangle \left\langle Q_2\right| \left.n\right\rangle . \tag{C.25}$$

The scalar products $\left\langle Q\right| \left.n\right\rangle$ can be expressed in terms of the Hermite potentials $H_n(Q)$, *i.e.*

$$\left\langle Q\right| \left.n\right\rangle = \frac{\pi^{-1/4}}{\sqrt{2^n n!}} e^{-\frac{Q^2}{2}} H_n(Q) . \tag{C.26}$$

The sum over n appearing in Eq. (C.25) can then be performed by means of Eq. (18.18.28) of Ref. [135], namely[1]

$$\sum_{n=0}^{\infty} \frac{H_n(x) H_n(y)}{2^n n!} z^n = \left(1-z^2\right)^{-1/2} \exp\left[\frac{2xyz - \left(x^2+y^2\right) z^2}{1-z^2}\right] , \tag{C.27}$$

[1] Hereafter, unless specified otherwise, the square root of a complex number $Z \notin \mathbb{R}^-$ is given by $\sqrt{Z} = \sqrt{\rho} e^{i\gamma/2}$, for $Z = \rho e^{i\gamma}$ with $-\pi < \gamma < \pi$. Notice that, for the square roots appearing in Eqs. (C.27) and (C.28), γ actually lies within $[-\pi/2, \pi/2]$.

with $|z|<1$. This gives rise to

$$\Psi_{2\mathrm{sq}}(Q_1,Q_2)=\frac{\exp\left[\frac{1}{2}A(r,\varphi)\,(Q_1^2+Q_2^2)+B(r,\varphi)Q_1Q_2\right]}{\cosh r\,\sqrt{\pi}\sqrt{1-e^{-4i\varphi}\tanh^2 r}} \tag{C.28}$$

where the functions $A(r,\varphi)$ and $B(r,\varphi)$ are given by

$$A(r,\varphi)=-\frac{1+e^{-4i\varphi}\tanh^2 r}{1-e^{-4i\varphi}\tanh^2 r},\quad B(r,\varphi)=\frac{2e^{-2i\varphi}\tanh r}{1-e^{-4i\varphi}\tanh^2 r}\,. \tag{C.29}$$

C.2 Correlation function of the evolution operator

In this appendix, we compute the two-point function of the evolution operator appearing in Eq. (6.15), namely $\left\langle \tilde{Q}_1,\tilde{Q}_2\right|\hat{U}(t_a)\hat{U}^\dagger(t_b)\left|\bar{Q}_1,\bar{Q}_2\right\rangle$. We first introduce the two-mode coherent states $|\boldsymbol{u}\rangle=|u_1,u_2\rangle$, which are eigenstates of the annihilation operators

$$\hat{c}_i\,|\boldsymbol{u}\rangle=u_i\,|\boldsymbol{u}\rangle \tag{C.30}$$

where $i=1$ or 2. Decomposing the eigenvalues into real and imaginary parts,

$$u_i=\frac{u_{i\mathrm{R}}+iu_{i\mathrm{I}}}{\sqrt{2}}, \tag{C.31}$$

and introducing the integration element $\mathrm{d}\boldsymbol{u}=\mathrm{d}u_{1\mathrm{R}}\mathrm{d}u_{1\mathrm{I}}\mathrm{d}u_{2\mathrm{R}}\mathrm{d}u_{2\mathrm{I}}$, they satisfy the closure relation

$$\int\frac{\mathrm{d}\boldsymbol{u}}{(2\pi)^2}\,|\boldsymbol{u}\rangle\,\langle\boldsymbol{u}|=1\,. \tag{C.32}$$

One can plug this closure relation on each side of the evolution operators in the two-point correlator we aim at computing, leading to

$$\begin{aligned}\left\langle \tilde{Q}_1,\tilde{Q}_2\right|\hat{U}(t_a)\hat{U}^\dagger(t_b)\left|\bar{Q}_1,\bar{Q}_2\right\rangle=\int\frac{\mathrm{d}\boldsymbol{u}}{(2\pi)^2}\int\frac{\mathrm{d}\boldsymbol{v}}{(2\pi)^2}\int\frac{\mathrm{d}\boldsymbol{w}}{(2\pi)^2}\left\langle\tilde{Q}_1\right|w_1\right\rangle\left\langle\tilde{Q}_2\right|w_2\right\rangle\\ \left\langle\boldsymbol{w}\right|\hat{U}(t_a)\left|\boldsymbol{u}\right\rangle\left\langle\boldsymbol{u}\right|\hat{U}^\dagger(t_b)\left|\boldsymbol{v}\right\rangle\left\langle v_1\right|\bar{Q}_1\right\rangle\left\langle v_2\right|\bar{Q}_2\right\rangle\end{aligned} \tag{C.33}$$

In this expression, $\left\langle\tilde{Q}_1\right|w_1\right\rangle$ is the wave function of the coherent state, and is given by

$$\left\langle\tilde{Q}_1\right|w_1\right\rangle=\frac{1}{\pi^{1/4}}\exp\left[-\frac{i}{2}w_{1\mathrm{R}}w_{1\mathrm{I}}+iw_{1\mathrm{I}}\tilde{Q}_1-\frac{1}{2}(\tilde{Q}_1-w_{1\mathrm{R}})^2\right], \tag{C.34}$$

with a similar expression for $\left\langle\tilde{Q}_2\right|w_2\right\rangle$, $\left\langle v_1\right|\bar{Q}_1\right\rangle$ and $\left\langle v_2\right|\bar{Q}_2\right\rangle$. Let us then consider $\left\langle\boldsymbol{w}\right|\hat{U}(t_a)\left|\boldsymbol{u}\right\rangle=\left\langle\boldsymbol{w}\right|\hat{U}_{\mathrm{S}}(t_a)\hat{R}(t_a)\left|\boldsymbol{u}\right\rangle$. By using the decomposition

$$|\boldsymbol{u}\rangle=e^{-\frac{|u_1|^2+|u_2|^2}{2}}\sum_{n_1=0}^{\infty}\sum_{n_2=0}^{\infty}\frac{u_1^{n_1}}{\sqrt{n_1!}}\frac{u_2^{n_2}}{\sqrt{n_2!}}\,|n_1,n_2\rangle\,, \tag{C.35}$$

Eq. (6.3) gives rise to

$$\hat{R}\,|\boldsymbol{u}\rangle = \sum_{m_1=0}^{\infty}\sum_{m_2=0}^{\infty} e^{-\frac{|u_1|^2+|u_2|^2}{2}} \sum_{n_1=0}^{\infty}\sum_{n_2=0}^{\infty} \frac{u_1^{n_1}}{\sqrt{n_1!}}\,(i\theta n_1)^{m_1}\,\frac{u_2^{n_2}}{\sqrt{n_2!}}\,(i\theta n_2)^{m_2}\,|n_1,n_2\rangle \tag{C.36}$$

$$= e^{-\frac{|u_1|^2+|u_2|^2}{2}} \sum_{n_1=0}^{\infty}\sum_{n_2=0}^{\infty} \frac{u_1^{n_1}}{\sqrt{n_1!}} e^{i\theta n_1} \frac{u_2^{n_2}}{\sqrt{n_2!}} e^{i\theta n_2}\,|n_1,n_2\rangle \tag{C.37}$$

$$= e^{-\frac{|u_1|^2+|u_2|^2}{2}} \sum_{n_1=0}^{\infty}\sum_{n_2=0}^{\infty} \frac{\left(u_1 e^{i\theta}\right)^{n_1}}{\sqrt{n_1!}} \frac{\left(u_2 e^{i\theta}\right)^{n_2}}{\sqrt{n_2!}}\,|n_1,n_2\rangle \tag{C.38}$$

$$= \left|e^{i\theta_a}u_1, e^{i\theta_a}u_2\right\rangle = \left|e^{i\theta}\boldsymbol{u}\right\rangle. \tag{C.39}$$

One thus has $\left\langle \boldsymbol{w}\middle|\,\hat{U}(t_a)\,\middle|\,\boldsymbol{u}\right\rangle = \left\langle \boldsymbol{w}\middle|\,\hat{U}_{\rm S}(t_a)\,\middle|\,e^{i\theta_a}\boldsymbol{u}\right\rangle$, where θ_a is a short-hand notation for $\theta(t_a)$. The next step is to use the operator ordered expression (C.23) for $\hat{U}_{\rm S}$. Recalling that $\hat{A} = \hat{c}_1\hat{c}_2$ and $\hat{B} = \hat{c}_1\hat{c}_1^\dagger + \hat{c}_2^\dagger\hat{c}_2 = 1 + \hat{n}_1 + \hat{n}_2$, Eq. (C.30) gives rise to $\hat{A}\,|\boldsymbol{u}\rangle = u_1u_2\,|\boldsymbol{u}\rangle$, hence $e^{z\hat{A}}\,|\boldsymbol{u}\rangle = e^{zu_1u_2}\,|\boldsymbol{u}\rangle$ for any complex number z. Similarly, one has $\langle w|\,e^{z\hat{A}^\dagger} = e^{zw_1^*w_2^*}\,\langle w|$.

Making use of Eq. (C.35), one also has

$$\langle \boldsymbol{w}|\,e^{z\hat{n}_1}\,|\boldsymbol{u}\rangle = e^{-\frac{|u_1|^2+|u_2|^2+|v_1|^2+|v_2|^2}{2}} \sum_{n,m,k} \frac{z^k n^k}{k!}\,\frac{(w_1^*u_1)^n}{n!}\,\frac{(w_2^*u_2)^m}{m!} \tag{C.40}$$

$$= e^{-\frac{|u_1|^2+|u_2|^2+|v_1|^2+|v_2|^2}{2}} \sum_{n,m} \frac{(w_1^*u_1e^z)^n}{n!}\,\frac{(w_2^*u_2)^m}{m!} \tag{C.41}$$

$$= e^{-\frac{|u_1|^2+|u_2|^2+|v_1|^2+|v_2|^2}{2}+w_1^*u_1e^z+w_2^*u_2} \tag{C.42}$$

for any complex number z, and a similar expression for $\langle \boldsymbol{w}|\,e^{z\hat{n}_1}\,|\boldsymbol{u}\rangle$. Similarly, one finds

$$\langle \boldsymbol{w}|\,e^{z\hat{B}}\,|\boldsymbol{u}\rangle = e^{-\frac{|u_1|^2+|u_2|^2+|v_1|^2+|v_2|^2}{2}+w_1^*u_1e^z+w_2^*u_2e^z+z}. \tag{C.43}$$

Combining the previous results, one obtains

$$\left\langle \boldsymbol{w}\middle|\,\hat{U}(t_a)\,\middle|\,\boldsymbol{u}\right\rangle = \frac{1}{\cosh r_a}\exp(\mathcal{F}), \tag{C.44}$$

where

$$\begin{aligned}\mathcal{F} &= e^{-2i\varphi_a}\tanh r_a w_1^*w_2^* - e^{2i\varphi_a}e^{2i\theta_a}\tanh r_a u_1u_2 \\ &\quad -\frac{1}{2}\left(|w_1|^2+|u_1|^2+|w_2|^2+|u_2|^2\right) + \frac{e^{i\theta_a}}{\cosh r_a}\left(w_1^*u_1+w_2^*u_2\right) \qquad \text{(C.45)}\\ &= \frac{1}{2}e^{-2i\varphi_a}\tanh r_a\left(w_{1\rm R}w_{2\rm R} - w_{1\rm I}w_{2\rm I} - iw_{1\rm R}w_{2\rm I} - iw_{1\rm I}w_{2\rm R}\right) \\ &\quad -\frac{1}{2}e^{2i\varphi_a}e^{2i\theta_a}\tanh r_a\left(u_{1\rm R}u_{2\rm R} - u_{1\rm I}u_{2\rm I} + iu_{1\rm R}u_{2\rm I} + iu_{1\rm I}u_{2\rm R}\right) \\ &\quad -\frac{1}{4}\left(w_{1\rm R}^2+w_{1\rm I}^2+w_{2\rm R}^2+w_{2\rm I}^2+u_{1\rm R}^2+u_{1\rm I}^2+u_{2\rm R}^2+u_{2\rm I}^2\right) \\ &\quad +\frac{1}{2}\frac{e^{i\theta_a}}{\cosh r_a}(w_{1\rm R}u_{1\rm R}+w_{1\rm I}u_{1\rm I}+iw_{1\rm R}u_{1\rm I}-iw_{1\rm I}u_{1\rm R} \\ &\qquad\qquad +w_{2\rm R}u_{2\rm R}+w_{2\rm I}u_{2\rm I}+iw_{2\rm R}u_{2\rm I}-iw_{2\rm I}u_{2\rm R}). \qquad \text{(C.46)}\end{aligned}$$

Here in the second expression, we have expanded u_1, u_2, w_1 and w_2 into their real and imaginary parts, see Eq. (C.31). The form $\mathcal{F}$ is quadratic in these variables, and since the argument of the exponential in Eq. (C.34) is also quadratic, our result for $\left\langle \tilde{Q}_1, \tilde{Q}_2 \middle| \hat{U}(t_a)\hat{U}^\dagger(t_b) \middle| \bar{Q}_1, \bar{Q}_2 \right\rangle$ can be written in matricial form if one introduces the 12-dimensional vector,

$$\alpha^{\mathrm{T}} \equiv [u_{1\mathrm{R}}, u_{1\mathrm{I}}, u_{2\mathrm{R}}, u_{2\mathrm{I}}, v_{1\mathrm{R}}, v_{1\mathrm{I}}, v_{2\mathrm{R}}, v_{2\mathrm{I}}, w_{1\mathrm{R}}, w_{1\mathrm{I}}, w_{2\mathrm{R}}, w_{2\mathrm{I}}], \tag{C.47}$$

in terms of which

$$\left\langle \tilde{Q}_1, \tilde{Q}_2 \middle| \hat{U}(t_a)\hat{U}^\dagger(t_b) \middle| \bar{Q}_1, \bar{Q}_2 \right\rangle = \frac{1}{64\pi^7} \frac{e^{-\left(\tilde{Q}_1^2+\tilde{Q}_2^2+\bar{Q}_1^2+\bar{Q}_2^2\right)/2}}{\cosh r_a \cosh r_b} \int \mathrm{d}^{12}\alpha e^{-\frac{1}{2}\alpha^{\mathrm{T}} M \alpha - J^{\mathrm{T}}\alpha}, \tag{C.48}$$

where

$$J^{\mathrm{T}} = \left[0, 0, 0, 0, -\bar{Q}_1, i\bar{Q}_1, -\bar{Q}_2, i\bar{Q}_2, -\tilde{Q}_1, -i\tilde{Q}_1, -\tilde{Q}_2, -i\tilde{Q}_2\right] \tag{C.49}$$

and

$$M = \begin{bmatrix}
1 & 0 & \Theta_a + \Theta_b^* & i\Theta_a - i\Theta_b^* & -C_b^* & -iC_b^* & 0 & 0 & -C_a & iC_a & 0 & 0 \\
0 & 1 & i\Theta_a - i\Theta_b^* & -\Theta_a - \Theta_b^* & iC_b^* & -C_b^* & 0 & 0 & -iC_a & -C_a & 0 & 0 \\
\Theta_a + \Theta_b^* & i\Theta_a - i\Theta_b^* & 1 & 0 & 0 & 0 & -C_b^* & -iC_b^* & 0 & 0 & -C_a & iC_a \\
i\Theta_a - i\Theta_b^* & -\Theta_a - \Theta_b^* & 0 & 1 & 0 & 0 & iC_b^* & -C_b^* & 0 & 0 & -iC_a & -C_a \\
-C_b^* & iC_b^* & 0 & 0 & \frac{3}{2} & -\frac{i}{2} & -T_b & -iT_b & 0 & 0 & 0 & 0 \\
-iC_b^* & -C_b^* & 0 & 0 & -\frac{i}{2} & \frac{1}{2} & -iT_b & T_b & 0 & 0 & 0 & 0 \\
0 & 0 & -C_b^* & iC_b^* & -T_b & -iT_b & \frac{3}{2} & -\frac{i}{2} & 0 & 0 & 0 & 0 \\
0 & 0 & -iC_b^* & -C_b^* & -iT_b & T_b & -\frac{i}{2} & \frac{1}{2} & 0 & 0 & 0 & 0 \\
-C_a & -iC_a & 0 & 0 & 0 & 0 & 0 & 0 & \frac{3}{2} & \frac{i}{2} & -T_a^* & iT_a^* \\
iC_a & -C_a & 0 & 0 & 0 & 0 & 0 & 0 & \frac{i}{2} & \frac{1}{2} & iT_a^* & T_a^* \\
0 & 0 & -C_a & -iC_a & 0 & 0 & 0 & 0 & -T_a^* & iT_a^* & \frac{3}{2} & \frac{i}{2} \\
0 & 0 & iC_a & -C_a & 0 & 0 & 0 & 0 & iT_a^* & T_a^* & \frac{i}{2} & \frac{1}{2}
\end{bmatrix}. \tag{C.50}$$

Here we have introduced $C_a = e^{i\theta_a}/(2\cosh r_a)$, $T_a = (1/2)e^{2i\varphi_a}\tanh r_a$ and $\Theta_a = e^{2i\theta_a}T_a$. If $\det M \neq 0$, the Gaussian integral can be performed, and one obtains[2]

$$\left\langle \tilde{Q}_1, \tilde{Q}_2 \middle| \hat{U}(t_a)\hat{U}^\dagger(t_b) \middle| \bar{Q}_1, \bar{Q}_2 \right\rangle = \frac{1}{\pi} \frac{1}{\cosh r_a \cosh r_b} \frac{1}{\sqrt{\det M}} e^{-\frac{1}{2}\left(\tilde{Q}_1^2+\tilde{Q}_2^2+\bar{Q}_1^2+\bar{Q}_2^2\right)+\frac{1}{2}J^{\mathrm{T}}M^{-1}J}. \tag{C.51}$$

[2]The precise meaning of $\sqrt{\det M}$ is a priori not obvious since $\det M$ is a complex number, and the branch cut of the complex square root function leaves the sign of $\sqrt{\det M}$ ambiguous. However, from Eq. (C.50), one can show that M is a symmetric normal matrix, *i.e.* $MM^\dagger = M^\dagger M$. This implies that the real part and the imaginary part of M commute, so they can be simultaneously diagonalized by an orthogonal matrix. The square root of $\det M$ thus stands for the product of the square roots of each eigenvalue of M. Since the square root of each eigenvalue is well-defined because all eigenvalues have a positive real part (otherwise the Gaussian integral could not be performed), this removes the ambiguity.

The determinant of M can be computed explicitly from Eq. (C.50), and is given by

$$\begin{aligned}\det M &= 4e^{2i\Delta\theta}\left[-\sin^2(\Delta\theta)+\sin^2(2\varphi_a+\Delta\theta)\tanh^2 r_a+\sin^2(2\varphi_b-\Delta\theta)\tanh^2 r_b\right.\\ &\qquad\left.-2\sin(2\varphi_a)\sin(2\varphi_b)\tanh r_a\tanh r_b-\sin^2(2\varphi_a-2\varphi_b+\Delta\theta)\tanh^2 r_a\tanh^2 r_b\right]\\ &\equiv f_M(a,b),\end{aligned} \tag{C.52}$$

where $\Delta\theta \equiv \theta_a - \theta_b$. This expression defines the function $f_M(a,b)$, which satisfies $f_M(b,a) = f_M^*(a,b)$.

Since the four first entries of J vanish, see Eq. (C.49), the 8×8 lower right block of M^{-1} is sufficient to compute $J^{\mathrm{T}}M^{-1}J$. We therefore focus on that 8×8 block, *i.e.* on the matrix $\tilde{M}$ defined as $\tilde{M}_{ij} = (M^{-1})_{i+4,j+4}$, with $i,j = 1\cdots 8$. It can be computed explicitly from Eq. (C.50), and its expression involves the four functions d_1, d_2, d_3, d_4, defined as

$$\begin{aligned}d_1(a,b) &= e^{2i\Delta\theta}\left\{f(2\varphi_a+\Delta\theta)\tanh^2 r_a+f(2\varphi_b-\Delta\theta)\tanh^2 r_b-f(\Delta\theta)\right.\\ &\quad -2\left[f(\varphi_a+\varphi_b)-f(\varphi_b-\varphi_a)\right]\tanh r_a\tanh r_b\\ &\quad \left.-f(2\varphi_b-2\varphi_a-\Delta\theta)\tanh^2 r_a\tanh^2 r_b\right\},\end{aligned} \tag{C.53}$$

$$\begin{aligned}d_2(a,b) &= 4ie^{2i\Delta\theta}\left[\sin(2\varphi_a)\tanh r_a-\sin(2\varphi_b-2\Delta\theta)\tanh r_b\right.\\ &\quad \left.-\sin(4\varphi_a-2\varphi_b+2\Delta\theta)\tanh^2 r_a\tanh r_b+\sin(2\varphi_a)\tanh r_a\tanh^2 r_b\right],\end{aligned} \tag{C.54}$$

$$d_3(a,b) = \frac{-4ie^{2i\Delta\theta}\left[\sin\Delta\theta+\sin(2\varphi_a-2\varphi_b+\Delta\theta)\tanh r_a\tanh r_b\right]}{\cosh r_a\cosh r_b}, \tag{C.55}$$

$$d_4(a,b) = \frac{4ie^{2i\Delta\theta}\left[\sin(2\varphi_a+\Delta\theta)\tanh r_a-\sin(2\varphi_b-\Delta\theta)\tanh r_b\right]}{\cosh r_a\cosh r_b}, \tag{C.56}$$

where $f(\theta) = 1-\cos 2\theta+2i\sin 2\theta$.[3] The matrix $\tilde{M}$ can be expressed as

$$\tilde{M} = \begin{bmatrix} \frac{1}{2} & \frac{i}{2} & 0 & 0 & 0 & 0 & 0 & 0\\ \frac{i}{2} & D_1 & 0 & D_2 & 0 & D_3 & 0 & D_4\\ 0 & 0 & \frac{1}{2} & \frac{i}{2} & 0 & 0 & 0 & 0\\ 0 & D_2 & \frac{i}{2} & D_1 & 0 & D_4 & 0 & D_3\\ 0 & 0 & 0 & 0 & \frac{1}{2} & -\frac{i}{2} & 0 & 0\\ 0 & D_3 & 0 & D_4 & -\frac{i}{2} & \bar{D}_1 & 0 & \bar{D}_2\\ 0 & 0 & 0 & 0 & 0 & 0 & \frac{1}{2} & -\frac{i}{2}\\ 0 & D_4 & 0 & D_3 & 0 & \bar{D}_2 & -\frac{i}{2} & \bar{D}_1 \end{bmatrix}, \tag{C.59}$$

where

$$D_i = \frac{d_i(a,b)}{f_M(a,b)} \quad \text{for} \quad i=1,2,3,4 \tag{C.60}$$

$$\bar{D}_i = \left[\frac{d_i(b,a)}{f_M(b,a)}\right]^* = \frac{d_i^*(b,a)}{f_M(a,b)} \quad \text{for} \quad i=1,2. \tag{C.61}$$

[3] In practice, the following relations satisfied by the function f turn out to be useful:

$$f(\theta) = 2\sin\theta(\sin\theta+2i\cos\theta) = \frac{1}{2}\left(e^{2i\theta}-3e^{-2i\theta}\right)+1 = 2\left[1-f\left(\frac{\theta}{2}-\frac{\pi}{4}\right)\right]\sin\theta, \tag{C.57}$$

and

$$f(-\theta) = f^*(\theta), \quad f(\theta\pm\pi) = f(\theta). \tag{C.58}$$

One can see that the bars denote the operation of taking the complex conjugate and flipping "a" and "b".

The calculation of $J^{\mathrm{T}}M^{-1}J$ can then be performed as follows. From Eq. (C.49), J can be written as $J^{\mathrm{T}} = [0, 0, 0, 0, (G \cdot X)^{\mathrm{T}}]$, with

$$G = \begin{bmatrix} -1 & 0 & 0 & 0 \\ i & 0 & 0 & 0 \\ 0 & -1 & 0 & 0 \\ 0 & i & 0 & 0 \\ 0 & 0 & -1 & 0 \\ 0 & 0 & -i & 0 \\ 0 & 0 & 0 & -1 \\ 0 & 0 & 0 & -i \end{bmatrix}, \quad X = \begin{bmatrix} \bar{Q}_1 \\ \bar{Q}_2 \\ \tilde{Q}_1 \\ \tilde{Q}_2 \end{bmatrix}. \tag{C.62}$$

Then $J^{\mathrm{T}}M^{-1}J = X^{\mathrm{T}}G^{\mathrm{T}}\tilde{M}GX = X^{\mathrm{T}}\mathcal{M}X$, where $\mathcal{M} \equiv G^{\mathrm{T}}\tilde{M}G$. $\mathcal{M}$ can be calculated from Eqs. (C.59) and (C.62), and one obtains

$$\mathcal{M} = \begin{bmatrix} \frac{3}{2} - \tilde{M}_{22} & -\tilde{M}_{24} & \tilde{M}_{26} & \tilde{M}_{28} \\ -\tilde{M}_{42} & \frac{3}{2} - \tilde{M}_{44} & \tilde{M}_{46} & \tilde{M}_{48} \\ \tilde{M}_{62} & \tilde{M}_{64} & \frac{3}{2} - \tilde{M}_{66} & -\tilde{M}_{68} \\ \tilde{M}_{82} & \tilde{M}_{84} & -\tilde{M}_{86} & \frac{3}{2} - \tilde{M}_{88} \end{bmatrix} = \begin{bmatrix} \frac{3}{2} - D_1 & -D_2 & D_3 & D_4 \\ -D_2 & \frac{3}{2} - D_1 & D_4 & D_3 \\ D_3 & D_4 & \frac{3}{2} - \bar{D}_1 & -\bar{D}_2 \\ D_4 & D_3 & -\bar{D}_2 & \frac{3}{2} - \bar{D}_1 \end{bmatrix} \tag{C.63}$$

Combining the above results together, one obtains

$$\left\langle \tilde{Q}_1, \tilde{Q}_2 \middle| \hat{U}(t_a)\hat{U}^{\dagger}(t_b) \middle| \bar{Q}_1, \bar{Q}_2 \right\rangle = \frac{\exp\left(\frac{1}{2}X^{\mathrm{T}}\tilde{\mathcal{M}}X\right)}{\pi \cosh r_a \cosh r_b \sqrt{\det M}}, \tag{C.64}$$

where

$$\tilde{\mathcal{M}} = \begin{bmatrix} \frac{1}{2} - D_1 & -D_2 & D_3 & D_4 \\ -D_2 & \frac{1}{2} - D_1 & D_4 & D_3 \\ D_3 & D_4 & \frac{1}{2} - \bar{D}_1 & -\bar{D}_2 \\ D_4 & D_3 & -\bar{D}_2 & \frac{1}{2} - \bar{D}_1 \end{bmatrix}. \tag{C.65}$$

This is the result we use in the main text to derive Eq. (6.16).

Appendix D

Formulae regarding Gaussian-type integrals

D.1 Gaussian integral over the quadrants

In this appendix, we consider the following integral

$$I \equiv \int_0^\infty \mathrm{d}x \int_0^\infty \mathrm{d}y \, e^{-ax^2-2bxy-cy^2} \,, \tag{D.1}$$

where $a, b, c \in \mathbb{C}$. Our goal is to derive a closed-form expression for I, and to carefully study the conditions under which that expression is valid. The result is used to derive Eq. (6.28), a formula for the temporal correlation function in the limit of infinite ℓ.

First, let us introduce the integral

$$J(\xi, \beta) \equiv \int_0^\infty \mathrm{d}x \, e^{-\xi x^2} \operatorname{erf}(\beta x) \,, \tag{D.2}$$

where $\xi, \beta \in \mathbb{C}$, and where the error function is defined as $\operatorname{erf}(z) = \frac{2}{\sqrt{\pi}} \int_0^z e^{-t^2} \mathrm{d}t$. Here, the integration variable t follows a straight line between 0 and z in the complex plane. The error function is an odd function, *i.e.* $\operatorname{erf}(-z) = -\operatorname{erf}(z)$. By replacing the error function by its definition, and upon changing the order of integration (the conditions for absolute integrability, which ensure the validity of Fubini's theorem, are discussed at the end of this appendix), J can be expressed as

$$\begin{aligned} J(\xi, \beta) &= \frac{2}{\sqrt{\pi}} \int_0^\infty \mathrm{d}x \, e^{-\xi x^2} \int_0^{\beta x} \mathrm{d}t \, e^{-t^2} \\ &= \frac{2}{\sqrt{\pi}} \int_0^\infty \mathrm{d}x \, e^{-\xi x^2} \beta x \int_0^1 \mathrm{d}u \, e^{-\beta^2 x^2 u^2} \\ &= \frac{2\beta}{\sqrt{\pi}} \int_0^1 \mathrm{d}u \int_0^\infty \mathrm{d}x \, x \, e^{-\left(\xi+\beta^2 u^2\right)x^2} \\ &= \frac{2\beta}{\sqrt{\pi}} \int_0^1 \mathrm{d}u \left[\frac{e^{-\left(\xi+\beta^2 u^2\right)x^2}}{-2\left(\xi+\beta^2 u^2\right)} \right]_0^\infty \,, \end{aligned} \tag{D.3}$$

where in the second line, we have performed the change of integration variable $t = \beta x u$. In order for this integral to converge, one must assume $\Re\mathrm{e}(\xi) > 0$ and $\Re\mathrm{e}(\xi + \beta^2) > 0$.

Then, one can proceed as

$$J(\xi,\beta) = \frac{\beta}{\sqrt{\pi}} \int_0^1 \frac{\mathrm{d}u}{\xi + \beta^2 u^2} = \frac{1}{\sqrt{\pi}\sqrt{\xi}} \int_0^{\beta/\sqrt{\xi}} \frac{\mathrm{d}v}{1+v^2}\,, \tag{D.4}$$

where we have performed the change of integration variable $v = \beta u/\sqrt{\xi}$. In this last expression, let us note that the result of the complex integral depends on the path followed in the complex plane, since the integrand has poles at $v = \pm i$. In the present case, however, as mentioned above, the path is a straight line, which leaves no ambiguity. This integral can then be expressed in terms of the arctangent function,

$$J(\xi,\beta) = \frac{1}{\sqrt{\pi}\sqrt{\xi}} \arctan\left(\frac{\beta}{\sqrt{\xi}}\right). \tag{D.5}$$

Here, the range of the real part of the arctangent is restricted to $[-\pi/2, \pi/2]$ as usual.

Let us now introduce a second integral, J_c, defined similarly to J but where the error function is replaced with the complementary error function

$$J_\mathrm{c}(\xi,\beta) \equiv \int_0^\infty \mathrm{d}x\, e^{-\xi x^2} \operatorname{erfc}(\beta x)\,. \tag{D.6}$$

The complementary error function is related to the error function by $\operatorname{erfc}(z) = 1 - \operatorname{erf}(z)$. By making use of Eq. (D.5) and of the relation [see Eq. (4.24.17) of Ref. [135]]

$$\arctan(z) + \arctan\left(\frac{1}{z}\right) = \begin{cases} \pi/2 & \text{for} \quad \Re\mathrm{e}(z) > 0 \\ -\pi/2 & \text{for} \quad \Re\mathrm{e}(z) < 0 \end{cases},$$

one has

$$J_\mathrm{c}(\xi,\beta) = \int_0^\infty \mathrm{d}x\, e^{-\xi x^2} \left[1 - \operatorname{erf}(\beta x)\right] \tag{D.7}$$

$$= \frac{\sqrt{\pi}}{2\sqrt{\xi}} - J(\xi,\beta) = \frac{\sqrt{\pi}}{2\sqrt{\xi}} - \frac{1}{\sqrt{\pi}\sqrt{\xi}} \arctan\left(\frac{\beta}{\sqrt{\xi}}\right) \tag{D.8}$$

$$= \begin{cases} \dfrac{1}{\sqrt{\pi}\sqrt{\xi}} \arctan\left(\dfrac{\sqrt{\xi}}{\beta}\right) & \text{for} \quad \Re\mathrm{e}\left(\dfrac{\beta}{\sqrt{\xi}}\right) > 0 \\ \dfrac{\sqrt{\pi}}{\sqrt{\xi}} + \dfrac{1}{\sqrt{\pi}\sqrt{\xi}} \arctan\left(\dfrac{\sqrt{\xi}}{\beta}\right) & \text{for} \quad \Re\mathrm{e}\left(\dfrac{\beta}{\sqrt{\xi}}\right) < 0 \end{cases}. \tag{D.9}$$

We now apply these results to the calculation of the integral I. By noticing that

$$-ax^2 - 2bxy - cy^2 = -c\left(y + \frac{bx}{c}\right)^2 + \left(\frac{b^2}{c} - a\right)x^2, \tag{D.10}$$

one obtains

$$I = \int_0^\infty \mathrm{d}x\, e^{-\left(a - \frac{b^2}{c}\right)x^2} \int_0^\infty \mathrm{d}y\, e^{-c\left(y + \frac{bx}{c}\right)^2} = \int_0^\infty \mathrm{d}x\, e^{-\left(a - \frac{b^2}{c}\right)x^2} \frac{1}{\sqrt{c}} \int_{bx/\sqrt{c}}^{\sqrt{c}(\infty + bx/c)} \mathrm{d}z\, e^{-z^2}, \tag{D.11}$$

where in the last expression, we have performed the change of integration variable $z = \sqrt{c}\left(y + \frac{bx}{c}\right)$. Assuming that $\Re\mathrm{e}(c) > 0$, one can write the integral over z in terms of the complementary error function,[1]

$$I = \frac{\sqrt{\pi}}{2\sqrt{c}} \int_0^\infty \mathrm{d}x\, e^{-\left(a-\frac{b^2}{c}\right)x^2} \mathrm{erfc}\left(\frac{b}{\sqrt{c}}x\right) = \frac{\sqrt{\pi}}{2\sqrt{c}} J_{\mathrm{c}}\left(a - \frac{b^2}{c}, \frac{b}{\sqrt{c}}\right). \tag{D.12}$$

According to the conditions given below Eq. (D.3), this expression is well defined if $\Re\mathrm{e}(a) > 0$ and $\Re\mathrm{e}\left(a - b^2/c\right) > 0$. Making use of Eq. (D.8), one obtains

$$I = \frac{1}{2\sqrt{c}\sqrt{a - \frac{b^2}{c}}} \left[\frac{\pi}{2} - \arctan\left(\frac{b}{\sqrt{c}\sqrt{a - \frac{b^2}{c}}}\right)\right]. \tag{D.13}$$

Note that $\sqrt{c}\sqrt{a - b^2/c} = \sqrt{ac - b^2}$ without ambiguity on the sign (in general, the branch cut of the complex square root function leaves the sign of $\sqrt{z}$ ambiguous) under the assumptions $\Re\mathrm{e}\,(c) > 0, \Re\mathrm{e}\,(a - b^2/c) > 0$.

In summary, we have showed that

$$\int_0^\infty \mathrm{d}x \int_0^\infty \mathrm{d}y\, e^{-ax^2-2bxy-cy^2} = \frac{1}{2\sqrt{ac-b^2}} \left[\frac{\pi}{2} - \arctan\left(\frac{b}{\sqrt{ac-b^2}}\right)\right] \tag{D.14}$$

under the conditions

$$\Re\mathrm{e}(a) > 0, \quad \Re\mathrm{e}(c) > 0, \quad \Re\mathrm{e}\left(a - \frac{b^2}{c}\right) > 0. \tag{D.15}$$

Let us note that the integral over other quadrants can be derived following the same lines. For instance, one has

$$\begin{aligned} \int_{-\infty}^0 \mathrm{d}x \int_0^\infty \mathrm{d}y\, e^{-ax^2-2bxy-cy^2} &= \int_0^\infty \mathrm{d}x \int_0^\infty \mathrm{d}y\, e^{-ax^2+2bxy-cy^2} \\ &= \frac{1}{2\sqrt{ac-b^2}} \left[\frac{\pi}{2} + \arctan\left(\frac{b}{\sqrt{ac-b^2}}\right)\right] \end{aligned} \tag{D.16}$$

under the same conditions (D.15). These expressions could be further simplified, as in Eq. (D.9), but one would then have to consider two branches, and we do not display the resulting formulas since they are not particularly insightful. The integrals over the two remaining quadrants can be readily derived from Eqs. (D.14) and (D.16) by exchanging the integration variables x and y, *i.e.* by swapping a and b in the formulas. In summary, for the integrals over the four quadrants to be well defined, the condition (D.15) must be satisfied *per se* and also after exchanging a and c, which leads to

$$\Re\mathrm{e}(a) > 0, \quad \Re\mathrm{e}(c) > 0, \quad \Re\mathrm{e}\left(a - \frac{b^2}{c}\right) > 0, \quad \Re\mathrm{e}\left(c - \frac{b^2}{a}\right) > 0. \tag{D.17}$$

[1] Note that in the limit $r \to \infty$, one has [see Eq. (7.12.1) of Ref. [135]]

$$\mathrm{erf}\left(re^{i\theta}\right) \underset{r\to\infty}{\longrightarrow} \begin{cases} 1 & \text{for} \quad -\pi/4 < \theta < \pi/4 \\ \text{divergent} & \text{otherwise} \end{cases}.$$

Let us finally discuss the convergence conditions for the integrals studied in this appendix. According to Fubini's theorem, a double integral can be evaluated by means of an iterated integral if the integrand is absolutely integrable. If one were to evaluate the Gaussian integral over the full two-dimensional plane, the condition for absolute convergence would be

$$\Re\mathrm{e}\,(a) > 0, \quad \Re\mathrm{e}\,(c) > 0, \quad \Re\mathrm{e}\,(a)\,\Re\mathrm{e}\,(c) - [\Re\mathrm{e}\,(b)]^2 > 0. \tag{D.18}$$

One should note that Eq. (D.17) is always true if Eq. (D.18) is satisfied, for the following reason. The conditions on $\Re\mathrm{e}\,(a)$ and $\Re\mathrm{e}\,(c)$ being the same, one needs to focus on the third and fourth conditions in Eqs. (D.17), and on the third condition in Eq. (D.18). By expanding b and c into their real and imaginary parts, one has

$$\Re\mathrm{e}\left(a - \frac{b^2}{c}\right) = \Re\mathrm{e}\,(a) - \frac{\Re\mathrm{e}^{\,2}(b)\Re\mathrm{e}\,(c) - \Im\mathrm{m}^{\,2}(b)\Re\mathrm{e}\,(c) - 2\Re\mathrm{e}\,(b)\Im\mathrm{m}\,(b)\Im\mathrm{m}\,(c)}{\Re\mathrm{e}^{\,2}(c) + \Im\mathrm{m}^{\,2}(c)} \tag{D.19}$$

Let us view this expression as a function of $\Im\mathrm{m}\,(b)$. Its derivative vanishes when $\Im\mathrm{m}\,(b) = -\Re\mathrm{e}\,(b)\Im\mathrm{m}\,(c)/\Re\mathrm{e}\,(c)$, and at that point, the second derivative reads $2\Re\mathrm{e}\,(c)/[\Re\mathrm{e}^{\,2}(c) + \Im\mathrm{m}^{\,2}(c)]$. Under the condition $\Re\mathrm{e}\,(c) > 0$, which is contained in both Eqs. (D.15) and (D.18), the second derivative is thus positive, hence $\Im\mathrm{m}\,(b) = -\Re\mathrm{e}\,(b)\Im\mathrm{m}\,(c)/\Re\mathrm{e}\,(c)$ is a global minimum. Evaluating Eq. (D.19) at that point, one thus obtains

$$\Re\mathrm{e}\left(a - \frac{b^2}{c}\right) > \Re\mathrm{e}\,(a) - \frac{\Re\mathrm{e}^{\,2}(b)}{\Re\mathrm{e}\,(c)} \qquad \text{if} \qquad \Re\mathrm{e}\,(c) > 0\,. \tag{D.20}$$

Since $\Re\mathrm{e}\,(c) > 0$ in Eq. (D.18), the third condition in Eq. (D.18) is equivalent to the requirement that the right-hand side of Eq. (D.20) is positive, and this implies the validity of the third condition in Eq. (D.17). Since the third condition in Eq. (D.18) is symmetric in a and b, this also implies the validity of the fourth condition in Eq. (D.17), which finishes proving that Eq. (D.18) implies Eq. (D.17).

The cases where Eq. (D.17) is valid while Eq. (D.18) is not are beyond the scope of Fubini's theorem and there, the correctness of the calculation performed in this appendix is a priori nontrivial. However, when this happens, we have checked with a direct numerical integration that our formulae are still valid. While Eq. (D.18) is a sufficient condition for making use of Fubini's theorem, it is not always necessary, and our results thus suggest that Eq. (D.17) is a necessary, and possibly sufficient, condition. In every physical situation we have looked at, we have checked that the conditions (D.17) are satisfied, which ensures that finite results are obtained.

D.2 Derivation of the small-ℓ expansion formula

In this appendix, we consider the small-ℓ limit of integrals of the form

$$I \equiv \sum_{n=-\infty}^{\infty} \sum_{m=-\infty}^{\infty} (-1)^{n+m} \int_{n\ell}^{(n+1)\ell} \mathrm{d}x \int_{m\ell}^{(m+1)\ell} \mathrm{d}y\, e^{-ax^2-2bxy-cy^2}\,, \tag{D.21}$$

where $a, b, c \in \mathbb{C}$. Let us first perform the change of integration variables $x' = (x - n\ell)/\ell$ and $y' = (y - n\ell)/\ell$, which allows us to rewrite I as

$$I = \ell^2 \sum_{n=-\infty}^{\infty} \sum_{m=-\infty}^{\infty} (-1)^{n+m} \int_0^1 \mathrm{d}x \int_0^1 \mathrm{d}y \, e^{-a(x+n)^2\ell^2 - 2b(x+n)(y+m)\ell^2 - c(y+m)^2\ell^2} \tag{D.22}$$

$$= \ell^2 \int_0^1 \mathrm{d}x \int_0^1 \mathrm{d}y \, e^{-(ax^2+2bxy+cy^2)\ell^2} \sum_{n=-\infty}^{\infty} (-1)^n e^{-2(ax+by)n\ell^2 - an^2\ell^2} \sum_{m=-\infty}^{\infty} (-1)^m e^{-2(bx+bn+cy)m\ell^2 - cm^2\ell^2} \tag{D.23}$$

$$= \ell^2 \int_0^1 \mathrm{d}x \int_0^1 \mathrm{d}y \, e^{-(ax^2+2bxy+cy^2)\ell^2} \sum_{n=-\infty}^{\infty} (-1)^n e^{-2(ax+by)n\ell^2 - an^2\ell^2} \vartheta_4 \left[i(bx+bn+cy)\ell^2, e^{-c\ell^2} \right] . \tag{D.24}$$

Here, in Eq. (D.23), we have exchanged the order by which we integrate over x and y and sum over n and m, which is possible since all integrals and sums are absolutely convergent under the conditions detailed in Appendix D.1, and in Eq. (D.24), we have recast the sum over m in terms of the elliptic theta function defined in Eq. (A.4). Using the Jacobi identity (A.19), one can write

$$\vartheta_4 \left[i(bx+bn+cy)\ell^2, e^{-c\ell^2} \right] = \frac{\sqrt{\pi}}{\ell\sqrt{c}} e^{(bx+bn+cy)^2 \frac{\ell^2}{c}} \vartheta_2 \left[-\frac{\pi(bx+bn+cy)}{c}, e^{-\frac{\pi^2}{c\ell^2}} \right] . \tag{D.25}$$

This allows us to obtain an expression in which the first argument of the elliptic theta function is independent of ℓ, and the second argument tends to 0 when ℓ tends to 0. Hence, in that limit, we can make use of an approximate expression (A.21). Combining these results, one obtains

$$I \simeq \frac{2\sqrt{\pi}\ell}{\sqrt{c}} e^{-\frac{\pi^2}{4c\ell^2}} \int_0^1 \mathrm{d}x \, e^{-\left(a - \frac{b^2}{c}\right)x^2\ell^2} \sum_{n=-\infty}^{\infty} (-1)^n e^{-\left(a-\frac{b^2}{c}\right)(n^2+2xn)\ell^2} \int_0^1 \mathrm{d}y \, \cos\left[\pi y + \frac{\pi b(x+n)}{c}\right] \tag{D.26}$$

$$= \frac{-4\ell}{\sqrt{\pi}\sqrt{c}} e^{-\frac{\pi^2}{4c\ell^2}} \int_0^1 \mathrm{d}x \, e^{-\left(a-\frac{b^2}{c}\right)x^2\ell^2} \sum_{n=-\infty}^{\infty} (-1)^n e^{-\left(a-\frac{b^2}{c}\right)(n^2+2xn)\ell^2} \sin\left[\frac{\pi b(x+n)}{c}\right] \tag{D.27}$$

$$= \frac{2i\ell}{\sqrt{\pi}\sqrt{c}} e^{-\frac{\pi^2}{4c\ell^2}} \int_0^1 \mathrm{d}x \, e^{-\left(a-\frac{b^2}{c}\right)x^2\ell^2} \left(J_+ - J_-\right) . \tag{D.28}$$

Here, in Eq. (D.27), we have performed the integral over y, and in Eq. (D.28), we have expanded the sine function in terms of exponentials, and introduced

$$J_\pm \equiv \sum_{n=-\infty}^{\infty} (-1)^n e^{-\left(a-\frac{b^2}{c}\right)(n^2+2xn)\ell^2 \pm i\pi b\frac{x+n}{c}} \tag{D.29}$$

$$= e^{\pm i\pi bx/c} \vartheta_4 \left[i\left(a - \frac{b^2}{c}\right)x\ell^2 \pm \frac{\pi b}{2c}, e^{-\left(a-\frac{b^2}{c}\right)\ell^2} \right] \tag{D.30}$$

where Eq. (A.4) has been used to express the sum over n as the elliptic theta function.

If one further assumes that $a - b^2/c$ has a positive real part, one can make use of the expansion formula (A.27) and rewrite $J_\pm$ as

$$J_\pm \simeq \frac{2\sqrt{\pi}}{\ell\sqrt{a-\frac{b^2}{c}}} \exp\left[-\frac{\pi^2\left(1+\frac{b^2}{c^2}\right)}{4\left(a-\frac{b^2}{c}\right)\ell^2} + \left(a-\frac{b^2}{c}\right)x^2\ell^2\right] C_\pm\,, \tag{D.31}$$

where

$$C_\pm \equiv \cosh\left[i\pi x \pm \frac{\pi^2 b}{2(ac-b^2)\ell^2}\right]\,. \tag{D.32}$$

Combining the above results, one obtains

$$I \simeq \frac{4i}{\sqrt{c}\sqrt{a-\frac{b^2}{c}}} \exp\left[-\frac{\pi^2(a+c)}{4(ac-b^2)\ell^2}\right] \int_0^1 \mathrm{d}x\ (C_+ - C_-)\ , \tag{D.33}$$

where the integral over x can be performed analytically and gives rise to

$$\int_0^1 \mathrm{d}x\, C_\pm = \pm\frac{2i}{\pi}\sinh\left[\frac{\pi^2 b}{2(ac-b^2)\ell^2}\right]\,. \tag{D.34}$$

Here again, as we mentioned below Eq. (D.13), $\sqrt{c}\sqrt{a-b^2/c} = \sqrt{ac-b^2}$ holds under the assumptions $\Re\mathrm{e}\,(c) > 0, \Re\mathrm{e}\,(a-b^2/c) > 0$, which we need for the integral to be convergent. One finally has

$$I \simeq \frac{-16}{\pi\sqrt{ac-b^2}} \exp\left[-\frac{\pi^2(a+c)}{4(ac-b^2)\ell^2}\right] \sinh\left[\frac{\pi^2 b}{2(ac-b^2)\ell^2}\right] \tag{D.35}$$

$$= \frac{8}{\pi\sqrt{ac-b^2}}\left(e^{p_+} - e^{p_-}\right)\ , \tag{D.36}$$

where

$$p_\pm \equiv -\frac{\pi^2(a+c\pm 2b)}{4(ac-b^2)\ell^2}\,. \tag{D.37}$$

These expressions are used to derive Eq. (6.29).

Bibliography

[1] A. Starobinsky, *A new type of isotropic cosmological models without singularity*, Phys. Lett. B **91** (1980), no. 1 99 – 102.

[2] K. Sato, *First-order phase transition of a vacuum and the expansion of the Universe*, Mon. Not. Roy. Astron. Soc. **195** (07, 1981) 467–479.

[3] A. H. Guth, *Inflationary universe: A possible solution to the horizon and flatness problems*, Phys. Rev. D **23** (Jan, 1981) 347–356.

[4] A. Linde, *A new inflationary universe scenario: A possible solution of the horizon, flatness, homogeneity, isotropy and primordial monopole problems*, Phys. Lett. B **108** (1982), no. 6 389 – 393.

[5] A. D. Linde, *Chaotic Inflation*, Phys. Lett. B **129** (1983) 177–181.

[6] V. F. Mukhanov and G. V. Chibisov, *Quantum Fluctuations and a Nonsingular Universe*, JETP Lett. **33** (1981) 532–535.

[7] V. F. Mukhanov and G. Chibisov, *The Vacuum energy and large scale structure of the universe*, Sov. Phys. JETP **56** (1982) 258–265.

[8] A. A. Starobinsky, *Dynamics of Phase Transition in the New Inflationary Universe Scenario and Generation of Perturbations*, Phys. Lett. B **117** (1982) 175–178.

[9] A. H. Guth and S. Pi, *Fluctuations in the New Inflationary Universe*, Phys. Rev. Lett. **49** (1982) 1110–1113.

[10] S. Hawking, *The Development of Irregularities in a Single Bubble Inflationary Universe*, Phys. Lett. B **115** (1982) 295.

[11] J. M. Bardeen, P. J. Steinhardt and M. S. Turner, *Spontaneous Creation of Almost Scale - Free Density Perturbations in an Inflationary Universe*, Phys. Rev. D **28** (1983) 679.

[12] **Planck** Collaboration, Y. Akrami et. al., *Planck 2018 results. X. Constraints on inflation*, Astron. Astrophys. **641** (2020) A10 [arXiv:1807.06211].

[13] G. Nicholson and C. R. Contaldi, *Reconstruction of the Primordial Power Spectrum using Temperature and Polarisation Data from Multiple Experiments*, JCAP **07** (2009) 011 [arXiv:0903.1106].

[14] G. Nicholson, C. R. Contaldi and P. Paykari, *Reconstruction of the Primordial Power Spectrum by Direct Inversion*, JCAP **01** (2010) 016 [arXiv:0909.5092].

[15] S. Bird, H. V. Peiris, M. Viel and L. Verde, *Minimally Parametric Power Spectrum Reconstruction from the Lyman-alpha Forest*, Mon. Not. Roy. Astron. Soc. **413** (2011) 1717–1728 [arXiv:1010.1519].

[16] L. P. Grishchuk and Y. V. Sidorov, *Squeezed quantum states of relic gravitons and primordial density fluctuations*, Phys. Rev. D **42** (Nov, 1990) 3413–3421.

[17] D. Polarski and A. A. Starobinsky, *Semiclassicality and decoherence of cosmological perturbations*, Class. Quant. Grav. **13** (1996) 377–392 [arXiv:gr-qc/9504030].

[18] J. Lesgourgues, D. Polarski and A. A. Starobinsky, *Quantum to classical transition of cosmological perturbations for nonvacuum initial states*, Nucl. Phys. B **497** (1997) 479–510 [arXiv:gr-qc/9611019].

[19] C. Kiefer and D. Polarski, *Why do cosmological perturbations look classical to us?*, Adv. Sci. Lett. **2** (2009) 164–173 [arXiv:0810.0087].

[20] J. Martin and V. Vennin, *Quantum Discord of Cosmic Inflation: Can we Show that CMB Anisotropies are of Quantum-Mechanical Origin?*, Phys. Rev. D **93** (2016), no. 2 023505 [arXiv:1510.04038].

[21] M. Revzen, P. A. Mello, A. Mann and L. M. Johansen, *Bell's inequality violation with non-negative wigner functions*, Physical Review A **71** (Feb, 2005).

[22] B. Hall, Quantum Theory for Mathematicians. Graduate Texts in Mathematics. Springer New York, 2013.

[23] J. Martin, *Cosmic Inflation, Quantum Information and the Pioneering Role of John S Bell in Cosmology*, Universe **5** (2019), no. 4 92 [arXiv:1904.00083].

[24] A. A. Starobinsky, *Stochastic De Sitter (inflationary) stage in the early universe*, Lect. Notes Phys. **246** (1986) 107–126.

[25] A. A. Starobinsky and J. Yokoyama, *Equilibrium state of a selfinteracting scalar field in the de Sitter background*, Phys. Rev. D **50** (1994) 6357–6368 [arXiv:astro-ph/9407016].

[26] N. Tsamis and R. Woodard, *Stochastic quantum gravitational inflation*, Nucl. Phys. B **724** (2005) 295–328 [arXiv:gr-qc/0505115].

[27] F. Finelli, G. Marozzi, A. Starobinsky, G. Vacca and G. Venturi, *Generation of fluctuations during inflation: Comparison of stochastic and field-theoretic approaches*, Phys. Rev. D **79** (2009) 044007 [arXiv:0808.1786].

[28] B. Garbrecht, G. Rigopoulos and Y. Zhu, *Infrared correlations in de Sitter space: Field theoretic versus stochastic approach*, Phys. Rev. D **89** (2014) 063506 [arXiv:1310.0367].

[29] V. Vennin and A. A. Starobinsky, *Correlation Functions in Stochastic Inflation*, Eur. Phys. J. C **75** (2015) 413 [arXiv:1506.04732].

[30] V. Onemli, *Vacuum Fluctuations of a Scalar Field during Inflation: Quantum versus Stochastic Analysis*, Phys. Rev. D **91** (2015) 103537 [arXiv:1501.05852].

[31] C. Burgess, R. Holman and G. Tasinato, *Open EFTs, IR effects & late-time resummations: systematic corrections in stochastic inflation*, JHEP **01** (2016) 153 [arXiv:1512.00169].

[32] R. J. Hardwick, V. Vennin, C. T. Byrnes, J. Torrado and D. Wands, *The stochastic spectator*, JCAP **10** (2017) 018 [arXiv:1701.06473].

[33] J. Tokuda and T. Tanaka, *Statistical nature of infrared dynamics on de Sitter background*, JCAP **02** (2018) 014 [arXiv:1708.01734].

[34] H. Kitamoto, *Infrared resummation for derivative interactions in de Sitter space*, Phys. Rev. D **100** (2019), no. 2 025020 [arXiv:1811.01830].

[35] T. Markkanen, A. Rajantie, S. Stopyra and T. Tenkanen, *Scalar correlation functions in de Sitter space from the stochastic spectral expansion*, JCAP **08** (2019) 001 [arXiv:1904.11917].

[36] A. A. Starobinsky, *Multicomponent de Sitter (Inflationary) Stages and the Generation of Perturbations*, JETP Lett. **42** (1985) 152–155.

[37] M. Sasaki and E. D. Stewart, *A General analytic formula for the spectral index of the density perturbations produced during inflation*, Prog. Theor. Phys. **95** (1996) 71–78 [arXiv:astro-ph/9507001].

[38] M. Sasaki and T. Tanaka, *Superhorizon scale dynamics of multiscalar inflation*, Prog. Theor. Phys. **99** (1998) 763–782 [arXiv:gr-qc/9801017].

[39] D. H. Lyth, K. A. Malik and M. Sasaki, *A General proof of the conservation of the curvature perturbation*, JCAP **05** (2005) 004 [arXiv:astro-ph/0411220].

[40] D. H. Lyth and Y. Rodriguez, *The Inflationary prediction for primordial non-Gaussianity*, Phys. Rev. Lett. **95** (2005) 121302 [arXiv:astro-ph/0504045].

[41] E. M. Lifshitz and I. M. Khalatnikov, *About singularities of cosmological solutions of the gravitational equations. I*, ZhETF **39** (1960) 149.

[42] A. A. Starobinsky, *Isotropization of arbitrary cosmological expansion given an effective cosmological constant*, JETP Lett. **37** (1983) 66–69.

[43] G. Comer, N. Deruelle, D. Langlois and J. Parry, *Growth or decay of cosmological inhomogeneities as a function of their equation of state*, Phys. Rev. D **49** (1994) 2759–2768.

[44] D. Wands, K. A. Malik, D. H. Lyth and A. R. Liddle, *A New approach to the evolution of cosmological perturbations on large scales*, Phys. Rev. D **62** (2000) 043527 [arXiv:astro-ph/0003278].

[45] I. Khalatnikov and A. Kamenshchik, *Comment about quasiisotropic solution of Einstein equations near cosmological singularity*, Class. Quant. Grav. **19** (2002) 3845–3850 [arXiv:gr-qc/0204045].

[46] D. H. Lyth and D. Wands, *Conserved cosmological perturbations*, Phys. Rev. D **68** (2003) 103515 [arXiv:astro-ph/0306498].

[47] J. Yokoyama, *Chaotic new inflation and formation of primordial black holes*, Phys. Rev. D **58** (Sep, 1998) 083510.

[48] K. Enqvist, S. Nurmi, D. Podolsky and G. Rigopoulos, *On the divergences of inflationary superhorizon perturbations*, JCAP **04** (2008) 025 [arXiv:0802.0395].

[49] T. Fujita, M. Kawasaki, Y. Tada and T. Takesako, *A new algorithm for calculating the curvature perturbations in stochastic inflation*, JCAP **12** (2013) 036 [arXiv:1308.4754].

[50] T. Fujita, M. Kawasaki and Y. Tada, *Non-perturbative approach for curvature perturbations in stochastic δN formalism*, JCAP **10** (2014) 030 [arXiv:1405.2187].

[51] M. Kawasaki and Y. Tada, *Can massive primordial black holes be produced in mild waterfall hybrid inflation?*, JCAP **08** (2016) 041 [arXiv:1512.03515].

[52] H. Assadullahi, H. Firouzjahi, M. Noorbala, V. Vennin and D. Wands, *Multiple Fields in Stochastic Inflation*, JCAP **06** (2016) 043 [arXiv:1604.04502].

[53] V. Vennin, H. Assadullahi, H. Firouzjahi, M. Noorbala and D. Wands, *Critical Number of Fields in Stochastic Inflation*, Phys. Rev. Lett. **118** (2017), no. 3 031301 [arXiv:1604.06017].

[54] C. Pattison, V. Vennin, H. Assadullahi and D. Wands, *Quantum diffusion during inflation and primordial black holes*, JCAP **10** (2017) 046 [arXiv:1707.00537].

[55] J. M. Ezquiaga, J. García-Bellido and V. Vennin, *The exponential tail of inflationary fluctuations: consequences for primordial black holes*, JCAP **03** (2020) 029 [arXiv:1912.05399].

[56] J. Grain and V. Vennin, *Stochastic inflation in phase space: Is slow roll a stochastic attractor?*, JCAP **05** (2017) 045 [arXiv:1703.00447].

[57] C. Pattison, V. Vennin, H. Assadullahi and D. Wands, *Stochastic inflation beyond slow roll*, JCAP **07** (2019) 031 [arXiv:1905.06300].

[58] V. Vennin, *Stochastic inflation and primordial black holes*, Habilitation thesis (2020) [arXiv:2009.08715].

[59] A. Einstein, B. Podolsky and N. Rosen, *Can quantum mechanical description of physical reality be considered complete?*, Phys. Rev. **47** (1935) 777–780.

[60] A. Heidmann, R. J. Horowicz, S. Reynaud, E. Giacobino, C. Fabre and G. Camy, *Observation of quantum noise reduction on twin laser beams*, Physical Review Letters **59** (Nov., 1987) 2555–2557.

[61] A. S. Villar, L. S. Cruz, K. N. Cassemiro, M. Martinelli and P. Nussenzveig, *Generation of Bright Two-Color Continuous Variable Entanglement*, Physical Review Letters **95** (Dec., 2005) 243603 [arXiv:quant-ph/0506139].

[62] A. Dutt, K. Luke, S. Manipatruni, A. L. Gaeta, P. Nussenzveig and M. Lipson, *On-Chip Optical Squeezing*, Physical Review Applied **3** (Apr., 2015) 044005.

[63] H. Vahlbruch, M. Mehmet, K. Danzmann and R. Schnabel, *Detection of 15 db squeezed states of light and their application for the absolute calibration of photoelectric quantum efficiency*, Phys. Rev. Lett. **117** (Sep, 2016) 110801.

[64] J. S. Bell, *On the Einstein-Podolsky-Rosen paradox*, Physics Physique Fizika **1** (1964) 195–200.

[65] J. F. Clauser, M. A. Horne, A. Shimony and R. A. Holt, *Proposed experiment to test local hidden variable theories*, Phys. Rev. Lett. **23** (1969) 880–884.

[66] A. Aspect, P. Grangier and G. Roger, *Experimental realization of Einstein-Podolsky-Rosen-Bohm Gedankenexperiment: A New violation of Bell's inequalities*, Phys. Rev. Lett. **49** (1982) 91–97.

[67] A. Aspect, J. Dalibard and G. Roger, *Experimental test of Bell's inequalities using time varying analyzers*, Phys. Rev. Lett. **49** (1982) 1804–1807.

[68] G. Weihs, T. Jennewein, C. Simon, H. Weinfurter and A. Zeilinger, *Violation of Bell's inequality under strict Einstein locality conditions*, Phys. Rev. Lett. **81** (1998) 5039–5043 [arXiv:quant-ph/9810080].

[69] B. Hensen et. al., *Loophole-free Bell inequality violation using electron spins separated by 1.3 kilometres*, Nature **526** (2015) 682–686 [arXiv:1508.05949].

[70] A. Palacios-Laloy, F. Mallet, F. Nguyen, P. Bertet, D. Vion, D. Esteve and A. N. Korotkov, *Experimental violation of a Bell's inequality in time with weak measurement*, Nature Physics **6** (Apr, 2010) 442–447.

[71] J. Maldacena, *A model with cosmological Bell inequalities*, Fortsch. Phys. **64** (2016) 10–23 [arXiv:1508.01082].

[72] J. Martin and V. Vennin, *Bell inequalities for continuous-variable systems in generic squeezed states*, Phys. Rev. **A93** (2016), no. 6 062117 [arXiv:1605.02944].

[73] S. Kanno and J. Soda, *Infinite violation of Bell inequalities in inflation*, Phys. Rev. **D96** (2017), no. 8 083501 [arXiv:1705.06199].

[74] S. Kanno and J. Soda, *Bell Inequality and Its Application to Cosmology*, Galaxies **5** (2017), no. 4 99.

[75] J. Martin and V. Vennin, *Obstructions to Bell CMB Experiments*, Phys. Rev. D **96** (2017), no. 6 063501 [arXiv:1706.05001].

[76] A. J. Leggett and A. Garg, *Quantum mechanics versus macroscopic realism: Is the flux there when nobody looks?*, Phys. Rev. Lett. **54** (1985) 857–860.

[77] C. Emary, N. Lambert and F. Nori, *Leggett-Garg inequalities*, Reports on Progress in Physics **77** (Jan., 2014) 016001 [arXiv:1304.5133].

[78] J. S. Bell, *EPR Correlations and EPW Distributions*, Annals of the New York Academy of Sciences **480** (Dec., 1986) 263–266.

[79] M. M. Wilde and A. Mizel, *Addressing the Clumsiness Loophole in a Leggett-Garg Test of Macrorealism*, Foundations of Physics **42** (Feb., 2012) 256–265 [arXiv:1001.1777].

[80] K. Ando and V. Vennin, *Power spectrum in stochastic inflation*, arXiv:2012.02031.

[81] K. Ando and V. Vennin, *Bipartite temporal Bell inequalities for two-mode squeezed states*, Phys. Rev. A **102** (2020), no. 5 052213 [arXiv:2007.00458].

[82] H. Kodama and M. Sasaki, *Cosmological Perturbation Theory*, Prog. Theor. Phys. Suppl. **78** (1984) 1–166.

[83] V. Mukhanov, Physical Foundations of Cosmology. Cambridge University Press, Oxford, 2005.

[84] K. A. Malik and D. Wands, *Cosmological perturbations*, Phys. Rept. **475** (2009) 1–51 [arXiv:0809.4944].

[85] N. S. Sugiyama, E. Komatsu and T. Futamase, *δN formalism*, Phys. Rev. **D87** (2013), no. 2 023530 [arXiv:1208.1073].

[86] J.-c. Hwang and H. Noh, *Cosmological perturbations with multiple scalar fields*, Phys. Lett. **B495** (2000) 277–283 [arXiv:astro-ph/0009268].

[87] M. Sasaki, *Large Scale Quantum Fluctuations in the Inflationary Universe*, Prog. Theor. Phys. **76** (1986) 1036.

[88] V. F. Mukhanov, *Quantum Theory of Gauge Invariant Cosmological Perturbations*, Sov. Phys. JETP **67** (1988) 1297–1302.

[89] R. H. Brandenberger, H. Feldman and V. F. Mukhanov, *Classical and quantum theory of perturbations in inflationary universe models*, in 37th Yamada Conference: Evolution of the Universe and its Observational Quest, pp. 19–30, 7, 1993. arXiv:astro-ph/9307016.

[90] J. Garriga and V. F. Mukhanov, *Perturbations in k-inflation*, Phys. Lett. B **458** (1999) 219–225 [arXiv:hep-th/9904176].

[91] J. M. Maldacena, *Non-Gaussian features of primordial fluctuations in single field inflationary models*, JHEP **05** (2003) 013 [arXiv:astro-ph/0210603].

[92] X. Chen, M.-x. Huang, S. Kachru and G. Shiu, *Observational signatures and non-Gaussianities of general single field inflation*, JCAP **01** (2007) 002 [arXiv:hep-th/0605045].

[93] E. Nelson, *Quantum Decoherence During Inflation from Gravitational Nonlinearities*, JCAP **03** (2016) 022 [arXiv:1601.03734].

[94] K. K. Boddy, S. M. Carroll and J. Pollack, *How Decoherence Affects the Probability of Slow-Roll Eternal Inflation*, Phys. Rev. D **96** (2017), no. 2 023539 [arXiv:1612.04894].

[95] J. Martin and V. Vennin, *Leggett-Garg Inequalities for Squeezed States*, Phys. Rev. **A94** (2016), no. 5 052135 [arXiv:1611.01785].

[96] L. Pinol, S. Renaux-Petel and Y. Tada, *A manifestly covariant theory of multifield stochastic inflation in phase space*, arXiv:2008.07497.

[97] L. Pinol, S. Renaux-Petel and Y. Tada, *Inflationary stochastic anomalies*, Class. Quant. Grav. **36** (2019), no. 7 07LT01 [arXiv:1806.10126].

[98] D. Cruces, C. Germani and T. Prokopec, *Failure of the stochastic approach to inflation beyond slow-roll*, JCAP **03** (2019) 048 [arXiv:1807.09057].

[99] H. Risken and H. Haken, The Fokker-Planck Equation: Methods of Solution and Applications Second Edition. Springer, 1989.

[100] S. E. Shreve, Stochastic Calculus for Finance II: Continuous-Time Models. Springer-Verlog New York, LLC, 2004.

[101] K. ITO, *109. stochastic integral*, Proceedings of the Imperial Academy **20** (1944), no. 8 519–524.

[102] R. L. Stratonovich, *A new representation for stochastic integrals and equations*, SIAM Journal on Control **4** (1966), no. 2 362–371 [arXiv:https://doi.org/10.1137/0304028].

[103] A. Mezhlumian and A. A. Starobinsky, *Stochastic inflation: New results*, in The First International A.D. Sakharov Conference on Physics, 10, 1991. arXiv:astro-ph/9406045.

[104] V. F. Mukhanov, *Gravitational Instability of the Universe Filled with a Scalar Field*, JETP Lett. **41** (1985) 493–496.

[105] B. S. Cirel'Son, *Quantum generalizations of Bell's inequality*, Letters in Mathematical Physics **4** (Mar., 1980) 93–100.

[106] J.-Å. Larsson, *Bell inequalities for position measurements*, Phys. Rev. A **70** (Aug, 2004) 022102.

[107] K. Banaszek and K. Wódkiewicz, *Testing quantum nonlocality in phase space*, Phys. Rev. Lett. **82** (Mar, 1999) 2009–2013.

[108] Z.-B. Chen, J.-W. Pan, G. Hou and Y.-D. Zhang, *Maximal violation of bell's inequalities for continuous variable systems*, Phys. Rev. Lett. **88** (Jan, 2002) 040406.

[109] N. Lambert, K. Debnath, A. F. Kockum, G. C. Knee, W. J. Munro and F. Nori, *Leggett-Garg inequality violations with a large ensemble of qubits*, Physical Review A **94** (July, 2016) 012105 [arXiv:1604.04059].

[110] J. P. Paz and G. Mahler, *Proposed test for temporal Bell inequalities*, Physical Review Letters **71** (Nov., 1993) 3235–3239.

[111] C. Brukner, S. Taylor, S. Cheung and V. Vedral, *Quantum Entanglement in Time*, arXiv e-prints (Feb., 2004) quant–ph/0402127 [arXiv:quant-ph/0402127].

[112] T. Fritz, *Quantum correlations in the temporal Clauser-Horne-Shimony-Holt (CHSH) scenario*, New Journal of Physics **12** (Aug., 2010) 083055 [arXiv:1005.3421].

[113] J. F. Clauser and A. Shimony, *REVIEW: Bell's theorem. Experimental tests and implications*, Reports on Progress in Physics **41** (Dec., 1978) 1881–1927.

[114] D. Rauch et. al., *Cosmic Bell Test Using Random Measurement Settings from High-Redshift Quasars*, Phys. Rev. Lett. **121** (2018), no. 8 080403 [arXiv:1808.05966].

[115] G. C. Ghirardi, A. Rimini and T. Weber, *A Unified Dynamics for Micro and MACRO Systems*, Phys. Rev. **D34** (1986) 470.

[116] P. M. Pearle, *Combining Stochastic Dynamical State Vector Reduction With Spontaneous Localization*, Phys. Rev. **A39** (1989) 2277–2289.

[117] G. C. Ghirardi, P. M. Pearle and A. Rimini, *Markov Processes in Hilbert Space and Continuous Spontaneous Localization of Systems of Identical Particles*, Phys. Rev. **A42** (1990) 78–79.

[118] A. Bassi and G. C. Ghirardi, *Dynamical reduction models*, Phys. Rept. **379** (2003) 257 [arXiv:quant-ph/0302164].

[119] J. Martin and V. Vennin, *A cosmic shadow on CSL*, Phys. Rev. Lett. **124** (2020), no. 8 080402 [arXiv:1906.04405].

[120] Y. Tada and V. Vennin, *Squeezed bispectrum in the δN formalism: local observer effect in field space*, JCAP **02** (2017) 021 [arXiv:1609.08876].

[121] J. Garcia-Bellido and E. Ruiz Morales, *Primordial black holes from single field models of inflation*, Phys. Dark Univ. **18** (2017) 47–54 [arXiv:1702.03901].

[122] C. Germani and T. Prokopec, *On primordial black holes from an inflection point*, Phys. Dark Univ. **18** (2017) 6–10 [arXiv:1706.04226].

[123] J. Martin, C. Ringeval and V. Vennin, *Encyclopædia Inflationaris*, Phys. Dark Univ. **5-6** (2014) 75–235 [arXiv:1303.3787].

[124] **Planck** Collaboration, N. Aghanim et. al., *Planck 2018 results. VI. Cosmological parameters*, Astron. Astrophys. **641** (2020) A6 [arXiv:1807.06209].

[125] J. Martin and C. Ringeval, *Inflation after WMAP3: Confronting the Slow-Roll and Exact Power Spectra to CMB Data*, JCAP **08** (2006) 009 [arXiv:astro-ph/0605367].

[126] J. Martin, C. Ringeval and V. Vennin, *Observing Inflationary Reheating*, Phys. Rev. Lett. **114** (2015), no. 8 081303 [arXiv:1410.7958].

[127] T. Papanikolaou, V. Vennin and D. Langlois, *Gravitational waves from a universe filled with primordial black holes*, arXiv:2010.11573.

[128] A. Moradinezhad Dizgah, G. Franciolini and A. Riotto, *Primordial Black Holes from Broad Spectra: Abundance and Clustering*, JCAP **11** (2019) 001 [arXiv:1906.08978].

[129] H. Ooguri and C. Vafa, *On the Geometry of the String Landscape and the Swampland*, Nucl. Phys. B **766** (2007) 21–33 [arXiv:hep-th/0605264].

[130] G. Obied, H. Ooguri, L. Spodyneiko and C. Vafa, *De Sitter Space and the Swampland*, arXiv:1806.08362.

[131] S. K. Garg and C. Krishnan, *Bounds on Slow Roll and the de Sitter Swampland*, JHEP **11** (2019) 075 [arXiv:1807.05193].

[132] H. Ooguri, E. Palti, G. Shiu and C. Vafa, *Distance and de Sitter Conjectures on the Swampland*, Phys. Lett. B **788** (2019) 180–184 [arXiv:1810.05506].

[133] Y. Tada and S. Yokoyama, *Primordial black hole tower: Dark matter, earth-mass, and LIGO black holes*, Phys. Rev. D **100** (2019), no. 2 023537 [arXiv:1904.10298].

[134] K. Vanderlinde, *Unveiling the radio cosmos*, Nature Astron. **1** (2017), no. 2 0037.

[135] I. Thompson, *NIST Handbook of Mathematical Functions, edited by Frank W.J. Olver, Daniel W. Lozier, Ronald F. Boisvert, Charles W. Clark*, Contemporary Physics **52** (Sept., 2011) 497–498.

[136] S. M. Barnett and P. M. Radmore, Methods in Theoretical Quantum Optics. Clarendon Press Publication, Oxford, 1997.